

STRUCTURAL DAMAGE ASSESSMENT AND FINITE ELEMENT  
MODEL REFINEMENT USING MEASURED MODAL DATA

By  
MOHAMED KAOUK

A DISSERTATION PRESENTED TO THE GRADUATE SCHOOL  
OF THE UNIVERSITY OF FLORIDA IN PARTIAL FULFILLMENT  
OF THE REQUIREMENTS FOR THE DEGREE OF  
DOCTOR OF PHILOSOPHY

UNIVERSITY OF FLORIDA

1993

A Mes Parents

Tout le mérite de ce travail, s'il en est, vous revient.

## ACKNOWLEDGEMENTS

I would like to express my sincere gratitude toward my advisor, Dr. David Zimmerman, for his expert guidance, friendship, endless encouragement and support. I will forever be indebted to him for inspiring me in my research and for the priceless education I acquired from him. I am also grateful for the financial support he provided me during the course of my graduate studies.

Words are not enough to express my deepest gratitude to my parents for their love, moral and financial support; it is these things that have made this work possible. I also wish to acknowledge my sisters and brothers for their continuous encouragement.

I would like to thank the members of my supervisory committee, Drs. Norman Fitz-Coy, Lawrence Malvern, Bhavani Sankar, and Kermit Sigmon, for their helpful advice.

I wish to thank my colleagues of the Dynamic Systems and Control Laboratory for their consideration and entertaining discussions. In particular, William Leath and Cinnamon Larson for their friendship and encouragement.

I would like to thank the staff of the Aerospace Engineering, Mechanics, and Engineering Science department for their assistance throughout the years, especially Shirley Robinson for making my life easier during registration, John Young for his prompt responses in fixing my computer problems, and Ronald Brown for his assistance in the machine shop and for many stimulating discussions.

I would like to acknowledge the financial support received from Harris Corporation, NASA/Florida Space Grant Consortium and Florida High Technology Council. I would like to thank Dr. T. A. Kashangaki of the NASA Langley Research Center and Dr. S. W. Smith of the University of Kentucky for providing the data of the Eight-Bay Truss used in this study.

Last, but not least, I am grateful to my good friends Joel Payabyab and Fadel Abdallah for their continuous support.

## TABLE OF CONTENTS

	<u>page</u>
ACKNOWLEDGEMENTS .....	iii
LIST OF TABLES .....	ix
LIST OF FIGURES .....	x
ABSTRACT .....	xiii
 CHAPTERS	
1 INTRODUCTION .....	1
1.1 Finite Element Model Refinement .....	1
1.1.1 Overview .....	1
1.1.2 Literature Survey .....	3
1.2 Structural Damage Assessment .....	6
1.3 Objective of the Present Study .....	8
 2 MATHEMATICAL PRELIMINARIES AND PRACTICAL ISSUES TO THE PROBLEMS OF MODEL REFINEMENT AND DAMAGE DETECTION .....	 11
2.1 Introduction .....	11
2.2 The Eigenvalue Problem of Discrete Systems .....	11
2.2.1 Undamped Models .....	15
2.2.2 Proportional Damped Models .....	16
2.3 Experimental Modal Analysis .....	16
2.4 Analytical/Experimental Model Dimensions Correlation .....	19
2.4.1 Model Reduction Methods .....	19
2.4.1.1 Static Reduction .....	21
2.4.1.2 IRS Reduction .....	22
2.4.1.3 Dynamic Reduction .....	22

2.4.2	Eigenvector Expansion Methods .....	23
2.4.2.1	Dynamic Expansion .....	23
2.4.2.2	Orthogonal Procrustes Expansion .....	24
2.5	Eigenvector Orthogonalization .....	26
2.5.1	Optimal Weighted Orthogonalization .....	27
2.5.2	Selective Optimal Orthogonalization .....	27
2.6	Load Path Preservation .....	28
3	INVERSE / HYBRID PROBLEM APPROACH FOR FINITE ELEMENT MODEL REFINEMENT .....	31
3.1	Introduction .....	31
3.2	Theoretical Formulation .....	31
3.3	Numerical Illustrations .....	35
3.3	Summary .....	37
4	SYMMETRIC EIGENSTRUCTURES ASSIGNMENT MODEL REFINEMENT ALGORITHM .....	39
4.1	Introduction .....	39
4.2	Problem Formulation .....	39
4.2.1	Standard Eigenstructure Assignment Formulation .....	40
4.2.2	Symmetric Eigenstructure Assignment Formulation .....	42
4.2.3	Best Achievable Eigenvectors .....	44
4.2.4	Selection of $B_0$ : The Subspace Rotation Method .....	46
4.3	Numerical Illustrations .....	47
4.3.1	Damage Detection: Kabe's Problem .....	48
4.3.1.1	Local to Global Mode Change .....	49
4.3.1.2	Consistent Modes .....	52
4.3.2	Model Refinement of a Cantilever Beam: Experimental Study .....	55
4.3.2.1	Modal Test Description .....	55
4.3.2.2	Finite Element Model Description .....	56
4.3.2.3	Application of SEAMRA .....	57
4.4	Discussion of the SEAMRA's Formulation .....	57
4.5	Summary .....	59

5	DAMAGE LOCATION: THE SUBSPACE ROTATION ALGORITHM .....	60
5.1	Introduction .....	60
5.2	The Subspace Rotation Algorithm: The Direct Method .....	60
5.3	The Subspace Rotation Algorithm: The Angle Perturbation Method .....	63
5.4	Practical Issues .....	64
5.4.1	Cumulative Damage Vectors .....	64
5.4.2	Eigenvector Filtering Algorithm .....	65
5.5	Summary .....	66
6	THE MINIMUM RANK PERTURBATION THEORY.....	67
6.1	Background .....	67
6.2	The Minimum Rank Perturbation Theory: Theoretical Background .....	68
6.3	Damage Extent: Undamped Structures .....	72
6.3.1	Damage Extent: Mass Properties .....	73
6.3.2	Damage Extent: Stiffness Properties .....	74
6.3.3	Damage Extent: Mass and Stiffness Properties .....	76
6.3.3.1	Application of the MRPT .....	76
6.3.3.2	Decomposition of Matrix B .....	77
6.4	Damage Extent: Proportionally Damped Structures .....	79
6.4.1	Damage Extent: Stiffness and Damping Properties .....	79
6.4.2	Damage Extent: Mass and Damping Properties .....	82
6.4.3	Damage Extent: Mass and Stiffness Properties .....	84
6.4.4	Damage Extent: Mass, Damping and Stiffness Properties ....	85
6.5	Damage Extent: Nonproportionally Damped Structures .....	87
6.5.1	Damage Extent: Damping and Stiffness Properties .....	89
6.5.2	Damage Extent: Mass and Damping Properties .....	90
6.5.3	Damage Extent: Mass and Stiffness Properties .....	92
6.6	Practical Issues .....	94
6.6.1	The Concept of “Best” Modes .....	95
6.6.2	Application of the Eigenvector Filtering Algorithm .....	97
6.7	Summary .....	97

7	VALIDATION AND ASSESSMENT OF THE SUBSPACE ROTATION ALGORITHM AND THE MINIMUM RANK PERTURBATION THEORY .....	98
7.1	Introduction .....	98
7.2	Kabe's Problem .....	98
7.2.1	Problem Description .....	98
7.2.2	Damage Location .....	100
7.2.3	Damage Extent .....	103
7.3	Damage Detection: Fifty-Bay Two-Dimensional Truss: Undamped FEM .....	105
7.3.1	Problem Description .....	105
7.3.2	Damage Location .....	106
7.3.3	Damage Extent .....	107
7.4	Experimental Study: The NASA 8-Bay Truss .....	112
7.4.1	Problem Description .....	112
7.4.2	Refinement of the Original FEM .....	115
7.4.3	Damage Location .....	118
7.4.4	Damage Extent .....	120
7.4.4.1	The Brute Force Method .....	121
7.4.4.2	The Damage Consistent Method .....	121
7.4.4.3	Application of the Eigenvector Filtering Algorithm .....	122
7.5	Experimental Study: Mass Loaded Cantilevered Beam .....	140
7.5.1	Problem Description .....	140
7.5.2	Analytical and Experimental Models Dimension Correlation .....	141
7.5.3	Refinement of the Original FEM .....	141
7.5.4	Damage Location .....	142
7.5.5	Damage Extent .....	143
7.6	Fifty-Bay Two-Dimensional Truss: Proportionally Damped FEM .....	144
7.6.1	Problem Description .....	144
7.6.2	Damage Location .....	145
7.6.3	Damage Extent .....	146



7.7	Eight-Bay Two-Dimensional Mass-Loaded Cantilevered Truss .....	148
7.7.1	Problem Description .....	148
7.7.2	Proportionally Damped Configuration: Damage of Small Order of Magnitude .....	149
7.7.2.1	Damage Location .....	150
7.7.2.2	Decomposition of Matrix B .....	150
7.7.2.3	Damage Extent .....	152
7.7.3	Undamped Configuration: Damage of Large Order of Magnitude .....	153
7.7.3.1	Noise Free Eigendata .....	153
7.7.3.2	Noisy Eigendata .....	154
7.8	Summary .....	156
8	CONCLUSION AND SUGGESTIONS FOR FUTURE WORK .....	159
	REFERENCES .....	162
	BIOGRAPHICAL SKETCH .....	167



## LIST OF TABLES

<u>Table</u>	<u>Page</u>
3.1 Kabe's Problem: Elemental Stiffness Components .....	38
4.1 Properties of the Cantilever Beam .....	56
4.2 Measured Natural Frequencies and Damping Ratios of the Cantilever Beam .....	56
4.3 Measured Mode Shapes of the Cantilevered Beam .....	56
7.1 Fifty-Bay Truss: Summary of Damage Detection Results using the MRPT .....	111
7.2 Mass Properties of the Eight Bay Truss .....	113
7.3 Strut Properties of the Eight Bay Truss .....	114
7.4 NASA 8-Bay: Truss Damage Case Definitions .....	115
7.5 Comparison of Analytical and Experimental Frequencies .....	116
7.6 Summary of the Filtering Process for Single Member Damage Cases .....	123
7.7 NASA 8-Bay Truss: Summary of the Damage Assessment Results .....	139
7.8 Mass Loaded Cantilevered Beam Properties .....	140
7.9 Analytical and Experimental Frequencies of the "Healthy" Structure .....	142
7.10 50-Bay 2-Dimensional Truss: Summary of the Percentage Error with Respect to the Exact Damage .....	147
7.11 Problem 7.7: Percentage Error of Damage Estimate with Respect to Exact Damage .....	156

## LIST OF FIGURES

<u>Figure</u>	<u>Page</u>
1.1 Overview of Finite Element Model Refinement .....	2
1.2 Overview of FEM Model Refinement Process Used for Damage Assessment .....	7
2.1 Components of a Vibration Measurement System for Modal Analysis .....	17
2.2 A simple Experimental Modal Analysis Setup .....	18
2.3 Flow Chart of the Iterative Load Preservation Path Algorithm .....	29
3.1 Kabe's Problem: Analytical Test Structure .....	36
4.1 Best Achievable Eigenvector Projection .....	45
4.2 Rotation of the Achievable Subspace .....	47
4.3 Kabe's Problem .....	48
4.4 Results for Kabe's Problem using the 1st Mode, Full Eigenvector .....	50
4.5 Results for Kabe's Problem Modes 1, 2, 3 and Eigenvectors Components 1, 2, 3 .....	51
4.6 Results for Kabe's Problem using Load Path Preservation, Modes 1, 2, 3 and Eigenvectors Components 1, 2, 3 .....	52
4.7 Results for Kabe's Problem using the 1st Mode, Full Eigenvector .....	53
4.8 Results for Kabe's Problem Modes 1, 2, 3 and Eigenvectors Components 1, 2, 6 .....	54
4.9 Experimental Cantilever Beam .....	55
4.10 Experimental and Analytical Frequency Response Function of the Cantilever Beam .....	58

7.1	Kabe's Problem .....	99
7.2	Kabe's Problem: Damage Location Results using the Subspace Rotation Direct Method with the Eigendata of the 1st Mode .....	101
7.3	Kabe's Problem: Damage Location Results using the Angle Perturbation Method with the Eigendata of the 1st Mode .....	101
7.4	Kabe's Problem: Damage Location Results using Lin's Algorithm with the Eigendata of the 1st Mode .....	102
7.5	Kabe's Problem: Damage Location Results using the Angle Perturbation Method with the Eigendata of the 1st and 2nd Modes .....	102
7.6	Kabe's Problem: Damage Location Results using Lin's Algorithm with the Eigendata of the 1st and 2nd Modes .....	103
7.7	Kabe's Problem: Damage Extent Results using the MRPT with the Eigendata of Mode 2 .....	104
7.8	Kabe's Problem: Damage Extent Results using Baruch's Method .....	105
7.9	Fifty-Bay Two-Dimensional Truss .....	106
7.10	Fifty-Bay Truss: Damage Location Results using the Subspace Rotation Algorithm with the Eigendata of the First Ten Modes .....	107
7.11	Fifty-Bay Truss: Damage Extent Results using the MRPT with the Eigendata of Modes 8 and 9 .....	109
7.12	Fifty-Bay Truss: Damage Extent Results using the MRPT with the Eigendata of the First Ten Modes .....	110
7.13	Fifty-Bay Truss: Damage Extent Results using Baruch's Algorithm .....	110
7.14	The NASA Eight-Bay Hybrid-Scaled Truss: Damage Cases .....	112
7.15	The NASA 8-Bay Truss: Lacing Pattern .....	113
7.16	NASA 8-Bay Truss: Typical Frequency Response Comparison .....	117
7.17	NASA 8-Bay Truss: Perturbation to the Original Stiffness Matrix that Resulted From the Refinement Process .....	118
7.18	NASA 8-Bay Truss: Cumulative Damage Vector Associated with Case F .....	124
7.19	NASA 8-Bay Truss: Damage Assessment of Case A .....	125
7.20	NASA 8-Bay Truss: Damage Assessment of Case C .....	126

7.21	NASA 8-Bay Truss: Damage Assessment of Case D .....	127
7.22	NASA 8-Bay Truss: Damage Assessment of Case E .....	128
7.23	NASA 8-Bay Truss: Damage Assessment of Case G .....	129
7.24	NASA 8-Bay Truss: Damage Assessment of Case H .....	130
7.25	NASA 8-Bay Truss: Damage Assessment of Case I .....	131
7.26	NASA 8-Bay Truss: Damage Assessment of Case J .....	132
7.27	NASA 8-Bay Truss: Damage Assessment of Case K .....	133
7.28	NASA 8-Bay Truss: Damage Assessment of Case L .....	134
7.29	NASA 8-Bay Truss: Damage Assessment of Case M .....	135
7.30	NASA 8-Bay Truss: Damage Assessment of Case N .....	136
7.31	NASA 8-Bay Truss: Damage Assessment of Case O .....	137
7.32	NASA 8-Bay Truss: Damage Assessment of Case P .....	138
7.33	The Mass Loaded Cantilevered Beam .....	140
7.34	Mass Loaded Cantilevered Beam: Damage Assessment .....	143
7.35	50-Bay 2-Dimensional Truss .....	145
7.36	50-Bay 2-Dimensional Truss: Damage Location .....	146
7.37	50-Bay 2-Dimensional Truss: Damage Extent .....	148
7.38	The Eight-Bay Two-Dimensional Mass-Loaded Cantilevered Truss .....	149
7.39	Problem 7.7: Cumulative Damage Location Vector: First Four Modes .....	150
7.40	Problem 7.7: Cumulative Vectors Associated with the Exact and Computed $B_m$ , $B_d$ , $B_k$ : First Three Modes .....	151
7.41	Problem 7.7: Exact and Computed $\Delta M_d$ , $\Delta D_d$ , $\Delta K_d$ .....	152
7.42	Problem 7.7: Cumulative Vector Associated with $B$ , $B_m$ , $B_d$ , $B_k$ $B$ Computed using Modes 1-4 $B_m$ , $B_d$ , $B_k$ Computed using Modes 3,4 & 5 .....	155
7.43	Problem 7.7: Exact and Computed $\Delta M_d$ , $\Delta D_d$ , $\Delta K_d$ .....	157

Abstract of Dissertation Presented to the Graduate School  
of the University of Florida in Partial Fulfillment of the  
Requirement for the Degree of Doctor of Philosophy

**STRUCTURAL DAMAGE ASSESSMENT AND FINITE ELEMENT  
MODEL REFINEMENT USING MEASURED MODAL DATA**

By

Mohamed Kaouk

August 1993

Chairperson: Dr. David C. Zimmerman

Major Department: Aerospace Engineering, Mechanics and Engineering Science

This study investigates the problems of model refinement and structural damage assessment. The essence of the model refinement problem is to adjust finite element models (FEMs) of structures with the intent of producing a correlation between experimental and analytical modal properties. Recently, the framework of model refinement has been adopted to determine the location and extent of structural damage. Damage will result in changes to the modal properties of the healthy structure. A further refinement of an accurate FEM of the structure using damaged modal parameters is expected to generate adjustments to the FEM at locations associated with damage. Analysis of these adjustments can then be used to assess damage. In this investigation, four algorithms relevant to the subjects of model refinement and damage detection are presented. The development of a model refinement algorithm with its basis in inverse theory is first presented. The algorithm, termed the inverse/hybrid approach, is illustrated in a comparative computer simulated study. Next, an existing eigenstructure assignment model refinement algorithm is improved to better approach the damage assessment problem. The enhanced algorithm is evaluated and compared to other techniques using simulated and experimental data. The algorithm is shown to perform well

in assessing damage and refining FEMs. A damage location algorithm that bypasses the general framework of model refinement is discussed. The damage location algorithm, termed the subspace rotation, is similar to the modal force error criteria proposed by several researchers. Greater insight to the modal force error criteria, along with a new viewpoint that reduces the effects of measurement noise, is discussed. Furthermore, an efficient damage extent algorithm based on a minimum rank perturbation theory (MRPT) is developed. The formulation of the MRPT is consistent with the effect of most structural damage on FEMs. The characteristics of the subspace rotation algorithm and the minimum rank perturbation theory are illustrated using simulated and experimental testbeds. The decomposition of the damage assessment problem into location and extent subproblems is shown to be advantageous from both for computational efficiency and for engineering insight.



## CHAPTER 1 INTRODUCTION

### 1.1 Finite Element Model Refinement

#### 1.1.1 Overview

An important aspect in the design process of a structure is the evaluation of its performance under expected dynamic loading conditions. Dynamic performance can be analyzed by using either analytical or experimental techniques. Experimental analyses are generally very costly, time consuming and can encounter technical difficulties. One example of a commonly encountered technical barrier is the ground base reproduction of a weightless environment for the testing of space structures. This shortcoming and the advent of computers have sparked a growing interest in the uses of analytical techniques. This type of analysis utilizes a mathematical model of the actual structure for computer simulated evaluation of structural performance. Presently, most analytical models used in industry are finite element models generated by using Finite Element Methods. The accuracy of a finite element model (FEM) can be improved to some extent by increasing the number of degrees of freedom (DOFs) included in the model. However, accuracy of the FEM may still be lacking due to uncertainties in material properties, geometric layout and fabrication induced errors. Thus, it is essential to “validate” these FEMs prior to their acceptance as a basis for analysis. One way to validate them is to compare their modal properties (eigenvalues/eigenvectors) with the measured modal parameters of the actual structure as obtained from experimental modal analysis (EMA). A FEM is acceptable when these two sets of modal properties are in agreement. Unfortunately, this agreement rarely occurs. As a result, the



FEM must be adjusted to produce a correlation of analytical and experimental modal properties. An overview of this procedure is schematically illustrated in Figure 1.1 (Zimmerman and Smith, 1992).

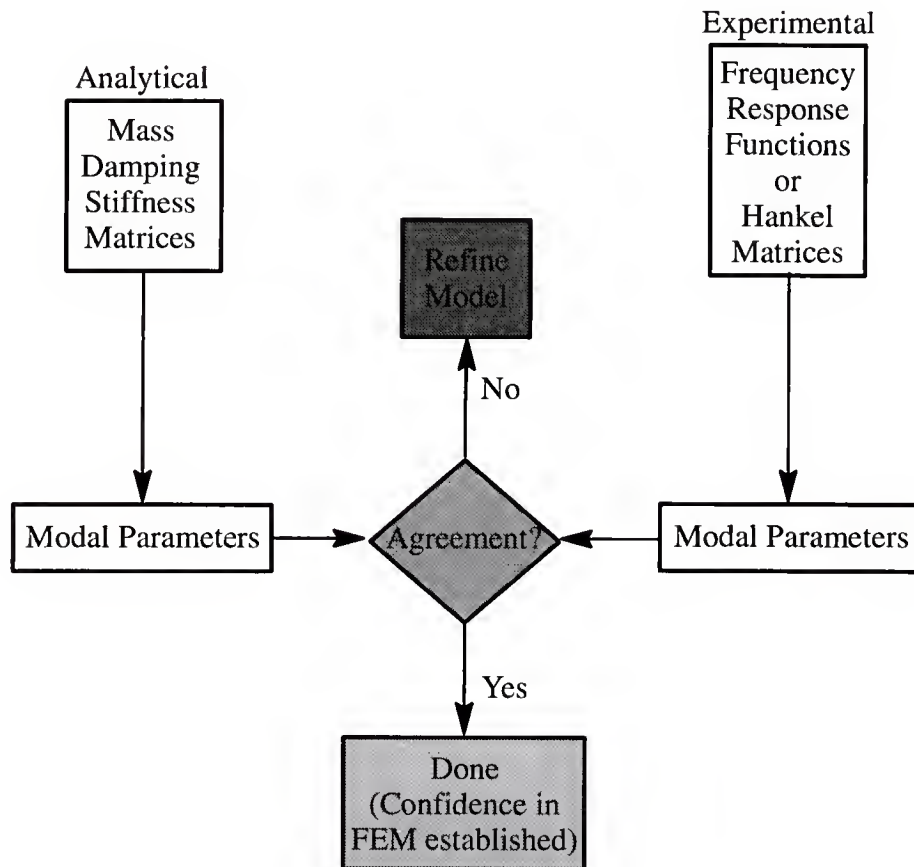


Figure 1.1 Overview of Finite Element Model Refinement (Zimmerman and Smith, 1992)

In the past, the process of adjusting FEMs was performed on an ad-hoc basis aided by engineering experience. This practice was naturally time consuming and in most cases inadequate for large-order, complex FEMs that are typically needed for accurate dynamic modelling. In the past years, growing interest has been focused on developing systematic procedures to produce correlated FEMs. These efforts have resulted in the development of a large number of algorithms. Finite element model adjustment procedures have been

commonly referred to in the literature as, FEM refinement, FEM adjustment, FEM correction, FEM correlation, and FEM identification.

### 1.1.2 Literature Survey

Comprehensive literature surveys covering a large portion of the work that addresses the model refinement problem can be found in the book chapter by Zimmerman and Smith (1992), and in the papers by Ibrahim and Saafan (1987) and Heylen and Saas (1987). For completeness and to properly underline the objective of the current study, it is appropriate to include a brief survey of the development made in this area.

The concept of using experimental modal data in analytical studies was initiated by an early work presented by Rodden (1967). In his work, Rodden explored the possibilities of generating mass and stiffness property matrices by using experimentally measured modal data. The experimentally generated mass and stiffness matrices were nonsymmetric. Brock (1968) improved the work of Rodden by proposing a strategy to insure symmetry of property matrices.

The essence of the model refinement concept, as adopted by most researchers, is to modify the finite element model (FEM) of systems with the intention of producing a correlation of test and analytical modal parameters. In general, this task has been approached through two different philosophies. The first amounts to modifying globally the finite element property matrices of the system. This approach is commonly referred to as the property matrix update. The alternative approach is to individually correct parameters of each element of the finite element model. This will be addressed here as the physical parameter update.

Property matrix update algorithms can be classified into two subclasses of methodologies: optimal-matrix update and control-based eigenstructure assignment techniques.

The basic philosophy of the optimal-matrix update is to minimize the correction to the FEM property matrices to accomplish the analytical/test modal correlation. The pioneering work in this area can be credited to Baruch and Bar Itzhack (1978). In their formulation, by assuming that the mass matrix is correct, the refinement of the stiffness matrix of an undamped FEM is cast as a constrained minimization problem. The objective of their formulation is to determine the minimal Frobenius-norm symmetric stiffness adjustment that satisfies the eigenvalue problem in terms of the experimentally measured eigenvalues and eigenvectors. A computationally efficient closed form solution was developed for the updated stiffness matrix. Berman and Nagy (1983) extended the Baruch and Bar Itzhack approach to the refinement of both the mass and stiffness matrices. This same methodology was further extended by Fuh et al. (1984) to update the mass, damping and stiffness matrices of damped FEMs. Fuh and his colleagues used cross-orthogonality relationships to correct the mass and damping matrices and a constrained minimization problem similar to the one proposed by Baruch and Bar Itzhack to determine the refined stiffness matrix. The problem of adjusting the mass, damping and stiffness matrices was also attempted by Hanagud et al. (1984). In their approach, all three property matrices of a nonproportionally damped FEM are incorporated in the constrained minimization problem.

The previously stated algorithms do not preserve the load path (sparsity pattern) of the original analytical property matrices. Kabe (1985) proposed a reformulation of the Baruch and Bar Itzhack algorithm that constrains the updated stiffness matrix to preserve the load path of the original stiffness matrix. In addition, in his reformulation, he adopted a percent weighting on the stiffness changes instead of mass matrix weighting as used in the Baruch and Bar Itzhack algorithm. Kammer (1987) proposed an alternative solution approach to the problem defined by Kabe that uses projection matrix theory and the Moore–Penrose generalized inverse. The algorithms formulated by Kabe and Kammer involve an excessive amount of computational effort. Another alternative and more efficient formulation of the

Kabe problem that utilized a generalization of Marwill-Toint updates was developed by Smith and Beattie (1991).

The other subclass of property matrix updates is based on the general framework of control-based eigenstructure assignment algorithms. The essence of this approach is to determine pseudo-controllers that would assign the experimentally measured modal parameters to the original analytical FEM. The pseudo-controllers are then translated into matrix adjustment to the original property matrices. This approach was initially formulated by Inman and Minas (1990) to adjust the damping and stiffness matrices of the original FEM. In their formulation, the symmetry of the adjusted property matrices was enforced through an iterative process that involves a numerical nonlinear optimization process. Zimmerman and Widengren (1989, 1990) proposed a formulation that replaces the iterative process of Inman and Minas with a generalized algebraic Riccati equation. Further details about this approach are treated in Chapter 4.

The alternative philosophy to the model refinement problem is the physical parameter update. The basic idea of this alternative approach consists of adjusting some or all structural physical parameters to produce test/analysis modal correlation. Structural parameters are design variables such as material densities, modulus of elasticity, cross-sectional areas, element lengths and others. This type of procedure results in corrected FEMs that are consistent with the framework of the original FEM.

Most methodologies that have adopted this philosophy have used the sensitivity derivatives of the system eigenvalues and/or eigenvectors with respect to the structural parameters. Generally, the refinement process amounts to solving for the corrected structural parameters through an iterative optimization problem directed by the sensitivity derivatives. Some notable work in this area was accomplished by Collins et al. (1974), Chen and Garba (1980), Adelman and Haftka (1986), Creamer and Hendricks (1987), Flanigan (1991), Martinez et al. (1991), to name only a few. In these studies, different sensitivity formulations and iterative optimization strategies are proposed. A direct approach that



bypasses the use of closed-form sensitivity derivatives was presented in the papers of Hajela and Soeiro (1990) and Soeiro (1990).

White and Maytum (1976) set forth another alternative methodology that can be classified in the physical parameter update group. In their approach, adjustments to the stiffness matrix are viewed as a collection of known submatrices, elements or group of elements. Each submatrix is multiplied by an unknown scaling factor. Correction of the original stiffness matrix amounts to determining the scaling factors that would improve the correlation of analytical and experimental modal properties. The scaling factors can be physically viewed as functions of the stiffness structural parameters. A large underdetermined system of equations in terms of the scaling factor is generated. The scaling factors are then computed by using a pseudo-inverse. An improvement to the White and Maytum approach is presented in the paper by Lim (1990).

## 1.2 Structural Damage Assessment

Structures, in general, are prone to structural damage during their service lives, that could affect their overall performance and could result in catastrophic failures. This is of critical concern when expensive systems and/or human lives are at stake. On this basis, it is highly desirable to monitor the structural health of systems such as airplanes, space systems, bridges, buildings, oil platforms, among others, to prevent such catastrophic events. Currently, the most common structural health monitoring methods involve visual inspections supplemented with X-rays, acoustic emission, magnetic resonance and ultrasonic testing. These approaches can be time consuming, costly and difficult to perform on inaccessible structural components. Additionally, none of these approaches provide a quantitative assessment of the magnitude of the damage.

In response to these shortcomings, structural health monitoring approaches based on the framework of existing model refinement techniques have been recently proposed by several researchers (Smith and Hendricks, 1987; Chen and Garba, 1988; Ricles and

Kosmatka, 1992; Zimmerman and Kaouk, 1992a,b; Kaouk and Zimmerman, 1993a,b). These techniques utilize the vibration signature of the pre- and post- damaged structure, in conjunction with an analytical model of the original structure, to assess both the location and extent of the structural damage. The pre-damage modal parameters are used to correct (refine) the original finite element model (FEM) to determine an “accurate” reference baseline. Once damaged, the post-damage modal properties of the structure are used to further “refine” the refined analytical model. This results in perturbations to the refined analytical model. Analysis of the perturbations could indicate the damage location and extent. An overview of the application of model refinement algorithms in assessing structural damage is summarized in Figure 1.2.

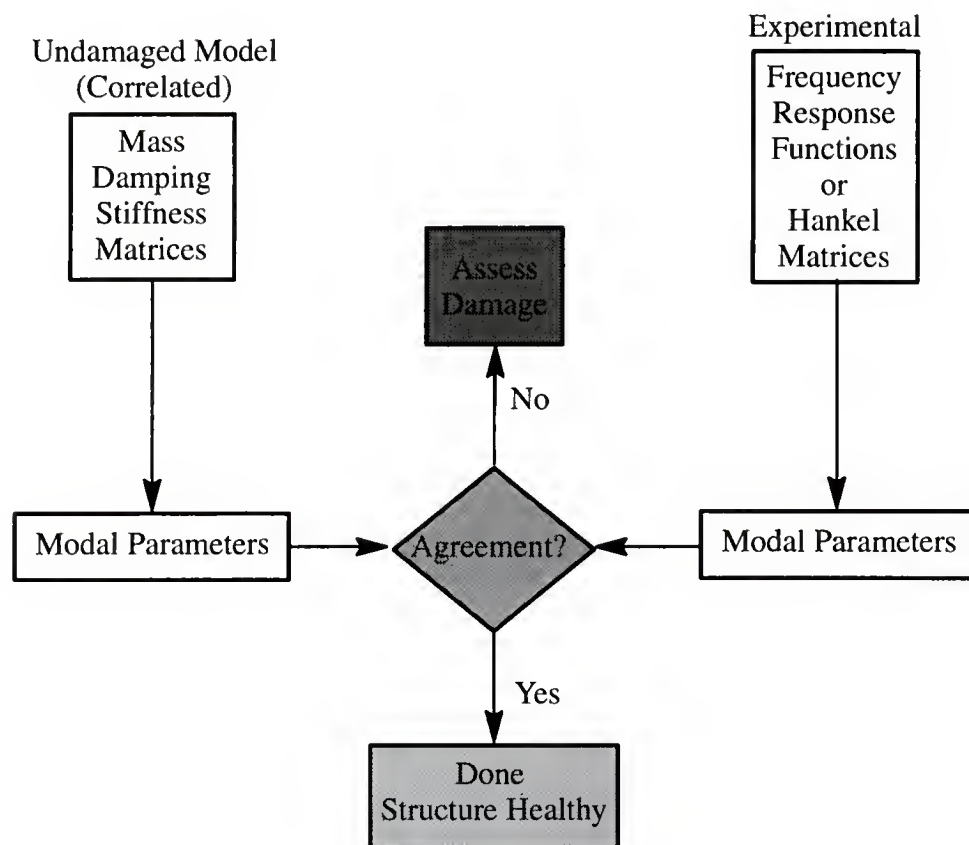


Figure 1.2 Overview of Finite Element Model Refinement Process Used for Damage Assessment

Notable exceptions to the direct use of FEM refinement algorithms to the damage detection problem are the work of Lin (1990), Ojalvo and Pilon (1988), and Gysin (1990). In the work of Lin, a flexibility matrix is determined using experimental data. This matrix is then multiplied by the original stiffness matrix, with those rows and/or columns that differ significantly from a row and/or column of the identity matrix indicating which degrees of freedom have been most affected by the damage. It is then assumed that damage has occurred in structural elements connecting those degrees of freedom. An overview of the work by Ojalvo and Pilon (1988), and Gysin (1990) is given in Chapter 5.

Although the problems of damage assessment and model refinement are related to one another, they have quite different characteristics. In essence, the model refinement concept is based on the philosophy of the minimum change to the original FEM. Naturally, this minimum change constraint has a tendency of smearing the changes throughout the entire FEM. This aspect is inconsistent with the effects of structural damage on FEMs which are usually localized perturbations of possibly large magnitude. In fact, structural damage often occurs at discrete locations and only affects a few elements of the FEM.

### 1.3 Objective of the Present Study

The present study investigates the development of new and promising model refinement and damage detection methodologies. Although considerable research has been done in these areas, no methodology has been fully successful in dealing with the refinement or the damage detection problem of “real life” systems. The main objective of this investigation is to formulate efficient model refinement algorithms that are consistent with the effect of structural damage.

In chapter 2, practical concepts and issues related to the general areas of model refinement are presented. First, the concept of the eigenvalue problem of discrete structural models is reviewed with emphasis on the associated cross-orthogonality conditions. A brief discussion of modal analysis follows. The problem associated with incomplete eigenvector



measurements is then investigated and already existing techniques to deal with this problem are presented. Furthermore, eigenvector orthogonalization techniques useful to a large number of model refinement algorithms are reported. Finally, an iterative approach to the problem of load path preservation encountered in a large number of property matrix update algorithms is discussed.

In chapter 3, the author proposes and formulates a new model refinement algorithm. The newly developed algorithm, named the inverse/hybrid method, is naturally based on the inverse problem. The model type under consideration is proportionally damped and the inaccuracies of the analytical model is assumed to be due to errors in the modelling of the damping and stiffness properties. A complete hybrid set of modal data is generated by approximating the unmeasured modal information by the corresponding analytical modes. Symmetry of the corrected stiffness and damping matrices is enforced by mass orthogonalization the complete hybrid eigenvector matrix. An orthogonalization procedure that assigns more confidence on the measured eigenvectors is proposed. A comparative study of the inverse/hybrid method and the algorithm proposed by Baruch and Bar Itzhack (1978) shows that both algorithms give similar results. However, it is shown that the inverse/hybrid approach is less computationally efficient.

Chapter 4 proposes improvements to the symmetric eigenstructure assignment model refinement algorithm (SEAMRA) formulated by Zimmerman and Widengren (1989). The author develops a technique to enhance eigenvector assignability. The technique, termed the subspace rotation method, is based on rotating the achievable eigenvector subspaces into the experimental eigenvectors. The subspace rotation method results in both a decrease in the computational burden and an increase in the accuracy of the assigned eigenvector. The enhanced SEAMRA is then evaluated and compared to other algorithms using both computer simulated and experimental testbeds. It is shown that the enhanced algorithm is suitable for damage detection applications.

In Chapter 5, an efficient damage location algorithm that utilizes modal data information but bypasses the general framework of the model refinement problem is presented. This location algorithm is an outgrowth of the subspace rotation method used to enhance eigenvector assignability of the SEAMRA. The proposed location algorithm is similar to the modal force error criteria presented by several researchers (Ojalvo and Pilon, 1988; Gysin, 1990). Further interpretation of the algorithm operation is given. Additionally, the author proposes and formulates a new viewpoint that reduces the effect of measurement noise for certain types of structures. Based on this formulation, an eigenvector filtering algorithm is also developed.

Chapter 6 presents the formulation of computationally attractive damage extent algorithms that are based on a minimum rank perturbation theory (MRPT) developed by the author. The formulation of the MRPT is consistent with the effect of many classes of structural damage on FEMs. Several MRPT based algorithms are formulated to accommodate structures with undamped, proportionally damped, and nonproportionally damped FEMs. For each type of FEM, several damage scenarios are considered. Discussions of the characteristics and properties of the developed algorithms are presented along with practical issues that can be used to improve their performance.

In Chapter 7, the algorithms developed in Chapters 5 and 6 are demonstrated and evaluated using both computer simulated and actual experimental data. The main objective of these example problems is to illustrate the potential of these algorithms in assessing structural damage. In all examples, the location of damage is first determined by using the algorithm presented in Chapter 5. An MRPT based algorithm is then utilized to assess the extent of the damage. Several key points made throughout the formulation in Chapters 5 and 6 are emphasized. In particular, it is shown that the damage extent calculations can be greatly enhanced by making use of the damage location algorithm.

In Chapter 8, summaries and conclusions of the issues discussed in this study are presented along with some suggestions for future work.

## CHAPTER 2

### MATHEMATICAL PRELIMINARIES AND PRACTICAL ISSUES RELATED TO THE PROBLEMS OF MODEL REFINEMENT AND DAMAGE DETECTION

#### 2.1 Introduction

In this chapter, general mathematical preliminaries and practical issues relevant to the areas of model refinement and damage detection are discussed. In Section 2.2, an overview of the general eigenvalue problem for discrete models is given. Further, the concept of modal analysis is introduced in Section 2.3. Section 2.4 deals with the concept of incomplete degrees of freedom measurement. Two alternative approaches are discussed as possible solutions to the incomplete measurement problem. Two eigenvector orthogonalization techniques are discussed in Section 2.5. Finally, in Section 2.6, an algorithm to preserve sparsity in updated property matrices is presented. The concepts discussed in this chapter will be frequently referred to in the course of the forthcoming chapters.

#### 2.2 The Eigenvalue Problem of Discrete Systems

In practice, most engineering structures are continuous systems with spatially distributed material properties. The vibration motion of these structures in terms of their distributed properties is usually governed by one or several partial differential equations. With complex systems, both the development and the analysis of partial differential equations of motion are tedious and in many cases impossible. These shortcomings and the advent of digital computers have motivated the development of approximate modelling of continuous systems in order to simplify the equations of motion. The general idea behind these approximations is to represent the exact distributed model of a system by a discrete one.

This concept is known as spatial discretization which eliminates the continuous spatial dependence of the distributed properties. The discrete model is of finite order and is described by a finite number of variables known as degrees of freedom (DOFs). The number of DOFs used in the discrete model depends on the desired accuracy in representing the continuous model. Commonly, the vibration motion of systems in terms of their discrete models is described by a set of simultaneous ordinary differential equations that are usually simpler to develop and analyze than the partial differential equations of the continuous system. One of the most commonly used approximate discrete modelling techniques is the finite element method. The model generated by a finite element method is called a finite element model (FEM). More elaborate discussions of the concepts of continuous and discrete models as well as finite element methods are covered in detail in the books of Meirovitch (1986, 1980), Inman (1989), and Hughes (1987).

Commonly, the free vibration motion of a structure in terms of an  $n^{\text{th}}$  order discrete model is represented by the following set of simultaneous ordinary differential equations

$$M\ddot{\underline{w}}(t) + D\dot{\underline{w}}(t) + K\underline{w}(t) = \underline{0} \quad (2.2.1)$$

where  $M$ ,  $D$  and  $K$  are termed, respectively, the mass, damping and stiffness matrices. They are models of the mass, damping and stiffness properties of the structure. Since the system model is order  $n$ , these matrices are of dimension  $n \times n$  and are generally real. The variable  $\underline{w}(t)$  represents the  $n$  displacements of the  $n$ -DOF model of the structure. The overdots represent differentiation with respect to time. The mass matrix,  $M$ , is always symmetric positive definite. The stiffness ( $K$ ) and damping ( $D$ ) matrices of nongyroscopic and noncirculatory systems are symmetric. In general, the modelling of the mass and stiffness properties of the structure is simpler and more accurate than the modelling of the damping properties. In the forthcoming discussion, it is assumed that the system under consideration is nongyroscopic and noncirculatory. The standard solution to Eq. (2.2.1) is of the form

$$\underline{w}(t) = \underline{v}e^{\lambda t} \quad (2.2.2)$$



where  $\underline{v}$  is a constant  $n \times 1$  vector and  $\lambda$  is a constant scalar. Substituting Eq. (2.2.2) into Eq. (2.2.1) and dividing the resultant equation by  $e^{\lambda t}$  yields the condition

$$M \underline{v} \lambda^2 + D \underline{v} \lambda + K \underline{v} = \underline{0} \quad (2.2.3)$$

There are  $n$  sets of nontrivial complex conjugate solutions  $(\lambda_i, \underline{v}_i)$  to Eq. (2.2.3). Note that since the property matrices  $(M, D, K)$  are real, if  $(\lambda_i, \underline{v}_i)$  is a solution set to Eq. (2.2.3), the complex conjugate of that set is also a solution. The problem of solving for these solutions is commonly known as the eigenvalue problem and is sometimes referred to as the characteristic value problem. The scalar  $\lambda_i$  and the vector  $\underline{v}_i$  are known, respectively, as the eigenvalue and eigenvector of the  $i^{\text{th}}$  mode of vibration of the structure. For a general damped system, eigenvalues and eigenvectors are both complex. Note that Eq. (2.2.3) can be easily rearranged in the more general mathematical eigenvalue problem format as

$$\begin{bmatrix} 0 & I_{n \times n} \\ -M^{-1}K & -M^{-1}D \end{bmatrix} \begin{bmatrix} \underline{v}_i \\ \underline{v}_i \lambda_i \end{bmatrix} = \lambda_i \begin{bmatrix} \underline{v}_i \\ \underline{v}_i \lambda_i \end{bmatrix} \quad (2.2.4)$$

where  $I_{n \times n}$  is the  $n \times n$  identity matrix. Equation (2.2.4) is called a state space representation of Eq. (2.2.3).

The eigenvalue and eigenvector can be related to some physical characteristic properties of structures. For that matter, the  $i^{\text{th}}$  eigenvalue is written as

$$\lambda_i = -\zeta_i \omega_i + j \omega_i \sqrt{1 - \zeta_i^2} \quad (2.2.5)$$

where  $j = \sqrt{-1}$ . Note that in writing this equation it is assumed that the system is underdamped. The real scalar  $\omega_i$  and  $\zeta_i$  are the natural frequency and damping ratio (or damping factor), respectively, of the  $i^{\text{th}}$  mode of the structure. The eigenvector  $\underline{v}_i$  indicates the “shape” of vibration of the  $i^{\text{th}}$  mode of the structure. The sets of frequencies, damping ratios and mode shapes are sometimes referred to as modal parameters.

The symmetric nature of the property matrices  $(M, D, K)$  constrains the eigenvectors to satisfy some cross-orthogonality relationships. For the purpose of discussing these

cross-orthogonality relationships, consider the following alternative state space representation of the eigenvalue problem in Eq. (2.2.3)

$$\begin{bmatrix} M & 0 \\ 0 & -K \end{bmatrix} \begin{bmatrix} V\Lambda & \overline{V\Lambda} \\ V & \overline{V} \end{bmatrix} \begin{bmatrix} \Lambda & 0 \\ 0 & \overline{\Lambda} \end{bmatrix} + \begin{bmatrix} D & K \\ K & 0 \end{bmatrix} \begin{bmatrix} V\Lambda & \overline{V\Lambda} \\ V & \overline{V} \end{bmatrix} = \begin{bmatrix} 0 \\ 0 \end{bmatrix} \quad (2.2.6)$$

$$\text{where } V = [ \underline{v}_1, \underline{v}_2, \dots, \underline{v}_n ]$$

$$\Lambda = \text{diag}(\lambda_1, \lambda_2, \dots, \lambda_n)$$

where the overbar denotes the matrix complex conjugate operator. Based on this particular representation and the fact that the state matrices of Eq. (2.2.6) are symmetric, by proper normalization of the eigenvectors, the cross-orthogonality relationship associated with the system are given by

$$\begin{bmatrix} V\Lambda & \overline{V\Lambda} \\ V & \overline{V} \end{bmatrix}^T \begin{bmatrix} M & 0 \\ 0 & -K \end{bmatrix} \begin{bmatrix} V\Lambda & \overline{V\Lambda} \\ V & \overline{V} \end{bmatrix} = I_{2n \times 2n} \quad (2.2.7)$$

$$\begin{bmatrix} V\Lambda & \overline{V\Lambda} \\ V & \overline{V} \end{bmatrix}^T \begin{bmatrix} D & K \\ K & 0 \end{bmatrix} \begin{bmatrix} V\Lambda & \overline{V\Lambda} \\ V & \overline{V} \end{bmatrix} = - \begin{bmatrix} \Lambda & 0 \\ 0 & \overline{\Lambda} \end{bmatrix} \quad (2.2.8)$$

Equations (2.2.7) and (2.2.8), respectively, clearly imply the following relations

$$\begin{bmatrix} V\Lambda \\ V \end{bmatrix}^* \begin{bmatrix} M & 0 \\ 0 & -K \end{bmatrix} \begin{bmatrix} V\Lambda \\ V \end{bmatrix} = \begin{bmatrix} 0 \\ 0 \end{bmatrix} \quad (2.2.9)$$

$$\begin{bmatrix} V\Lambda \\ V \end{bmatrix}^* \begin{bmatrix} D & K \\ K & 0 \end{bmatrix} \begin{bmatrix} V\Lambda \\ V \end{bmatrix} = \begin{bmatrix} 0 \\ 0 \end{bmatrix} \quad (2.2.10)$$

where  $[ \ ]^*$  denotes the complex conjugate transpose operator ( $[ \ ]^* = [\overline{\ ]}^T$ ). Note that, contrary to Eqs. (2.2.7–8), no particular normalization of the eigenvector is needed in order for Eqs. (2.2.9–10) to be satisfied.

Another state space representation of Eq. (2.2.3) is given by

$$\begin{bmatrix} 0 & M \\ M & D \end{bmatrix} \begin{bmatrix} V\Lambda & \overline{V\Lambda} \\ V & \overline{V} \end{bmatrix} \begin{bmatrix} \Lambda & 0 \\ 0 & \overline{\Lambda} \end{bmatrix} + \begin{bmatrix} -M & 0 \\ 0 & K \end{bmatrix} \begin{bmatrix} V\Lambda & \overline{V\Lambda} \\ V & \overline{V} \end{bmatrix} = \begin{bmatrix} 0 \\ 0 \end{bmatrix} \quad (2.2.11)$$

Based on the same argument discussed earlier, the cross-orthogonality conditions that arise from this representation are

$$\begin{bmatrix} V\Lambda & \overline{V\Lambda} \\ V & \overline{V} \end{bmatrix}^T \begin{bmatrix} 0 & M \\ M & D \end{bmatrix} \begin{bmatrix} V\Lambda & \overline{V\Lambda} \\ V & \overline{V} \end{bmatrix} = I_{2n \times 2n} \quad (2.2.12)$$

$$\begin{bmatrix} V\Lambda & \overline{V\Lambda} \\ V & \overline{V} \end{bmatrix}^T \begin{bmatrix} -M & 0 \\ 0 & K \end{bmatrix} \begin{bmatrix} V\Lambda & \overline{V\Lambda} \\ V & \overline{V} \end{bmatrix} = - \begin{bmatrix} \Lambda & 0 \\ 0 & \overline{\Lambda} \end{bmatrix} \quad (2.2.13)$$

Again, the following two relationships follow,

$$\begin{bmatrix} V\Lambda \\ V \end{bmatrix}^* \begin{bmatrix} 0 & M \\ M & D \end{bmatrix} \begin{bmatrix} V\Lambda \\ V \end{bmatrix} = \begin{bmatrix} 0 \\ 0 \end{bmatrix} \quad (2.2.14)$$

$$\begin{bmatrix} V\Lambda \\ V \end{bmatrix}^* \begin{bmatrix} -M & 0 \\ 0 & K \end{bmatrix} \begin{bmatrix} V\Lambda \\ V \end{bmatrix} = \begin{bmatrix} 0 \\ 0 \end{bmatrix} \quad (2.2.15)$$

### 2.2.1 Undamped Models

In the modelling of structures, it is often assumed that the damping is negligible and hence is set to zero. For these type of system models, the eigenvalue problem in matrix form is given by

$$MV\Lambda^2 + KV = [0] \quad (2.2.16)$$

The matrices  $V$  and  $\Lambda$  are as defined earlier. For undamped systems, the eigenvalues  $\lambda_i$  are pure imaginary and the eigenvectors  $\underline{v}_i$  are real. Note that the eigenvalues are related to the system natural frequency by

$$\lambda_i^2 = -\omega_i^2 \quad (2.2.17)$$

Furthermore, by proper normalization of the eigenvectors, the cross-orthogonality relations associated with this type of systems are



$$V^T M V = I_{n \times n} \quad (2.2.18)$$

$$V^T K V = \text{diag}(\omega_1^2, \omega_2^2, \dots, \omega_n^2) \quad (2.2.19)$$

### 2.2.2 Proportionally Damped Models

When the damping of the structure is accounted for, it is sometimes modelled to be proportional,

$$D = \alpha M + \beta K \quad (2.2.20)$$

where  $\alpha$  and  $\beta$  are real scalars. The eigenvectors of a proportionally damped system are the same as the eigenvectors associated with the corresponding undamped system. The cross-orthogonality relationships associated with proportionally damped models are

$$V^T M V = I_{n \times n} \quad (2.2.21)$$

$$V^T D V = \text{diag}(2\zeta_1 \omega_1, 2\zeta_2 \omega_2, \dots, 2\zeta_n \omega_n) \quad (2.2.22)$$

$$V^T K V = \text{diag}(\omega_1^2, \omega_2^2, \dots, \omega_n^2) \quad (2.2.23)$$

where all variables have the same definitions as in the previous discussion.

A more detailed development of the eigenvalue problem can be found in the books of Meirovitch (1986, 1980) and Inman (1989).

## 2.3 Experimental Modal Analysis

The vibration characteristics of structures can also be measured experimentally. Recall that the structural vibration characteristics are given by natural frequencies, damping ratios and mode shapes (eigenvectors). The process of measuring the modal parameters is known as modal testing or experimental modal analysis. An introductory treatment of the concept of experimental modal analysis can be found in the book of Inman (1989); a more rigorous coverage is treated in the book of Ewins (1986).

The hardware components needed in a modal analysis experiment are identified in Figure 2.1 (Inman, 1989). A schematic of a simple modal vibration measurement test setup

is shown in Figure 2.2. Brief descriptions of some of the components and their functions are given below.

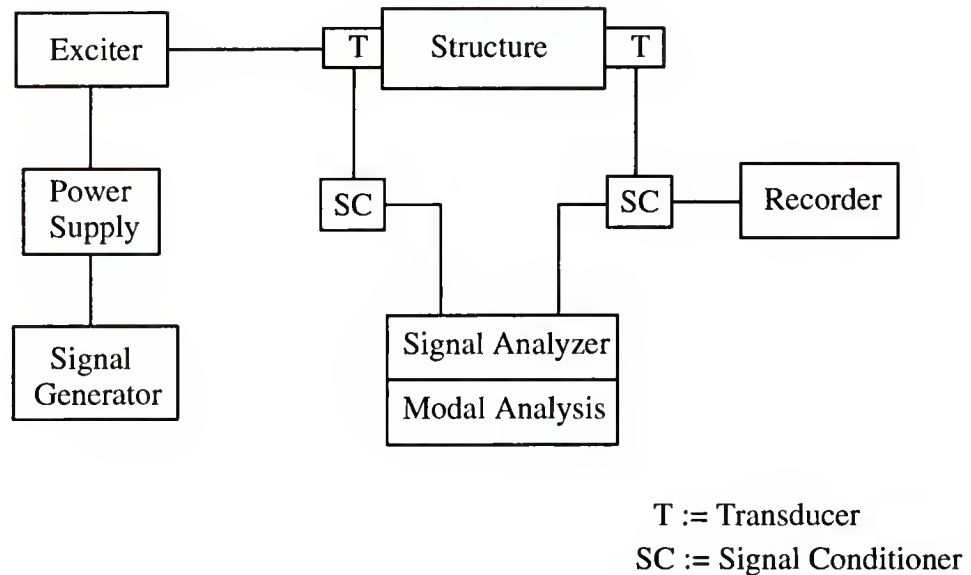


Figure 2.1 Components of a Vibration Measurement System For Modal Analysis (Inman, 1989).

The exciter is used to deliver the driving force that puts the structure in motion. The two most commonly used exciters are the shaker and the impulse hammer.

Transducers are devices that measure the driving force as well as the response of the structure. They sense mechanical forces or motions and, then, convert them into electrical signals. Mechanical forces are usually recorded by a force transducers. Commonly, the vibration response of structures is measured by accelerometers. Accelerometers are mounted directly on the structure and, naturally, record the local accelerations.

Signal conditioners are used to match the signal, received from the transducers, to the specification of the analyzer. These devices can also be used to amplify the signals.

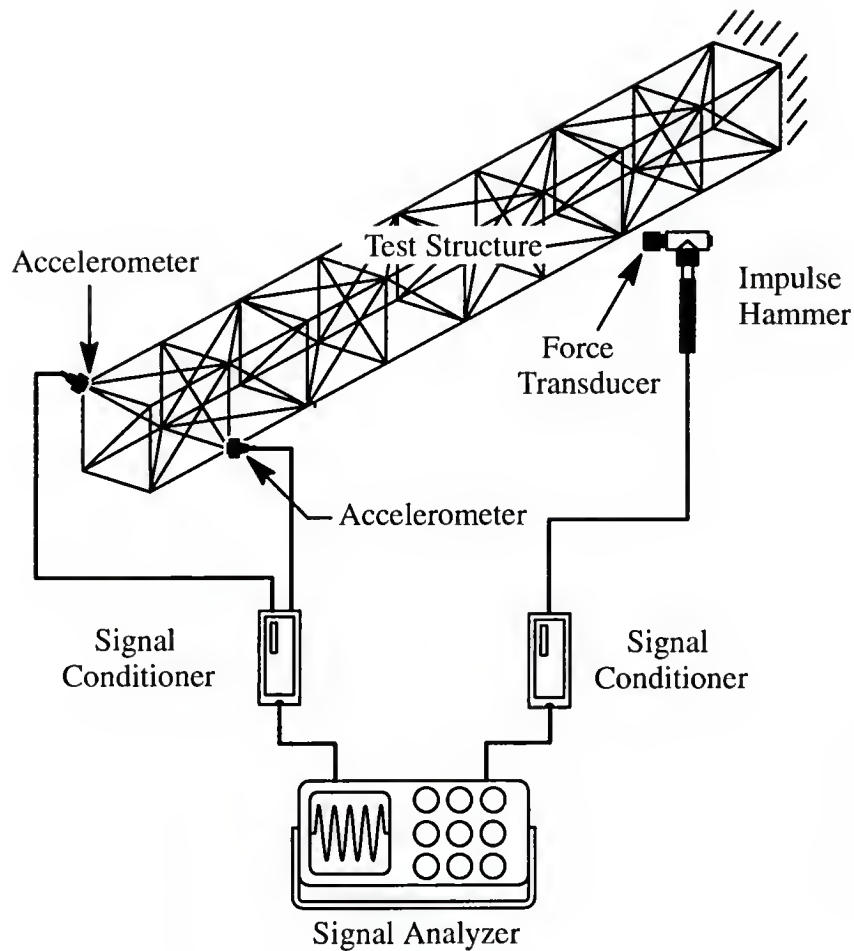


Figure 2.2 A Simple Experimental Modal Analysis Setup.

The signal analyzer processes the electrical signal received from the signal conditioners. The standard type of analyzer allows time domain signals to be viewed in the frequency domain via a Fast Fourier Transform (FFT) algorithm. In an FFT, the signals are first filtered, digitized and then transformed into discrete frequency spectra. The frequency spectra can then be manipulated to compute the modal properties of the structure.

It is important to note that the experimentally identified modal parameters are usually affected by unpredictable measurement noise. Typically, natural frequencies are identified to within 1 to 2% repeatability; damping ratios to within 5 to 15% repeatability, and mode shapes to within 5 to 10% repeatability. In practice, due to testing limitations, the set of

structural modal parameters identified experimentally is incomplete with respect to the analytical model. Experimental incompleteness is manifested in two forms, (i) a limited number of measured modes of vibration, (ii) a limited number of eigenvector DOF measurements.

## 2.4 Analytical and Experimental Model Dimensions Correlation

One major prerequisite common to most model refinement algorithms is to match the number of degrees of freedom (DOFs) in the experimentally measured eigenvector and in the discrete analytical model. Two different approaches have been commonly used to resolve this matching problem when an incomplete set of eigenvector DOFs have been measured. The first approach consists of reducing the dimension of the discrete analytical model to the number of the measured DOFs. The other approach is to expand the measured eigenvector to the size of the analytical model. A good evaluative survey of a number of analytical model reduction techniques has been compiled by McGowan (1991). The subject of eigenvector expansion is discussed in fair detail in the papers by Gysin (1990), and Zimmerman and Kaouk (1992a). In the next two sections, some commonly used model reduction and eigenvector expansion algorithms are reported and described.

### 2.4.1 Model Reduction Methods

In this section the general framework of the model reduction concept is first presented. Then formulations of three commonly used model reduction techniques are summarized. Mostly, the concept of model reduction has only been studied for undamped models. In this presentation no attempt has been made to generalize these concepts to damped models.

For the purpose of reporting the general concept of model reduction, consider the eigenvalue problem associated with an undamped model,

$$MVA^2 + KV = [0] \quad (2.4.1)$$

where, as defined earlier,  $M$  and  $K$  are, respectively, the mass and stiffness matrix;  $V$  is the eigenvector matrix and  $\Lambda$  is the diagonal eigenvalue matrix. Assume that only a subset of the eigenvector DOFs has been experimentally measured.

Equation (2.4.1) can be reordered such that the DOFs associated with the measured DOFs are in the upper rows of the equation,

$$M_o V_o \Lambda^2 + K_o V_o = [0] \quad (2.4.2)$$

$$\text{where } V_o = \begin{bmatrix} V_m \\ V_u \end{bmatrix} \quad K_o = \begin{bmatrix} K_{mm} & K_{mu} \\ K_{um} & K_{uu} \end{bmatrix} \quad M_o = \begin{bmatrix} M_{mm} & M_{mu} \\ M_{um} & M_{uu} \end{bmatrix}$$

The matrices  $M_o$ ,  $K_o$ , and  $V_o$  are, respectively, the reordered mass, stiffness and eigenvector matrices. In the above equation, the subscripts “m” and “u” denote, respectively, the components associated with the measured and unmeasured DOFs. A transformation matrix  $P$ , that relates matrices  $V_u$  and  $V_m$  can be defined as

$$V_u = P V_m \quad (2.4.3)$$

A substitution of this relationship in the reordered eigenvector matrix  $V_o$  results in

$$V_o = \begin{bmatrix} I \\ P \end{bmatrix} V_m = T V_m \quad (2.4.4)$$

Substituting Eq. (2.4.4) into Eq. (2.4.2) and premultiplying by  $T^T$  yields the eigenvalue problem of the reduced model,

$$M_r V_m \Lambda^2 + K_r V_m = [0] \quad (2.4.5)$$

$$\text{where } M_r = T^T M_o T$$

$$K_r = T^T K_o T$$

where  $M_r$  and  $K_r$  are the reduced mass and stiffness matrices, respectively. In terms of the partitioned matrices, the reduced matrices are defined as

$$\mathbf{M}_r = \mathbf{M}_{mm} + \mathbf{P}^T \mathbf{M}_{um} + \mathbf{M}_{mu} \mathbf{P} + \mathbf{P}^T \mathbf{M}_{uu} \mathbf{P} \quad (2.4.6)$$

$$\mathbf{K}_r = \mathbf{K}_{mm} + \mathbf{P}^T \mathbf{K}_{um} + \mathbf{K}_{mu} \mathbf{P} + \mathbf{P}^T \mathbf{K}_{uu} \mathbf{P} \quad (2.4.7)$$

At this point, the only condition placed on  $\mathbf{P}$  is the relationship of Eq. (2.4.3). Naturally, matrix  $\mathbf{P}$  can be computed directly from Eq. (2.4.3) if the eigenvectors of the system are available. This approach is known as the exact reduction method and has been discussed in the papers by Kammer (1987) and O'Callahan et al. (1989). The exact reduction method requires solving for a large number of eigenvectors, which can be computationally expensive. The three reduction methods that are presented in the forthcoming discussions propose alternative techniques to compute matrix  $\mathbf{P}$ . The first two do not require the computation of the system eigenvalue problem. The last one requires the knowledge of one eigenvalue which is computationally admissible.

#### 2.4.1.1 Static Reduction

This reduction method is often referred to as Guyan (1965) reduction. In the static reduction, the mass properties associated to the unmeasured DOFs are assumed negligible. With that assumption, Eq. (2.4.2) can be written as

$$\begin{bmatrix} \mathbf{M}_{mm} & 0 \\ 0 & 0 \end{bmatrix} \begin{bmatrix} \mathbf{V}_m \\ \mathbf{V}_u \end{bmatrix} \Lambda^2 + \begin{bmatrix} \mathbf{K}_{mm} & \mathbf{K}_{mu} \\ \mathbf{K}_{um} & \mathbf{K}_{uu} \end{bmatrix} \begin{bmatrix} \mathbf{V}_m \\ \mathbf{V}_u \end{bmatrix} = \begin{bmatrix} 0 \\ 0 \end{bmatrix} \quad (2.4.8)$$

The second row of this matrix equation can then be manipulated as

$$\mathbf{V}_u = -\mathbf{K}_{uu}^{-1} \mathbf{K}_{um} \mathbf{V}_m \quad (2.4.9)$$

From comparing Eq. (2.4.9) to Eq. (2.4.3), it can be deduced that the transformation matrix,  $\mathbf{P}$ , computed using the Guyan approach is given by

$$\mathbf{P}_g = -\mathbf{K}_{uu}^{-1} \mathbf{K}_{um} \quad (2.4.10)$$

The reduced mass and stiffness matrices can then be computed by substituting matrix  $\mathbf{P}_g$  for matrix  $\mathbf{P}$  in Eqs. (2.4.6) and (2.4.7). Naturally, the Guyan assumption (Eq. (2.4.8))



suggests that if the mass properties of the omitted DOFs are not small, the accuracy of the Guyan reduced model could be lacking.

#### 2.4.1.2 IRS Reduction

The improved reduction method (IRS) was formulated by O'Callahan (1989). It is an improvement over the Guyan reduction in that it accounts for the mass properties of the unmeasured DOFs. In the formulation of the IRS method, the Guyan reduced model is corrected to include the mass influence of the unmeasured DOFs. This formulation is somewhat lengthy and the interested reader is referred back to the paper of O'Callahan (1989) or the thesis of McGowan (1991). The transformation matrix  $P$  computed using the IRS reduction is

$$P_{IRS} = P_g + K_{uu}^{-1} [ M_{um} + M_{uu}P_g ] M_{r_g}^{-1} K_{r_g} \quad (2.4.11)$$

The reduced IRS model is then computed by substituting matrix  $P_{IRS}$  in Eqs. (2.4.6–7).

#### 2.4.1.3 Dynamic Reduction

The dynamic reduction was proposed as another improvement to the Guyan reduction (Kidder, 1973; Miller, 1980; and Paz, 1984). This reduction utilizes the dynamic equation associated with a single mode of vibration to compute the transformation matrix  $P$ . In this technique, the transformation matrix  $P$  is arrived at by considering the reordered dynamic equation associated with the  $i^{\text{th}}$  mode,

$$\begin{bmatrix} \lambda_i^2 M_{mm} + K_{mm} & \lambda_i^2 M_{mu} + K_{mu} \\ \lambda_i^2 M_{um} + K_{um} & \lambda_i^2 M_{uu} + K_{uu} \end{bmatrix} \begin{bmatrix} \underline{y}_{m_i} \\ \underline{y}_{u_i} \end{bmatrix} = \begin{bmatrix} 0 \\ 0 \end{bmatrix} \quad (2.4.12)$$

where  $\lambda_i$  is the  $i^{\text{th}}$  eigenvalue;  $\underline{y}_{m_i}$  and  $\underline{y}_{u_i}$  are, respectively, the measured and unmeasured eigenvector DOFs associated with the  $i^{\text{th}}$  mode of vibration. Based on this partition, two equations can be generated. By using the rows that correspond to the unmeasured DOFs (lower rows), the following relationship is obtained,



$$\underline{v}_{u_i} = - \left[ M_{uu} \lambda_i^2 + K_{uu} \right]^{-1} \left[ M_{um} \lambda_i^2 + K_{um} \right] \underline{v}_{m_i} \quad (2.4.13)$$

Hence, the transformation matrix associated with the  $i^{\text{th}}$  mode is defined by

$$P_{d_i} = - \left[ M_{uu} \lambda_i^2 + K_{uu} \right]^{-1} \left[ M_{um} \lambda_i^2 + K_{um} \right] \quad (2.4.14)$$

The reduced mass and stiffness matrices are then computed by using Eqs. (2.4.6) and (2.4.7).

Note that different modes will result in different transformation matrices  $P_{d_i}$  and, hence, different reduced mass and stiffness matrices.

## 2.4.2 Eigenvector Expansion Methods

Alternatively, the dimension of the measured eigenvectors can be correlated to the dimension of the analytical model by using eigenvector expansion algorithms. The common basis of these algorithms is the interpolation of the unmeasured eigenvector components. In the forthcoming sections, two eigenvector expansion algorithms are reviewed.

### 2.4.2.1 Dynamic Expansion

The dynamic expansion technique (Berman and Nagy, 1983) is one of the most commonly used eigenvector expansion algorithms. A slight modification of the Berman and Nagy formulation is presented here to accommodate damped systems (Fuh et al., 1984). In the formulation of the dynamic expansion, it is assumed that the measured modes satisfy the eigenvalue problem involving the property matrices of the original model ( $M, D, K$ ). For the  $i^{\text{th}}$  measured mode, this assumption takes the form

$$\left( \lambda_{e_i}^2 M + \lambda_{e_i} D + K \right) \underline{v}_{e_i} = \underline{0} \quad (2.4.15)$$

where  $\lambda_{e_i}$  and  $\underline{v}_{e_i}$  are, respectively, the  $i^{\text{th}}$  experimental eigenvalue and eigenvector. The matrices  $M, D$  and  $K$  have the same definitions as in the earlier sections. Assume that only a subset of the DOFs of eigenvector  $\underline{v}_{e_i}$  has been measured. Equation (2.4.15) can be reordered, as in Section 2.4.1, such that the measured eigenvector DOFs reside in the upper half of the equation,

$$\left\{ \begin{bmatrix} M_{mm} & M_{mu} \\ M_{um} & M_{uu} \end{bmatrix} \lambda_{e_i}^2 + \begin{bmatrix} D_{mm} & D_{mu} \\ D_{um} & D_{uu} \end{bmatrix} \lambda_{e_i} + \begin{bmatrix} K_{mm} & K_{mu} \\ K_{um} & K_{uu} \end{bmatrix} \right\} \begin{bmatrix} \underline{v}_{em_i} \\ \underline{v}_{eu_i} \end{bmatrix} = \begin{bmatrix} 0 \\ 0 \end{bmatrix} \quad (2.4.16)$$

where  $\underline{v}_{em_i}$  and  $\underline{v}_{eu_i}$  are, respectively, the measured and unmeasured DOFs of  $\underline{v}_{e_i}$ . The subscripts “m” and “u” denote masured and unmeasured components. A rearrangement of Eq. (2.4.16) yields

$$\begin{bmatrix} \lambda_{e_i}^2 M_{mm} + \lambda_{e_i} D_{mm} + K_{mm} & \lambda_{e_i}^2 M_{mu} + \lambda_{e_i} D_{mu} + K_{mu} \\ \lambda_{e_i}^2 M_{um} + \lambda_{e_i} D_{um} + K_{um} & \lambda_{e_i}^2 M_{uu} + \lambda_{e_i} D_{uu} + K_{uu} \end{bmatrix} \begin{bmatrix} \underline{v}_{em_i} \\ \underline{v}_{eu_i} \end{bmatrix} = \begin{bmatrix} 0 \\ 0 \end{bmatrix} \quad (2.4.17)$$

From Eq. (2.4.17), two matrix equations in function of  $\underline{v}_{em_i}$  and  $\underline{v}_{eu_i}$  can be generated. By using the equation associated with the second row of the partition, the unmeasured components of the  $i^{\text{th}}$  experimental eigenvector are computed to be

$$\underline{v}_{eu_i} = - \left[ M_{uu} \lambda_{e_i}^2 + D_{uu} \lambda_{e_i} + K_{uu} \right]^{-1} \left[ M_{um} \lambda_{e_i}^2 + D_{um} \lambda_{e_i} + K_{um} \right] \underline{v}_{em_i} \quad (2.4.18)$$

Note that this expansion works on a single mode at a time. Also, notice that it involves the original analytical model (M, D, K). This implies that the accuracy of the expansion depends on the validity of the original analytical model.

#### 2.4.2.2 Orthogonal Procrustes Expansion

Another expansion process that has shown great promise is the orthogonal Procrustes (OP) expansion method presented in the papers of Smith and Beattie (1990) and Zimmerman and Kaouk (1992a). The technique uses the general mathematical framework of the orthogonal Procrustes problem (Golub and Van Loan, 1983).

Let  $V_{em}$  be the experimentally measured eigenvector component matrix and  $V_{am}$  be the corresponding analytical eigenvector component matrix. The essence of the OP expansion is to find a unitary transformation matrix  $P_{op}$  that closely rotates  $V_{am}$  into  $V_{em}$ . This is attempted by solving the following problem,

$$\begin{aligned} \text{Minimize} \quad & \| V_{em} - V_{am}P_{op} \|_F \\ \text{subject to} \quad & P_{op}^T P_{op} = I \end{aligned} \quad (2.4.19)$$

The solution to this general problem is discussed in the book of Golub and Van Loan and is given by

$$P_{op} = YZ^T \quad (2.4.20)$$

where  $Y$  and  $Z$  are, respectively the left and right singular matrices of matrix  $\Phi$  defined by

$$\Phi = V_{am}^T V_{em} \quad (2.4.21)$$

Let  $V_{au}$  be the eigenvector matrix associated with the unmeasured DOFs. In the orthogonal Procrustes expansion, it is assumed that the transformation matrix computed above also rotates  $V_{au}$  into the unmeasured “experimental” eigenvector component matrix,  $V_{eu}$ , as

$$V_{eu} = V_{au}P_{op} \quad (2.4.22)$$

Two different approaches have been defined to generate the expanded experimental eigenvector matrix. The first is suggested in the paper by Smith and Beattie (1990),

$$V_e = \begin{bmatrix} V_{am} \\ V_{au} \end{bmatrix} P_{op} \quad (2.4.23)$$

In this definition, the expanded “experimental” eigenvector matrix is the rotated analytical eigenvector matrix. The actual experimental measured eigenvector components  $V_{em}$  are replaced by matrix  $V_{am}P_{op}$ . The advantage of the approach is that the resulting “experimental” eigenvector satisfies the cross-orthogonality conditions (see Section 2.4).

The second viewpoint was proposed by Zimmerman and Kaouk (1992a),

$$V_e = \begin{bmatrix} V_{em} \\ V_{au}P_{op} \end{bmatrix} \quad (2.4.24)$$

Here, the unaltered eigenvector components measured experimentally are inserted in  $V_e$ . In this viewpoint, if cross-orthogonalization of the expanded experimental eigenvectors is

required, a separated orthogonality algorithm can be used (Section 2.5). In the paper by Smith et al. (1993), it is shown that for actual model refinement problems, both viewpoints give equivalent eigenvector expansion results. However, for damage detection problems, a preliminary study indicates that eigenvectors expanded by using the viewpoint defined in Eq. (2.4.24) give better assessment of the damage.

## 2.5 Eigenvector Orthogonalization

Most matrix update algorithms require the measured eigenvectors to satisfy a cross-orthogonality condition. This is especially true in matrix update algorithms in which (i) the model of the structure is assumed undamped and the modelling errors are assumed to be in only one of the two property matrices ( $M$  or  $K$  is assumed correct) or (ii) the system is modeled by a proportionally damped model with errors in only two of the three property matrices ( $M$ ,  $D$  or  $K$ ). In these situations, in order to insure symmetry of the updated property matrices, it is required that the expanded experimental eigenvectors be orthogonal with respect to the property matrix assumed accurate. This situation is encountered in the optimal update algorithms developed by Baruch and Bar Itzhack (1978), Kabe (1985), Kammer (1985), and Smith and Beattie (1991), Zimmerman and Kaouk (1992b), Kaouk and Zimmerman (1993b) among others. In most of these algorithms, it is assumed that the mass matrix is correct. This assumption is used in a number of the model refinement algorithms since the inertial properties of structures are known to a good extent. In these cases, one would expect the expanded experimental eigenvectors to be mass orthogonal. However, because of measurements errors, this condition rarely occurs. For this reason, a great deal of effort was focussed on the development of mass orthogonalization techniques. Some of the most notable work in that area was performed by Targoff (1976), Baruch and Bar Itzhack (1978), and Baruch (1979). In the next two sections, two orthogonalization techniques (Baruch and Bar Itzhack, 1978; Baruch, 1979) are discussed. Both techniques are mass orthogonalization techniques; however, with obvious modifications, these techniques can be

adopted to solve the orthogonalization problem of the eigenvectors with respect to the stiffness or the damping matrices.

### 2.5.1 Optimal Weighted Orthogonalization

The essence of the standard mass orthogonalization technique is to modify the measured eigenvectors such that the mass cross-orthogonality condition is satisfied. Baruch and Bar Itzhack (1978) proposed an elegant solution to that problem. An overview of their problem statement and solution is given below.

Assuming that  $V_e$  is a matrix of expanded experimental eigenvectors that need to be mass orthogonalized. The present formulation searches for the optimal mass weighted change of matrix  $V_e$  such that the mass cross-orthogonality condition is satisfied. This problem is cast as

$$\text{Minimize } \| N (V_{eo} - V_e) \|_F \quad (2.5.1)$$

$$\text{subject to } V_{eo}^T M V_{eo} = I \quad (2.5.2)$$

where  $N=M^{1/2}$  and  $M$  is the mass matrix. By means of a Lagrange multiplier, Eq. (2.5.2) can be incorporated into Eq. (2.5.1); then the application of the optimality conditions yields the following expression for  $V_{eo}$ ,

$$V_{eo} = V_e (V_e^T M V_e)^{-1/2} \quad (2.5.3)$$

Before being incorporated into the orthogonalization process, the measured eigenvectors have to be unit mass normalized, i.e.,

$$\underline{v}_{e_i} = \underline{v}_{e_i} (\underline{v}_{e_i}^T M \underline{v}_{e_i})^{-1/2} \quad (2.5.4)$$

where  $\underline{v}_{e_i}$  is the  $i^{\text{th}}$  expanded experimental eigenvector ( $i^{\text{th}}$  column of  $V_e$ ).

### 2.5.2 Selective Optimal Orthogonalization

Some structures exhibit rigid body modes (modes with zero eigenvalues). It is desirable to preserve these rigid body modes in the refinement process. However, some matrix update



algorithms require the rigid body modes and the experimental eigenvectors to be mass orthogonal to insure symmetry of the updated property matrices (see Chapter 6). Naturally, the rigid body modes will be corrupted if they are incorporated along with the expanded experimental eigenvectors in the above orthogonalization process. Thus, Baruch (1979) presented a modification of the procedure in Section 2.5.1 to deal with such a problem. The resulting problem is a selective orthogonalization and is formulated as follows,

$$\text{minimize} \quad \| N (V_{eo} - V_e) \|_F \quad (2.5.5)$$

$$\text{Subject to} \quad V_{eo}^T M V_{eo} = I \quad (2.5.6)$$

$$\text{and} \quad V_{eo}^T M V_r = [0] \quad (2.5.7)$$

In the above equations,  $V_e$  and  $V_r$  are, respectively, the expanded experimental eigenvector matrix and the rigid body mode matrix. Again, the Lagrange multiplier is used, and the orthogonalized experimental eigenvector matrix that satisfies the conditions in Eqs. (2.5.6) and (2.5.7) is found to be

$$V_{eo} = Q(Q^T M Q)^{-1/2} \quad (2.5.8)$$

$$\text{where} \quad Q = V_e - V_r V_r^T M V_e$$

Note that, as in previous process, the expanded experimental eigenvectors have to be unit mass normalized.

## 2.6 Load Path Preservation

Many matrix update algorithms introduce additional load paths in their updated models, i.e., elements of the mass, damping or stiffness matrices that were originally zero may become nonzero. Whether or not preserving the original load path is a practical problem is still a matter of current debate. It seems that for damage assessment of truss structures it is desired to maintain load paths. In the paper of Zimmerman and Kaouk (1992a), an iterative approach to preserve the load path of the original property matrices was developed. The

approach was presented in the context of the symmetric eigenstructure assignment model refinement algorithm (discussed in Chapter 4); however, its application can also be extended to other model refinement algorithms. In Figure 2.3, a flow chart of the iterative load preservation algorithm is presented. The procedure is illustrated for a general model refinement scenario in which all three property matrices ( $M$ ,  $D$ ,  $K$ ) are being updated. However, it can be easily modified to accommodate other refinement problems.

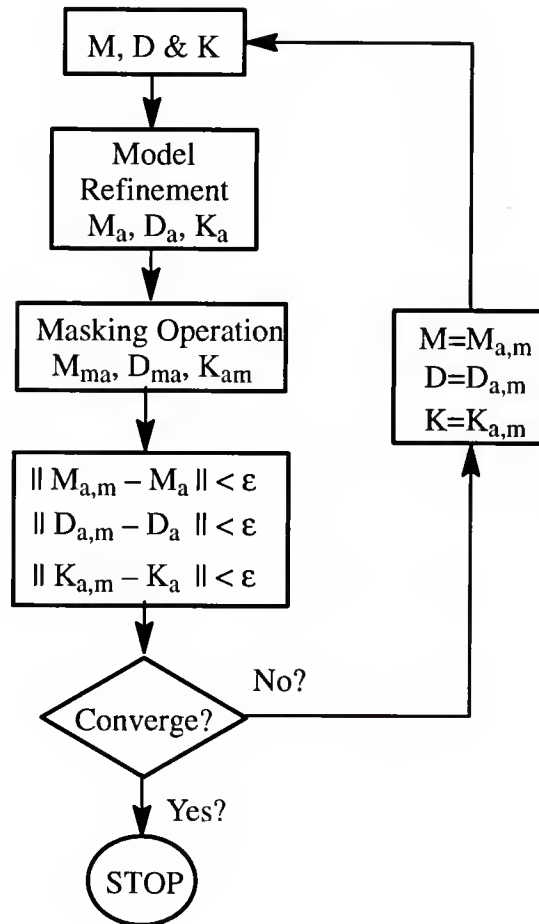


Figure 2.3 Flow Chart of the Iterative Load Path Preservation Algorithm

In the flow chart, the matrices  $M_{a,m}$ ,  $D_{a,m}$ , and  $K_{a,m}$  are respectively the adjusted masked mass, damping and stiffness matrices defined by

$$\begin{aligned}
M_{a,m} &= M_a \odot M_m \\
D_{a,m} &= D_a \odot D_m \\
K_{a,m} &= K_a \odot K_m
\end{aligned}
\tag{2.6.2}$$

where  $M_a$ ,  $D_a$ , and  $K_a$  are the adjusted mass damping and stiffness matrices. The matrices  $M_m$ ,  $D_m$ , and  $K_m$  are the masking matrices associated with the original mass, damping and stiffness matrix. By definition, the masking matrix,  $A_m$ , associated with matrix  $A$  is given by

$$\begin{aligned}
A_m(i,j) &= 1 \quad \text{if } A(i,j) \neq 0 \\
A_m(i,j) &= 0 \quad \text{if } A(i,j) = 0
\end{aligned}
\tag{2.6.1}$$

In Eqs. (2.6.2), the operator  $\odot$  is the element-by-element (scalar) matrix multiplication. Let  $B$  and  $C$  be two  $n \times n$  matrices, then the element-by-element multiplication of  $B$  and  $C$  is given by

$$S = B \odot C \Rightarrow S(i,j) = B(i,j) * C(i,j) \quad i,j = 1, \dots, n \tag{2.6.3}$$

At every iteration, the norms of the matrix differences between corresponding adjusted and adjusted masked property matrices are computed. At a given iteration, if the three computed norms are equal to zero or within user set limits, then the load paths of the original three property matrices have been exactly achieved or achieved within user state guidelines. Thus, the procedure is halted, and the refined model consists of the adjusted property matrices computed at that particular iteration. It should be noted that there is no formal guarantee of convergence in using this iterative procedure. Experience gained in using the present algorithm indicates that if the experimental modal data are consistent with the sparsity pattern, the procedure will converge. Consistent data means that there exist mass, damping and stiffness matrices that have the same sparsity pattern as the original matrices and also exhibit the measured test data. Otherwise, if the data are inconsistent, the original sparsity patterns will not be exactly preserved. In this case, the added load path terms of  $M_a$ ,  $D_a$  and  $K_a$  which should be zero will be closer to zero after application of the algorithm.

## CHAPTER 3 INVERSE / HYBRID APPROACH FOR FINITE ELEMENT MODEL REFINEMENT

### 3.1 Introduction

The inverse eigenvalue problem is concerned with the construction of the property matrices (mass, damping or stiffness) of a dynamic model using experimentally measured modal data. These techniques require complete modal properties. Thus, for an n-DOF model, n natural frequencies, damping ratios and mode shapes (eigenvectors) must be measured, and the identified mode shapes must be of dimension n. Due to practical testing limitations, this is rarely accomplished for typical large structures. In this chapter, the application of the inverse problem is extended to model updating by combining experimental measurements and original analytical FEM modal information. Again, refinement implies correlating the measured and analytical modal properties.

### 3.2 Theoretical Formulation

The dynamic structure under consideration is assumed to be successfully modelled by an n-DOF proportionally damped nongyroscopic and noncirculatory (symmetric property matrices) FEM. The free vibration motion of such a dynamic structure can be analytically represented by a differential equation of the form

$$M\ddot{\underline{w}}(t) + D\dot{\underline{w}}(t) + K\underline{w}(t) = \underline{0} \quad (3.2.1)$$

where the variables M, D, and K are nxn real symmetric matrix models of the mass, damping and stiffness properties of the structure. The nx1 time varying vector  $\underline{w}(t)$  represents the n

displacements of the n-DOF model of the system. The overdots represent differentiation with respect to time. The eigenvalue problem associated with the differential equation shown in Eq. (3.2.1) is of the form

$$\mathbf{M}\underline{\dot{v}}_i \lambda_i^2 + \mathbf{D}\underline{\dot{v}}_i \lambda_i + \mathbf{K}\underline{v}_i = \underline{0} \quad (3.2.2)$$

where  $\lambda_i$  and  $\underline{v}_i$  are, respectively, the eigenvalue and eigenvector of the  $i^{\text{th}}$  mode of vibration. In this problem, it is assumed that the accuracy of the original FEM is lacking and, hence, needs improvement. Furthermore, it is assumed that the inaccuracy of the original FEM is solely due to modeling errors in the stiffness and damping properties.

The model refinement, proposed herein, exploits the cross-orthogonality relations that arise from the symmetric nature of the property matrices and the proportional damping assumption. As discussed in Chapter 2, by proper normalization of the eigenvectors these cross-orthogonality relations have the form

$$\mathbf{V}^T \mathbf{M} \mathbf{V} = \mathbf{I}_{n \times n} \quad (3.2.3a)$$

$$\mathbf{V}^T \mathbf{D} \mathbf{V} = \text{diag}(2\zeta_1\omega_1, \dots, 2\zeta_n\omega_n) = \Sigma \quad (3.2.3b)$$

$$\mathbf{V}^T \mathbf{K} \mathbf{V} = \text{diag}(\omega_1^2, \dots, \omega_n^2) = \Omega \quad (3.2.3c)$$

$$\mathbf{V} = [ \underline{v}_1, \dots, \underline{v}_n ]$$

where  $\omega_i$  and  $\zeta_i$  are the natural frequency and damping ratio, respectively, of the  $i^{\text{th}}$  mode of the structure. The matrix  $\mathbf{I}_{n \times n}$  is the  $n \times n$  identity matrix. It is important to recognize that Eq. (3.2.3a) represents necessary and sufficient conditions for conserving symmetry and damping proportionality when updating the stiffness and damping properties of proportionally damped systems.

Suppose that  $p$  ( $p \ll n$ ) modes of an existing structure have been experimentally identified (mode shapes or eigenvectors, frequencies and damping ratios). Assume that the dimension of measured eigenvectors is equal to the dimension of the FEM, i.e., all  $n$  components of the measured eigenvectors are available. It is widely accepted that in the



absence of specific experimental measurements a good approximation to the unmeasured modes is their corresponding analytical modal information. With that in mind, a complete hybrid set of modal data is generated by combining experimental and analytical information

$$\begin{aligned}
 V_{ea} &= [V_e \quad V_a] \\
 \Omega_{ea} &= \begin{bmatrix} \Omega_e & 0 \\ 0 & \Omega_a \end{bmatrix} \\
 \Sigma_{ea} &= \begin{bmatrix} \Sigma_e & 0 \\ 0 & \Sigma_a \end{bmatrix}
 \end{aligned} \tag{3.2.4}$$

where  $V$  is the eigenvector matrix;  $\Omega$  and  $\Sigma$  are diagonal matrices of frequencies squared and damping ratios, respectively. The subscripts  $e$  and  $a$  denote, respectively, experimental and analytical sets. At this point, the complete “hybrid” set of eigenvectors,  $V_{ea}$ , does not satisfy the cross-orthogonality conditions defined in Eq. (3.2.3a); thus the conditions in Eqs. (3.2.3b) and (3.2.3c) are not met. One possible solution to this problem is to modify all of  $V_{ea}$  in an optimal way to comply with the orthogonality requirement. This approach treats all parts of  $V_{ea}$  equally, and thus overlooks the fact that the experimental modes are known with a higher confidence. Naturally, a technique that assigns a higher credibility to the experimental eigenvectors,  $V_e$ , is preferable. This can be achieved by incorporating  $V_{ea}$  into the orthogonalization process group by group in the order of their descending credibility (experimental then analytical). If the problem is set such that the experimental modes,  $V_e$ , are corrected first, it is clear that the analytical modes,  $V_a$ , will be subject to larger correction when incorporated into the orthogonalization process since they will be subject to more constraints.

The experimental modes,  $V_e$ , are orthogonalized by using the orthogonalization technique formulated by Baruch and Bar Itzhack (1978). The general formulation of this orthogonalization technique is discussed in Chapter 2. For this particular application, the problem consists of finding the matrix,  $V_{eo}$ , that satisfies the cross-orthogonality condition,

$$V_{eo}^T M V_{eo} = I_{p \times p} \quad (3.2.5)$$

and that minimizes the weighted Euclidean norm,

$$\Phi = \| N (V_{eo} - V_e) \|_F \quad (3.2.6)$$

where  $N = M^{1/2}$

The solution to this problem, as reported in Chapter 2, is

$$V_{eo} = V_e (V_e^T M V_e)^{-1/2} \quad (3.2.7)$$

The next step is to invoke the orthogonality requirement on the analytical eigenvector matrix,  $V_a$ , by searching for a matrix  $V_{ao}$  that satisfies the following two conditions,

$$V_{ao}^T M V_{ao} = I_{(n-p) \times (n-p)} \quad (3.2.8)$$

$$\text{and } V_{ao}^T M V_{eo} = [0] \quad (3.2.9)$$

while minimizing the objective function,

$$\Gamma = \| N (V_{ao} - V_a) \|_F \quad (3.2.10)$$

where  $N = M^{1/2}$

A similar problem was also treated by Baruch (1980) in a different context. A brief discussion of the solution approach can be found in Chapter 2. The set of eigenvectors,  $V_{ao}$  that satisfies this problem is given by

$$V_{ao} = Q (Q^T M Q)^{-1/2} \quad (3.2.11)$$

$$Q = V_a - V_{eo} V_{eo}^T M V_a$$

Clearly, the resultant matrix,  $V_{eao} = [V_{eo}, V_{ao}]$ , satisfies Eq. (3.2.3a). The corrected stiffness and damping matrices are then computed using Eqs. (3.2.2b) and (3.2.2c).

$$K_a = M V_{eao} \Omega_{ea} V_{eao}^T M \quad (3.2.12a)$$

$$D_a = M V_{eao} \Theta_{ea} V_{eao}^T M \quad (3.2.12a)$$

$$\text{where } \Theta_{ea} = 2\Pi_{ea}\Omega_{ea}$$

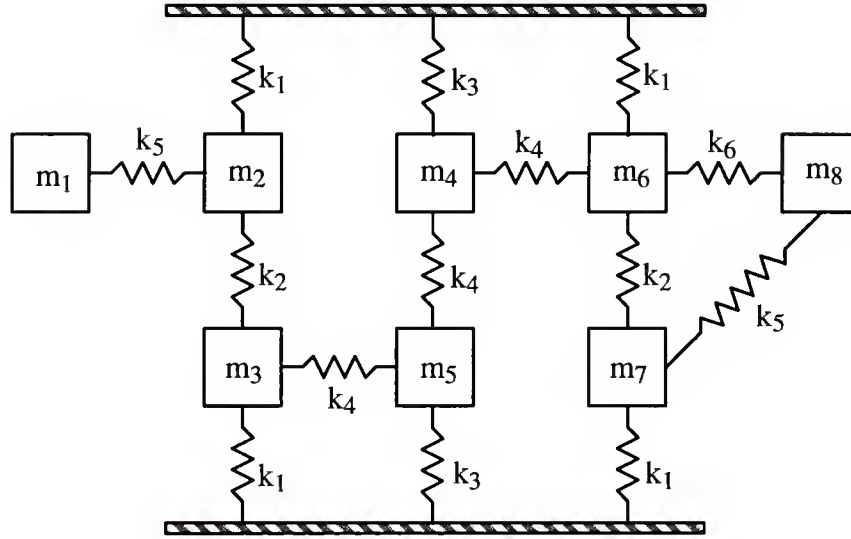
Note that the matrices  $K_a$  and  $D_a$  computed from Eqs. (3.2.12a,b) will be symmetric. The above formulation suggests that the system modelled by the original mass matrix ( $M$ ) and the stiffness ( $K_a$ ) and damping ( $D_a$ ) matrices computed from Eqs. (3.2.12a,b) will have eigenvectors  $V_{eao}$ , frequencies  $\Omega_{ea}$ , and damping ratios  $\Pi_{ea}$ . Some structures exhibit rigid body modes of vibration. Commonly, it is desirable to preserve these rigid body modes in the updated model. The above formulation also suggest that the updated model will preserve the original rigid body modes.

The procedure developed above can be easily contracted to address the case when the system model does not account for the effects of damping (undamped model). The contraction can be obtained by setting to zeros matrices  $D$ ,  $\Theta_{ea}$ , and  $\Pi_{ea}$  in Eqs. (3.2.2–4).

The computational burden limits the size of the FEM which can be updated (order of 200). Essentially, the limiting factor is that all mode shapes of the structure that are not available from experimental measurements must be calculated analytically by solving the eigenvalue / eigenvector problem.

### 3.3 Numerical Illustration

The system addressed in this investigation is the commonly used eight degrees of freedom model shown in Figure 3.1. This model was developed by Kabe (1985) to give a common testbed for the evaluation of the performance of model refinement algorithms. An original undamped analytical model of the system was generated by using the mass and stiffness properties shown in Figure 3.1. The elements of the original analytical stiffness matrix are displayed in the second column of Table 3.1. In this problem, it is assumed that the original stiffness matrix of the model is incorrect. These inaccuracies were simulated by



$$m_1 = 0.001 \quad m_8 = 0.002 \quad m_j = 1.0 \quad j = 2, \dots, 7$$

$$k_1 = 1000 \quad k_2 = 10 \quad k_3 = 900 \quad k_4 = 100 \quad k_5 = 1.5 \quad k_6 = 2.0$$

Figure 3.1 Kabe's Problem: Analytical Test Structure.

using incorrect stiffness constants for most of the springs. The elements of the actual correct stiffness matrix are given in the last column of Table 3.1. Note that the present model refinement problem is very challenging and because of the large difference between the stiffness matrices of the original and exact model. In this study, two cases will be considered. In the first case, it is assumed that only the modal parameters (eigenvalue and eigenvector) of the first mode were measured. In the other, the modal parameters of first three modes are assumed to be available. In both cases, the measured eigenvectors are supposed to be full (all degrees of freedom of the eigenvector(s) are measured).

The main objective of this investigation is to compare the performance of the inverse/hybrid method to the algorithm proposed by Baruch and Bar Itzhack (1978). The Baruch and Bar Itzhack model update technique is one of the most commonly used model refinement algorithm. One of the main reasons for its common use is because the algorithm is computationally efficient. The updated stiffness matrices generated by using the Baruch and Bar Itzhack approach for the one mode and three mode cases are shown in the third and

fourth column of Table 3.1, respectively. The fifth and sixth columns of Table 3.1 display the results of using the inverse/hybrid algorithm for the one mode and three modes cases. For both cases, it is clear that the performances of both algorithms is lacking in predicting the exact stiffness matrix. As expected, It can also be seen that both algorithms generate better results when using three measured modes. A comparison of the results generated using the Baruch and Bar Itzhack approach and the inverse/hybrid method shows that both algorithms give the same type of results. This similarity of results was also encountered in other example problems.

### 3.4 Summary

A model refinement approach that uses a hybrid set of experimental and analytical modal properties was formulated. The developed approach, termed the inverse/hybrid algorithm, was illustrated by using a computer simulated example. Part of the evaluation of the proposed algorithm was the comparison of its performance with the performance of the Baruch and Bar Itzhack algorithm. It was found that both algorithms give the same type of results. However, the computations involved in the inverse/hybrid approach exceed those involved in the Baruch and Bar Itzhack algorithm. Essentially, the inverse/hybrid approach requires the computation of all eigenvalues and eigenvectors of the structure that are not available from experimental measurements. As will be illustrated in the forthcoming chapter, the Baruch type approaches are not suited for damage assessment applications. For these reasons, further development of the Inverse/Hybrid algorithm was not investigated and new formulations (Chapters 4 & 6) were considered.



Table 3.1 Kabe's Problem: Elemental Stiffness Components.

Element #	Original	Baruch		Inverse/Hybrid		Exact
		Mode 1	Modes 1-3	Mode 1	Modes 1-3	
(1,1)	2.0	2.0	2.0	2.0	2.0	1.5
(1,2)	-2.0	-2.0	-3.0	-2.0	-3.0	-1.5
(1,3)	0.0	0.0	-0.1	0.0	-0.1	0.0
(1,4)	0.0	0.0	-0.1	0.0	-0.1	0.0
(1,5)	0.0	0.0	-0.1	0.0	0.1	0.0
(1,6)	0.0	0.0	0.1	0.0	0.1	0.0
(1,7)	0.0	0.0	0.1	0.0	0.0	0.0
(1,8)	0.0	0.0	0.0	0.0	0.0	0.0
(2,2)	1512.0	1508.6	1024.2	1510.6	1024.3	1011.5
(2,3)	-10.0	-31.5	-68.5	-21.5	-71.4	-10.0
(2,4)	0.0	-8.9	-9.0	-15.0	-8.4	0.0
(2,5)	0.0	-8.9	-20.9	-15.0	23.8	0.0
(2,6)	0.0	-21.6	38.5	-11.5	35.2	0.0
(2,7)	0.0	-3.9	-9.1	-1.6	-8.7	0.0
(2,8)	0.0	-0.1	0.1	-0.1	0.1	0.0
(3,3)	1710.0	1574.6	1560.8	1624.1	1612.2	1110.0
(3,4)	0.0	-44.9	-49.8	-75.6	-76.2	0.0
(3,5)	-200.0	-244.8	-244.1	-275.6	-276.9	-100.0
(3,6)	0.0	-136.5	-123.4	-86.2	-74.5	0.0
(3,7)	0.0	-24.6	50.8	-13.1	46.8	0.0
(3,8)	0.0	-0.4	-0.1	-0.4	0.0	0.0
(4,4)	850.0	1083.1	1087.9	1102.1	1099.9	1100.0
(4,5)	-200.0	3.27	25.1	51.8	48.0	-100.0
(4,6)	-200.0	-254.3	-242.2	-276.5	-274.9	-100.0
(4,7)	0.0	-10.1	27.0	-17.2	30.8	0.0
(4,8)	0.0	-0.2	-0.1	-0.2	-0.2	0.0
(5,5)	850.0	1082.2	1089.5	1101.4	1101.1	1100.0
(5,6)	0.0	-45.2	-49.5	-76.5	-75.1	0.0
(5,7)	0.0	-10.1	-12.4	-17.2	-11.7	0.0
(5,8)	0.0	-0.2	-0.1	-0.2	-0.2	0.0
(6,6)	1714.0	1576.4	1565.0	1617.5	1610.8	1112.0
(6,7)	-10.0	-34.8	-82.6	-23.1	-76.2	-10.0
(6,8)	-4.0	-4.4	-4.7	-4.4	-4.5	-2.0
(7,7)	1512.0	1507.5	1027.9	1510.1	1028.0	1011.5
(7,8)	-2.0	2.1	-4.1	-2.1	-4.2	-1.5
(8,8)	6.0	6.0	6.0	6.0	6.0	3.5

## CHAPTER 4

### SYMMETRIC EIGENSTRUCTURE ASSIGNMENT MODEL REFINEMENT ALGORITHM

#### 4.1 Introduction

Eigenstructure assignment is a control concept used to alter the transient response of linear systems. This is done by forcing the system to have some predetermined eigenvalues and eigenvectors. A detailed overview of eigenstructure assignment theories can be found in the paper by Andry et al. (1983). Inman and Minas (1990), Zimmerman and Widengren (1989, 1990), and Widengren (1989) have developed model refinement algorithms based on the mathematical framework of eigenstructure assignment. The basic idea of these model refinement techniques is to design the pseudo-controller which is required to produce the measured modal properties (natural frequencies, damping ratios and mode shapes) with the original finite element model (FEM) of the structure. The pseudo-controller is then translated into matrix adjustments applied to the initial FEM.

In this work, the eigenstructure assignment based model refinement algorithm proposed by Zimmerman and Widengren (1989, 1990) is extended to better approach the damage assessment problem. A subspace rotation algorithm is developed to enhance eigenvector assignability. Finally, the enhanced algorithm is tested and compared to other techniques on both “simulated” and actual experimental data.

#### 4.2 Problem Formulation

In this section, a review of the Zimmerman and Widengren (1989, 1990) refinement technique, which is termed the symmetric eigenstructure assignment model refinement

algorithm (SEAMRA), is presented. This review is essential in order to properly introduce and discuss the extension and improvement proposed in this work.

#### 4.2.1 Standard Eigenstructure Assignment Formulation

Consider the standard differential equation of motion of an  $n$  degrees of freedom damped, nongyroscopic and noncirculatory structure with control feedback,

$$M\ddot{\underline{w}}(t) + D\dot{\underline{w}}(t) + K\underline{w}(t) = B_0\underline{u}(t) \quad (4.2.1)$$

Again,  $M$ ,  $D$ , and  $K$  are  $n$ -by- $n$  real symmetric matrix models of the mass, damping and stiffness properties of the structure. Assume that these matrices were generated using the finite element method. The  $n \times 1$  time varying vector,  $\underline{w}(t)$ , represents the  $n$  displacements of the  $n$ -DOF FEM of the system. The overdots represent differentiation with respect to time. In control terminology,  $B_0$  is the  $n \times m$  ( $m \ll n$ ) control influence matrix describing the actuator force distributions and  $\underline{u}(t)$  is the  $m \times 1$  vector of output feedback control forces defined by

$$\underline{u}(t) = F\underline{y}(t) \quad (4.2.2)$$

In Eq. (4.2.2),  $F$  is the  $m \times r$  feedback gain matrix and  $\underline{y}(t)$  is the  $r \times 1$  output of sensor measurements defined by

$$\underline{y}(t) = C_0\underline{w} + C_1\dot{\underline{w}} \quad (4.2.3)$$

in which  $C_0$  and  $C_1$  are the  $r \times n$  output influence matrices corresponding to position and velocity, respectively. A substitution of Eqs. (4.2.2) and (4.2.3) into Eq. (4.2.1) yields

$$M\ddot{\underline{w}}(t) + (D - B_0FC_1)\dot{\underline{w}}(t) + (K - B_0FC_0)\underline{w}(t) = \underline{0} \quad (4.2.4)$$

It is clear, from Eq. (4.2.4), that the feedback controller results in residual changes,  $B_0FC_0$  and  $B_0FC_1$ , to the stiffness and damping matrices, respectively. These changes can be viewed as perturbations to the initial finite element model (FEM) such that the adjusted FEM matches closely the experimentally measured modal properties. The adjusted FEM consists of the original mass matrix and the adjusted stiffness and damping matrices given by

$$\begin{aligned} K_a &= K - B_0 F C_0 \\ D_a &= D - B_0 F C_1 \end{aligned} \quad (4.2.5)$$

Assume that modal analysis of the structure under consideration has been performed and that  $p$  modes ( $p$  eigenvalues  $\lambda_{e_i}$ , and  $p$  eigenvectors  $\underline{v}_{e_i}$ ) have been identified. As discussed earlier in Chapter 2, in practice  $p$  is typically much less than  $n$ . The feedback gain matrix  $F$ , such that the adjusted FEM eigendata matches the experimental modal parameters, is computed using standard eigenstructure assignment theories (Andry et al. 1983):

$$F = [Z - A_u V] \left\{ [C_0 \ C_1] \begin{bmatrix} W & \bar{W} \\ W\Lambda & \bar{W}\Lambda \end{bmatrix} \right\}^{-1} \quad (4.2.6)$$

where

$$A = \begin{bmatrix} 0 & I_{n \times n} \\ -M^{-1}K & -M^{-1}D \end{bmatrix} \quad B = \begin{bmatrix} 0 \\ -M^{-1}K \end{bmatrix} \quad T = [B \ P]$$

$$\tilde{A} = T^{-1}AT = \begin{bmatrix} A_u \\ A_l \end{bmatrix} \quad \tilde{B} = T^{-1}B = \begin{bmatrix} I_{m \times m} \\ 0 \end{bmatrix}$$

$$V = T^{-1} \begin{bmatrix} W & \bar{W} \\ W\Lambda & \bar{W}\Lambda \end{bmatrix} \quad \Lambda = \text{diag}(\lambda_{e_1}, \lambda_{e_2}, \dots, \lambda_{e_p}) \quad W = [\underline{v}_{ea_1}, \underline{v}_{ea_2}, \dots, \underline{v}_{ea_p}]$$

$$Z = S^{-1} \left[ \begin{bmatrix} W \\ W\Lambda \end{bmatrix} \Lambda \begin{bmatrix} \bar{W} \\ \bar{W}\Lambda \end{bmatrix} \bar{\Lambda} \right] \quad T^{-1} = \begin{bmatrix} S_1 \\ S_2 \end{bmatrix}$$

The overbar in the above equations indicates the complex conjugate operator. The vectors  $\underline{v}_{ea_i}$  in matrix  $W$  are the expanded “best achievable” eigenvectors associated with the experimentally measured eigenvectors  $\underline{v}_{e_i}$ . An explanation of the concept of “best

achievable" eigenvectors is discussed in Section 4.2.3. The submatrix  $P$  of matrix  $T$  is arbitrary as long as  $T$  is invertible.

At this point, the variables  $B_0$ ,  $C_0$  and  $C_1$  are still arbitrary. A random selection of these variables will usually result in nonsymmetric perturbation matrices and, consequently nonsymmetric adjusted stiffness and damping matrices. This clearly conflicts with the fundamental symmetry requirement of most structures' FEM. In the formulation of Inman and Minas (1990), the resulting perturbation matrices from the pseudo-controller are forced to be symmetric through a nonlinear unconstrained optimization problem. Zimmerman and Widengren (1989, 1990) proposed a non-iterative and computationally more efficient approach to satisfy the symmetry requirement. This approach is discussed in the following section.

#### 4.2.2 Symmetric Eigenstructure Assignment Formulation

The perturbation matrices are symmetric if the following conditions are met,

$$\begin{aligned} B_0 F C_0 &= C_0^T F^T B_0^T & (a) \\ B_0 F C_1 &= C_1^T F^T B_0^T & (b) \end{aligned} \quad (4.2.7)$$

At this point, two additional assumptions are made. As a prerequisite to the existence of the inverse of some matrices used in the computations, it is assumed that the number of pseudo sensors and actuators is equal to twice the number of measured modes ( $m=r=2p$ ). The other assumption consists of restricting the matrices  $C_0$  and  $C_1$  by the conditions

$$\begin{aligned} C_0 &= G_0 B_0^T & (a) \\ C_1 &= G_1 B_0^T & (b) \end{aligned} \quad (4.2.8)$$

where  $G_0$  and  $G_1$  are  $m \times m$  invertible matrices. A substitution of Eq. (4.2.8) into Eq. (4.2.7) simplifies the symmetry conditions to the following relationships,

$$\begin{aligned} F G_0 &= G_0^T F^T & (a) \\ F G_1 &= G_1^T F^T & (b) \end{aligned} \quad (4.2.9)$$



By using the conditions in Eq. (4.2.9), along with the expression for the feedback gain matrix (Eq. (4.2.6)), a necessary but not sufficient condition on  $G_0$  and  $G_1$ , for symmetric perturbation matrices, is expressed in the form of a generalized algebraic Riccati equation,

$$A_1X + XA_2 + XA_3X + A_4 = [0] \quad (4.2.10)$$

where

$$X = G_1^{-1}G_0$$

$$A_1 = \left[ \sigma^* \alpha^{-1} \sigma^{-1} (\alpha^* \tau^* - \tau \alpha) - \tau^* \right] \sigma^{-*}$$

$$A_2 = \tau^* \alpha^{-1} \sigma^{-1} \alpha^*$$

$$A_3 = \tau^* \alpha^{-1} \sigma^{-1} (\alpha^* \tau^* - \tau \alpha) \sigma^{-*}$$

$$A_4 = \sigma^* \alpha^{-1} \sigma^{-1} \alpha^* - I_{m \times m}$$

$$\tau = \begin{bmatrix} W^* B_0 \\ \overline{W}^* B_0 \end{bmatrix} \quad \sigma = \begin{bmatrix} \Lambda W^* B_0 \\ \overline{\Lambda W}^* B_0 \end{bmatrix} \quad \alpha = Z - A_1 V$$

The matrices  $A_1$ ,  $W$ ,  $Z$ , and  $V$  are defined in Eqs. (4.2.6). The superscript  $( )^{-*}$  indicates the inverse of the complex conjugate transpose matrix. Equation (4.2.10) can be solved for  $X$  by using the techniques described in the papers of Potter (1966) or Martensson (1971). In general, there exist multiple solutions ( $X$ 's) to this generalized algebraic Riccati equation. With all solutions computed, the next step is to decompose these solutions into  $G_0$ 's and  $G_1$ 's. It is shown in the paper by Zimmerman and Widengren (1989) that for a given solution  $X$ , any selection of  $G_0$  and  $G_1$  satisfying  $X = G_1^{-1}G_0$  results in the same adjusted damping ( $D_a$ ) and stiffness ( $K_a$ ) matrices. Hence, either  $G_1$  (or  $G_0$ ) can be chosen arbitrarily, as long as its inverse exists. Then,  $G_0$  (or  $G_1$ ) is calculated from the relationship  $X = G_1^{-1}G_0$ .

For each set ( $G_0$ ,  $G_1$ ), a feedback gain matrix  $F$  is calculated from Eq. (4.2.6), and the corresponding adjusted damping ( $D_a$ ) and stiffness ( $K_a$ ) matrices are computed using Eqs.

(4.2.5). At this point, a rationale is proposed to choose the most meaningful adjusted damping and stiffness matrices. Among all computed sets  $(D_a, K_a)$ , it is apparent that only the ones that are real and symmetric are acceptable. When dealing with a model refinement problem, among all acceptable solutions, the final selection could be made by choosing the set  $(D_a, K_a)$  that minimizes the cost function,

$$J = q \| K - K_a \|_F + \| D - D_a \|_F \quad (4.2.11)$$

$$\text{where } q = \frac{\| D \|_F}{\| K \|_F}$$

Clearly, this process selects the set  $(D_a, K_a)$  that results in a minimum change from the original set  $(D, K)$ . The scale factor  $q$  in Eq. (4.2.11) is used to give equal weight to the changes in  $D$  and  $K$ . For the damage detection problem, there is no unique rationale to choose the “best” set  $(D_a, K_a)$ . A physically intuitive approach is to use engineering judgement in selecting the “best” updated model. Thus, all acceptable “adjusted” sets of solutions should be inspected to determine which best provides information concerning the state of damage.

#### 4.2.3 Best Achievable Eigenvectors

From standard eigenstructure assignment theory (Andry, et al. 1983), it is shown that the measured eigenvectors are not always exactly assignable to the adjusted finite element model. In fact, it can be shown that the measured eigenvectors are assigned exactly if and only if they lie in their respective achievable subspace. The achievable subspace associated to the  $i^{\text{th}}$  mode is defined by

$$L_i = (M\lambda_i^2 + D\lambda_i + K)^{-1}B_0 \quad (4.2.12)$$

where  $\lambda_i$  is the measured eigenvalue of the  $i^{\text{th}}$  mode. When all  $n$  components of the experimental eigenvectors are available, the  $i^{\text{th}}$  best achievable eigenvectors is defined as the

least square projection of the  $i^{\text{th}}$  experimental eigenvector  $\underline{v}_{e_i}$  on the  $i^{\text{th}}$  achievable subspace  $L_i$ . This projection is schematically illustrated in Figure 4.1.

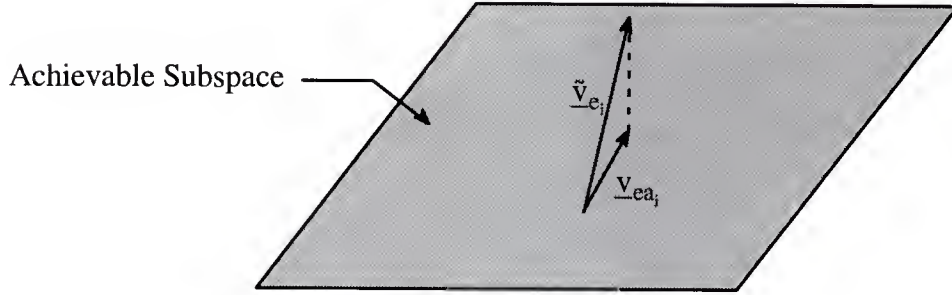


Figure 4.1 Best Achievable Eigenvector Projection.

This best achievable eigenvector is given by

$$\underline{v}_{ea_i} = L_i [L_i^* L_i]^{-1} L_i^* \underline{v}_{e_i} \quad (4.2.13)$$

When only a subset  $s$  of the eigenvector components are measured,  $s < n$ , the least square projection discussed above can be used to simultaneously expand and project the measured eigenvectors. In this case, the  $i^{\text{th}}$  expanded best achievable experimental eigenvector is given by

$$\underline{v}_{ea_i} = L_i [\tilde{L}_i^* \tilde{L}_i]^{-1} \tilde{L}_i^* \underline{v}_{e_i} \quad (4.2.14)$$

where  $\tilde{L}_i$  are the rows of  $L_i$  which correspond to the measured eigenvector components. Notice that the calculation of the  $p$  achievable subspace using Eq. (4.2.13) requires  $p$  inversions of an  $n \times n$  matrix. Although the matrix to be inverted is typically banded, this may present a practical computational burden when dealing with large FEMs. The next section discusses an approach that does not require the actual computation of the achievable subspaces and hence avoids this computational burden.

#### 4.2.4 Selection of $B_0$ : The Subspace Rotation Method

So far, the control influence matrix has not yet been completely defined. The preceding formulation suggest that different  $B_0$  may possibly result in different adjusted FEM. Hence, it is essential to develop a physically meaningful rationale to select  $B_0$ .

Zimmerman and Widengren (1989, 1990) proposed an approach, termed the mode selection method, that consists in selecting  $B_0$  such that the unmeasured modes of the structure are nearly unchanged. In other word,  $B_0$  is selected such that only the measured modes of the structure are corrected. This selection technique fixes the achievable subspaces in which the eigenvectors must lie, and hence places a limitation on the assignment process. In most studied cases, the experimental eigenvectors were not assigned exactly since their assignment “success” depends on the locations vis-a-vis the achievable subspaces set by the selection of  $B_0$ .

In this work, a new method of selecting  $B_0$ , termed the subspace rotation method, is proposed. The subspace rotation method is based on selecting  $B_0$  such that the measured eigenvectors lie exactly in the achievable eigenvectors subspaces. This procedure is illustrated in Figure 4.2 and is accomplished by setting  $B_0$  as

$$B_0 = \begin{bmatrix} b_{r_1}, & b_{r_2}, & \dots, & b_{r_p} & | & b_{i_1}, & b_{i_2}, & \dots, & b_{i_p} \end{bmatrix} \quad (4.2.15)$$

$$\left. \begin{array}{l} \text{where } b_{r_j} = \text{real} \left[ \left( M\lambda_j^2 + D\lambda_j + K \right) \underline{v}_{e_j} \right] \\ b_{i_j} = \text{imaginary} \left[ \left( M\lambda_j^2 + D\lambda_j + K \right) \underline{v}_{e_j} \right] \end{array} \right\} \quad j = 1, \dots, p$$

where  $\underline{v}_{e_j}$  is the eigenvector associated with the  $j^{\text{th}}$  experimentally measured mode, and it is assumed that all  $n$  components of the experimental eigenvectors are available. This could be accomplished by any of the procedures discussed in Chapter 2. Clearly, when  $B_0$  is selected as shown in Eq. (4.2.15), the measured expanded eigenvectors lie exactly in the achievable subspaces defined in Eq. (4.2.12). Hence, there is no need for the projection operations defined in Eq. (4.2.13). This eliminates the required  $p$  inverses of  $n \times n$  matrices

involved in computing the achievable subspaces. As will be seen in Chapters 5 and 6, the elements of  $B_0$ , as defined by Eq. (4.2.15), give an indication to the pseudo-controller about the extent of modification of each DOF in order for the structure to exhibit the  $j^{\text{th}}$  measured eigenvalue and eigenvector.

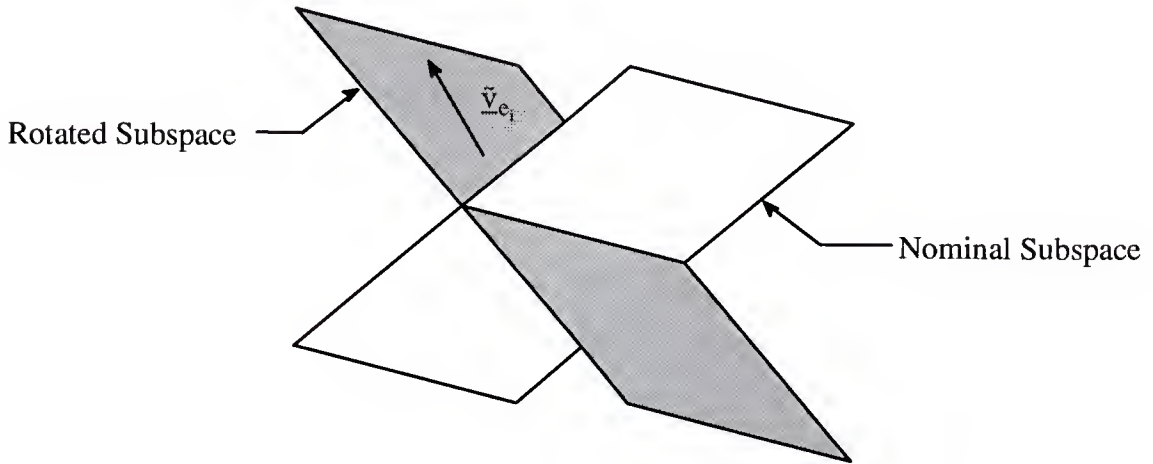


Figure 4.2 Rotation of the Achievable Subspace.

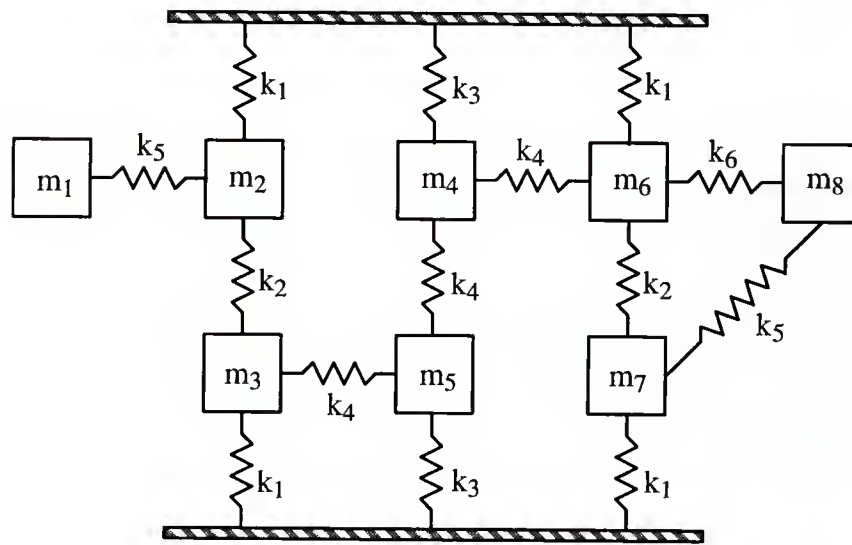
### 4.3 Numerical Illustrations

In this section, the characteristics of the proposed enhancement to the symmetric eigenstructure assignment model refinement algorithm (SEAMRA) are evaluated and compared to other refinement techniques for two example problems. The first problem is a widely-used spring-mass computer simulated example (Kabe, 1985). It is used here for the purposes of illustrating model refinement for a large local discrepancy, analogous to a damage detection situation. The phenomena of global/local mode switching and load path preservation are examined in this problem. The second problem is used to illustrate the characteristics of the enhanced SEAMRA in updating the finite element model (FEM) of a laboratory cantilever beam using actual measured modal parameters.



#### 4.3.1 Damage Detection: Kabe's Problem

Kabe's eight degree of freedom spring-mass system is shown in Figure 4.3. The mass and stiffness properties of the system are included in the figure. This problem presents a challenging situation for damage detection in that stiffness values of various magnitudes are included. The model exhibits closely-spaced frequencies and both local and global modes of vibration.



$$m_1 = 0.001 \quad m_8 = 0.002 \quad m_j = 1.0 \quad j = 2, \dots, 7$$

$$k_1 = 1000 \quad k_2 = 10 \quad k_3 = 900 \quad k_4 = 100 \quad k_5 = 1.5 \quad k_6 = 2.0$$

Figure 4.3 Kabe's Problem.

A variation of Kabe's original problem is used here. Rather than the standard initial model commonly used, which has incorrect values for all of the connecting springs, only a single spring constant is changed. This is reflective of the fact that damage may occur as a large local change in the stiffness of a structural member.

#### 4.3.1.1 Local to Global Mode Change

In the first problem, Kabe's initial model is only incorrect for the spring between masses 3 and 5. A value of 500, five times that of the exact spring, is assumed in this problem. Changing the spring value from 500 to 100 also causes a local mode of vibration to be replaced by a global mode, thus presenting a difficult challenge for damage detection.

Figure 4.4 presents element-by-element stiffness matrix results for applying the Baruch and Bar Itzhack update (1978) and the symmetric eigenstructure assignment model refinement algorithm. Baruch Damage indicates that the update was made using Baruch and Bar Itzhack's algorithm. SEA-M Damage indicates that the update was made using the SEAMRA with  $B_0$  selected by using the modal (M) selection method. SEA-SR Damage indicates that the update was made by using the SEAMRA with  $B_0$  selected using Subspace Rotation (SR) method. The x-coordinate on all plots are the indices of a column vector constructed by storing the upper triangular portion of the stiffness matrix in a column vector. The y-coordinate on each plots consists of the difference between the updated stiffness matrix elements and the original stiffness matrix.

In the first case, as shown in Figure 4.4, it is assumed that only the fundamental mode of vibration is measured, but all eigenvector components have been measured. Thus, no expansion of eigenvectors is required. It is evident from Figure 4.4 that the Baruch update is unable to discern the damage, but that both the SEA-M and SEA-SR are able to clearly locate the damage. In fact, the SEA-SR was able to exactly reproduce the correct stiffness matrix. This was true independent of which mode was used in the update. Also, it should be noted that the Baruch update tends to focus elemental changes in the third and fifth row of the stiffness matrix, indicating the possibility of damage between these degrees of freedom, but certainly giving no clear indication to the extent of damage. As is evident from the plot, the Baruch update has spread errors over several elements. Using the algorithm of Lin (1990), the damage vector is given as  $\underline{\alpha} = [1.0 \ 0.93 \ 0.72 \ 0.83 \ 0.70 \ 0.90 \ 0.97 \ 1.0]^T$ , where the element number corresponds to the structural DOFs and a number less than 1 indicates the

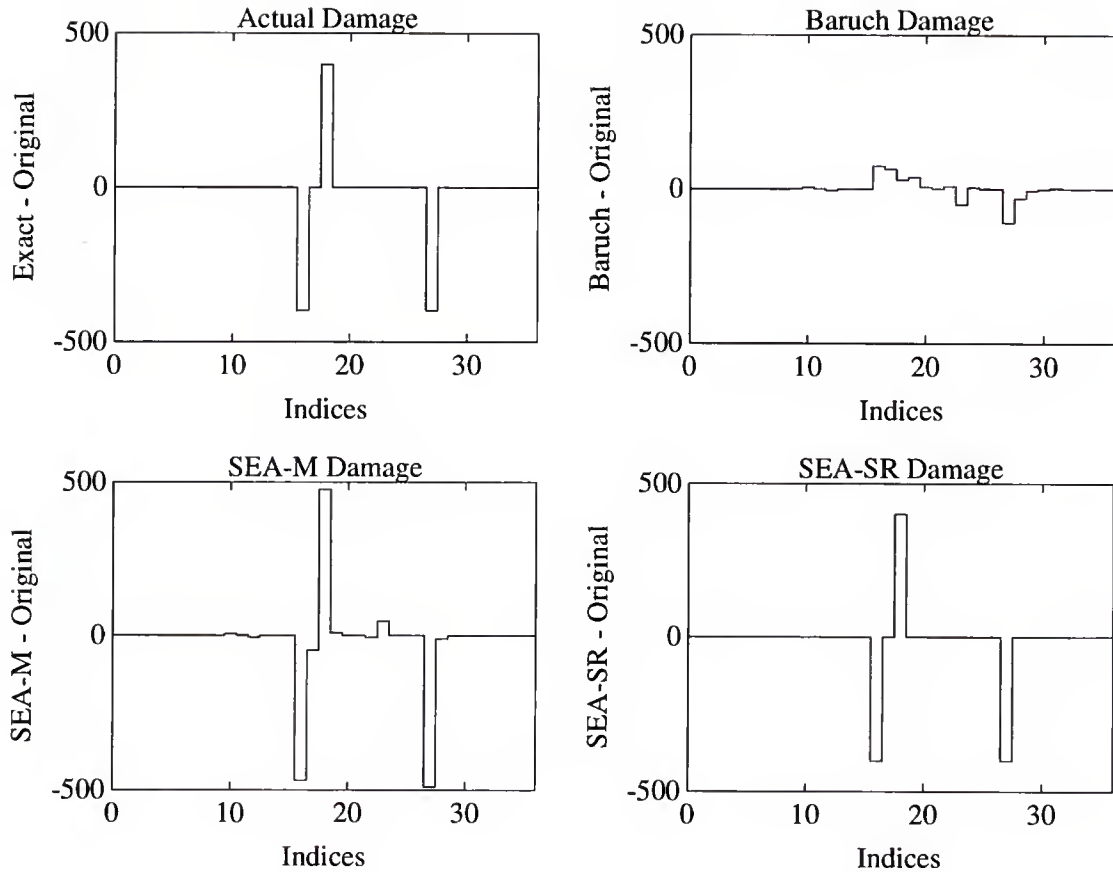


Figure 4.4 Results for Kabe's Problem using the 1st Mode, Full Eigenvector.

possibility of damage affecting that DOF. It is obvious that DOFs 3 and 5 are affected by damage, but the results also indicate strong damage of DOF 4.

In the second case, as shown in Figure 4.5, it is assumed that the first three modes of vibration have been measured, but only the first three components of the eigenvectors have been measured. The eigenvectors components were expanded for the Baruch update using dynamic expansion (Berman and Nagy, 1983) with subsequent orthogonalization (Baruch and Bar Itzhack, 1978). The least squares expansion was used for the SEA-M update. The SEA-SR update utilized the orthogonal Procrustes expansion (Chapter 2). In comparing Figure 4.5 to Figure 4.4, it is clear that the damage detection capabilities of all three algorithms have been degraded when using expanded mode shapes, even though more modes have been measured. However, both the SEA-M and SEA-SR updates give a clear

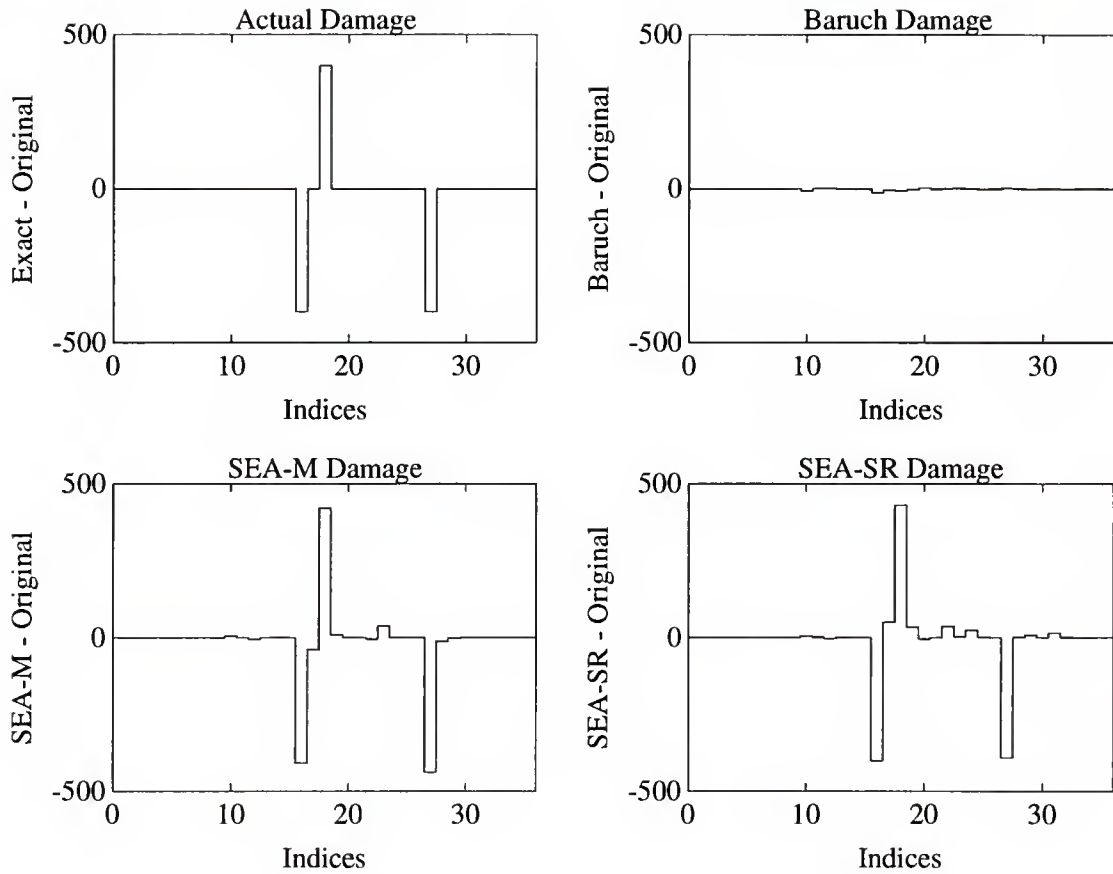


Figure 4.5 Results for Kabe's Problem using Modes 1, 2, 3, and Eigenvectors Components 1, 2, 3.

indication to both the location and extent of damage. Using Lin's algorithm, the damage vector is given as  $\underline{\alpha} = [1.0 \ 0.81 \ 0.75 \ 0.83 \ 0.82 \ 0.79 \ 0.85 \ 1.0]^T$ . It is difficult from inspection of  $\alpha$  to determine the location of damage.

The effect of applying the iterative load path algorithm described in Chapter 2 in the update procedure is shown in Figure 4.6. For the Baruch update, 100 iterations were performed. For the SEA-M and SEA-SR updates 2 and 3 iterations respectively, were performed. The iterations were halted early for both SEA updates because the discrepancy between the eigenstructure before and after masking was within the numerical precision of the symmetric eigenstructure assignment software. It is seen that the load path enforcement further enhances the damage detection capability of both SEA updates.

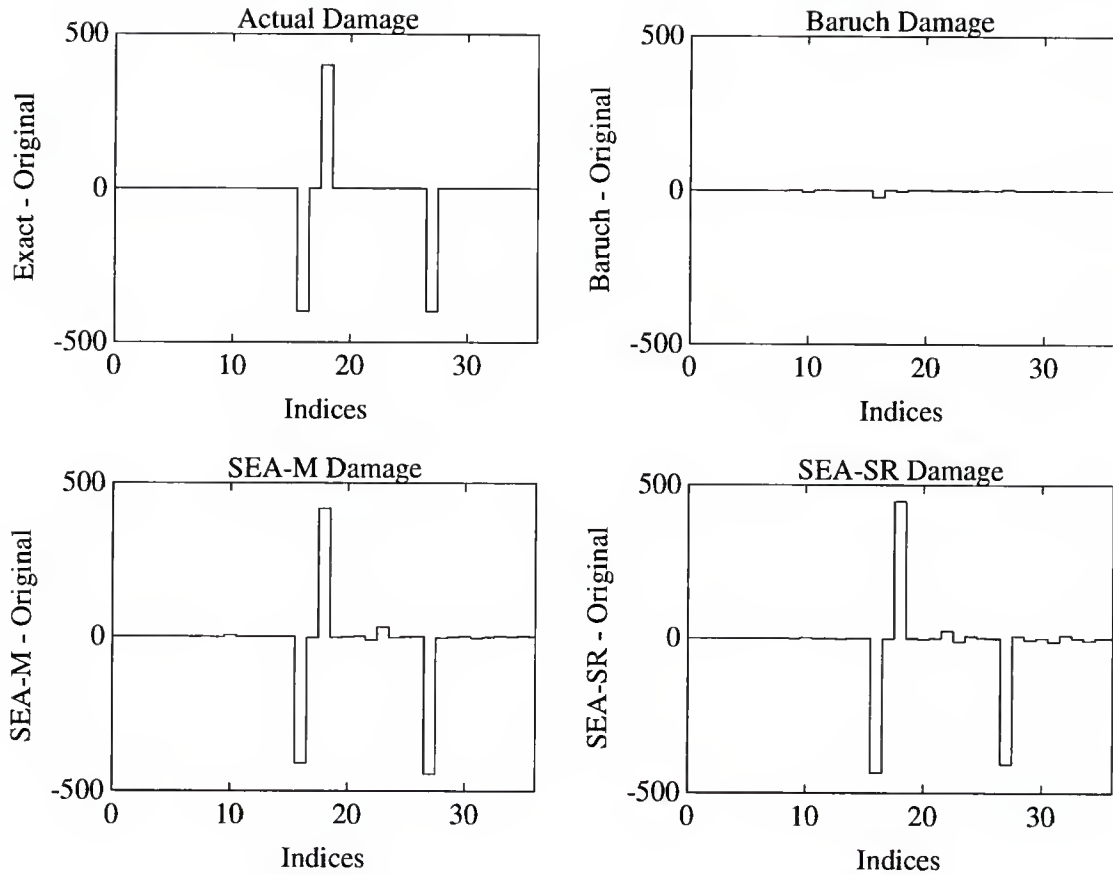


Figure 4.6 Results for Kabe's Problem using Load Path Preservation, Modes 1, 2, 3, and Eigenvectors Components 1, 2, 3.

#### 4.3.1.2 Consistent Modes

In the second problem, the initial model is only incorrect for the spring between masses 4 and 6. A value of 200, two times that of the exact spring, is assumed in this problem. In this problem, all global and local modes remain global and local modes respectively after damage. It should be noted that finding a problem with this feature was difficult.

In the first case, as shown in Figure 4.7, it is assumed that only the fundamental mode of vibration is measured, but all eigenvector components have been measured. It is evident from Figure 4.7 that the Baruch and SEA-M update are unable to discern the damage, but that the SEA-SR is able to clearly locate damage. In fact, the SEA-SR was able to exactly reproduce the correct stiffness matrix. Again, this was true independent of which mode was



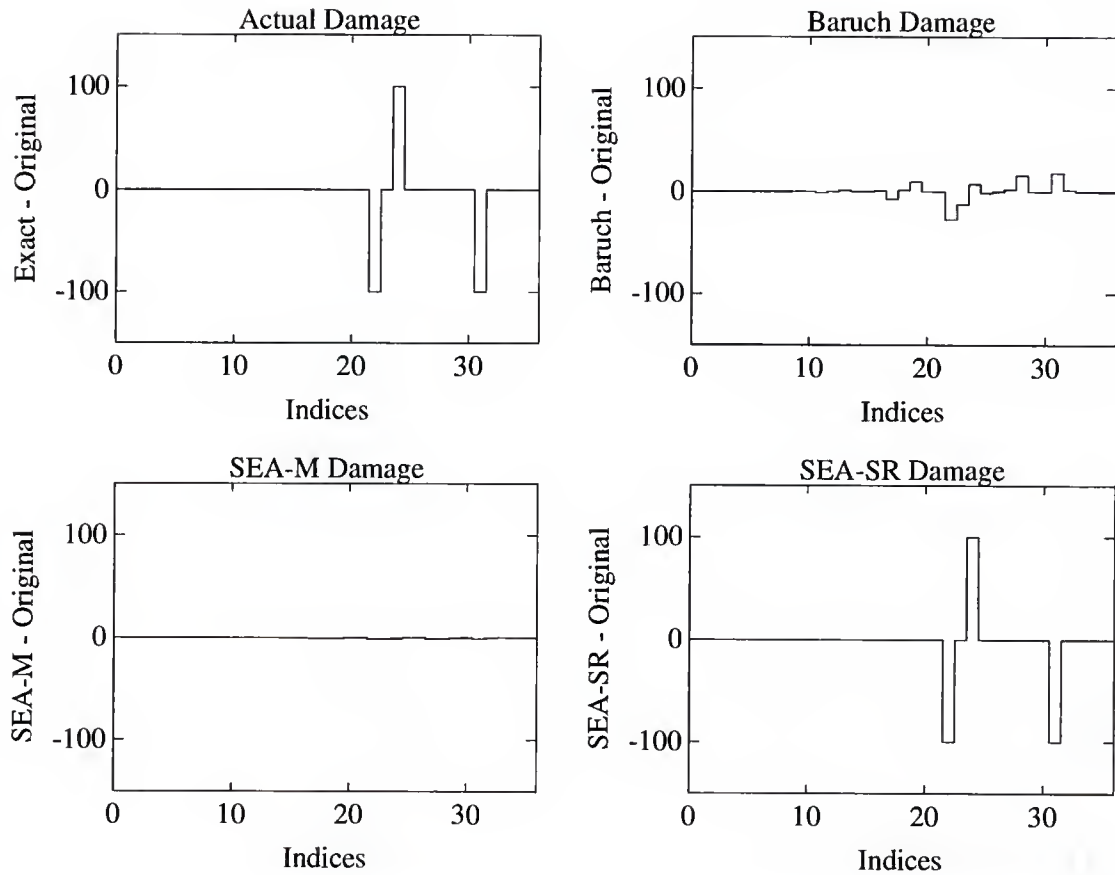


Figure 4.7 Results for Kabe's Problem using the 1st Mode, Full Eigenvectors.

used in the update. It should be noted that the Baruch and SEA-M update tends to focus elemental changes in the fourth and sixth rows of the stiffness matrix, indicating the possibility of damage between these degrees of freedom, but certainly giving no clear indication to the extent of damage. Using Lin's algorithm, the damage vector is given as  $\alpha = [1.0 \ 0.98 \ 0.92 \ 0.85 \ 0.87 \ 0.84 \ 0.95 \ 1.0]^T$ . This algorithm does not clearly identify the damage location.

In the second case, as shown in Figure 4.8, it is assumed that the first three modes of vibration have been measured, but only DOFs 1,3, and 6 of the eigenvectors have been measured. In comparing Figure 4.8 to Figure 4.7, it is clear that the damage detection capability of all three algorithms has again been degraded when using expanded mode shapes. Only the SEA-SR update gives a clear indication to the location of damage, but is

unable to predict the exact extent. Using Lin's algorithm, the damage vector is given as  $\underline{\alpha} = [0.99 \ 0.18 \ 0.55 \ 0.34 \ 0.52 \ 0.33 \ 0.41 \ 1.0]^T$ . Again, it is difficult from inspection of  $\underline{\alpha}$  to determine the location of damage. In fact, inspection of  $\underline{\alpha}$  indicates that DOF 2 is the most likely damaged DOF.

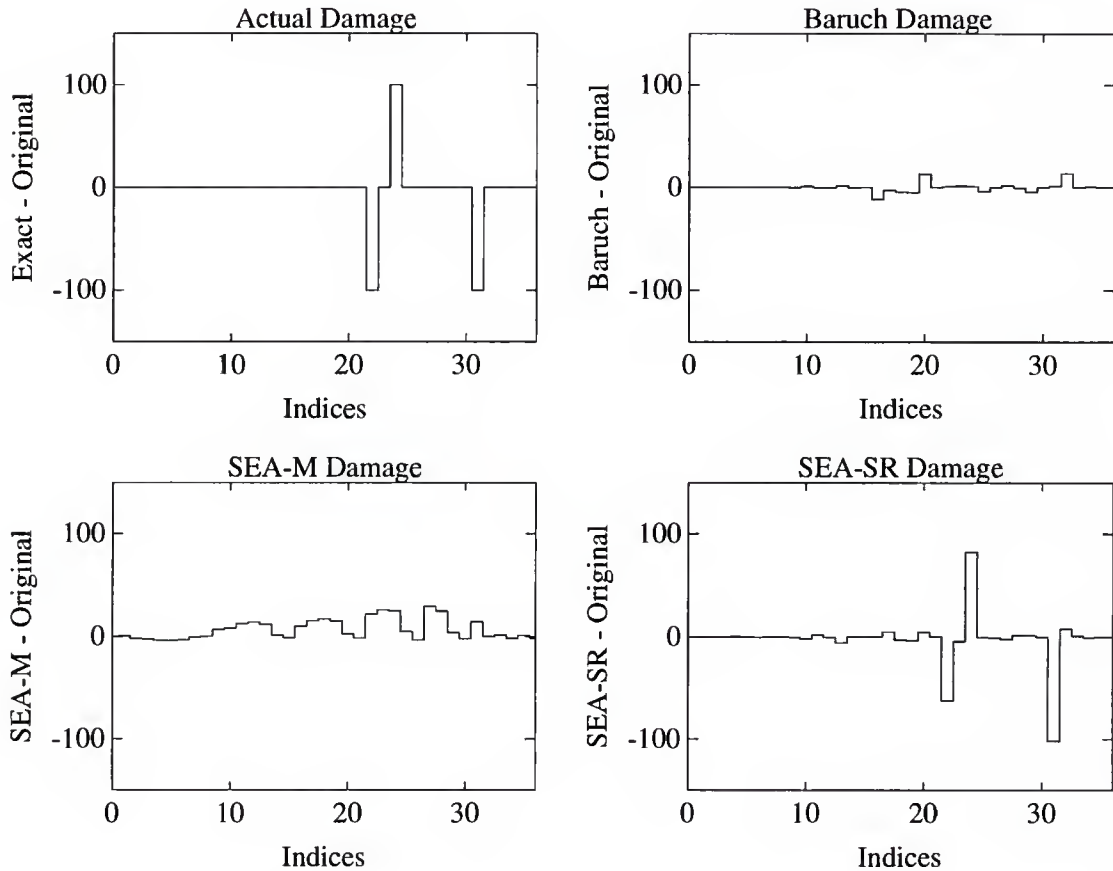


Figure 4.8 Results for Kabe's Problem using Modes 1, 2, 3, and Eigenvectors Components 1, 2, 6.

It should be noted that in this problem, it was critical to have the proper DOFs measured. When the second test case was run with the first three DOFs measured, no algorithm was able to locate damage. In this case, the eigenvectors components were relatively unaffected by damage, thus causing substantial error in the eigenvector expansion process.

### 4.3.2 Model Refinement of a Cantilever Beam: Experimental Study

#### 4.3.2.1 Modal Test Description

The structure used in this investigation is the aluminum cantilevered beam shown in Figure 4.9. The dimensions and material properties of the beam are given in Table 4.1. Experimental modal analysis of the beam was performed to measure its modal properties. Six equally spaced translational degrees of freedom shown in Figure 4.9 were selected as measurement locations. The modal properties of the first three modes of vibration were determined using frequency domain techniques and single degree of freedom curve fitting algorithms. The excitation source used in the testing was an impact hammer and the driving point measurement was an accelerometer mounted at the free end of the beam. Impact and exponential windows were utilized to improve frequency response calculations. At each measured degree of freedom, five frequency response measurements were made and averaged to reduce the effects of measurement noise. Natural frequencies, damping ratios and mode shapes of the beam's first three modes of vibration were identified and are reported in Tables 4.2 and 4.3.

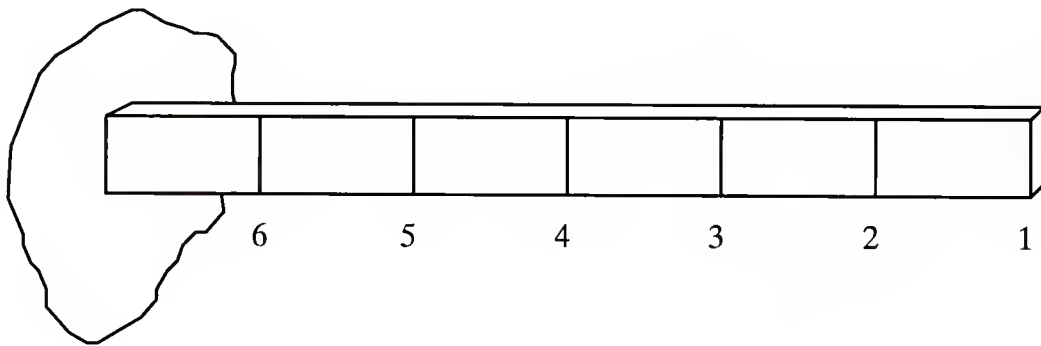


Figure 4.9 Experimental Cantilever Beam.

Table 4.1 Structural Properties of the Cantilever Beam.

Length – 0.84 m
Mass/Length – 2.364 kg/m
Moment of Inertia – $3.02\text{e-}9 \text{ m}^4$
Youngs Modulus – 70 GPa

Table 4.2 Measured Natural Frequencies and Damping Ratios of the Cantilever Beam.

Mode #	Natural Frequency (Hz)	Damping Ratio (%)
1	7.25	4.41
2	45.55	0.68
3	127.01	0.33

Table 4.3 Measured Mode Shapes of the Cantilever Beam.

Mode	1	2	3
DOF			
1	1.00	1.00	1.00
2	0.95	0.16	-0.30
3	0.65	-0.53	-0.61
4	0.36	-0.72	0.20
5	0.15	-0.52	0.75
6	0.03	-0.12	0.28

#### 4.3.2.2 Finite Element Model Description

A twelve DOF undamped finite element model (FEM) of the beam was generated using six equal length beam elements as shown in Figure 4.9. The beam element has two degrees of freedom (DOFs) at each node; bending and rotation. This model was then reduced using

Guyan reduction (1965) eliminating the rotational degrees of freedom. There are several possible errors affecting the accuracy of this FEM. The most obvious is the fact that a perfect cantilever condition is assumed. In addition, an artificial error was purposely introduced by selecting the Young's Modulus higher than that often assumed for aluminum.

#### 4.3.2.3 Application of the SEAMRA.

Because the “true” finite element model is unknown, a comparison between the “true” and updated structural matrices is not possible. Besides such comparison, a fair and useful judgement on the quality of SEAMRA updating capability can be obtained by comparing actual experimental frequency response functions with those predicted by the initial and updated FEMs. Figure 4.10 shows a comparison of frequency response functions measured between degrees of freedom 1 and 3 (i.e. sensor measurement at DOF 1 and impact excitation at DOF 3). The solid curve corresponds to the experimental data, while the dotted line corresponds to that predicted by the original analytical FEM. It is apparent that the discrepancies between the frequency response function increases as the frequency of excitation increases. This is in part due to the fact that the assumption of a perfect cantilever condition affects the higher modes of vibration to a greater extent. The dashed lines in this figure corresponds to the SEA-SR updated finite element model. It is clear from this comparison that the SEA-SR provided a great deal of improvement to the original analytical FEM. Inspection of the updated stiffness matrix indicates that changes occur throughout the matrix, indicating that the discrepancy between the original and refined FEMs was due to degradation of some global structural property (Young's Modulus), as opposed to some form of local damage, as seen in the previous problem.

### 4.4 Discussion of the SEAMRA's Formulation

In some problems SEAMRA in conjunction with either the subspace rotation or the modal selection method, failed to find a symmetric updated FEM (symmetric  $D_a$  and  $K_a$ ). This shortcoming was especially encountered in practical situations when the experimental



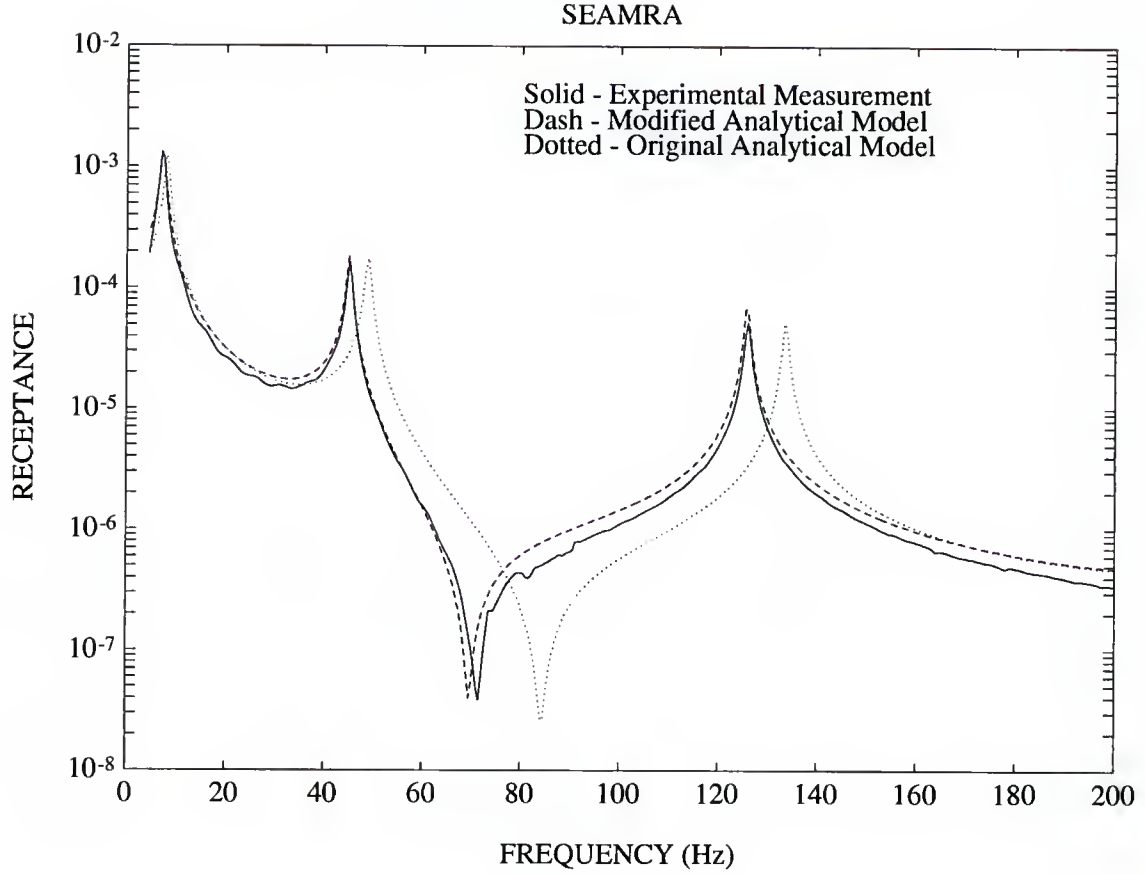


Figure 4.10 Experimental and Analytical Frequency Response Functions of the Cantilever Beam.

modal properties were corrupted by measurement errors. This can be attributed to the fact that there is no symmetric updated FEM that is consistent with the present SEAMRA's formulation. Recall that SEAMRA's modifications to the initial stiffness and damping matrices in its updating process are given by

$$\begin{aligned} \Delta K &= B_0 H_0 B_0^T & \text{with } H_0 &= F G_0 \\ \Delta D &= B_0 H_1 B_0^T & \text{with } H_1 &= F G_1 \end{aligned} \quad (4.5.1)$$

Clearly, from Eq. (4.5.1), the perturbations (i.e. modifications) to the initial stiffness and damping matrices are constrained by the relationship

$$\text{range}(\Delta K) = \text{range}(\Delta K^T) = \text{range}(\Delta D) = \text{range}(\Delta D^T) \quad (4.5.2)$$

This relationship can always be satisfied for the cases when the experimental modal properties are consistent with an update in which (i) either  $\Delta K$  or  $\Delta D$  is zero or (ii)  $\Delta K$  is proportional to  $\Delta D$  ( $\Delta K = \beta \Delta D$ ,  $\beta$  is a scalar). For all other cases, SEAMRA might fail to produce symmetric  $\Delta K$  and  $\Delta D$ . A more flexible and general formulation that accounts for such shortcoming is proposed in Section 6.5 of Chapter 6. The formulation as presented in Chapter 6 is more elegant, efficient and guarantees, for all situations, a symmetric updated FEM.

#### 4.5 Summary

A previously developed model refinement algorithm based on the general mathematical framework of eigenstructure assignment theory (Zimmerman and Widengren, 1989, 1990) has been extended and improved. A technique to enhance eigenvector assignability of the algorithm has been developed. The method consists of rotating the achievable eigenvector subspaces into the experimentally measured eigenvectors. The subspace rotation method, used in conjunction with one of eigenvector expansion techniques discussed in Chapter 2, results in both a decrease in the computational burden as well as an increase in the accuracy of the assigned eigenvectors. Finally, the improved algorithm (SEA-SR) was tested for its suitability for model refinement and structural damage assessment. The performances of SEA-SR in a damage assessment problem on a challenging simulated structure was presented and compared to other algorithms. The results acquired using the SEA-SR were superior.

## CHAPTER 5

### DAMAGE LOCATION: THE SUBSPACE ROTATION ALGORITHM

#### 5.1 Introduction

In this chapter, a computationally attractive algorithm is proposed to provide an insight to the location of structural damage. The proposed algorithm is similar to the Modal Force Error Criteria proposed by several researchers ( Ojalvo and Pilon 1988; Gysin, 1990). However, a greater insight of the Modal Force Error criteria is provided. Further, a new viewpoint which allows for the reduction of the effects of measurement errors in the experimental modal parameters for a certain class of structures is also discussed. As will be shown in the next sections, the proposed damage location algorithm requires only matrix-scalar and matrix-vector multiplication.

#### 5.2 The Subspace Rotation Algorithm: The Direct Method

Assume that an n-DOF finite element model of the “healthy” (undamaged) structure exists. As seen in the earlier chapters, the standard differential equation governing the dynamic motion of such structures is given by

$$M\ddot{\underline{w}} + D\dot{\underline{w}} + K\underline{w} = \underline{0} \quad (5.2.1)$$

where M, D, and K are the n x n analytical mass, damping, and stiffness matrices,  $\underline{w}$  is a n x 1 vector of positions and the overdots represent differentiation with respect to time. The eigenvalue problem associated with Eq. (5.2.1) in second order (lambda) form is given as

$$\left( \lambda_{h_i}^2 M + \lambda_{h_i} D + K \right) \underline{v}_{h_i} = \underline{0} \quad (5.2.2)$$

where  $\lambda_{h_i}$  and  $\underline{v}_{h_i}$  denote the  $i^{\text{th}}$  eigenvalue and eigenvector, respectively, of the pre-damaged “healthy” structure. It is assumed that Eq. (5.2.2) is satisfied for all measured “healthy” eigenvalues/eigenvectors. This can be enforced by correlating the original FEM ( $M, D$ , and  $K$ ), possibly through the use of a model refinement procedure.

Next, consider that the  $p$  eigenvalues and eigenvectors,  $\lambda_{d_i}$  and  $\underline{v}_{d_i}$ , of a post-damage modal survey of the structure are available, in which  $\lambda_{d_i} \neq \lambda_{h_i}$ ,  $\underline{v}_{d_i} \neq \underline{v}_{h_i}$ . In the present formulation, it is assumed that the dimension of the measured eigenvector is the same as the analytical eigenvector. As discussed in Chapter 2, this is true (i) when all FEM DOFs are measured (ii) after the application of an eigenvector expansion algorithm, or (iii) after the application of a finite element model reduction algorithm. The ideal situation would be to measure all FEM DOFs since the eigenvector expansion process would introduce additional errors in the “expanded” eigenvectors and the model reduction process would introduce errors in the FEM. It should be noted that in both cases the additional errors may become significant as the ratio of measured to unmeasured DOFs become smaller.

Let  $\Delta M_d$ ,  $\Delta D_d$ , and  $\Delta K_d$  be the exact perturbation matrices that reflect the nature of the structural damage. For localized damage, the exact perturbation matrices are sparse matrices with the nonzero elements reflecting the state of damage. The lambda equation for the damaged structure is, defined by

$$\left( \lambda_{d_i}^2 (M - \Delta M_d) + \lambda_{d_i} (D - \Delta D_d) + (K - \Delta K_d) \right) \underline{v}_{d_i} = \underline{0} \quad (5.2.3)$$

Although only  $p$  of the  $n$  eigenvalues/eigenvectors are assumed measured,  $p \ll n$ , Eq. (5.2.3) holds for any particular eigenvalue and eigenvector of the damaged structure because the perturbation matrices are assumed to be exact. Grouping all perturbation matrices on the right-hand side defines a damage vector  $\underline{d}_i$ ,

$$\underline{d}_i \equiv Z_{d_i} \underline{v}_{d_i} \quad (5.2.4a)$$

$$= \left( \lambda_{d_i}^2 \Delta M_d + \lambda_{d_i} \Delta D_d + \Delta K_d \right) \underline{v}_{d_i} \quad (5.2.4b)$$

$$\text{where } Z_{d_i} \equiv \lambda_{d_i}^2 M + \lambda_{d_i} D + K$$

Although Eqs. (5.2.4a, b) yield the same damage vector, it should be noted that  $Z_{d_i}$  and the coefficient matrix of Eq. (5.2.4b) are not equal. When the measured eigendata are not corrupted by noise, an inspection of  $\underline{d}_i$  in terms of the Eq. (5.2.4b) reveals that the  $j^{\text{th}}$  element of  $\underline{d}_i$  will be zero when the  $j^{\text{th}}$  rows of the perturbation matrices are zero, i.e. the finite element model for the  $j^{\text{th}}$  degree of freedom is not directly affected by damage. Conversely, a degree of freedom whose finite element model has been affected by damage will result in a nonzero entry in  $\underline{d}_i$ . Thus, the degrees of freedom which have been affected by damage can be determined by inspecting the elements of  $\underline{d}_i$ . Vector  $\underline{d}_i$  as defined in Eq. (5.2.4b) also reveals that only a single mode of vibration needs to be measured exactly to determine the damage locations exactly. This is true in even multiple member damage situations. More importantly, the vector  $\underline{d}_i$  can be determined from the original finite element model (M,D,K) and the measured eigenvalues and eigenvectors,  $\lambda_{d_i}$  and  $\underline{v}_{d_i}$ , using Eq. (5.2.4a). Thus, there is no need to use a model refinement algorithm to attempt to estimate the exact perturbation matrices in order to locate the damage. If the damping term is ignored, Eq. (5.2.4a) is essentially the Modal Force Error criteria as proposed by Ojalvo (1988) for use as a diagnostic “tool” to locate modelling errors in FEMs. A physical interpretation of Eq. (5.2.4a) provided by Ojalvo was “...  $\underline{d}_i$  is the applied harmonic force error distribution, applied at frequency  $\lambda_{d_i}$ , which is necessary to cause the analytical model to vibrate with mode shape  $\underline{v}_{d_i}$  ...”. However, Eq. (5.2.4b) provides a much clearer interpretation of the damage vector  $\underline{d}_i$  for the damage location problem in which the perturbation matrices are sparse.

In practice, the perfect zero/nonzero pattern of the damage vector  $\underline{d}_i$  rarely occurs due to errors present in the experimentally measured eigenvalues and eigenvectors. This scenario was studied and discussed for the undamped case by Gysin (1990) in the context of eigenvector expansion techniques. Gysin (1990) observed that in certain specific cases of eigenvector expansion errors, the damage vector defined by Eq. (5.2.1a) may lead to incorrect conclusions concerning the location of damage. The next section proposes a new



viewpoint which allows for the reduction of the effects of measurement errors for certain classes of structures.

### 5.3 The Subspace Rotation Algorithm: The Angle Perturbation Method

In order to provide an alternative view of the state of damage, Eq. (5.2.4a) is rewritten as

$$d_i^j \equiv \underline{z}_{d_i}^j \underline{v}_{d_i} = \|\underline{z}_{d_i}^j\| \|\underline{v}_{d_i}\| \cos(\theta_i^j) \quad (5.3.1)$$

where  $d_i^j$  is the  $j^{\text{th}}$  component (or  $j^{\text{th}}$  DOF) of the  $i^{\text{th}}$  damage vector,  $\underline{z}_{d_i}^j$  is the  $j^{\text{th}}$  row of the matrix  $\underline{Z}_{d_i}$  and  $\theta_i^j$  is the angle between the vectors  $\underline{z}_{d_i}^j$  and  $\underline{v}_{d_i}$ .

In the case when the measurements are free of error, a zero  $d_i^j$  corresponds to a  $\theta_i^j$  of ninety degrees, whereas a nonzero  $d_i^j$  corresponds to a  $\theta_i^j$  different from ninety degrees. Errors in the experimental measurements of modal parameters will cause slight perturbations in the angles  $\theta_i^j$  that destroy the zero/nonzero pattern of the damage vector. One would initially expect that the components of  $\underline{d}_i$  corresponding to the damaged DOFs would be substantially larger than the other elements. However, by inspecting Eq. (5.3.1), a large  $\underline{d}_i$  component could be due to a  $\underline{z}_{d_i}^j$  row norm substantially larger than other rows of  $\underline{Z}_{d_i}$ , coupled with a slight deviation of  $\theta_i^j$  from ninety degrees due to measurement noise. Hence, when dealing with a structure whose FEM results in  $\underline{z}_{d_i}^j$  row norms of different order of magnitude, it is more reasonable to use the deviation of the angles,  $\theta_i^j$ , from ninety degrees for damage location,

$$\alpha_i^j = \theta_i^j \left( \frac{180^\circ}{\pi} \right) - 90^\circ \quad (5.3.2)$$

$$\text{where } \theta_i^j = \cos^{-1} \left[ \frac{d_i^j}{\|\underline{z}_{d_i}^j\| \|\underline{v}_{d_i}\|} \right]$$

The angle  $\theta_i^j$  is determined from Eq. (5.3.2) and  $\alpha_i^j$  is the  $j^{\text{th}}$  component of  $\underline{\alpha}_i$ .

## 5.4 Practical Issues

### 5.4.1 Cumulative Damage Location Vectors

The discussion in the previous section suggests that for a given mode, the damage is locatable if the perturbation to the angle,  $\theta_i^j$  due to the measurement error is less than the angle perturbation due to the damage. Hence, modes that are highly affected by the damage are expected to provide better assessment to the location of the damage when errors are present in the measured eigendata. As will be seen in example problems (Chapter 7), certain modes are more susceptible to a given state of damage than others. This is mainly due to the fact that different elements of the structure have different levels of contribution to the total strain energy of a given mode (Kashangaki 1992). Furthermore, a particular part of the structure usually has different orders of strain energy contribution for different modes. Usually, if the damage occurs in a region of high strain energy for a given mode, that mode would be highly susceptible to the damage and, hence would reflect the state of damage. To accommodate this type of problem, when the number of measured modes  $p$  is greater than one, two different composite damage vectors may be defined as

$$\underline{d} = \frac{1}{p} \sum_{i=1}^p \frac{\underline{d}_i}{\|\underline{v}_{d_i}\|} \quad (5.4.1)$$

$$\underline{\alpha} = \frac{1}{p} \sum_{i=1}^p |\underline{\alpha}_i| \quad (5.4.2)$$

In Eq. (5.4.1), the damage vectors,  $\underline{d}_i$ , are normalized with respect to their corresponding eigenvectors,  $\underline{v}_{d_i}$ . The reason for this normalization is such that the composite vector ignores the inherent “weighting” of  $\|\underline{v}_{d_i}\|$ , which is usually of different orders of magnitudes for different measured modes. It should be noted that in the multi-mode measurement case, Eq. (5.4.2) is preferable when the values of  $\|\underline{z}_{d_i}^j\|$  are of different orders of magnitude for different measured modes. Again, in practice, the DOFs affected by the damage are expected

to have substantially larger  $\underline{d}$  or  $\underline{\alpha}$ . Finally, the damaged areas of the structure can then be located using the knowledge of the “damaged” DOFs and the connectivity of the FEM.

It is interesting to note that Eqs. (5.2.4a, b) reveal an interesting relationship between various model refinement algorithms. Model refinement techniques attempt to approximate the exact perturbation matrices by using limited modal data, but do so in different manners. However, Eq. (5.2.4a, b) indicates that if the model refinement technique has satisfaction of the eigenproblem as an equality constraint, the calculated perturbation matrices  $\Delta M$ ,  $\Delta D$ , and  $\Delta K$  are constrained to be related to the original finite element model  $M$ ,  $D$  and  $K$  and the measured eigendata by Eqs. (5.2.4a, b).

#### 5.4.2 Eigenvector Filtering Algorithm

In a modal survey, the errors associated with the measured eigenvectors are typically greater than the error associated with the measured eigenvalues. In addition, in the case of incomplete eigenvector component measurements, these measurement errors are often compounded with eigenvector expansion induced errors. A simple eigenvector noise filtering algorithm is proposed assuming the measured eigenvalues to be correct. From the cumulative damage vector defined in Eqs. (5.2.4a) or (5.2.4b), and the original FEM connectivity, the engineer can deduce which DOFs have been damaged. It is reasonable to assume that nonzero elements in each damage vector  $\underline{d}_i$  associated with “undamaged DOFs” are due to eigenvector errors. These elements can then be set to zero. In addition, the magnitude of the elements of  $\underline{d}_i$  at the “damaged” DOFs can be adjusted by using knowledge of DOF connectivity and the properties of the element property matrices connecting the “damaged DOFs.” The element property matrices provide constraints relating the effect of damage on each element DOF. The noise filtering algorithm consists simply of replacing the  $\underline{d}_i$  vectors by  $\underline{d}_{f_i}$ , where  $\underline{d}_{f_i}$  is obtained from  $\underline{d}_i$  as described above. The  $i^{\text{th}}$  filtered eigenvector,  $\underline{v}_{df_i}$ , can then be obtained from solving

$$\left( \lambda_{d_i}^2 M + \lambda_{d_i} D + K \right) \underline{v}_{df_i} = \underline{d}_{f_i} \quad (5.4.3)$$

using Gaussian elimination. In this calculation, the bandedness of typical FEM matrices should be exploited. Essentially, the filtered eigenvector is just the eigenvector that if measured would have produced the damage vector  $\underline{d}_f$ . Experience gained in using the eigenvector filtering algorithm indicates that it is best to use structural matrix properties (M, D, K) that (i) are finite element consistent, and (ii) have not been “corrupted” by measurement noise. By finite element consistent, it is meant that the property matrices can be achieved by a finite element program. Note that measurement noise can be introduced in the property matrix through a FEM refinement algorithm. Hence, the property matrices that should be used are the original property matrices (unrefined). The present eigenvector filtering algorithm can be useful in improving the damage extent assessment. This concept is discussed in Chapters 6 and 7.

### 5.5 Summary

A computationally attractive algorithm to determine the location of damage in structures was developed. The algorithm completely bypasses the general framework of the model refinement problem and involves only matrix-scalar and matrix-vector multiplications. The effect of measurement error in the eigendata was discussed and techniques to reduce these effect were presented. Furthermore, a simple eigenvector filtering algorithm was developed. Practical example problems to illustrate and evaluate the performance of the developed algorithm will be presented in Chapter 7.

## CHAPTER 6

### THE MINIMUM RANK PERTURBATION THEORY

#### 6.1 Background

The theory developed in Chapter 5 is limited to determining the location of structural damage. In a practical situation, it is essential to determine the extent of the damage to get a good estimate about the overall integrity of the structure. In general, the extent problem, as discussed in Chapter 1, has been approached by several researchers using existing model refinement algorithms. The formulations of these algorithms were obviously based on the “model refinement philosophy”: minimum change made to the original FEM. The minimum change constraint has a clear tendency to smear the changes throughout the entire FEM. However, in most cases, this philosophy is not consistent with the effect of structural damage on FEMs. In fact, the effects of structural damage on FEMs are usually “non-minimal” localized perturbations. Structural damage often occurs at discrete locations. The effect of damage on the analytical model is often restricted to just a few elements of the finite element model. The rank of each element mass, damping or stiffness matrix is dependent on the number of degrees of freedom defined by the element and the shape functions utilized. However, it should be noted that in general the element matrices are not of full rank. For example, the rank of the 6x6 element stiffness matrix of a three dimensional truss element is just one. Thus, instead of using the matrix Frobenius norm minimization formulation to arrive at unique perturbation matrices, minimum rank perturbation constraints are enforced.

In this Chapter, a computationally attractive damage extent algorithm is proposed. The proposed damage extent algorithm is a minimum rank perturbation, which is consistent with the effects of many classes of structural damage on a FEM.



Assume that “p damaged” eigenvalues and eigenvectors have been measured and that the original FEM has been corrected such that its modal properties match the measured modal properties of the healthy model. The eigenvalue problem of a damaged structure shown in Eq. (5.2.3), for all p measured modes, can be written in matrix form, as

$$MV_d\Lambda_d^2 + DV_d\Lambda_d + KV_d = \Delta M_d V_d \Lambda_d^2 + \Delta D_d V_d \Lambda_d + \Delta K_d V_d \equiv B \quad (6.1.1)$$

$$\text{where } \Lambda_d = \text{diag}(\lambda_{d_1}, \lambda_{d_2}, \dots, \lambda_{d_p})$$

$$V_d = \begin{bmatrix} \underline{v}_{d_1}, \underline{v}_{d_2}, \dots, \underline{v}_{d_p} \end{bmatrix}$$

$$B = \begin{bmatrix} \underline{d}_1, \underline{d}_2, \dots, \underline{d}_p \end{bmatrix}$$

where all variables have the same definitions as in the previous chapter. Note that matrix B can be determined from the FEM (M, D, K) and the “p” measured eigenvalues and eigenvectors. As discussed earlier, the damage extent problem consist of finding the perturbation matrices,  $\Delta M_d$ ,  $\Delta D_d$ , and  $\Delta K_d$ , such that Eq. (6.1.1) is satisfied. As already discussed in Chapter 2, structures can be modelled using either undamped, proportionally damped or nonproportionally damped finite element models. The proposed extent algorithm is formulated to accommodate all three types of structural models. For each type of model, several scenarios of damage effects are considered. Practical issues that can be used to improve the damage extent estimate are also presented.

## 6.2 The Minimum Rank Perturbation Theory: Theoretical Background

In this section, the theoretical foundation of the Minimum Rank Perturbation Theory (MRPT) is derived. This theory will be extensively used throughout the remainder of this chapter.

**PROPOSITION 6.1** Suppose that  $X, Y \in \mathbb{R}^{n \times p}$  are given where  $p < n$  and  $\text{rank}(X)=\text{rank}(Y)=p$ .

Define  $\mathcal{K}$  to be the set of matrices A in  $\mathbb{R}^{n \times n}$  that satisfy,

$$AX = Y \quad \text{with} \quad A^T = A \quad (6.2.1)$$

Then,

(1.a) If the set  $\mathcal{K}$  is nonempty, the minimum rank of any matrix,  $A$ , in  $\mathcal{K}$  is  $p$ .

Next, define  $\mathcal{K}^p$  to be a subset of  $\mathcal{K}$  comprised of all  $A$  such that  $\text{rank}(A) = p$ .

Then

(1.b) If the matrix  $Y^T X$  is symmetric, then one member of  $\mathcal{K}^p$  is given by

$$A^p = YHY^T \quad (6.2.2)$$

$$\text{with} \quad H = (Y^T X)^{-1}$$

and

(1.c) The matrix defined by Eq. (6.2.2) is the unique member of  $\mathcal{K}^p$ .

Proof:

To prove Proposition (6.1.a), note that Eq. (6.2.1) is exactly satisfied if and only if  $\text{range}(Y)$  is included in  $\text{range}(A)$ , which is also the  $\text{range}(A^T)$  by symmetry. This implies that  $\text{rank}(Y) = p \leq \text{rank}(A)$ .

///

To investigate Proposition (6.1.b), assume that the expanded singular value decomposition of one member,  $A^{pj}$ , of  $\mathcal{K}^p$  to be of the form

$$A^{pj} = U^j \Sigma^j U^{jT} \quad (6.2.3)$$

$$\text{where} \quad U^j = [\underline{u}_1^j, \underline{u}_2^j, \dots, \underline{u}_p^j]$$

$$\Sigma^j = \text{diag}(\sigma_1^j, \sigma_2^j, \dots, \sigma_p^j)$$

where the superscript  $j$  indicates the  $j^{\text{th}}$  family member of  $\mathcal{K}^p$ , the  $\underline{u}_i^j$  are the left and right singular vectors and the  $\sigma_i^j$  are the non-zero singular values of  $A^{pj}$ . In the expanded singular value decomposition, the  $(p+1)$  to  $n$  singular vectors are not shown in the factorization because of their corresponding zero singular values. Note that the left and right singular vectors are the same because  $A^{pj}$  is restricted to be symmetric. For Eq. (6.2.1) to be satisfied, the range of  $Y$ ,  $A^{pj}$ ,  $A^{pjT}$  and  $U^j$  must be equal. Thus, any column of  $Y$  can be written as a linear combination of the  $\underline{u}_i^j$ 's. The matrices  $Y$  and  $U^j$  are then related by a unique  $p \times p$  invertible matrix  $Q^j$ ,

$$Y = U^j Q^j \quad (6.2.4)$$

Substituting Eq. (6.2.4) into Eq. (6.2.3) gives

$$A^{pj} = Y(Q^{j-1}\Sigma^jQ^{j-T})Y^T = YH^jY^T \quad (6.2.5)$$

Thus, each family member is uniquely defined by the factorization of Eq. (6.2.3). From Eq. (6.2.5), it is evident that  $H^j$  is of full rank because its inverse exists ( $H^{j-1} = Q^{jT}\Sigma^{j-1}Q^j$ ).

Inspection of Eq. (6.2.5) reveals that the only unknown term in the factorization is  $H^j$ . By using the factorization of  $A^{pj}$  as defined by Eq. (6.2.5), Eq. (6.2.5) can be rewritten as

$$Y = A^{pj}X = (YH^jY^T)X = Y(H^jY^TX) \quad (6.2.6)$$

Equation (6.2.6) is satisfied if and only if  $H^jY^TX = I_{p \times p}$ , where  $I_{p \times p}$  is the  $p \times p$  identity matrix. This is true because  $Y$  and  $X$  are of full column rank. Thus,  $H^j$  is uniquely calculated to be

$$H^j = (Y^TX)^{-1} \quad (6.2.7)$$

///

Proposition (6.1.c) follows immediately by inspecting the right hand side of Eq. (6.2.7). Inspection reveals that  $H^j$  is the same for all members of  $\mathcal{K}^p$ . This fact, in conjunction with

Eq. (6.2.5) leads to the conclusion that  $A^{pj}$  is the unique member of the set  $\mathcal{K}^p$ . This member is given by Eq. (6.2.2).

///

■

At this point, the MRPT as defined in Proposition 6.1 assumes that the matrices  $X$  and  $Y$  are of full rank. In practical uses, as will be seen later, matrix  $X$  is usually of full rank. The rank requirement on matrix  $Y$  can be of some concern since it is directly related to the rank of matrix  $A$ . The next proposition addresses the case in which matrix  $Y$  is rank deficient.

**PROPOSITION 6.2** Suppose that  $X, Y \in \mathbb{R}^{n \times m}$  are given and  $\text{rank}(X)=m$  and  $\text{rank}(Y)=p$ , where  $p < m < n$ . Further, suppose that the matrix  $Y^T X$  is symmetric.

Define  $\mathcal{U}$  to be the set of matrices  $A$  in  $\mathbb{R}^{n \times n}$  that satisfies the problem,

$$A^p X^p = Y^p \quad \text{with} \quad (A^p)^T = A^p \quad (6.2.8)$$

where the superscript  $p$  indicates a rank  $p$  matrix. In Eq. (6.2.8),  $X^p, Y^p \in \mathbb{R}^{n \times p}$  are corresponding full rank submatrices of  $X$  and  $Y$ .

Then

The set  $\mathcal{U}$  contains a single member,  $A^p$ , that can be calculated from Eq. (6.2.2) using any corresponding  $X^p$  and  $Y^p$ .

Proof:

The  $j^{\text{th}}$  member of the set  $\mathcal{U}$  is given by

$$A^{pj} = Y^{pj} H^j Y^{pjT} \quad (6.2.9)$$

$$\text{with} \quad H^j = (Y^{pjT} X^{pj})^{-1}$$

where the additional superscript  $(\ )^{-j}$  indicates the  $j^{\text{th}}$  member of  $\mathcal{U}$ . Note that  $H^j$  is symmetric since  $Y^T X$  is symmetric. The range of any  $Y^p$  is equal to the range of  $Y$ , thus the  $Y^{p,i}$  and  $Y^{p,j}$  are related by

$$Y^{p,i} = Y^{pj} Q^{ij} \quad (6.2.10)$$

where  $Q^{ij} \in \mathbb{R}^{p \times p}$  and  $\text{rank}(Q^{ij}) = p$ . By utilizing Eq. (6.2.10), Eq. (6.2.9) can be written for the  $i^{\text{th}}$  member of  $\mathcal{U}$  as

$$A^{p,i} = Y^{pj} (Q^{ij} H^i Q^{ijT}) Y^{pjT} \quad (6.2.11)$$

$$\text{with } H^i = (Q^{ijT} Y^{pjT} X^{p,i})^{-1}$$

Again,  $H^i$  is symmetric because  $Y^T X$  is symmetric. In comparing Eqs. (6.2.9) and (6.2.11), it is seen that  $A^{pj} = A^{p,i}$  if

$$H^j = Q^{ij} H^i Q^{ijT} \quad (6.2.12)$$

or equivalently,

$$H^{j^{-1}} = Q^{ij^{-T}} H^{i^{-T}} Q^{ij^{-1}} \quad (6.2.13)$$

where Eq. (6.2.13) makes use of the symmetry of  $H^i$ . By using the definitions of  $H^i$  and  $H^j$ , Eq. (6.2.13) can be written as

$$Y^{pjT} X^{pj} = Q^{ij^{-T}} X^{p,iT} Y^{pj} \quad (6.2.14)$$

Pre-multiplying Eq. (6.2.14) by  $Q^{ijT}$  and utilizing the relation in Eq. (6.2.10) gives the condition such that  $A^{pj} = A^{p,i}$ , namely

$$Y^{p,iT} X^{pj} = X^{p,iT} Y^{pj} \quad (6.2.15)$$

This condition is clearly satisfied since  $Y^T X$  is symmetric. ■

The actual uses of Proposition 6.1 and Proposition 6.2 will be clearly seen in the next sections. The practical implication of Proposition 6.2 is discussed in detail in Section 6.6.

### 6.3 Damage Extent: Undamped Structures

In some cases, the damping of the system under consideration is assumed to be negligible. For this type of system, MRPT based algorithms will be developed assuming that



the structural damage affects (i) only the mass properties, or (ii) only the stiffness properties, or (iii) simultaneously the mass and stiffness properties.

### 6.3.1 Damage Extent: Mass Properties

In this case, it is assumed that the effect of damage on the stiffness properties of the structure is negligible. With this assumption, Eq. (6.1.1) can be rewritten as

$$MV_d\Lambda_d^2 + KV_d = \Delta M_d V_d \Lambda_d^2 \equiv B \quad (6.3.1)$$

Note that the eigenvectors are real and the eigenvalues are purely imaginary. Further, the eigenvectors are linearly independent, which implies that the matrix product  $V_d\Lambda_d^2$  is of full column rank if rigid body modes are not included. Assume, for the moment, that B is of full rank ( $\text{rank}(B) = p$ ). Then, Proposition 6.1 can be applied to determine the perturbation matrix,  $\Delta M_d$ , as

$$\Delta M_d = B(B^T V_d \Lambda_d^2)^{-1} B^T \quad (6.3.2)$$

by letting  $Y=B$  and  $X=V_d\Lambda_d^2$ . Note that the required inversion is that of a  $p \times p$  matrix, where “p” is the number of measured modes. As discussed in Proposition 6.1, this inversion is feasible if matrix B is of full rank and the rigid body modes of the system are omitted in the computations. When matrix B is rank deficient, Proposition 6.2 should be used to render the computation possible.

The properties associated with  $\Delta M_d$  as computed in Eq. (6.3.2) are as follows:

**PROPERTY 6.3.1** The perturbation matrix,  $\Delta M_d$ , defined in Eq. (6.3.2) will be symmetric if the eigenvectors,  $V_d$ , are stiffness orthogonal, i.e., the eigenvectors are orthogonal with respect to the original stiffness matrix, K.

Proof:

Proposition (6.1.c) in conjunction with Proposition (6.1.b) implies that the existence of the unique symmetric rank p  $\Delta M_d$  requires the symmetry of the matrix product  $B^T V_d \Lambda_d^2$ . The symmetric equivalence associated with this matrix product is

$$B^T V_d \Lambda_d^2 \equiv \Lambda_d^2 V_d^T B \quad (6.3.3)$$

Substituting the expression for B from Eq. (6.3.1) into Eq. (6.3.3) gives

$$\Lambda_d^2 V_d^T M V_d \Lambda_d^2 + V_d^T K V_d \Lambda_d^2 \equiv \Lambda_d^2 V_d^T M V_d \Lambda_d^2 + \Lambda_d^2 V_d^T K V_d \quad (6.3.4)$$

where the symmetry of M, K and  $\Lambda_d^2$  has been used in writing Eq. (6.3.4). From Eq. (6.3.4), it is clear that the equivalence is true if

$$(V_d^T K V_d) \Lambda_d^2 \equiv \Lambda_d^2 (V_d^T K V_d) \quad (6.3.5)$$

Equation (6.3.5) will obviously be satisfied if the measured eigenvectors are stiffness orthogonal. Baruch (1978) treated one approach to mass orthogonalize the measured eigenvectors. A similar approach can be used to orthogonalize the measured eigenvectors with respect to the stiffness matrix.



**PROPERTY 6.3.2** The updated finite element model (FEM) defined by the original mass and stiffness matrix along with the perturbation mass matrix computed using Eq. (6.3.2) preserve the rigid body characteristics of the original FEM.

Proof:

This is apparent in that the original stiffness matrix is unchanged and that the rigid body modes are defined as modes whose eigenvectors lie in the null space of the stiffness matrix.

### 6.3.2 Damage Extent: Stiffness Properties

Here, it is assumed that the effect of damage on the mass properties of the structure is negligible. With this assumption, Eq. (6.1.1) can be rewritten as

$$M V_d \Lambda_d^2 + K V_d = \Delta K_d V_d \equiv B \quad (6.3.6)$$

For this problem, the eigenvectors are real and the eigenvalues are purely imaginary. The eigenvectors are also linearly independent, which implies that matrix  $V_d$  is of full rank. If

matrix  $B$  is assumed to be of full rank ( $\text{rank}(B)=p$ ), Proposition 6.1 can be used to determine the perturbation to the original stiffness matrix,

$$\Delta K_d = B(B^T V_d)^{-1} B^T \quad (6.3.7)$$

This expression for  $\Delta K_d$  is determined by setting  $Y=B$  and  $X=V_d$  in Eq. (6.1.3).

The properties associated with  $\Delta K_d$  as computed by Eq. (6.3.7) are as follow.

**PROPERTY 6.3.3** The matrix  $\Delta K_d$  will be symmetric if the eigenvectors are mass orthogonal, i.e., the eigenvectors are orthogonal with respect to the original mass matrix.

The proof of Property 6.3.3 follows very much the same pattern as the one presented for  $\Delta M_d$  (Property 6.3.1).

**PROPERTY 6.3.4** The updated FEM defined by the original mass and stiffness matrices and the perturbation stiffness matrix,  $\Delta K_d$ , preserves the rigid body mode characteristics if the measured eigenvectors and the rigid body modes are mass orthogonal.

Proof:

The original rigid body modes of an undamped system are defined by the eigenvalue problem,

$$K \underline{v}_r = \lambda_r M \underline{v}_r = \underline{0} \quad (6.3.8)$$

where the subscript  $r$  denotes the rigid body mode(s) and  $\lambda_r$  is equal to zero. Thus, the rigid body modes lie in the null space of the original stiffness matrix. The rigid body modes of the system will be preserved in the updated model if the original rigid body modes lie in the null space of the updated stiffness matrix,

$$\underline{e} = (K - \Delta K_d) \underline{v}_r \quad (6.3.9a)$$

$$= - \Delta K_d \underline{v}_r \quad (6.3.9b)$$

where vector  $\underline{e}$  is zero if the the rigid body modes are preserved. Equation (6.3.8) has been used to arrive at the expression shown in Eq. (6.3.9b). Substituting Eq. (6.3.7) into (6.3.9b) gives

$$\underline{e} = -B(B^T V_d)^{-1} B^T \underline{v}_r \quad (6.3.10)$$

By utilizing the symmetry of the original mass and stiffness matrices, along with Eq. (6.3.6), Eq. (6.3.10) can be expanded as

$$\underline{e} = -B(B^T V_d)^{-1} [V_d^T K \underline{v}_r + \Lambda_d V_d^T M \underline{v}_r] \quad (6.3.11)$$

The first term in the parenthesis is zero because the matrix-vector product  $K \underline{v}_r$  is zero by definition. The second term will be zero if the rigid body modes and the measured mode shapes are mass orthogonal.

### 6.3.3 Damage Extent: Mass and Stiffness Properties

In this case, it is assumed that the structural damage affects simultaneously the mass and stiffness properties of the structure. With this assumption, Eq. (6.1.1) can be rewritten as

$$M V_d \Lambda_d^2 + K V_d = \Delta M_d V_d \Lambda_d^2 + \Delta K_d V_d \equiv B \quad (6.3.12)$$

#### 6.3.3.1 Application of The MRPT

Assume that Eq. (6.1.12) can be decoupled as follows,

$$\Delta M_d V_d = B_m \quad (6.3.13a)$$

$$\Delta K_d V_d = B_k \quad (6.3.13b)$$

Then, the MRPT, as formulated in Proposition 6.1, can be applied to determine the perturbation matrices  $\Delta M_d$  and  $\Delta K_d$ , as

$$\Delta M_d = B_m (B_m^T V_d)^{-1} B_m^T \quad (6.3.14a)$$

$$\Delta K_d = B_k (B_k^T V_k)^{-1} B_k^T \quad (6.3.14b)$$

Note that the matrices  $B_m^T V_d$  and  $B_k^T V_d$  are invertible if  $B_m$  and  $B_k$  are of full rank. When these rank requirements are not met, Proposition 6.2 can be used to make the computations possible.

### 6.3.3.2 Decomposition of Matrix B

The decomposition problem as illustrated in the previous section is equivalent to the problem of solving for the matrices  $B_m$  and  $B_k$ . So far, the only constraint that these unknown matrices must satisfy is given by the expression,

$$B = B_m \Lambda_d^2 + B_k \quad (6.3.15)$$

which results from Eqs. (6.3.12) and (6.3.13). Naturally, there is an infinite set of solutions  $(B_m, B_k)$  that satisfy Eq. (6.3.15). To arrive at a unique solution, additional physically meaningful constraints can be enforced. The decomposition proposed herein exploits the cross-orthogonality relations that arise from the symmetric nature of the property matrices and the undamped assumption. By measuring mass normalized “damaged” eigenvectors (which is possible if a driving point measurement is made), the cross-orthogonality relations associated with the damaged structure can be written as

$$V_d^T (M - \Delta M_d) V_d = I_{p \times p} \quad (6.3.16a)$$

$$V_d^T (K - \Delta K_d) V_d = \text{diag}(\omega_{d_1}^2, \dots, \omega_{d_p}^2) = \Omega_d \quad (6.3.16b)$$

in which  $\omega_{d_i}$  is the natural frequency of the  $i^{\text{th}}$  mode of the “damaged” structure. Matrix  $I_{p \times p}$  is the  $p \times p$  identity matrix. A rearrangement of Eq. (6.3.16) yields

$$V_d^T \Delta M_d V_d = V_d^T M V_d - I_{p \times p} \equiv V_d^T B_m \quad (6.3.17a)$$

$$V_d^T \Delta K_d V_d = V_d^T K V_d - \Omega_d \equiv V_d^T B_k \quad (6.3.17b)$$

Clearly, the matrices  $B_m$  and  $B_k$  can be computed from Eqs. (6.3.17). In the rare situation that the number of measured modes is equal to the number of DOFs in the FEM ( $p = n$ ), these can be computed by simply inverting matrix  $V_d$ . Unfortunately, as discussed earlier, the number of measured modes is usually much less than the number of FEM DOFs ( $p \ll n$ ). In this case, the solution that naturally comes to mind is to use the pseudo-inverse of matrix  $V_d^T$ . The inconvenience of this approach is that the sparsity pattern of matrix B will not be



reflected in the computed matrices  $B_m$  and  $B_k$ . Remember that the sparsity pattern of  $B$ , as discussed in Chapter 5, indicates the location of the damage affecting the structure. A more physically intuitive approach is to constrain  $B_m$  and  $B_k$  to exhibit the same sparsity pattern as matrix  $B$ . This is done by casting  $B$  in an equation similar to the expressions of Eqs. (6.3.17). The problem in question is then to find an  $n \times p$  matrix  $P$  that satisfies

$$P(V_d^T B) = B \quad (6.3.18)$$

Matrix  $P$  can be computed as

$$P = B (V_d^T B)^{-1} \quad (6.3.19)$$

The inverse involved in this computation is that of a  $p \times p$  matrix which is invertible if matrix  $B$  is of full rank. Now that  $P$  is computed,  $B_m$  and  $B_k$  can be computed using Eq. (6.3.19) as

$$B_m = P (V_d^T M V_d - I_{p \times p}) \quad (6.3.20a)$$

$$B_k = P (V_d^T K V_d - \Omega_d) \quad (6.3.20b)$$

It is clear from Eq. (6.3.19) that  $P$  will have the same sparsity pattern as matrix  $B$ . Hence  $B_m$  and  $B_k$  will also reflect the important sparsity pattern of  $B$ . The computed matrices  $B_m$  and  $B_k$  can also be used to determine the effect of the damage, respectively, on the mass, and stiffness properties. As in Chapter 5, cumulative vectors associated to  $B_m$  and  $B_k$  can also be defined when more than one measured mode is available.

$$\underline{d}_m = \frac{1}{p} \sum_{i=1}^p \frac{|\underline{d}_{m_i}|}{\|\underline{v}_{di}\|} \quad (6.3.21a)$$

$$\underline{d}_k = \frac{1}{p} \sum_{i=1}^p \frac{|\underline{d}_{k_i}|}{\|\underline{v}_{di}\|} \quad (6.3.21b)$$

where  $\underline{d}_{m_i}$  and  $\underline{d}_{k_i}$  are, respectively, the  $i^{\text{th}}$  column of matrix  $B_m$  and  $B_k$ .

**PROPERTY 6.3.5** The perturbation matrices ( $\Delta M_d$ ,  $\Delta K_d$ ) computed from the MRPT using the  $B_m$  and  $B_k$  resulting from the decomposition discussed above will be symmetric.

Proof:

The perturbation matrices  $\Delta M_d$  and  $\Delta K_d$  will be symmetric because they satisfy the relationships in Eqs. (6.3.17) and the right hand sides of these equations are symmetric.

#### 6.4 Damage Extent: Proportionally Damped Structures

Since many structures have non-negligible damping, it is of practical interest to extend the MRPT to address damped structures. In this analysis, the structure under consideration is assumed to exhibit proportional damping.

##### 6.4.1 Damage Extent: Stiffness and Damping Properties

It is assumed that the effect of the structural damage on the mass properties is negligible. In this context, Eq. (6.1.1) is rewritten as

$$M V_d \Lambda_d^2 + D V_d \Lambda_d + K V_d = \Delta D_d V_d \Lambda_d + \Delta K_d V_d \equiv B \quad (6.4.1)$$

The complex conjugate of Eq. (6.4.1) is

$$\Delta D_d V_d \bar{\Lambda}_d + \Delta K_d V_d = \bar{B} \quad (6.4.2)$$

where the overbar indicates the complex conjugate operator, and the fact that  $\Delta D_d$ ,  $\Delta K_d$  and  $V_d$  are real has been used in writing Eq. (6.4.2). Subtracting Eq. (6.4.2) from Eq. (6.4.1) gives

$$\Delta D_d V_d (\Lambda_d - \bar{\Lambda}_d) = (B - \bar{B}) \quad (6.4.3)$$

If  $(B - \bar{B})$  is assumed to be of full rank, Proposition 6.1 can be applied to determine the perturbation matrix,  $\Delta D_d$ , as

$$\Delta D_d = (B - \bar{B}) H_d (B - \bar{B})^T \quad (6.4.4)$$

$$\text{with } H_d = \left[ (B - \bar{B})^T V_d (\Lambda_d - \bar{\Lambda}_d) \right]^{-1}$$

Note that  $\Delta D_d$  as defined by Eq. (6.4.4) is real. Post-multiplying Eq. (6.4.1) by  $\bar{\Lambda}_d$  and Eq. (6.4.2) by  $\Lambda_d$  and subtracting the two equations leads to

$$\Delta K_d V_d (\bar{\Lambda}_d - \Lambda_d) = (B \bar{\Lambda}_d - \bar{B} \Lambda_d) \quad (6.4.5)$$

where the fact that  $\bar{\Lambda}_d$  and  $\Lambda_d$  are diagonal matrices has been used in writing Eq. (6.4.5). If  $(B \bar{\Lambda}_d - \bar{B} \Lambda_d)$  is assumed to be of full rank, Proposition 6.1 can also be applied to determine the perturbation matrix,  $\Delta K_d$ , as

$$\begin{aligned} \Delta K_d &= (B \bar{\Lambda}_d - \bar{B} \Lambda_d) H_k (B \bar{\Lambda}_d - \bar{B} \Lambda_d)^T \\ \text{with } H_k &= \left[ (B \bar{\Lambda}_d - \bar{B} \Lambda_d)^T V_d (\bar{\Lambda}_d - \Lambda_d) \right]^{-1} \end{aligned} \quad (6.4.6)$$

Note that  $\Delta K_d$  as defined by Eq. (33) is also real.

**PROPERTY 6.4.1** The perturbation matrices  $\Delta D_d$  and  $\Delta K_d$ , as computed above, will be symmetric if the measured eigenvectors,  $V_d$ , are mass orthogonal; i.e., the eigenvectors are orthogonal with respect to the original unperturbed mass matrix.

Proof:

Matrix  $\Delta D_d$  is symmetric if  $H_d$  is symmetric or, equivalently, if  $H_d^{-1}$  is symmetric. Hence, to get a symmetric  $\Delta D_d$ , the following equivalence must be satisfied.

$$(B - \bar{B})^T V_d (\Lambda_d - \bar{\Lambda}_d) \equiv (\Lambda_d - \bar{\Lambda}_d) V_d^T (B - \bar{B}) \quad (6.4.7)$$

Substituting the expressions for  $B$  and  $\bar{B}$ , from Eqs. (6.4.1) and (6.4.2), respectively, into Eq. (6.4.7) yields

$$\begin{aligned} & \left( \Lambda_d^2 V_d^T M + \Lambda_d V_d^T D - \bar{\Lambda}_d^2 V_d^T M - \bar{\Lambda}_d V_d^T D \right) V_d (\Lambda_d - \bar{\Lambda}_d) \\ & \equiv (\Lambda_d - \bar{\Lambda}_d) V_d^T \left( M V_d \Lambda_d^2 + D V_d \Lambda_d - M V_d \bar{\Lambda}_d^2 + D V_d \bar{\Lambda}_d \right) \end{aligned} \quad (6.4.8)$$

Note that in Eq. (6.4.8) the terms involving matrix  $\Delta K_d$  canceled out. A further expansion and simplification of Eq. (6.4.8) yields

$$\left(\Lambda_d^2 - \bar{\Lambda}_d^2\right) V_d^T M V_d (\Lambda_d - \bar{\Lambda}_d) \equiv (\Lambda_d - \bar{\Lambda}_d) V_d^T M V_d \left(\Lambda_d^2 - \bar{\Lambda}_d^2\right) \quad (6.4.9)$$

which is clearly satisfied if the measured “damaged” eigenvectors,  $V_d$ , are mass orthogonal.

///

Likewise, the perturbation matrix  $\Delta K_d$  as computed in Eq. (6.4.6) is symmetric if  $H_k$  is symmetric or, equivalently, if  $H_k^{-1}$  is symmetric. This symmetry requirement yields the following equivalence.

$$(B\bar{\Lambda}_d - \bar{B}\Lambda_d)^T V_d (\bar{\Lambda}_d - \Lambda_d) \equiv (\bar{\Lambda}_d - \Lambda_d) V_d^T (B\bar{\Lambda}_d - \bar{B}\Lambda_d) \quad (6.4.10)$$

Substitution of the expressions for  $B$  and  $\bar{B}$  into Eq. (6.4.10) yields

$$\begin{aligned} & \left(\bar{\Lambda}_d \Lambda_d^2 V_d^T M + \bar{\Lambda}_d V_d^T K - \Lambda_d \bar{\Lambda}_d^2 V_d^T M - \Lambda_d V_d^T K\right) V_d (\Lambda_d - \bar{\Lambda}_d) \\ & \equiv (\bar{\Lambda}_d - \Lambda_d) V_d^T \left(M V_d \Lambda_d^2 \bar{\Lambda}_d + K V_d \bar{\Lambda}_d - M V_d \bar{\Lambda}_d^2 \Lambda_d^2 - K V_d \Lambda_d\right) \end{aligned} \quad (6.4.11)$$

in which the terms involving matrix  $\Delta D_d$  cancel. Manipulating and simplifying Eq. (6.4.11) yields

$$\left(\bar{\Lambda}_d \Lambda_d^2 - \Lambda_d \bar{\Lambda}_d^2\right) V_d^T M V_d (\bar{\Lambda}_d - \Lambda_d) \equiv (\bar{\Lambda}_d - \Lambda_d) V_d^T M V_d \left(\bar{\Lambda}_d \Lambda_d^2 - \Lambda_d \bar{\Lambda}_d^2\right) \quad (6.4.12)$$

This equivalence is obviously satisfied if the eigenvectors are mass orthogonal.

///

■

**PROPERTY 6.4.2** The updated FEM, defined by the original FEM and the perturbation matrices  $\Delta D_d$  and  $\Delta K_d$  computed from Eqs. (6.4.4) and (6.4.6), preserves the original rigid body modes if the measured eigenvectors and the rigid body modes are mass orthogonal.

Proof:

As discussed earlier, a rigid body mode is defined as a mode whose eigenvalue is equal to zero and whose eigenvector lies in the null space of the FEM stiffness matrix. Hence, the rigid body modes of the original system are preserved in the updated FEM if they lie in the null space of the perturbed stiffness matrix. Consider the relationship

$$\underline{e} = (\mathbf{K} - \Delta\mathbf{K}_d)\underline{v}_r \quad (6.4.13)$$

where  $\underline{v}_r$  is a rigid body mode eigenvector. Clearly, the rigid body mode associated to eigenvector  $\underline{v}_r$  is preserved if  $\underline{e} = \underline{0}$ . By definition,  $\underline{v}_r$  is a rigid body eigenvector of the original system, hence Eq. (6.4.13) can be simplified as

$$\underline{e} = -\Delta\mathbf{K}_d\underline{v}_r \quad (6.4.14)$$

Substituting the expression for  $\Delta\mathbf{K}_d$  as defined in Eq. (6.4.6), into Eq. (6.4.14) gives

$$\underline{e} = -(\mathbf{B}\bar{\Lambda}_d - \bar{\mathbf{B}}\Lambda_d)\mathbf{H}_k(\mathbf{B}\bar{\Lambda}_d - \bar{\mathbf{B}}\Lambda_d)^T\underline{v}_r \quad (6.4.15)$$

Substitution of the expressions for  $\mathbf{B}$  and  $\bar{\mathbf{B}}$  into this equation yields

$$\underline{e} = -(\mathbf{B}\bar{\Lambda}_d - \bar{\mathbf{B}}\Lambda_d)\mathbf{H}_k \left[ \bar{\Lambda}_d\Lambda_d^2\mathbf{V}_d^T\mathbf{M} + \bar{\Lambda}_d\mathbf{V}_d^T\mathbf{K} - \Lambda_d\bar{\Lambda}_d^2\mathbf{V}_d^T\mathbf{M} - \Lambda_d\mathbf{V}_d^T\mathbf{K} \right] \underline{v}_r \quad (6.4.16)$$

By using the fact that  $\underline{v}_r$  is a rigid body eigenvector of the original system (i.e.  $\mathbf{K}\underline{v}_r = \underline{0}$ ), Eq. (6.3.16) can be simplified as

$$\underline{e} = -(\mathbf{B}\bar{\Lambda}_d - \bar{\mathbf{B}}\Lambda_d)\mathbf{H}_k \left( \bar{\Lambda}_d\Lambda_d^2 - \Lambda_d\bar{\Lambda}_d^2 \right) \mathbf{V}_d^T\mathbf{M}\underline{v}_r \quad (6.4.17)$$

It is clear from Eq. (6.4.17) that  $\underline{e} = \underline{0}$  if the rigid body mode  $\underline{v}_r$  and the measured eigenvectors  $\mathbf{V}_d$  are mass orthogonal (i.e.  $\mathbf{V}_d^T\mathbf{M}\underline{v}_r = \underline{0}$ ).

■

#### 6.4.2 Damage Extent: Mass and Damping Properties

In this case it is assumed that the effect of the structural damage on the stiffness properties is negligible. In this context, Eq. (6.1.1) is rewritten as



$$MV_d\Lambda_d^2 + DV_d\Lambda_d + KV_d = \Delta M_d V_d \Lambda_d^2 + \Delta D_d V_d \Lambda_d \equiv B \quad (6.4.18)$$

By using an approach similar to one used in the preceding section, Eq. (6.4.18) and its complex conjugate can be manipulated to yield the following decomposition

$$\Delta M_d V_d (\Lambda_d^2 \bar{\Lambda}_d - \bar{\Lambda}_d^2 \Lambda_d) = (B \bar{\Lambda}_d - \bar{B} \Lambda_d) \quad (6.4.19)$$

$$\Delta D_d V_d (\Lambda_d \bar{\Lambda}_d^2 - \bar{\Lambda}_d \Lambda_d^2) = (B \bar{\Lambda}_d^2 - \bar{B} \Lambda_d^2) \quad (6.4.20)$$

Again by applying the MRPT to the preceding equations,  $\Delta M_d$  and  $\Delta D_d$  are determined to be

$$\begin{aligned} \Delta M_d &= (B \bar{\Lambda}_d - \bar{B} \Lambda_d) H_m (B \bar{\Lambda}_d - \bar{B} \Lambda_d)^T \\ \text{with } H_m &= \left[ (B \bar{\Lambda}_d - \bar{B} \Lambda_d)^T V_d (\Lambda_d^2 \bar{\Lambda}_d - \bar{\Lambda}_d^2 \Lambda_d) \right]^{-1} \end{aligned} \quad (6.4.21)$$

$$\begin{aligned} \Delta D_d &= (B \bar{\Lambda}_d^2 - \bar{B} \Lambda_d^2) H_d (B \bar{\Lambda}_d^2 - \bar{B} \Lambda_d^2)^T \\ \text{with } H_d &= \left[ (B \bar{\Lambda}_d^2 - \bar{B} \Lambda_d^2)^T V_d (\Lambda_d \bar{\Lambda}_d^2 - \bar{\Lambda}_d \Lambda_d^2) \right]^{-1} \end{aligned} \quad (6.4.22)$$

Clearly, the perturbation matrices  $\Delta M_d$  and  $\Delta D_d$  as defined by Eqs. (6.4.21) and (6.4.22) are real.

**PROPERTY 6.4.3** The perturbation matrices  $\Delta M_d$  and  $\Delta D_d$ , as computed above, will be symmetric if the measured eigenvectors,  $V_d$ , are stiffness orthogonal; i.e., the eigenvectors are orthogonal with respect to the original unperturbed stiffness matrix.

**PROPERTY 6.4.4** The updated FEM, defined by the original FEM and the perturbation matrices,  $\Delta M_d$  and  $\Delta D_d$ , preserves the original rigid body modes.

The proof of Property 6.4.4 is straightforward since the original stiffness matrix is unchanged (see Property 6.3.2). The proof of Property 6.4.4 follows very much the same pattern as the proof of Property 6.4.2 .

### 6.4.3 Damage Extent: Mass and Stiffness Properties

In this problem, it is assumed that the effect of the structural damage on the damping properties is negligible. For this situation, the general eigenvalue problem defined in Eq. (6.1.1) associated to this case can be simplified as

$$MV_d\Lambda_d^2 + DV_d\Lambda_d + KV_d = \Delta M_d V_d \Lambda_d^2 + \Delta K_d V_d \equiv B \quad (6.4.23)$$

Algebraic manipulations of Eq. (6.4.23) and its complex conjugate yield the following decomposition

$$\Delta M_d V_d (\Lambda_d^2 - \bar{\Lambda}_d^2) = (B - \bar{B}) \quad (6.4.24)$$

$$\Delta K_d V_d (\bar{\Lambda}_d^2 - \Lambda_d^2) = (B\bar{\Lambda}_d^2 - \bar{B}\Lambda_d^2) \quad (6.4.25)$$

The perturbation matrices  $\Delta M_d$  and  $\Delta K_d$  can then be computed using the MRPT.

$$\Delta M_d = (B - \bar{B}) H_m (B - \bar{B})^T$$

$$\text{with } H_m = \left[ (B - \bar{B})^T V_d (\Lambda_d^2 - \bar{\Lambda}_d^2) \right]^{-1} \quad (6.4.26)$$

$$\Delta K_d = (B\bar{\Lambda}_d^2 - \bar{B}\Lambda_d^2) H_k (B\bar{\Lambda}_d^2 - \bar{B}\Lambda_d^2)^T$$

$$\text{with } H_k = \left[ (B\bar{\Lambda}_d^2 - \bar{B}\Lambda_d^2)^T V_d (\bar{\Lambda}_d^2 - \Lambda_d^2) \right]^{-1} \quad (6.4.27)$$

Note that  $\Delta M_d$  and  $\Delta K_d$  as defined by Eqs. (6.4.26) and (6.4.27) are real.

**PROPERTY 6.4.5** The perturbation matrices  $\Delta M_d$  and  $\Delta K_d$ , as computed above, will be symmetric if the measured eigenvectors,  $V_d$ , are damping orthogonal; i.e., the eigenvectors are orthogonal with respect to the original unperturbed damping matrix.

**PROPERTY 6.4.6** The updated FEM, defined by the original FEM and the perturbation matrices,  $\Delta M_d$  and  $\Delta K_d$ , preserves the original rigid body modes if the measured eigenvectors and the rigid body modes are damping orthogonal.

These proofs of the above two properties are not reported here. They follow very much the same pattern as the proofs in Section 6.4.2 .

#### 6.4.4 Damage Extent: Mass, Damping and Stiffness Properties

The eigenvalue problem of a proportionally damped system with all property matrices simultaneously affected by damage can be rearranged into the form

$$MV_d\Lambda_d^2 + DV_d\Lambda_d + KV_d = \Delta M_d V_d \Lambda_d^2 + \Delta D_d V_d \Lambda_d + \Delta K_d V_d \equiv B \quad (6.4.28)$$

The theory developed in Section 6.3.3 can be expanded to address this particular problem. The cross-orthogonality relationships associated with this type of structures are

$$V_d^T(M - \Delta M_d)V_d = I_{p \times p} \quad (6.4.29a)$$

$$V_d^T(D - \Delta D_d)V_d = \text{diag}\left(2\zeta_{d_1}\omega_{d_1}, \dots, 2\zeta_{d_p}\omega_{d_p}\right) = \Sigma_d \quad (6.4.29b)$$

$$V_d^T(K - \Delta K_d)V_d = \text{diag}\left(\omega_{d_1}^2, \dots, \omega_{d_p}^2\right) = \Omega_d \quad (6.4.29c)$$

Notice that the cross-orthogonality relationships in Eqs. (6.4.29a) and (6.4.29c) are exactly the same as the ones associated with undamped systems reported in Eqs. (6.3.16a) and (6.3.16b). As before, these cross-orthogonality conditions can also be rearranged as

$$V_d^T \Delta M_d V_d = V_d^T M V_d - I_{p \times p} \equiv V_d^T B_m \quad (6.4.30a)$$

$$V_d^T \Delta D_d V_d = V_d^T D V_d - \Sigma_d \equiv V_d^T B_d \quad (6.4.30b)$$

$$V_d^T \Delta K_d V_d = V_d^T K V_d - \Omega_d \equiv V_d^T B_k \quad (6.4.30c)$$

Following the exact same argument discussed for undamped systems in Section 6.3.3, an  $n \times p$  matrix  $P$  that satisfies the relation,

$$P(V_d^T B) = B \quad (6.4.31)$$

is sought, where  $B$  is computed using Eq. (6.4.18) and  $(V_d^T B)$  is a  $p \times p$  matrix. Although  $B$  is a complex matrix, the  $n \times p$  matrix  $P$  is real, since  $V_d$  is real. Hence, for computational efficiency, matrix  $P$  can be computed from

$$P = B_r \left( V_d^T B_r \right)^{-1} \quad (6.4.32)$$

where  $B_r$  is the real part of  $B$ . In Eq. (6.4.32), it is assumed that matrix  $(V_d^T B)$  is invertible. With  $P$  computed, the next step is to determine the decomposed damage vectors that indicate the effects of the damage on the mass, damping and stiffness matrices,

$$B_m \equiv \Delta M V_d = P (V_d^T M V_d - I_{p \times p}) \quad (6.4.33a)$$

$$B_d \equiv \Delta D V_d = P (V_d^T D V_d - \Sigma_d) \quad (6.4.33b)$$

$$B_k \equiv \Delta K V_d = P (V_d^T K V_d - \Omega_d) \quad (6.4.33c)$$

The minimum rank perturbation theory (MRPT), as formulated in Proposition 6.1, can again be applied to determine the perturbation matrices,  $\Delta M_d$ ,  $\Delta D_d$  and  $\Delta K_d$ , as

$$\Delta M_d = B_m (B_m^T V_d)^{-1} B_m^T \quad (6.4.34a)$$

$$\Delta D_d = B_d (B_d^T V_d)^{-1} B_d^T \quad (6.4.34b)$$

$$\Delta K_d = B_k (B_k^T V_k)^{-1} B_k^T \quad (6.4.34c)$$

Note that the matrices  $B_m^T V_d$ ,  $B_d^T V_d$  and  $B_k^T V_d$  are  $p \times p$  matrices that are invertible if  $B_m$ ,  $B_d$  and  $B_k$  are of full rank. As in all other cases already studied, Proposition 6.2 can be used to deal with the situation when any one of these matrices are rank deficient. The cumulative damage location vector associated to  $B_m$  and  $B_k$ , defined in Eqs. 6.3.21, are also applicable to this problem. An additional cumulative damage vector associated to the perturbations in the damping properties can be similarly defined as

$$\underline{d}_d = \frac{1}{p} \sum_{i=1}^p \frac{|\underline{d}_{d_i}|}{\|\underline{v}_{d_i}\|} \quad (6.4.35)$$

where  $\underline{d}_{d_i}$  is the  $i^{\text{th}}$  column of matrix  $B_d$ .

**PROPERTY 6.4.5** The perturbation matrices ( $\Delta M_d$ ,  $\Delta D_d$ ,  $\Delta K_d$ ) as computed above will be symmetric.

**Proof:**

This is true since these perturbation matrices are constrained to satisfy the relationships in Eqs. (6.4.30). Notice that the right hand sides of Eqs. (6.4.30) are symmetric.

### 6.5 Damage Extent: Nonproportionally Damped Structures

As reported earlier in the beginning of the chapter, the eigenvalue problem associated with the dynamic differential equation of motion of a damaged nonproportionally damped system can be written as

$$MV_d\Lambda_d^2 + DV_d\Lambda_d + KV_d = \Delta M_d V_d\Lambda_d^2 + \Delta D_d V_d\Lambda_d + \Delta K_d V_d \equiv B \quad (6.5.1)$$

where the matrices  $M$ ,  $D$ ,  $K$ ,  $\Delta M_d$ ,  $\Delta D_d$ ,  $\Delta K_d$ ,  $V_d$ , and  $\Lambda_d$  have the same definitions as in the previous sections. A number of cross-orthogonality relationships associated to general nonproportionally damped systems have been reported in Chapter 2. The cross-orthogonality conditions that are relevant to the following formulations are

$$\begin{bmatrix} V_d\Lambda_d \\ V_d \end{bmatrix}^* \begin{bmatrix} (M - \Delta M_d) & 0 \\ 0 & -(K - \Delta K_d) \end{bmatrix} \begin{bmatrix} V_d\Lambda_d \\ V_d \end{bmatrix} = \begin{bmatrix} 0 \\ 0 \end{bmatrix} \quad (6.5.2)$$

$$\begin{bmatrix} V_d\Lambda_d \\ V_d \end{bmatrix}^* \begin{bmatrix} (D - \Delta D_d) & (K - \Delta K_d) \\ (K - \Delta K_d) & 0 \end{bmatrix} \begin{bmatrix} V_d\Lambda_d \\ V_d \end{bmatrix} = \begin{bmatrix} 0 \\ 0 \end{bmatrix} \quad (6.5.3)$$

$$\begin{bmatrix} V_d\Lambda_d \\ V_d \end{bmatrix}^* \begin{bmatrix} 0 & (M - \Delta M_d) \\ (M - \Delta M_d) & (D - \Delta D_d) \end{bmatrix} \begin{bmatrix} V_d\Lambda_d \\ V_d \end{bmatrix} = \begin{bmatrix} 0 \\ 0 \end{bmatrix} \quad (6.5.4)$$

In the above equations, the notation  $[ \ ]^*$  denotes the complex conjugate transpose operator.

Expansion of the above three equations yield, respectively, the following relations,

$$\Lambda_d^* V_d^* (M - \Delta M_d) V_d \Lambda_d - V_d^* (K - \Delta K_d) V_d = [0] \quad (6.5.5)$$



$$\Lambda_d^* V_d^* (D - \Delta D_d) V_d \Lambda_d + \Lambda_d^* V_d^* (K - \Delta K_d) V_d + V_d^* (K - \Delta K_d) V_d \Lambda_d = [0] \quad (6.5.6)$$

$$V_d^* (M - \Delta M) V_d \Lambda_d + \Lambda_d^* V_d^* (M - \Delta M_d) V_d + V_d^* (D - \Delta D) V_d = [0] \quad (6.5.7)$$

These equations can be further manipulated to become, respectively,

$$\begin{aligned} W_1 &\equiv \Lambda_d^* V_d^* M V_d \Lambda_d - V_d^* K V_d \\ &= \Lambda_d^* V_d^* \Delta M_d V_d \Lambda_d - V_d^* \Delta K_d V_d \end{aligned} \quad (6.5.8)$$

$$\begin{aligned} W_2 &\equiv \Lambda_d^* V_d^* D V_d \Lambda_d + \Lambda_d^* V_d^* K V_d + V_d^* K V_d \Lambda_d \\ &= \Lambda_d^* V_d^* \Delta D_d V_d \Lambda_d + \Lambda_d^* V_d^* \Delta K_d V_d + V_d^* \Delta K_d V_d \Lambda_d \end{aligned} \quad (6.5.9)$$

$$\begin{aligned} W_3 &\equiv V_d^* M V_d \Lambda_d + \Lambda_d^* V_d^* M V_d + V_d^* D V_d \\ &= V_d^* \Delta M_d V_d \Lambda_d + \Lambda_d^* V_d^* \Delta M_d V_d + V_d^* \Delta D_d V_d \end{aligned} \quad (6.5.10)$$

Notice that  $W_1$ ,  $W_2$  and  $W_3$  can be computed using the equations in terms of known matrices  $M$ ,  $D$ ,  $K$ ,  $V_d$ , and  $\Lambda_d$ .

The above cross-orthogonality conditions are derived from two different state space representations of the equation of motion shown in Eq. (6.5.1) (see Chapter 2). From each representation, two cross-orthogonality condition were derived. The two sets provide exactly the same information about Eq. (6.5.1) but in a different format. Hence, only two of the three cross-orthogonality relations are linearly independent. In fact, Eq. (6.5.8) can be generated by subtracting Eq. (6.5.9) from (6.5.10). Any set of two linearly independent cross-orthogonality relationships can be viewed as a decoupling of the equation of motion (Eq. (6.5.1)). Hence, for the present problem, there are only two distinct (linearly independent) matrix equations for the three unknown perturbation matrices ( $\Delta M_d$ ,  $\Delta D_d$ ,  $\Delta K_d$ ). Naturally, if the problem consists of solving for all three unknown matrices, there will exist an infinite number of solutions. Additional constraints are hence needed to get a better defined problem. In this formulation, it is assumed that the damage only affects two of the three property matrices. Mathematically, this can be translated as a constraint on one of three perturbation matrices (either  $\Delta M_d$  or,  $\Delta D_d$  or,  $\Delta K_d$ ) to be equal to zero.

### 6.5.1 Damage Extent: Damping and Stiffness Properties

In this case, it is assumed that the effects of the damage on the mass properties are negligible ( $\Delta M_d = 0$ ). The corresponding eigenvalue equation and the cross-orthogonality conditions relevant to this problem are

$$MV_d \Lambda_d^2 + DV_d \Lambda_d + KV_d = \Delta D_d V_d \Lambda_d + \Delta K_d V_d \equiv B \quad (6.5.11)$$

$$V_d^* \Delta K_d V_d = -W_1 \quad (6.5.12)$$

$$V_d^* \Delta D_d V_d = W_3 \quad (6.5.13)$$

The approach used in this formulation follows very much the same pattern as the one developed in Section 3.3.3. The basic idea is to generate from Eqs. (6.5.11-13) problems that can take the advantage of the already existing MRPT concept. Based on the same argument as in Section 3.3.3, a matrix  $P \in \mathbb{C}^{n \times p}$  is sought such that

$$P(V_d^* B) = B \quad (6.5.14)$$

It is Assumed that  $(V_d^T B)$  is invertible; then matrix  $P$  is given by

$$P = B (V_d^* B)^{-1} \quad (6.5.15)$$

Matrix  $P$  can then be used in Eqs. (6.5.11) and (6.5.12) to yield

$$\Delta K_d V_d = -PW_1 \quad (6.5.16a)$$

$$\Delta D_d V_d = PW_3 \quad (6.5.16b)$$

In order to force the perturbation matrices  $\Delta D_d$  and  $\Delta K_d$  to be real, the complex conjugates of Eqs. (6.5.16a) and (6.5.16b) are introduced,

$$\Delta K_d \bar{V}_d = -\bar{P}\bar{W}_1 \quad (6.5.17a)$$

$$\Delta D_d \bar{V}_d = \bar{P}\bar{W}_3 \quad (6.5.17b)$$

A combination of Eqs. (6.5.16a, b) and (6.5.17a, b) implies

$$\Delta K_d \begin{bmatrix} (V_d)_R & | & (V_d)_I \end{bmatrix} = - \begin{bmatrix} (PW_1)_R & | & (PW_1)_I \end{bmatrix} \quad (6.5.18a)$$

$$\Delta D_d \begin{bmatrix} (V_d)_R & | & (V_d)_I \end{bmatrix} = \begin{bmatrix} (PW_3)_R & | & (PW_3)_I \end{bmatrix} \quad (6.5.18b)$$

where the notation  $(X)_R$  and  $(X)_I$  indicate, respectively, the real and imaginary part of matrix  $X$ . The MRPT can now be applied to determine the perturbation matrices  $\Delta D_d$  and  $\Delta K_d$ .

$$\Delta D_d = F_d \left( F_d^T U_d \right)^{-1} F_d^T \quad (6.5.19a)$$

$$\Delta K_d = F_k \left( F_k^T U_d \right)^{-1} F_k^T \quad (6.5.19b)$$

where

$$\begin{aligned} U_d &= \begin{bmatrix} (V_d)_R & | & (V_d)_I \end{bmatrix} \\ F_k &= - \begin{bmatrix} (PW_1)_R & | & (PW_1)_I \end{bmatrix} \\ F_d &= \begin{bmatrix} (PW_3)_R & | & (PW_3)_I \end{bmatrix} \end{aligned}$$

Remember that  $W_1$  and  $W_3$  can be computed in terms of known matrices as shown in Eqs. (6.5.8) and (6.5.10). The computations in Eqs. (6.5.19a) and (6.5.19b) require that  $(F_d^T U_d)$  and  $(F_k^T U_d)$  be invertible. As discussed in the earlier sections, Proposition 6.2 can be used when these inverse requirements are not met.

### 6.5.2 Damage Extent: Mass and Damping Properties

Here, it is assumed that the damage effects on the stiffness properties are negligible ( $\Delta K_d = 0$ ). By considering this assumption, the eigenvalue equation associated with this problem is found to be

$$M V_d \Lambda_d^2 + D V_d \Lambda_d + K V_d = \Delta M_d V_d \Lambda_d^2 + \Delta D_d V_d \Lambda_d \equiv B \quad (6.5.20)$$

The cross-orthogonality conditions relevant to the present development are obtained from Eqs. (6.5.8) and (6.5.9) by setting  $\Delta K_d$  to zero.

$$\Lambda_d^* V_d^* \Delta M_d V_d \Lambda_d = W_1 \quad (6.5.21)$$

$$\Lambda_d^* V_d^* \Delta D_d V_d \Lambda_d = W_2 \quad (6.5.22)$$

The solution procedure to the problem of determining  $\Delta M_d$  and  $\Delta D_d$  is exactly the same as the one formulated in the preceding section. First, equations (6.5.21) and (6.5.22) are cast in the following form.

$$\Delta M_d V_d \Lambda_d = P W_1 \quad (6.5.23a)$$

$$\Delta D_d V_d \Lambda_d = P W_2 \quad (6.5.23b)$$

$$\text{where } P = B (\Lambda_d^* V_d^* B)^{-1}$$

The above two equations involve complex matrices. To guarantee that the perturbation matrices  $\Delta M_d$  and  $\Delta D_d$  are real, Eqs. (6.5.23a) and (6.5.23b) are used in conjunction with their corresponding complex conjugates. The combinations of the two sets of complex conjugate pairs yield

$$\Delta M_d \left[ (V_d \Lambda_d)_R \mid (V_d \Lambda_d)_I \right] = \left[ (P W_1)_R \mid (P W_1)_I \right] \quad (6.5.24a)$$

$$\Delta D_d \left[ (V_d \Lambda_d)_R \mid (V_d \Lambda_d)_I \right] = \left[ (P W_2)_R \mid (P W_2)_I \right] \quad (6.5.24b)$$

Finally, the perturbation matrices  $\Delta M_d$  and  $\Delta D_d$  are, respectively, determined from Eqs. (6.5.24a) and (6.5.24b) by using the MRPT.

$$\Delta M_d = F_m (F_m^T U_d)^{-1} F_m^T \quad (6.5.25a)$$

$$\Delta D_d = F_d (F_d^T U_d)^{-1} F_d^T \quad (6.5.25b)$$

where

$$U_d = \left[ (V_d \Lambda_d)_R \mid (V_d \Lambda_d)_I \right]$$

$$F_m = \left[ (P W_1)_R \mid (P W_1)_I \right]$$

$$F_d = \left[ (P W_2)_R \mid (P W_2)_I \right]$$

Again, the computations in Eq. (6.5.25a) and (6.5.25b) are feasible if and only if  $(F_m^T U_d)$  and  $(F_d^T U_d)$  are both invertible.

### 6.5.3 Damage Extent: Mass and Stiffness Properties

In some situations, structural damage is such that it only affects the mass and stiffness properties of the system. The following expression are the results of setting the damping perturbation to zero ( $\Delta D_d = 0$ ) in Eqs. (6.5.1), (6.5.9) and (6.5.10).

$$M V_d \Lambda_d^2 + D V_d \Lambda_d + K V_d = \Delta M_d V_d \Lambda_d^2 + \Delta K_d V_d \equiv B \quad (6.5.26)$$

$$\Lambda_d^* V_d^* \Delta K_d V_d + V_d^* \Delta K_d V_d \Lambda_d = W_2 \quad (6.5.27)$$

$$\Lambda_d^* V_d^* \Delta M_d V_d + V_d^* \Delta M_d V_d \Lambda_d = W_3 \quad (6.5.28)$$

Equation (6.5.26) is the rearranged eigenvalue problem associated with the present case. The expressions in Eqs. (6.5.12) and (6.5.13) are the “rearranged” cross-orthogonality conditions that are relevant to the forthcoming formulation. First, Eqs. (6.5.27) and (6.5.28) are conveniently simplified to the standard format encountered in the previous two sections. Since  $\Lambda_d$  and  $\Lambda_d^*$  are diagonal matrices, Eqs. (6.5.27) can be written as

$$V_d^* \Delta K_d V_d = Q_2 \quad (6.5.29)$$

$$\text{where } q_{2ij} = w_{2ij} / (\lambda_{dii}^* + \lambda_{djj})$$

The variables  $q_{2ij}$  and  $w_{2ij}$  are the components in the  $i^{\text{th}}$  row and  $j^{\text{th}}$  column of matrix  $Q_k$  and  $W_2$ , respectively;  $\lambda_{dii}$  is the  $i^{\text{th}}$  diagonal component of the eigenvalue matrix  $\Lambda_d$ . Similarly, Eq. (6.5.28) can also be written as

$$V_d^* \Delta M_d V_d = Q_3 \quad (6.5.30)$$

$$\text{where } q_{3ij} = w_{3ij} / (\lambda_{dii}^* + \lambda_{djj})$$

Equations (6.5.29) and (6.5.30) can then be transformed as



$$\Delta K_d V_d = PQ_2 \quad (6.5.31a)$$

$$\Delta M_d V_d = PQ_3 \quad (6.5.31b)$$

$$\text{where } P = B (V_d^* B)^{-1}$$

Notice that the above computations require that matrix  $(V_d^* B)$  be invertible. The sought perturbation matrices,  $\Delta M_d$  and  $\Delta K_d$ , are ensured to be real by supplementing Eqs. (6.5.31a) and (6.5.31b) with their complex conjugates. The complex conjugate pairs are then combined together in the following fashion

$$\Delta K_d \begin{bmatrix} (V_d)_R & | & (V_d)_I \end{bmatrix} = \begin{bmatrix} (PQ_2)_R & | & (PQ_2)_I \end{bmatrix} \quad (6.5.32a)$$

$$\Delta M_d \begin{bmatrix} (V_d)_R & | & (V_d)_I \end{bmatrix} = \begin{bmatrix} (PQ_3)_R & | & (PQ_3)_I \end{bmatrix} \quad (6.5.32b)$$

At this point, the MRPT is applied to Eqs. (6.5.32a) and (6.5.32b) and the perturbation matrices,  $\Delta M_d$  and  $\Delta K_d$ , are determined

$$\Delta K_d = F_k (F_k^T U_d)^{-1} F_k^T \quad (6.5.33a)$$

$$\Delta M_d = F_m (F_m^T U_d)^{-1} F_m^T \quad (6.5.33b)$$

where

$$U_d = \begin{bmatrix} (V_d)_R & | & (V_d)_I \end{bmatrix}$$

$$F_k = \begin{bmatrix} (PQ_2)_R & | & (PQ_2)_I \end{bmatrix}$$

$$F_m = \begin{bmatrix} (PQ_3)_R & | & (PQ_3)_I \end{bmatrix}$$

Again, it is assumed that Proposition 6.2 has been applied, if necessary, to ensure that the inverses of the matrices  $(F_m^T U_d)$  and  $(F_k^T U_d)$  exist.

**PROPERTY 6.5.1** In the above three damage configurations considered for nonproportionally damped structures, the computed perturbation matrices ( $\Delta M_d$ ,  $\Delta D_d$  or  $\Delta K_d$ ) from the MRPT will be symmetric.

Proof:

This is true since the developed formulations require the perturbation matrices along with the “healthy” FEM to satisfy the cross orthogonality conditions in Eqs. (6.5.2-4). These cross-orthogonality conditions are satisfied if and only if the corresponding state matrices are symmetric; that is

$$\begin{bmatrix} (M - \Delta M_d) & 0 \\ 0 & -(K - \Delta K_d) \end{bmatrix} = \begin{bmatrix} (M - \Delta M_d) & 0 \\ 0 & -(K - \Delta K_d) \end{bmatrix}^T \quad (6.5.34)$$

$$\begin{bmatrix} (D - \Delta D_d) & (K - \Delta K_d) \\ (K - \Delta K_d) & 0 \end{bmatrix} = \begin{bmatrix} (D - \Delta D_d) & (K - \Delta K_d) \\ (K - \Delta K_d) & 0 \end{bmatrix}^T \quad (6.5.35)$$

$$\begin{bmatrix} 0 & (M - \Delta M_d) \\ (M - \Delta M_d) & (D - \Delta D_d) \end{bmatrix} = \begin{bmatrix} 0 & (M - \Delta M_d) \\ (M - \Delta M_d) & (D - \Delta D_d) \end{bmatrix}^T \quad (6.5.36)$$

Since the matrices  $M$ ,  $D$ ,  $K$  are known to be symmetric, the above relationships are satisfied if and only if the perturbation matrices  $\Delta M_d$ ,  $\Delta D_d$  and  $\Delta K_d$  are symmetric.

■

## 6.6 Practical Issues

In all cases discussed in the previous sections of this Chapter, the damage extent problem boiled down to solving problems of the form

$$AX = Y \quad (6.6.1)$$

in which  $A$  is an unknown  $n \times n$  matrix representing one of the perturbation matrices ( $\Delta M_d$ ,  $\Delta D_d$  and  $\Delta K_d$ ) and  $X$  and  $Y$  are known  $n \times p$  complex matrices. Matrix  $X$  is a function of the damaged structure eigenvector ( $V_d$ ) and eigenvalue ( $\Lambda_d$ ) matrices. Recall that  $p$  represents the number of modes and  $n$  is the total number of DOFs in the structure's FEM. As discussed in Chapter 5, the columns of matrix  $Y$  provide useful information in determining the location

of the structural damage. For each problem, a cumulative damage vector associated to the columns of matrix  $Y$  can be defined as

$$\underline{d} = \frac{1}{p} \sum_{i=1}^p \frac{|\underline{y}_{di}|}{\|\underline{v}_{di}\|} \quad (6.6.2)$$

Recall that the DOFs of the FEM affected by the damage are associated with the components of vector  $\underline{d}$  which are substantially larger than the other components of  $\underline{d}$ .

Considering the present generic problem, the extent problem consists of determining a symmetric real matrix  $A$  that satisfies Eq. (6.6.1). A solution to this problem based on the Minimum Rank Perturbation Theory (MRPT) was developed in Proposition 6.1. The solution technique presented in Proposition 6.1 requires the  $p \times p$  matrix  $(Y^T X)$  to be invertible. Proposition 6.2 was then presented to deal with the case when matrix  $(Y^T X)$  is not invertible. In the forthcoming discussions, two strategies to improve the extent calculation are presented.

#### 6.6.1 The Concept of “Best” Modes

Note that for the sake of generality, the forthcoming discussion is based on the generic problem shown in Eq. (6.6.1); however it should be viewed as representative of all extent problems discussed in the earlier sections of this chapter.

Although Proposition 6.2 deals with noise free measurements, its practical usefulness is for the case when the eigenvalue / eigenvector measurements are corrupted by noise (either through actual measurement error or eigenvector expansion induced errors). In general, matrix  $Y$  will typically be of full column rank due to the presence of noise ( $\text{rank}(Y)=p$ ), even though the actual damage has only induced a rank  $r$  ( $r < p$ ) change to the FEM property matrix ( $M, D$  or  $K$ ) associated to  $A$  ( $\Delta M_d, \Delta D_d$  or  $\Delta K_d$ ). Application of the extent algorithm at this point will result in a rank  $r$  perturbation to the property matrix  $A$ . A better estimate of the true extent of the damage can be obtained by estimating the “true” rank of  $Y$  (and thus  $A$ ), where the true rank of  $Y$  is defined by the limiting case when there are no

eigenvalue/eigenvector measurement errors. There are two possible techniques for estimating the “true” rank of  $Y$ . The first technique, which amounts to a brute-force numerical computation, is to calculate the Singular Value Decomposition (SVD) of  $Y$ . Various rank criteria measures, as formulated by Juang and Pappa (1985) in their work on system realization theory, in conjunction with engineering judgement, can be used to arrive at an estimate of the true rank of  $Y$  and, hence,  $A$ . However, this would greatly increase the computational burden of the extent algorithm, and may not even be practical if the number of DOFs of the original FEM is large. A computationally inexpensive technique for estimating the true rank of  $Y$  is to make use of the damage location results. The cumulative damage vector associated to the perturbation matrix  $A$  defined in Eq. (6.6.2) indicates which structural DOFs have been directly affected by the damage. Using connectivity information from the original FEM in conjunction with knowledge of the damaged DOFs allows for the determination of which elements of the FEM have been damaged. The “true” rank of  $Y$  can be estimated by adding up the ranks of the element matrices associated with each damaged element.

Once the true rank of  $Y$  has been estimated, corresponding columns of  $X$  and  $Y$  are eliminated such that the actual rank of  $B$  is set to the estimated true rank of  $Y$ . In Proposition 6.2, it was shown that with noise free measurements it does not matter which  $r$  modes from the set of  $p$  measured modes are used in the extent calculation. However, when the measurements are corrupted by noise, it is best to use those modes which best reflect the damage state as indicated by the cumulative damage vector Eq. (6.6.2). As will be illustrated in the example problems presented in Chapter 7, the concept discussed here improves the damage extent estimation. This is especially true when the rank of the perturbation matrix ( $r$ ) due to the damage is less than the number of measured modes ( $p$ ). The reason is twofold. First, the rank of the computed perturbation matrix is consistent with the rank of the actual perturbation matrix. Second, the measurement errors in the experimental modes that do not reflect the actual state of the damage are not included in the computation.

### 6.6.2 Application of the Eigenvector Filtering Algorithm

Another technique that can be used to improved the damage extent estimation is the eigenvector filtering algorithm developed in Chapter 5. The modes that should be filtered and used in the extent computation are the ones that reflect the overall structure cumulative damage vector defined in Eqs. (5.4.1) or (5.4.2) of Chapter 5. The characteristics of the eigenvector filtering algorithm are illustrated in Chapter 7. It should be pointed out that it is not a requirement of the extent algorithm to use the eigenvector filtering algorithm, but certainly it does allow for more engineering judgement to enter into the extent calculation. The choice of whether or not to use the filtering algorithm is dependent on (i) the errors in the eigenvectors as seen from the damage vectors, (ii) the requirement on accuracy of the extent calculation and (iii) the size of the FEM, which defines the additional computational burden.

## 6.7 Summary

A computationally attractive algorithm was developed to provide an insight to the extent of structural damage. The developed theory, called the Minimum Rank Perturbation Theory (MRPT), makes use of an existing finite element model of the “healthy” structure and a subset of experimentally measured modal properties of the “damaged” structure. The MRPT formulation is consistent with the effects of many classes of structural damage on a finite element model. The MRPT was applied to assess the damage in undamped, proportionally damped and nonproportionally damped models. For each type of model, several different damage scenarios were considered. The performance of the MRPT will be investigated in Chapter 7 along with the subspace rotation damage location algorithm using both simulated and actual experimental data. As will be shown in Chapter 7, the MRPT can also be used to refine finite element models.



## CHAPTER 7

### VALIDATION AND ASSESSMENT OF THE SUBSPACE ROTATION ALGORITHM AND THE MINIMUM RANK PERTURBATION THEORY

#### 7.1 Introduction

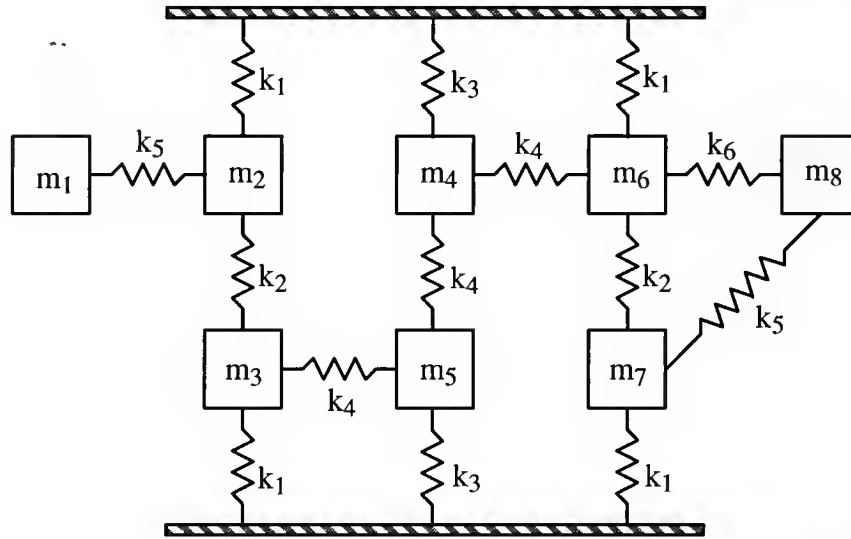
In this chapter, the characteristics of the subspace rotation algorithm (Chapter 5) and the minimum rank perturbation theory (Chapter 6) are illustrated by using both simulated and actual experimental data. The main objective is to show that the algorithms are suited to assess damage in structures. Additionally, it is shown that the minimum rank perturbation theory formulated in Chapter 6 is also suited to update finite element models. The computer simulated example problems provide a controlled setting in which key points made throughout the formulation of both algorithms are emphasized. Actual experimental examples are used to demonstrate the practicality of the algorithms in handling “real-life” systems.

#### 7.2 Kabe’s Problem

##### 7.2.1 Problem Description

Kabe’s eight degree of freedom spring-mass problem is shown in Figure 7.1, which includes the stiffness and mass values for the exact model. The main objective of this problem is to illustrate the damage location algorithm formulated in Chapter 5. The Subspace Rotation algorithm direct method is compared to the Angle Perturbation Method. Key points discussed in the formulation will be highlighted. Application of the damage

extent algorithm of Chapter 6 is also addressed. Both algorithms will be evaluated using noisy modal measurements in an attempt to reproduce a practical testing situation.



$$m_1 = 0.001 \quad m_8 = 0.002 \quad m_j = 1.0 \quad j = 2, \dots, 7$$

$$k_1 = 1000 \quad k_2 = 10 \quad k_3 = 900 \quad k_4 = 100 \quad k_5 = 1.5 \quad k_6 = 2.0$$

Figure 7.1 Kabe's Problem.

A variation of Kabe's original problem is used here. Rather than the standard model commonly used, which has incorrect values for all of the connecting springs, only a single spring constant is changed. This is reflective of the fact that damage may occur as a large local change in the stiffness of a structural member. In this problem, the initial model is incorrect for the spring between masses seven (7) and eight (8). Damage will be modeled as a change in spring constant from 1.5 to 0.1. Changing the spring in this fashion causes the damage to occur at degrees of freedom which have a small  $\|Z_{d_i}\|$  in comparison to other DOFs. Thus, it would be expected that damage would best be located using the Angle Perturbation method as defined in Eq. (5.3.1). In this problem, it is assumed that only the first two modes of vibration are measured. Note that the damage does not affect the mass properties of the structure.

### 7.2.2 Damage Location

Figures 7.2 and 7.3 show, respectively, the damage location results of using the Subspace Rotation direct ( $\underline{d}_i$ ) method and the Angle Perturbation Method ( $\underline{\alpha}_i$ ). Figure 7.4 provides the damage vector as defined by Lin's algorithm (1990). These results were generated using only the fundamental mode of vibration eigendata. In these figures, the x-coordinate represents the elements of the damage vector  $\underline{d}_i$  (or  $\underline{\alpha}_i$ ), where the  $i^{\text{th}}$  element of  $\underline{d}_i$  ( $\underline{\alpha}_i$ ) corresponds to the  $i^{\text{th}}$  degree of freedom.

The upper left plot represents the damage vector if the exact perturbation matrices are used. The upper right plot corresponds to the case where the exact eigenvector information is provided to the algorithm. The lower left and lower right plots correspond to the case where the exact eigenvector has been corrupted with five and ten percent random noise, respectively. In practice, the noise in eigenvector information could be due to both measurement and/or expansion induced errors.

As shown in Figures (7.2) and (7.3), the location algorithm is able to exactly locate the correct damage when provided with only a single correct eigenvalue/eigenvector pair as guaranteed by Eq. (5.2.4). From the lower plots, it is seen that the algorithm experiences a degradation in damage detection capability as the error in the eigenvector is increased. In fact, when presented with 10% eigenvector noise, the direct subspace rotation method incorrectly identifies the damage. However, when using the angle perturbation method the location algorithm is able to discern damage with a 10% noise level. As shown in Figure 7.4, Lin's algorithm is unable to discern damage in this particular test problem.

Figures 7.5 and 7.6 show the results of using the angle perturbation method and Lin's algorithm when provided with complete first and second mode eigenvalue/eigenvector information. Again, the angle perturbation method is able to cleanly detect damage even when presented with eigenvector information corrupted with ten percent noise. Again, Lin's algorithm is unable to discern damage.

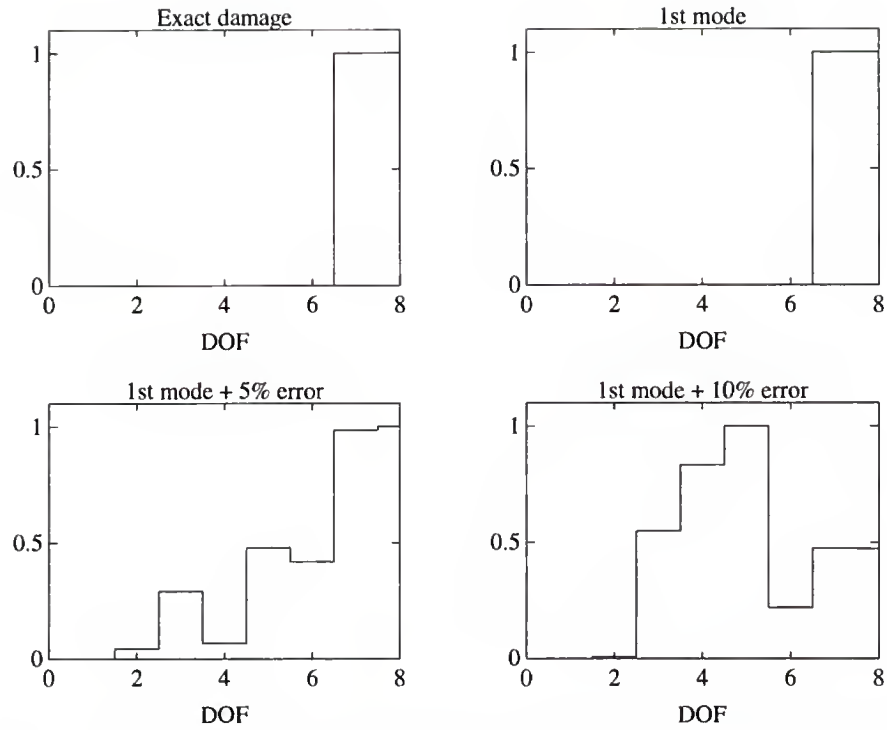


Figure 7.2 Kabe's Problem: Damage Location Results using the Subspace Rotation Direct Method with the Eigendata of the 1st Mode.

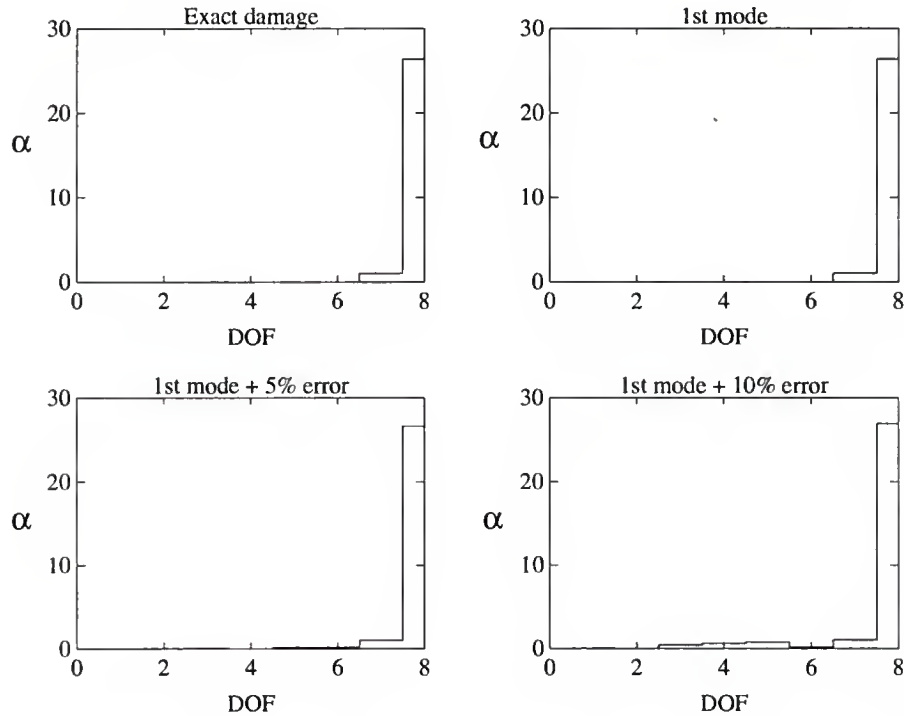


Figure 7.3 Kabe's Problem: Damage Location Results using the Angle Perturbation Method with the Eigendata of the 1st Mode.

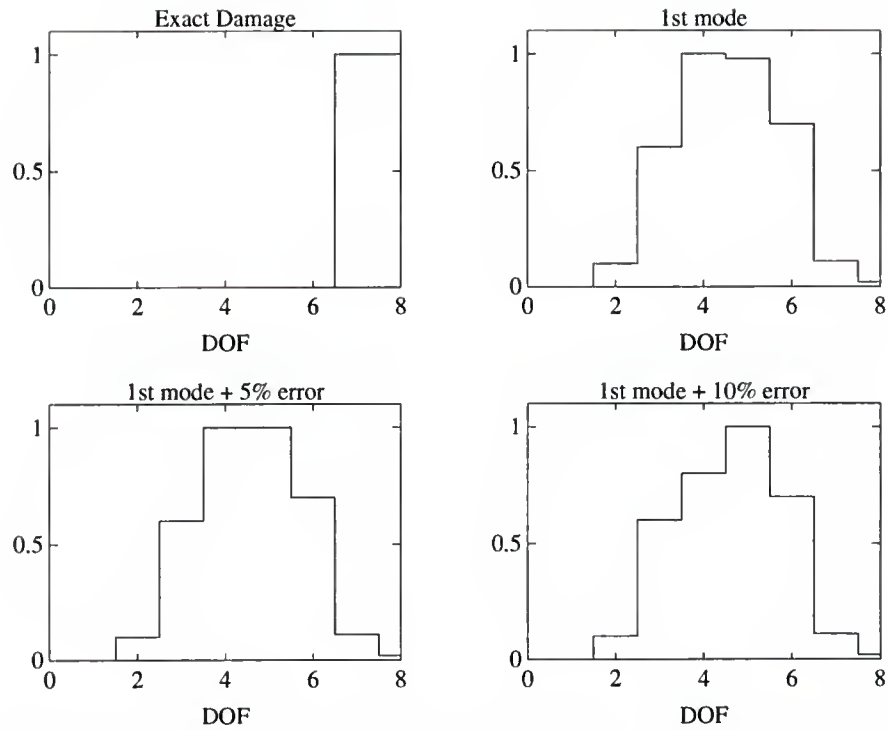


Figure 7.4 Kabe's Problem: Damage Location Results using Lin's Algorithm with the Eigendata of the 1st Mode.

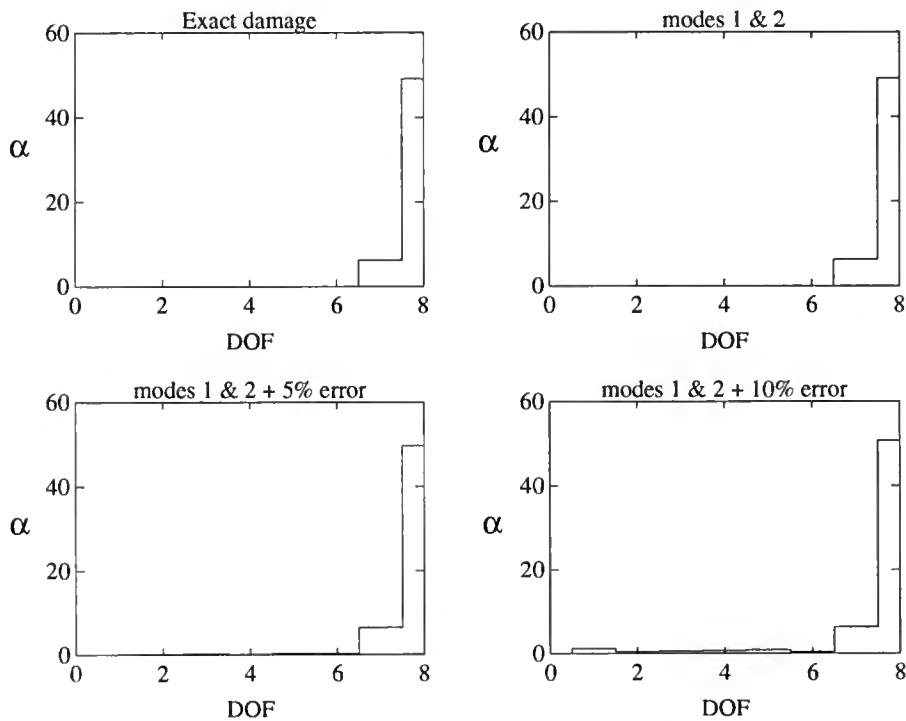


Figure 7.5 Kabe's Problem: Damage Location Results using the Angle Perturbation Method with the Eigendata of the 1st and 2nd Modes.



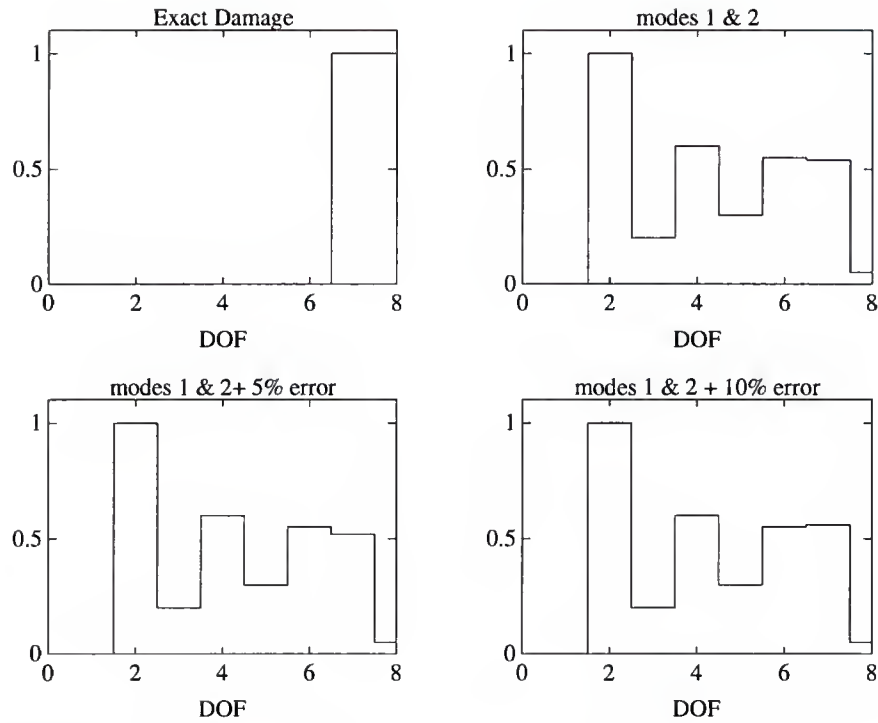


Figure 7.6 Kabe's Problem: Damage Location Results using Lin's Algorithm with the Eigendata of the 1st and 2nd Modes.

### 7.2.3 Damage Extent

In the previous two-mode noisy test case, inspection of the cumulative damage vector clearly indicates that the 7th and 8th degrees of freedom have experienced damage. Inspecting the structural connectivity, it can be deduced that the spring between mass 7 and 8 has been damaged. The rank of the single spring “element” matrix is one. Thus, the rank of the “true” perturbation to the stiffness matrix due to damage is one. From Proposition 6.1 and 6.2, it is clear that only experimental data from one mode of vibration should be used to compute the extent of damage. In the noisy cases, as discussed in Section 6.6.1, the mode that should be used in the extent calculation is the one associated with a  $\underline{d}_i$  that most clearly demonstrates the damage location shown in Figure 7.5. A simple inspection of the individual  $\underline{d}_i$  of the two measured modes indicates that mode 2 provides the best insight into the state of damage. Figure 7.7 presents element-by-element stiffness perturbation matrix results from the application of the extent algorithm, formulated in Section 6.3.3, using mode 2

eigendata. The x-coordinates on each plot are the indices of a column vector constructed by storing the upper triangular portion of the perturbation stiffness matrix ( $\Delta K_d$ ) in a column vector. The y-coordinate on all plots consists of the difference between the updated stiffness matrix and the original stiffness matrix (i.e.  $\Delta K_d$ ). In the noise free case, it should be noted that the exact damage would be computed using any single set of eigenvalue/eigenvector measurement. The extent algorithm experiences a modest degradation as the measurements are corrupted by noise.

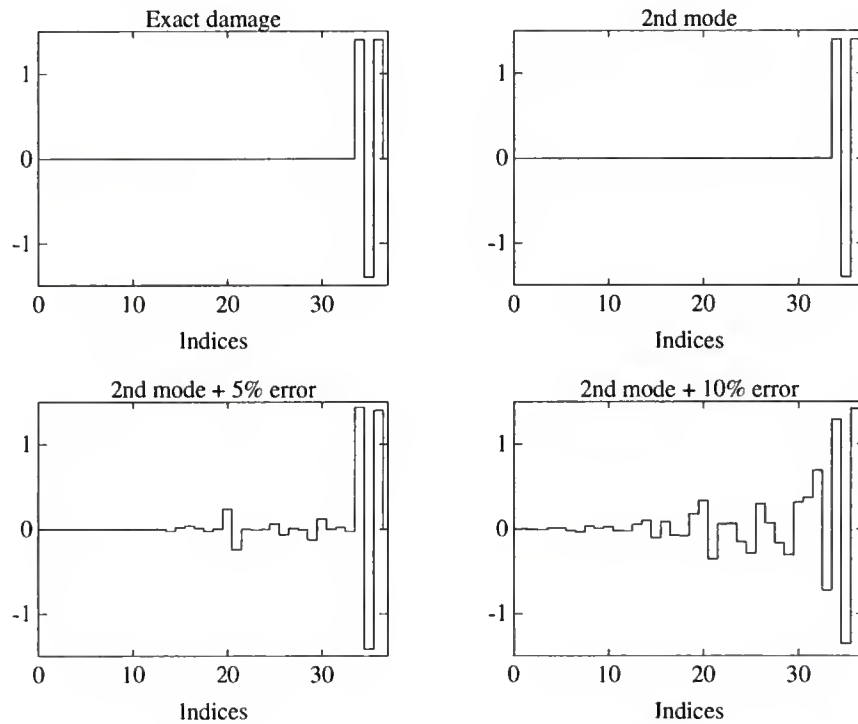


Figure 7.7 Kabe's Problem: Damage Extent Results using the MRPT with the Eigendata of Mode 2.

To contrast the proposed minimum rank perturbation approach to the optimal matrix update approaches, consider the application to the current problem of the commonly used method formulated by Baruch and Bar Itzhack (1978). Although this algorithm was developed from a model refinement viewpoint, it has been investigated for possible uses in damage detection (Smith, 1992). It is evident from Figure 7.8 that this algorithm is unable to discern the damage for this particular example when provided with (i) the second mode's exact eigendata, or (ii) the first six modes' exact eigendata. In fact, it can be seen in the upper

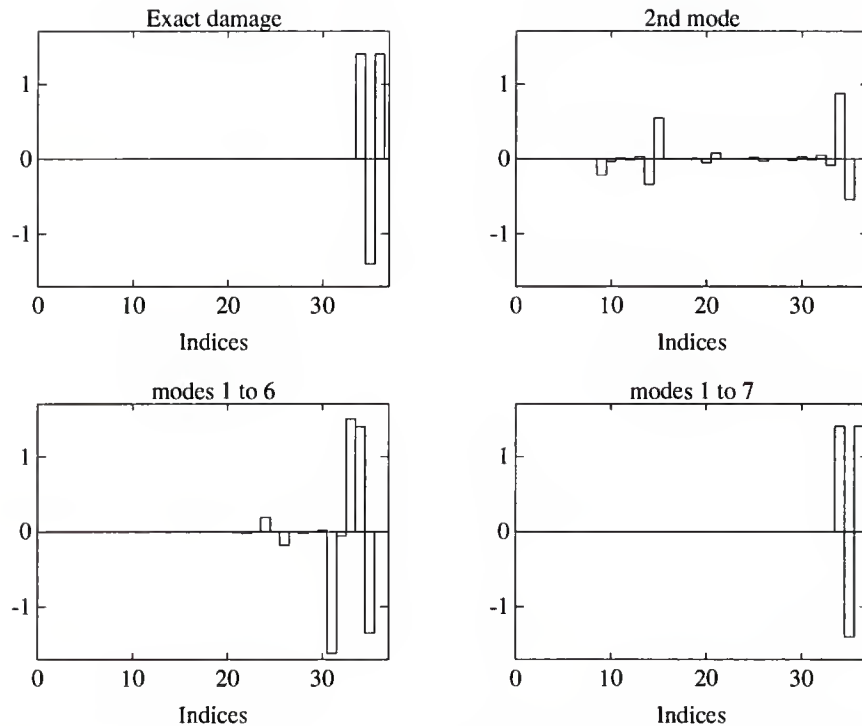


Figure 7.8 Kabe's Problem: Damage Extent Results using Baruch's Method.

right plot of Figure 7.8 that, consistent with the minimum Frobenius norm change formulation, the approach tends to “smear” the changes throughout the entire stiffness matrix instead of localizing them at the damage location. In this problem, this method is only able to cleanly ascertain the damage when provided with the exact eigendata of the first seven modes.

### 7.3 Damage Detection: Fifty-Bay Two-Dimensional Truss: Undamped FEM

#### 7.3.1 Problem Description

The 50-bay, 2-dimensional truss used in this example is shown in Figure 7.9. The geometric and material properties of the truss are also given in the figure. Each truss member was modeled as a rod element. The finite element model of the structure has 201 degrees of freedom and is undamped. In this example, damage is simulated by reducing the Young's modulus of two members. One of the damaged members is the upper longeron of the third

bay. In this member, the Young's modulus is decreased from  $E=2.0 \times 10^{11}$  Pa ( $29 \times 10^6$  psi) to  $6.895 \times 10^6$  Pa ( $1 \times 10^3$  psi). The other member is the lower longeron of bay forty. This member is subjected to a complete loss of stiffness (Young's modulus equal to zero). It is assumed that only the first ten modes of vibration are measured.

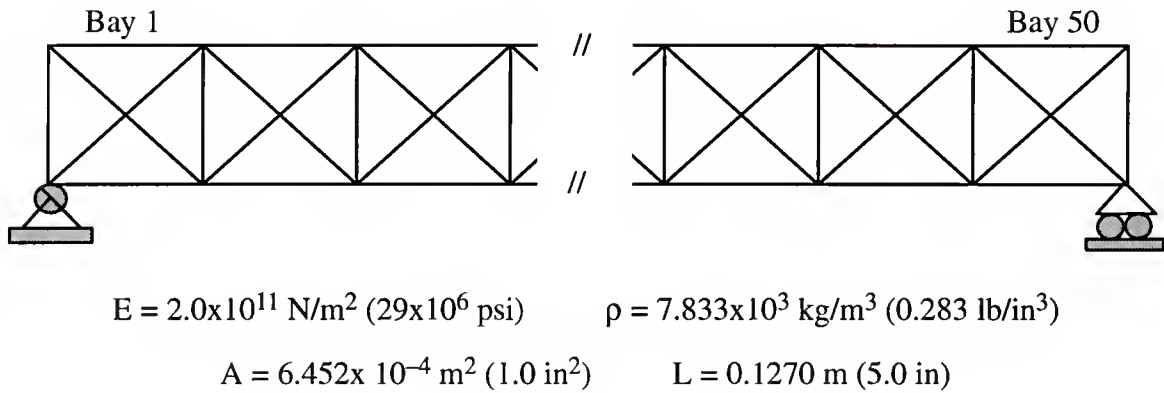


Figure 7.9 Fifty-Bay Two-Dimensional Truss.

### 7.3.2 Damage Location

The first task in this analysis is to use the damage location algorithm to determine the location of the damage. Since the  $\underline{z}_{d_i}^j$  row norms (defined in Section 5.3) associated with this particular FEM are of the same order of magnitude, either the subspace rotation direct method or the angle perturbation method can be used to locate the damage. The results from the application of the subspace rotation direct method are summarized in Figure 7.10. The upper left plot of Figure 7.10 represents the exact damage location. The upper right plot corresponds to the case where the exact (noise free) “damaged” eigenvector information is provided to the algorithm. The lower left and right plots correspond to the case where the exact “damaged” eigenvectors have been corrupted with 2.5% and 5% random noise, respectively. As shown in Figure 7.10, the location algorithm is able to exactly locate the damage when presented with noise free information. It is also seen that the algorithm

experiences a degradation in detecting damage as the error in the eigenvectors is increased; however the damage is still locatable.

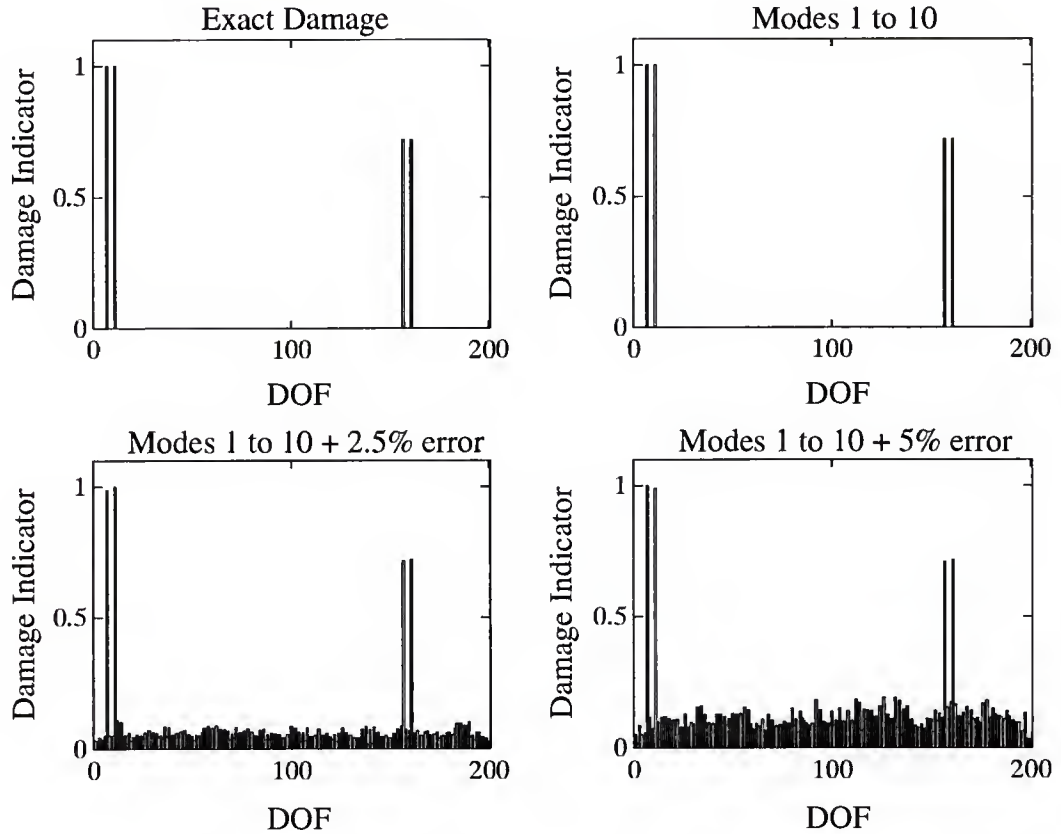


Figure 7.10 Fifty-Bay Truss: Damage Location Results using the Subspace Rotation Algorithm with the Eigendata of the First Ten Modes.

### 7.3.3 Damage Extent

With knowledge of the location of damage from the previous analysis, the rank of the “true” perturbation to the stiffness matrix,  $\Delta K_d$  can be found by adding the rank of the element stiffness matrix of the damaged members. Hence, the rank of the perturbation to the stiffness matrix due to damage is two because two members having rank one element matrices are damaged. From Proposition 6.1 and 6.2, it is clear that only experimental eigendata from two modes of vibration should be used to compute the extent of the damage. In the noisy cases, the two modes that should be used are the ones with  $\underline{d}_i$ ’s that most clearly demonstrate the damage shown in Figure 7.10. These modes can be determined by



inspecting the individual damage vectors  $\underline{d}_i$  associated with the measured modes. In reviewing the individual  $\underline{d}_i$ , it was determined that modes 8 and 9 provide the best insight into the state of the damage. The results of applying the extent algorithm to determine the perturbations to the stiffness matrix due to the damage,  $\Delta K_d$ , are shown in Figure 7.11. The mesh plots are 3-dimensional representations of the perturbation matrices. The rows and columns of the mesh plots correspond to the rows and columns of the perturbation matrices. The “height” of each peak represents the magnitude of the perturbation made to each matrix element. In Figure 7.11, the upper left mesh plot represents the exact damage. The upper right plot corresponds to the case where exact eigendata are used in computing the extent of damage. Note that with only two noise free eigenvalues / eigenvectors (modes 8 and 9), the algorithm is able to reproduce the exact damage. As stated and proved in Proposition 6.2, the exact damage can be computed using any two noise free modes that have a corresponding  $B$  (defined in Section 6.3.2) of rank two. The left and right mesh plots of the second row of Figure 7.11 correspond to the cases where the eigenvectors have been corrupted with 2.5% and 5% random noise, respectively. The algorithm again demonstrates good performance when faced with noisy eigendata (middle plots). The results of applying the eigenvector filtering algorithm described in Section 6.6.2 to predict the extent using modes 8 and 9 are shown in the left and right lower plots of Figure 7.11. It is obvious that the filtering process greatly enhances the accuracy of the extent algorithm. Figure 7.12 displays the MRPT’s assessment of the damage extent, for the noisy eigenvector cases, when the eigendata of the first ten modes of vibration are used. A comparison of the results in Figure 7.12 and those in the second row of Figure 7.11 shows that the above procedure which resulted in the use of only modes 8 and 9 to assess the extent provided cleaner results. In the mesh plots of Figure 7.12, additional numerical values appear at the “undamaged” DOFs which can be attributed to the noise added by the addition of the extra modes. The resultant perturbation matrices when using all ten modes are of rank 10 which is not consistent with the “actual” damage perturbation which is of rank 2. Furthermore, this “ten modes procedure” is less

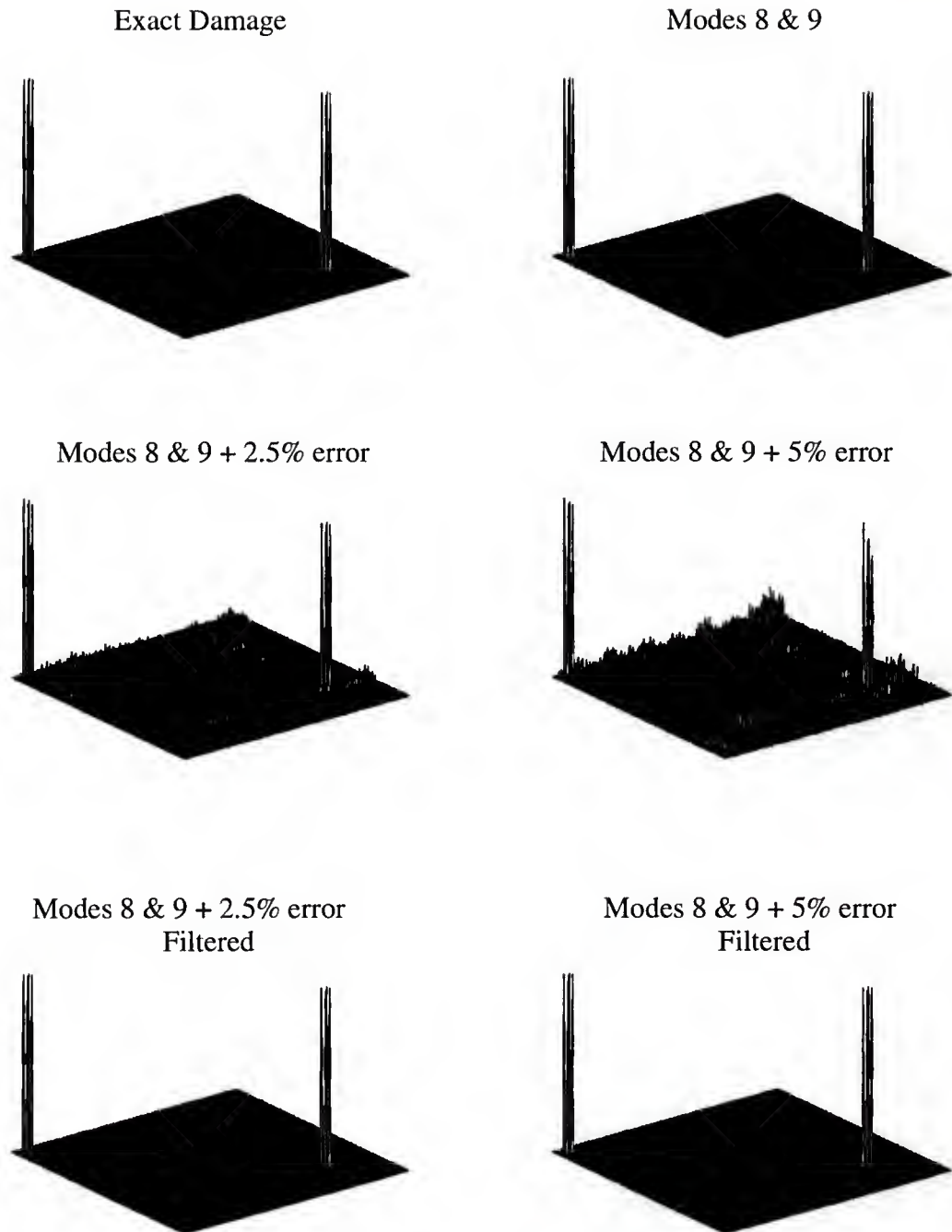


Figure 7.11 Fifty-Bay Truss: Damage Extent Results using the MRPT with the Eigendata of Modes 8 and 9.

efficient since it requires the inversion of a 10-by-10 matrix, contrasted to the 2-by-2 inverse used in the “two modes procedure.” The percentage errors of the predicted damage extent with respect to the exact stiffness damage for all studied cases, with and without filtering,

are listed in Table 7.1. It can be seen from the table, the results obtained when the eigenvector filtering process is used are much more accurate. The results from the “two modes procedure” are, in all cases, but one, better than the “ten modes procedure”.

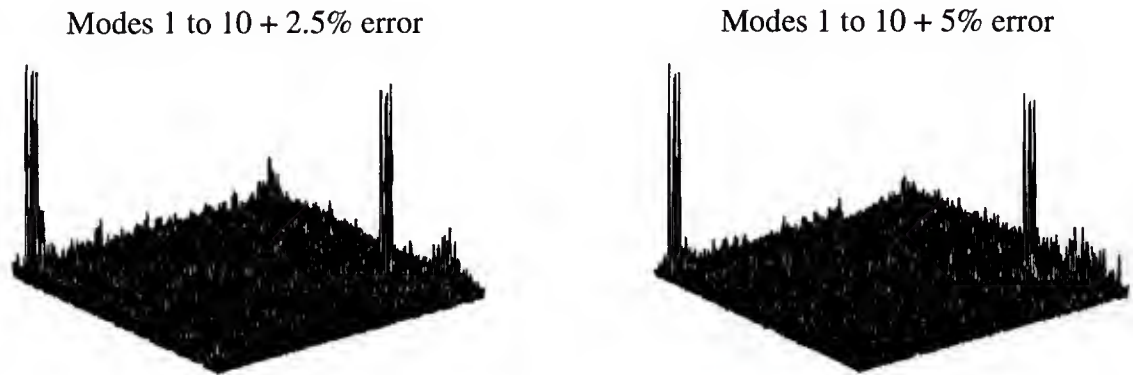


Figure 7.12 Fifty-Bay Truss: Damage Extent Results using the MRPT With the Eigendata of the First Ten Modes.

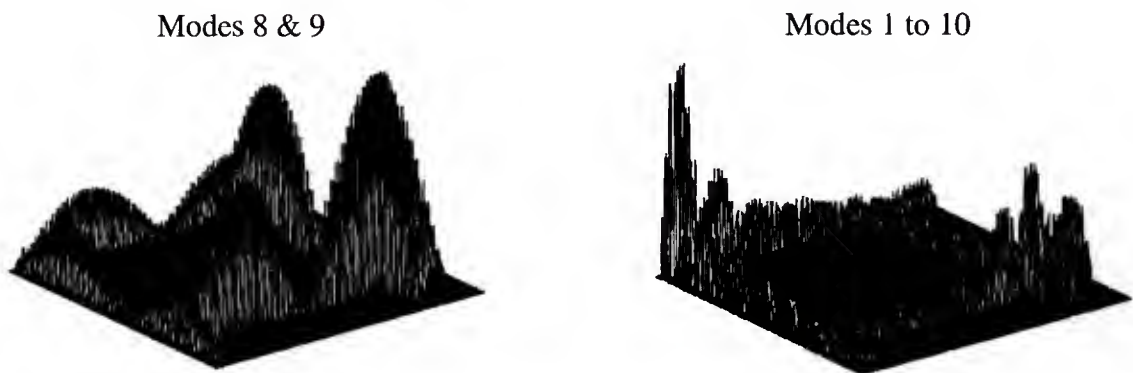


Figure 7.13 Fifty-Bay Truss: Damage Extent Results using Baruch's Algorithm.

For the sake of comparison, results from the application of Baruch and Bar Itzhack's algorithm (1978) are provided in Figure 7.13. These results were obtained using (i) noise free eigendata from modes 8 and 9, and (ii) noise free eigendata from the first ten modes. In both cases, Baruch's algorithm fails to ascertain the extent of the damage. In the first case, the approach completely “smeared” the changes throughout the entire stiffness matrix. In the second case, the changes are more localized around the damaged areas.

Table 7.1 Fifty-Bay Truss: Summary of Damage Extent Results using the MRPT.

Percentage Error with Respect to the Exact Damage						
	Without Filtering – Modes 1 to 10		Without Filtering – Modes 8 & 9		With Filtering – Modes 8 & 9	
	Upper Longeron of Bay Three	Lower Longeron of Bay Forty	Upper Longeron of Bay Three	Lower Longeron of Bay Forty	Upper Longeron of Bay Three	Lower Longeron of Bay Forty
Eigenvectors Error						
0.0%	Not Applicable	Not Applicable	0.00%	0.00%	Not Applicable	Not Applicable
2.5%	7.90%	13.03%	3.49%	7.89%	0.00%	0.07%
5.0%	14.70%	20.30%	13.31%	24.89%	0.00%	0.00%

## 7.4 Experimental Study: The NASA 8-bay Truss

### 7.4.1 Problem Description

The eight bay hybrid-scaled truss used in this investigation is part of a series of structures designed for research in dynamic scale model ground testing of large structures at the NASA Langley Research Center. Among other studies, a complete analytical and experimental analysis of this truss was performed to generate a realistic testbed for structural damage location/extent algorithms (Kashangaki et al., 1992; Kashangaki, 1992). The truss configuration used in this analysis was cantilevered and instrumented with ninety-six accelerometers to measure all three translational degrees of freedom at each of the thirty-two unconstrained nodes. A schematic of this truss is shown in Figure 7.14. Figure 7.15 shows a close-up of the truss lacing pattern along with strut definitions that will be used in the remainder of this study.

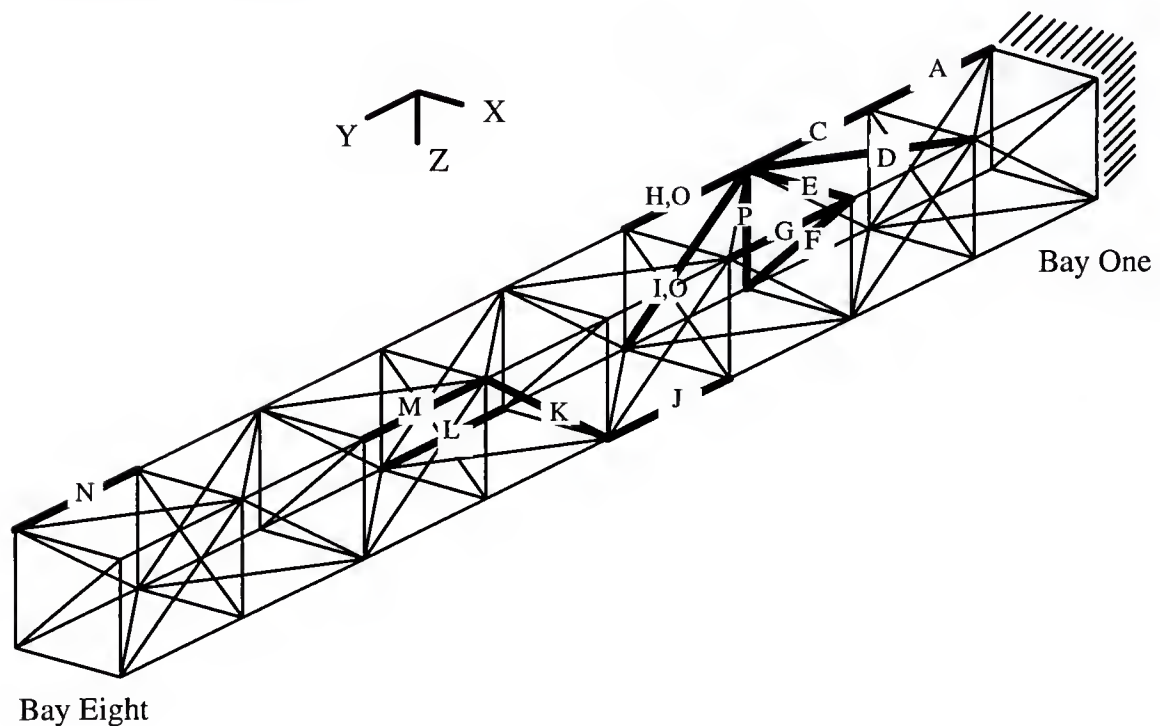


Figure 7.14 The NASA Eight-Bay Hybrid-Scaled Truss: Damage Cases.



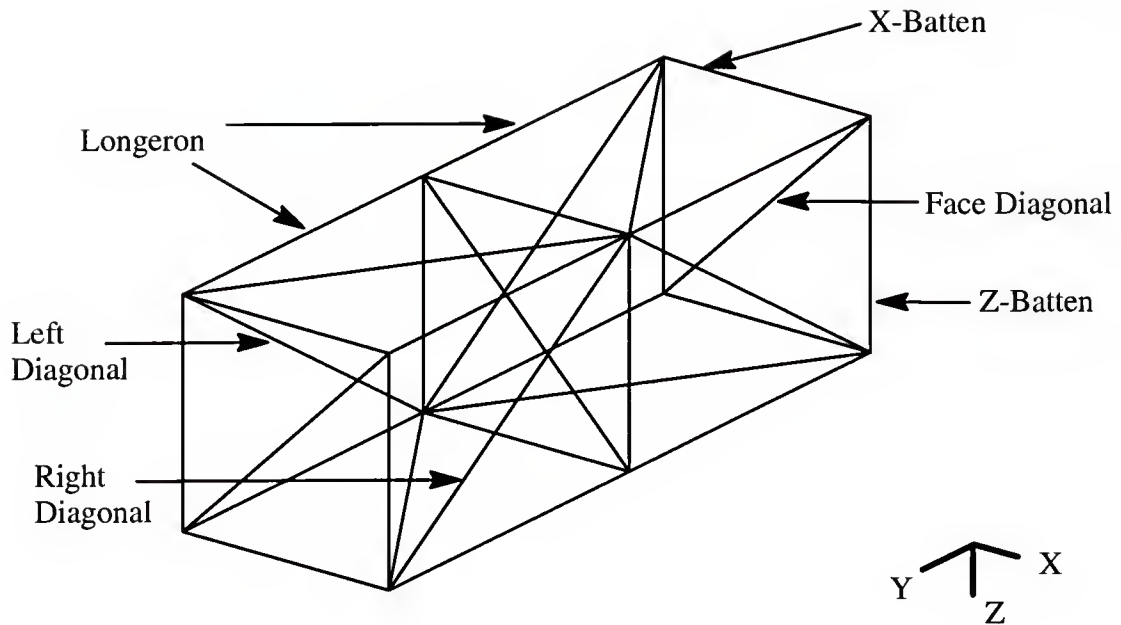


Figure 7.15 The NASA 8-Bay Truss: Lacing Pattern.

A ninety-six degree of freedom undamped finite element model (FEM) of the original “healthy” truss was generated using MSC/NASTRAN. In this FEM, each truss strut was modeled as a rod element. Concentrated masses were added at each node to account for the joint and instrumentation mass properties (Kashangaki, 1992). The mass and strut properties of the truss are summarized in Tables 7.2 and 7.3.

Table 7.2 Mass Properties of the Eight Bay Truss.

	Weight (Pounds)	Total Number in Eight Bay Truss	Total Weight (Pounds)
Node Ball	0.0128	36	2.6935
Longeron Strut	0.0396	68	2.4524
Diagonal Strut	0.0598	41	0.4608
Joint Assembly	0.0170	218	3.7001
Triax + Block	0.0243	32	0.7760
Total Weight of the Truss			10.0776

Table 7.3 Strut Properties of the Eight Bay Truss.

	Longeron	Diagonal
Strut Length	19.685 in	27.839 in
Strut Stiffness $(EA/L)_{eff}$	13,040 lb/in	9,013 lb/in

Experimental modal analysis of the truss was performed for the “no damage” and sixteen damage cases. In the testing, the excitation source was provided by two shakers. Modal parameters were identified from the measured frequency response functions using the Polyreference complex exponential technique. For each case, five modes of vibration were identified. Each measured mode consists of a natural frequency and its corresponding mode shape with measurements at all ninety-six FEM degrees of freedom. For the “no damage” case, the first, second, fourth and fifth mode are bending modes; and the third mode is the first torsional mode. In the damage cases, the same five modes were measured; however their order varies, since in some cases, the damage could cause mode switching. It should be noted that during the testing process, two accelerometers at node fifteen failed. These defective accelerometers would affect the component of the measured modes associated with DOFs 44 and 45.

Data for fifteen of the sixteen damage cases tested were received from NASA. The fifteen damage cases that were received are identified in the schematic of the truss shown in Figure 7.14. For each damage case, the type of element and the FEM degrees of freedom affected by damage are shown in Table 7.4.

In damage cases A to N, structural damage consisted of the full removal of one strut from the truss. Case O damage consists of the full removal of two struts. In Case P, one of the struts was buckled to illustrate a partial damage scenario. Note that the forthcoming analysis of the fifteen damage cases was performed with no a priori knowledge of the actual damage locations.

Table 7.4 NASA 8-Bay Truss Damage Case Definitions.

Damage Case	Element Type	Damaged DOFs
A	Longeron	86
C	Longeron	74, 86
D	Upper Diagonal	73, 74, 88, 89
E	X-Batten	73, 76
F	Face Diagonal	76, 78, 79, 81
G	Longeron	65, 77
H	Longeron	62, 74
I	Left Diagonal	68, 69, 74, 75
J	Longeron	59, 71
K	Right Diagonal	41, 42, 59, 60
L	Longeron	44, 56
M	Longeron	29, 41
N	Longeron	2, 14
O*	Longeron & Diagonal	62, 68, 69, 74, 75
P**	Z-Batten	75, 81

\* Two struts removed

\*\* Buckled strut

#### 7.4.2 Refinement of the Original FEM

The original FEM provided by NASA is a first generation analytical model that was not modified to match the experimentally measured modal parameters. It was found that the original FEM does not accurately predict the dynamic behavior of the actual structure. As an illustration to the inaccuracy of the original FEM, Table 7.5 shows a comparison between the analytically computed and experimentally measured natural frequencies. Another commonly used criterion to judge the accuracy of the original analytical FEM is to compare

its frequency response functions to those measured experimentally. One such comparison is shown in Figure 7.16. It is clear from this typical frequency response comparison that the original FEM is lacking in accuracy.

Table 7.5 Comparison of Analytical and Experimental Frequencies

MODE #	Natural Frequencies (Hz)	
	Analytical	Experimental
1	13.9245	13.8757
2	14.4407	14.4783
3	46.7445	48.4122
4	66.0067	64.0332
5	71.1420	67.4631

Hence, the first step in this study was to refine the original FEM. For the refinement process, it was assumed that the original mass matrix is an accurate representation of the truss' mass properties. The inaccuracy of the original FEM was believed to be solely due to modeling errors in the stiffness properties. The minimum rank perturbation theory discussed in Chapter 6 (Section 6.3.2) was used to correct the original stiffness matrix. In order to get a symmetric updated stiffness matrix, the measured mode shapes (eigenvectors) were mass orthogonalized using the Optimum Weighted Orthogonalization technique (Baruch 1978).

A mesh plot of the changes made to the stiffness matrix ( $\Delta K$ ) from the refinement process is shown in Figure 7.17. As can be seen in the figure, there are three areas of major change made to the original stiffness matrix. One area of change corresponds to the cantilever end of the truss. This change was expected since a perfect cantilever condition was assumed in generating the original FEM. Note that it is common knowledge that perfect cantilever conditions cannot be produce in practice. Other changes can be seen in the middle of the mesh plot. These changes occur at and around DOFs 44 and 45 which are the location of the bad sensors. Hence, these changes were attributed to the effect of the bad sensors. Yet,

another area of changes can be seen near the free end. These areas coincide with the locations of the two shakers. The reason for the perturbation at these shaker locations is that their localized stiffness effects were not modelled in the original FEM. The improvement made to the original analytical FEM from the MRPT refinement process can also be seen in Figure 7.16. It is apparent from comparing the frequency response functions corresponding to experimental measurement, original FEM and the refined FEM that the MRPT provided a great deal of improvement to the original FEM. The amplitude mismatch between the experimental data and refined FEM prediction can be attributed to the fact that the actual effects of the damping were not considered in the analytical models. Note that the actual damping of the truss is small and negligible but it is nonzero.

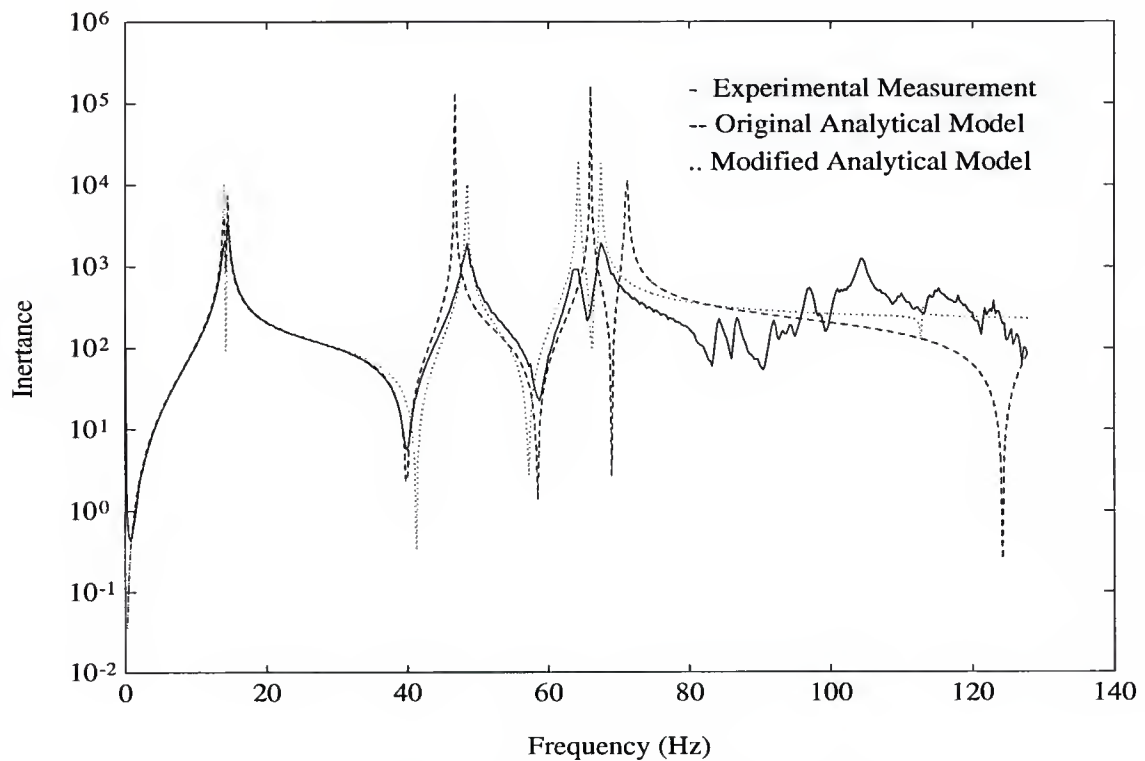


Figure 7.16 NASA 8-bay Truss: Typical Frequency Response Comparison.



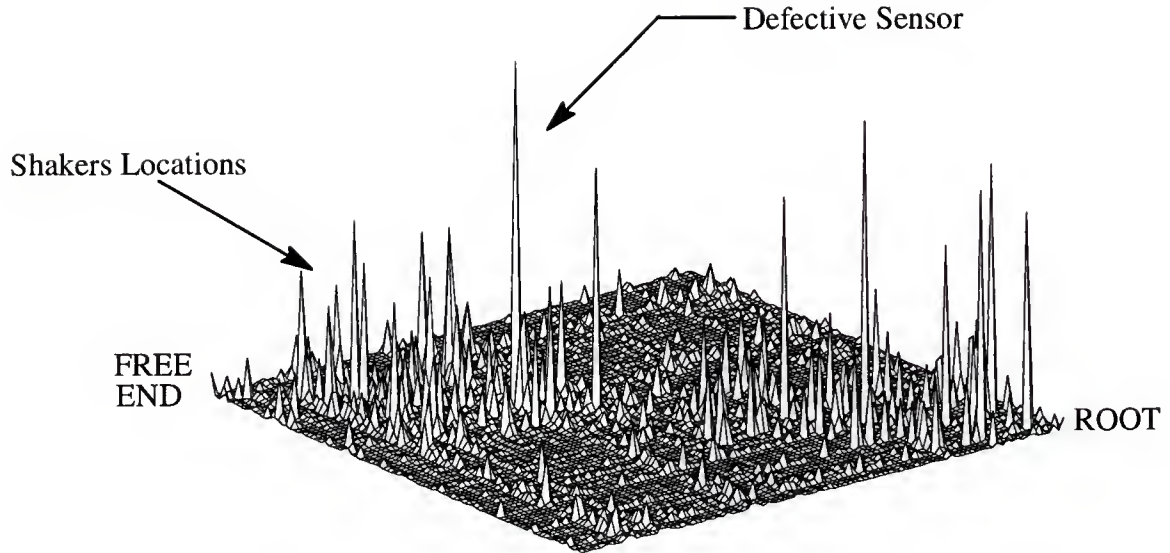


Figure 7.17 NASA 8-bay Truss: Perturbation to the Original Stiffness Matrix that Resulted from the Refinement Process.

#### 7.4.3 Damage Location

For each damage case, the modal parameters of the five measured modes were used to compute a cumulative damage location vector (CDLV) to determine the location of the structural damage. Since the values of  $\| \underline{z}_{d_i}^j \|$ , as defined in Section 5.3, are of the same orders of magnitude for all DOFs and all five measured modes, the cumulative damage location vector (CDLV) could be computed using either Eq. (5.4.1) or Eq. (5.4.2). The angle perturbation CDLV (Eq. (5.4.2)) associated to damage case F is shown in Figure (7.18). The upper left corners of Figures (7.19) to (7.32) display plots of the cumulative damage location vectors as calculated by Eq. (5.4.2) for all cases where the damage was successfully located. In these plots, the CDLV were unit normalized and their elements were plotted versus the FEM DOFs. The performance of the location algorithm for each damage case is summarized in the second column of Table 7.7. A summary of the procedures used in the interpretation of the CDLV of each damage case is as follows:

- (1) Initially, a comparative study of the CDLV for all cases was performed to deduce the effects of the bad accelerometers. A fairly large numerical component at DOF 44 was detected in most of the fifteen CDLV. This component was believed to be due to the “bad” sensor located at DOF 44. Hence, for all cases, it was decided to ignore the component of the CDLV at DOF 44.
- (2) For damage cases A, C, D, G, H, I, J, K, M, N and O, the location of the damage was determined by simply considering the DOFs associated with the substantially larger numerical components of the CDLV's as being the damaged DOFs. The smaller numerical components of the CDLV's at the other DOFs can be attributed to measurement errors. Notice that for cases D, I, J, M and N, the component of the CDLV at DOF 44 is fairly small and hence negligible. It should be also noted that the damage in Case A affects only one degree of freedom (86) since the strut involved is a longeron connected to the cantilevered end.
- (3) For damage case E, the DOFs associated with the CDLV components of greater order of magnitude are 42, 73, 75, 76 and 81. By utilizing the connectivity of the original FEM, the combinations of these DOFs that are physically meaningful, i.e. bound a strut, are (73, 76) and (75, 81). Based on these results, it was decided that two struts connecting DOF (73, 76) and (75, 81) were damaged. However, in actuality the only damaged strut is the one connecting DOFs (73, 76).
- (4) For damage case L, by ignoring DOF 44 ( the “bad” sensor), the only DOF that is clearly damaged is 56. No strut with DOF 56 is connected to the wall. The damage of a strut not connected to the cantilevered end must affect at least two DOFs . Since DOF 56 is in the y-direction, it was deduced that the most probable damaged strut is a longeron connected at one end to DOF 56. The two candidate struts are the ones bounded by DOFs (44, 56) and (56, 68). However, the component of the CDLV associated with

DOF 68 is small and is in no way affected by damage. This prompted the deduction that the strut connecting DOFs 44 and 56 is the damaged member in Case L.

- (5) For damage case P, the substantially larger components of the CDLV occur at DOFs 42, 75 and 81 (DOF 44 ignored). Again, with the use of the connectivity of the original FEM, it is deduced that the only combination of these three DOFs that are connected by a strut is (75, 81). These DOFs are exactly the damaged DOFs of Case P.
- (6) Damage Case F is the only case where the location algorithm failed to locate the damage. The cumulative damage vector for this case is shown in Figure 7.18. The reason the damage was not located in this case is that it involves a face diagonal strut. Face diagonal struts, in general, affect only the axial modes and have slight or no effects on the bending and torsional modes. As reported earlier, the only available (measured) modes are bending and torsional modes. It was determined analytically that the first axial mode of the truss occurs at the sixth mode.

Kashangaki et al. (1992) performed a pure analytical study to compile a list of the elements of the 8-bay truss that have a substantial contribution to the total strain energy for each of the five measured modes. The present study confirms that the damage in struts that have a substantial contribution to the total modal strain energy for the measured modes is detectable. However, our study also shows that damage of non-highly strained struts for the measured modes can also be located as illustrated in cases G and N. Note that the damage in cases E and F involves struts with low strain energy for the measured modes.

#### 7.4.4 Damage Extent

Because the truss under investigation is light weight and very flexible, the effect of structural damage is considered (i) negligible on the overall inertial properties, and (ii) a substantial stiffness loss. Using the extent algorithm discussed in Section 6.3.2, the perturbation to the stiffness matrix ( $\Delta K_d$ ) due to the damage is calculated for each damage case where the damage was successfully located. To insure the symmetry of  $\Delta K_d$ , the

eigenvectors used in these calculations were first mass orthogonalized using the Optimum Weighted Orthogonalization technique (Baruch and Bar Itzhack, 1978).

#### 7.4.4.1 The Brute Force Method

The upper right corners of Figures 7.19 to 7.32 display mesh plots of the calculated  $\Delta K_d$ 's using the modal parameters of all five measured modes. From these mesh plots, it is clear that on the average the extent algorithm failed to concentrated the major changes at the damaged DOFs. This unsatisfactory performance of the extent algorithm can be attributed to the measurement error of the defective accelerometers. In most cases, the major changes are concentrated at DOF 44, which corresponds to the location of a defective accelerometer. In addition, for any given damage case, as discussed in Section 6.6.1, only a subset of the measured modes are highly affected by damage. Using modes that are not highly affected by damage only introduces their associated measurement noise in the extent calculation.

#### 7.4.4.2 The Damage Consistent Method

As discussed in Section 6.6.1 and illustrated in the previous example, for each damage case, the performance of the extent algorithm can be improved by only using as many modes as the rank of the “actual”  $\Delta K_d$ . The rank of the “actual”  $\Delta K_d$  can be estimated by adding the rank of all element stiffness matrices which connect damaged DOFs. Since the elemental stiffness matrix of the truss under investigation is rank one, the rank of the “actual”  $\Delta K_d$ , for each damage case, is equal to the number of damaged struts. Hence, only modal parameters from one mode are needed to compute the damage extent of all cases featuring one damaged strut. For Case O, since two struts are damaged, data from two modes are needed. For each case, the modes that should be used are the ones that most cleanly demonstrate the state of damage of that case. These modes can be simply determined by inspecting the individual damage location vector  $\underline{d}_i$ . The modes that provide the best insight into the state of the damage for each damage case are reported in the third column of Table 7.7. The unit normalized damage location vectors associated with the “best” modes for all cases are



plotted versus the FEM DOFs in the middle left of Figures 7.19 to 7.32. The mesh plots of the  $\Delta K_d$ 's computed using only the “best” mode(s) for all damage cases are shown in the middle right corners of Figures 7.19 to 7.32. It is clear that the performance of the extent algorithm for all cases has been greatly improved in comparison to its performance when all five measured modes were used. The estimated effective stiffness loss (lb/in) for all damage cases, computed from this process, are reported in the fourth column of Table 7.7. For each damage case, the effective stiffness loss was calculated by averaging the stiffness changes ( $\Delta K_d$ ) associated with the damaged DOFs. In the original FEM, the longerons, X-battens and Z-battens have an effective stiffness of 13,040 lb/in, while the effective stiffness of the diagonal struts is 9,013 lb/in (Kashangaki, 1992). The removal of any strut results in the complete loss of the stiffness of that strut. The fifth column of Table 7.7 reports the percentage error of the estimated stiffness losses with respect to the original FEM. The percentage error for Case P (buckled strut) was not computed since the damage extent is unknown.

#### 7.4.4.3 Application of the Eigenvector Filtering Algorithm

The damage extent assessment can be further improved by using the eigenvector filtering algorithm discussed in Section 5.4.2. For consistency, the mode(s) used in the filtering process are the “best” mode(s) as determined above and reported in the third column of Table 7.7. For each case, the “undamaged” components of the damage vectors  $\underline{d}_i$  are first set to zero. The components of  $\underline{d}_i$  associated to the “damaged” DOFs are then constrained to be consistent with the actual effect of the damage as dictated by the element stiffness matrix of the damage struts. The damage in X-battens, longerons or Z-battens affects two DOFs (one DOF at each of the two nodes of the strut). In order for the damage to be finite element consistent, the component associated with these two DOFs should be equal in magnitude and of opposite sign. Damage in upper, face, left or right diagonal struts affects four DOFs (two at each node of the strut). These four DOFs can be classified into two sets of two DOFs in the same direction (x, y or z). The DOFs of a given set are, in general, equal in magnitude and of



opposite signs. In the 8-bay truss, all upper, face, left or right diagonals are either at a  $45^\circ$  or  $-45^\circ$  angle with respect to their in-plane global coordinate axis. This constrains the DOFs of the two sets to have the same magnitude in order to be consistent with the FEM. The DOFs associated with a given node have the same sign when the angle is  $45^\circ$ ; they are of opposite sign when the angle is  $-45^\circ$ . For the cases where a single strut is damaged the magnitude of a DOF could be set arbitrarily. The reason is that eigenvectors are unique in a relative sense; i.e., if  $\underline{u}_i$  is an eigenvector associated to a given mode then  $\alpha \underline{u}_i$  is also an eigenvector associated to that same mode,  $\alpha$  being any scalar. Thus, the components of the damage vector are also a function of the scalar  $\alpha$ . These components can be set to any values by varying  $\alpha$ . For the single member damage cases under study, this process is summarized in Table 7.6.

Table 7.6 Summary of the Filtering Process for Single Member Damage Cases.

	Node 1			Node 2		
DOF	X	Y	Z	X	Y	Z
X-Batten	$\beta$	0	0	$-\beta$	0	0
Longeron	0	$\beta$	0	0	$-\beta$	0
Z-Batten	0	0	$\beta$	0	0	$-\beta$
Case D ( $-45^\circ$ )	$\beta$	$-\beta$	0	$-\beta$	$\beta$	0
Case I ( $45^\circ$ )	$\beta$	0	$\beta$	$-\beta$	0	$-\beta$
Case K ( $-45^\circ$ )	$\beta$	0	$-\beta$	$-\beta$	0	$\beta$

where  $\beta$  is any scalar

Note that cases A, C, E, G, H, J, L, M, N and P involve the damage of either an X-batten, longeron or Z-batten. As discussed earlier, all DOFs of the filtered damage vector  $\underline{d}_f$ , associated to a given damage member have the same magnitude,  $\beta$ . Experience gained by using the eigenvector filtering algorithm indicates that in the multiple member damage scenario (case O), the ratio between the  $\beta$ 's from different damaged struts contains important

information about the relative damage extent among the damaged struts. Hence, in case O, a given  $\beta$  associated with a given damaged strut cannot be chosen arbitrary. This  $\beta$  should be estimated by averaging the components of the unfiltered damage vector  $\underline{d}_i$  corresponding to the damaged strut in question. The absolute value of the unit normalized filtered damage location vectors associated with all cases are plotted versus the FEM DOFs in the bottom left corners of Figures 7.19 to 7.32. Now that the “filtered” damage vectors are generated, the next step is to compute the corresponding filtered damage eigenvector using Eq. 5.4.3. The process of computing the perturbation due to the damage using the filtered eigenvectors is as in the previous section. For all damage cases, the mesh plots of the  $\Delta K_d$ 's computed using the “filtered” mode(s) are displayed in the bottom right corners of Figures 7.19 to 7.32. The effective stiffness loss computed using the filtering process, for each damage case, is reported in the sixth column of Table 7.7. The seventh column of Table 7.7 reports the percentage error of the estimated stiffness losses with respect to the original FEM. A comparison of these results to the one acquired from the previous section shows that the eigenvector filtering algorithm greatly enhances the extent estimate.

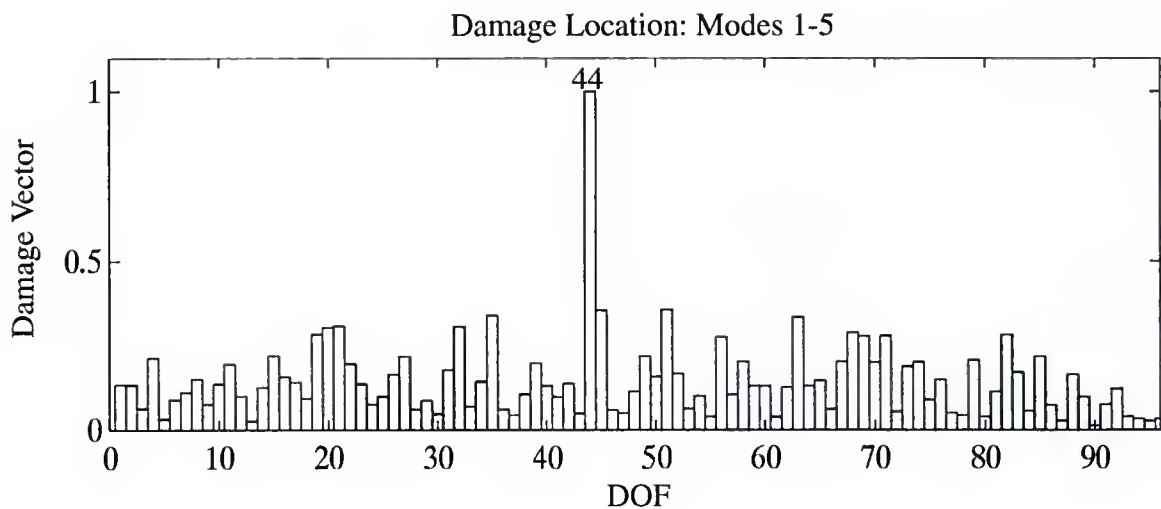


Figure 7.18 NASA 8-bay Truss: Cumulative Damage Vector Associated to Case F.

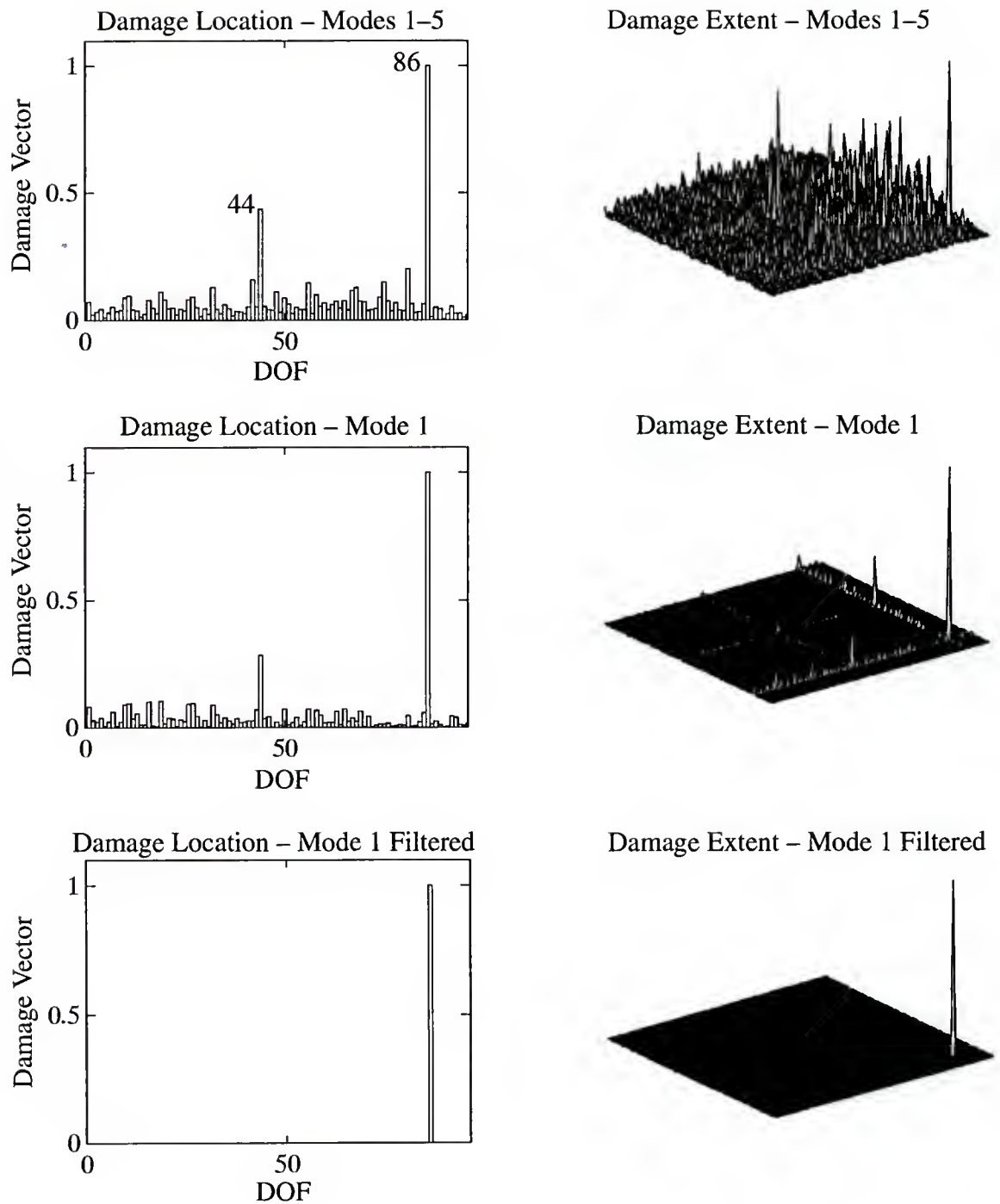


Figure 7.19 NASA 8-bay Truss: Damage Assessment of Case A.

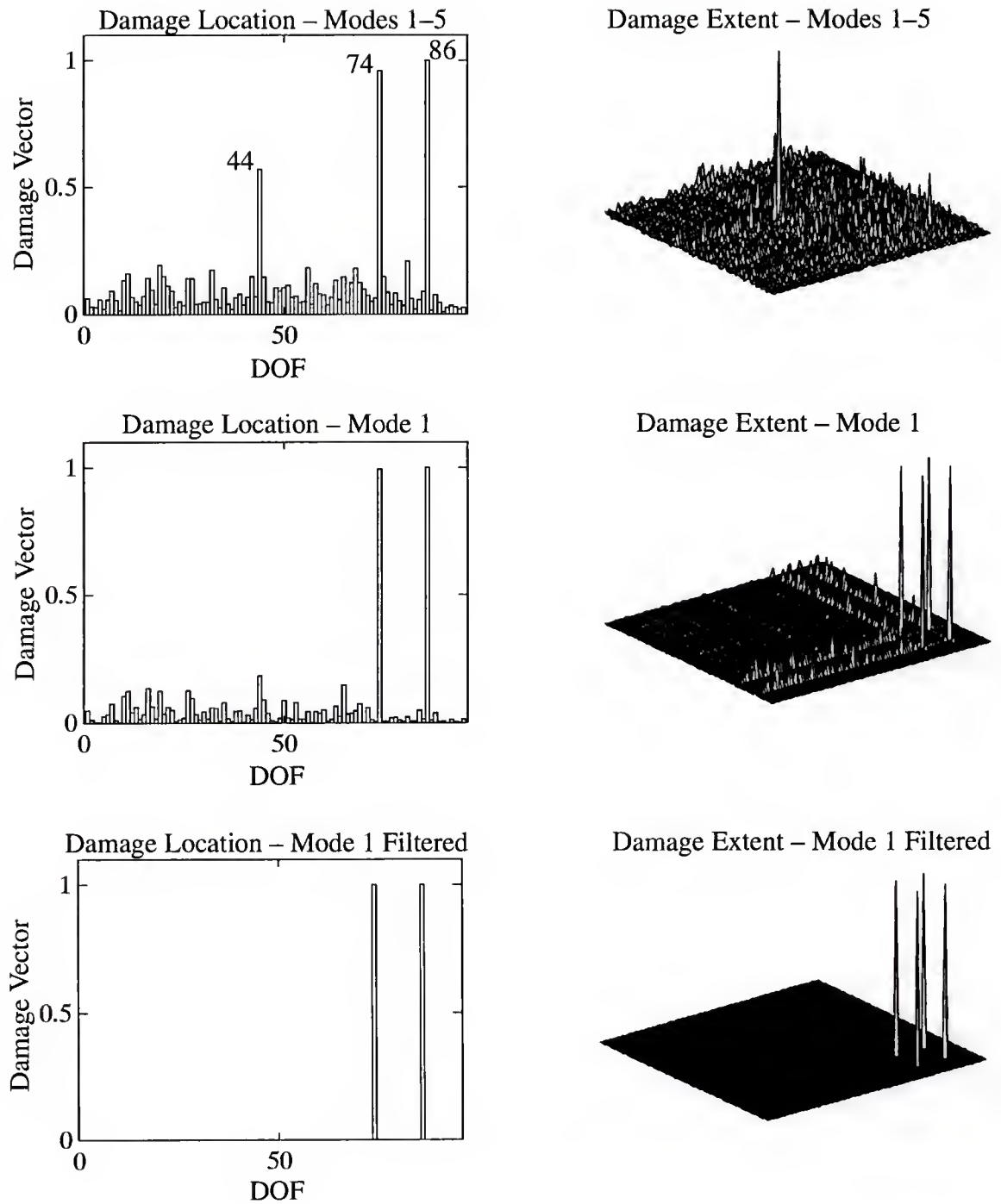
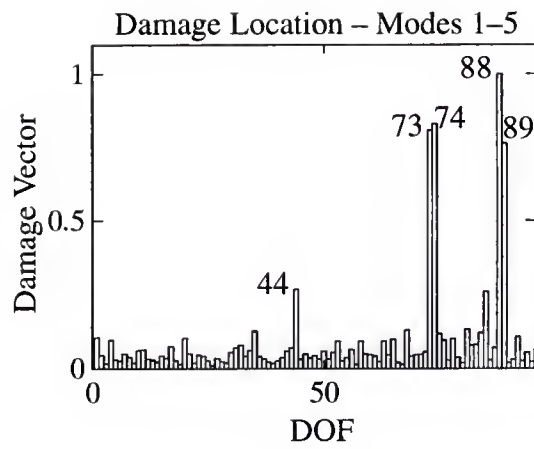
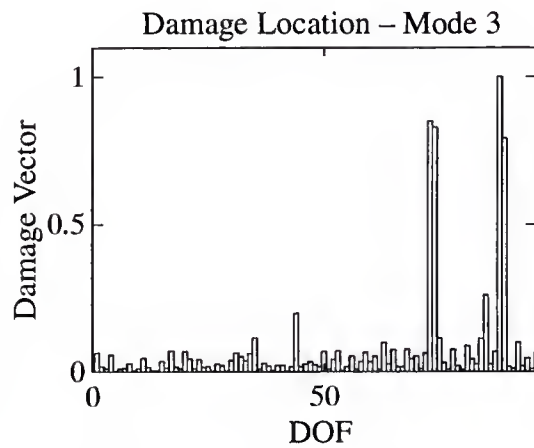
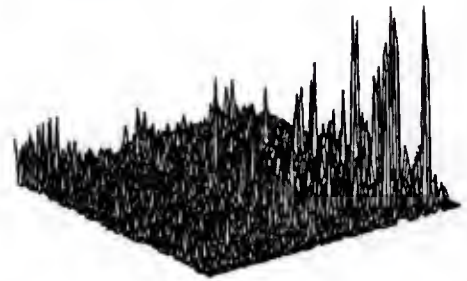


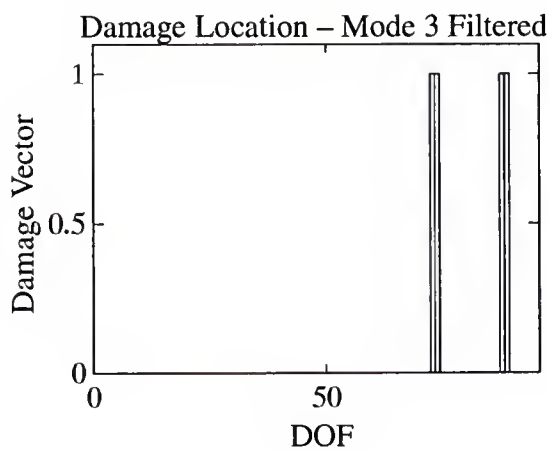
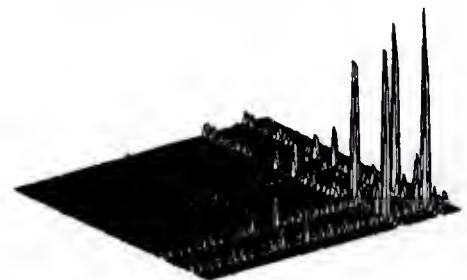
Figure 7.20 NASA 8-bay Truss: Damage Assessment of Case C.



Damage Extent – Modes 1–5



Damage Extent – Mode 3

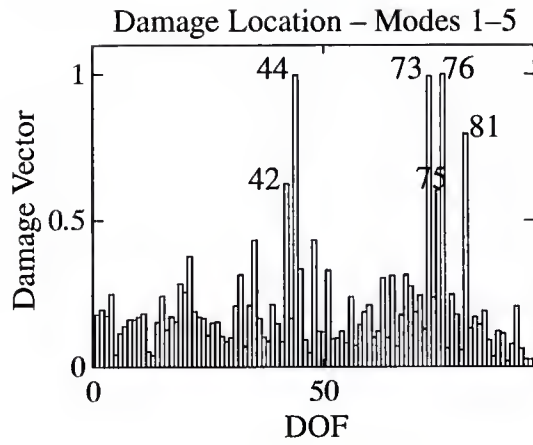


Damage Extent – Mode 3 Filtered

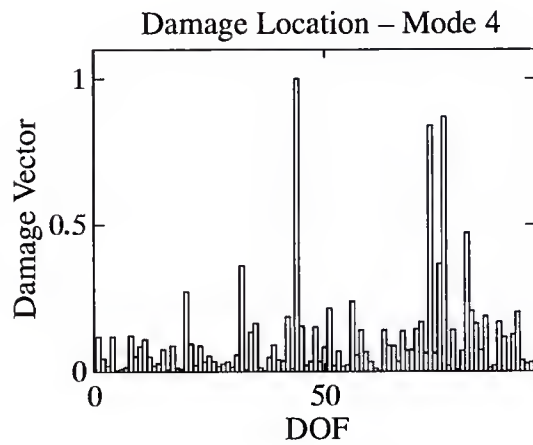
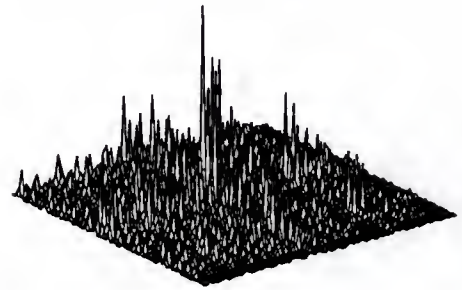


Figure 7.21 NASA 8-bay Truss: Damage Assessment of Case D.

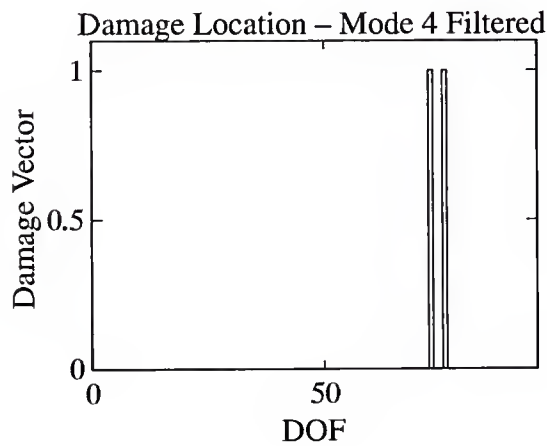
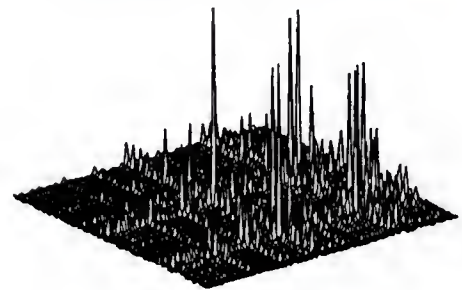




Damage Extent – Modes 1–5



Damage Extent – Mode 4



Damage Extent – Mode 4 Filtered



Figure 7.22 NASA 8-bay Truss: Damage Assessment of Case E.

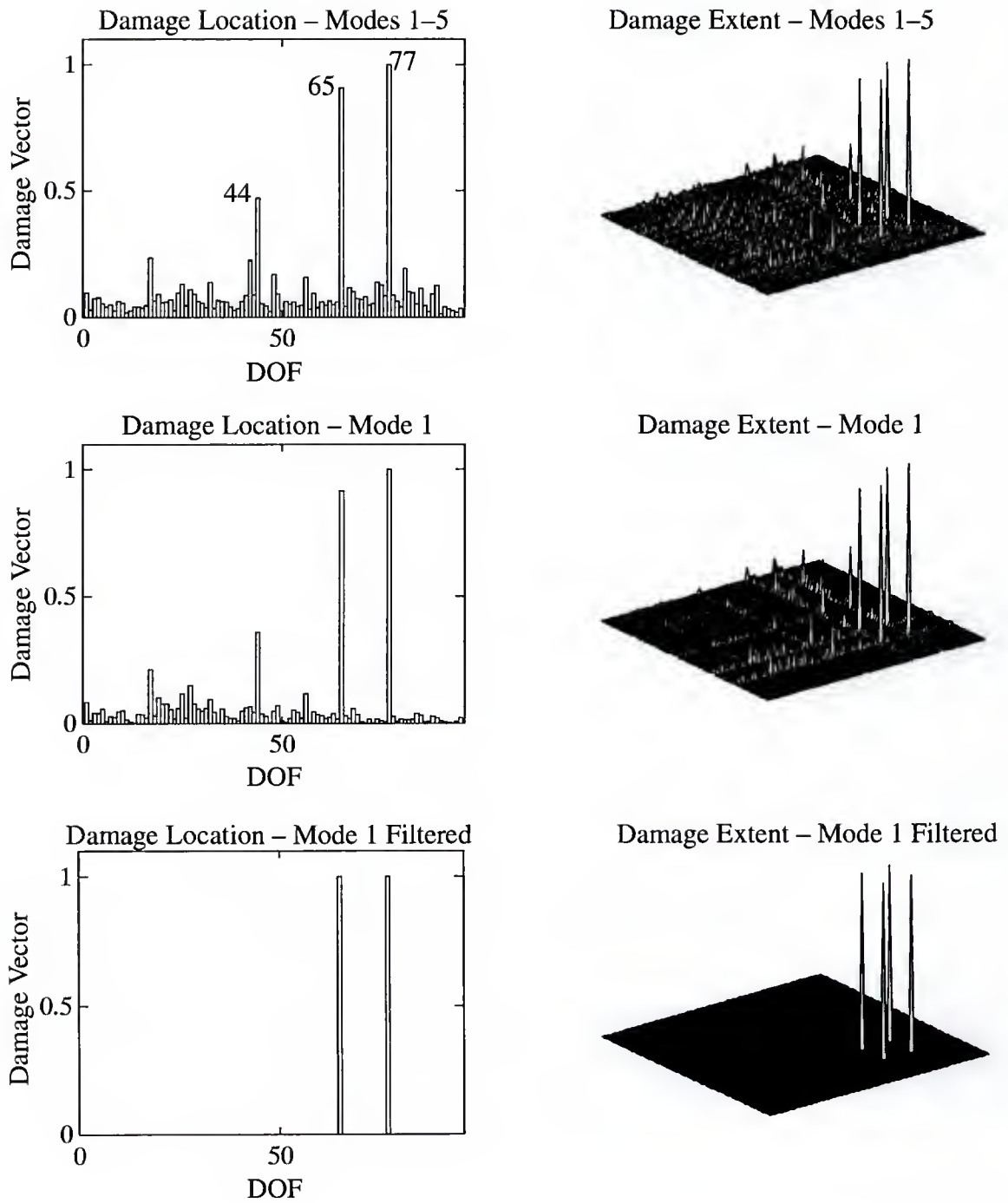


Figure 7.23 NASA 8-bay Truss: Damage Assessment of Case G.

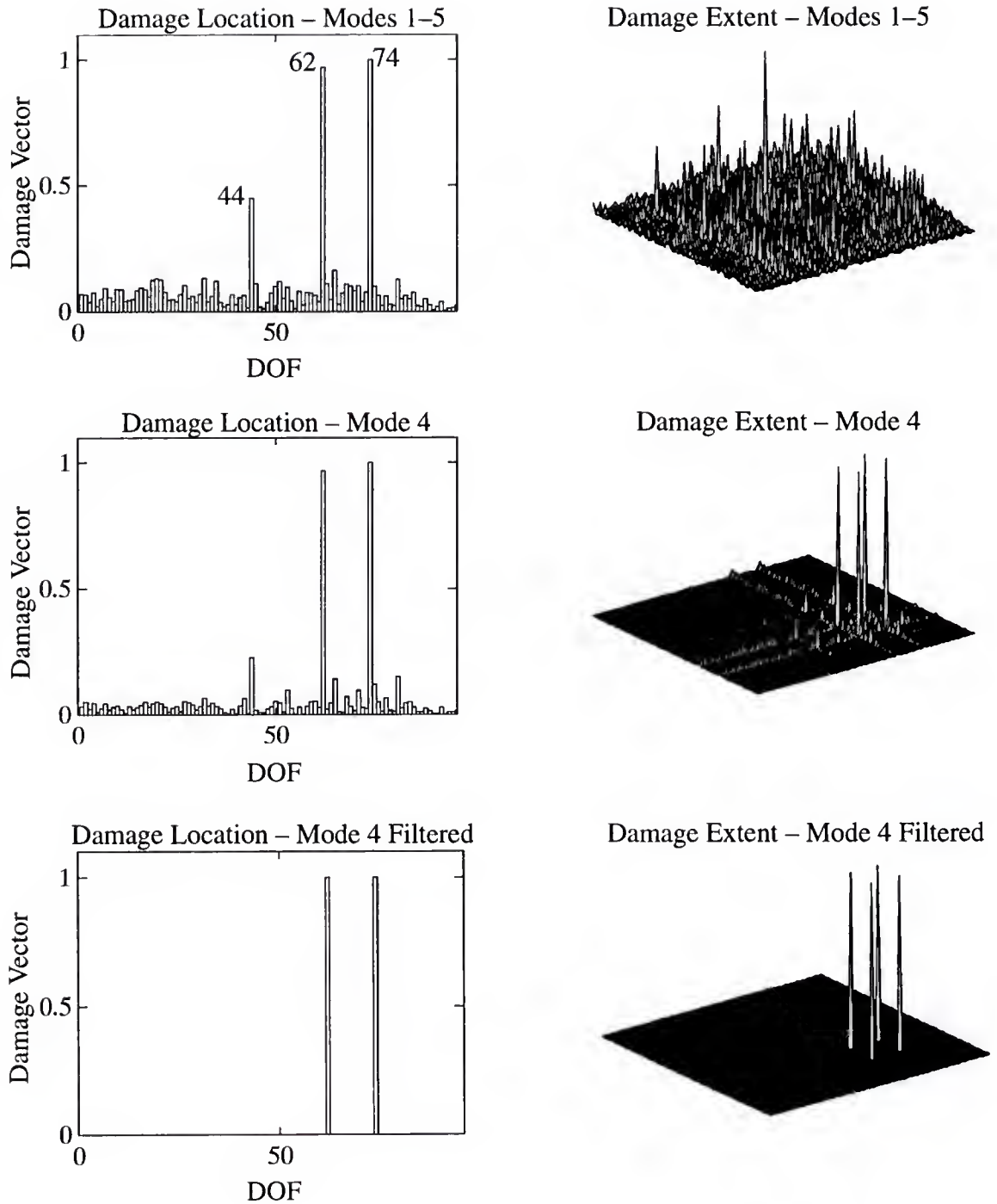


Figure 7.24 NASA 8-bay Truss: Damage Assessment of Case H.

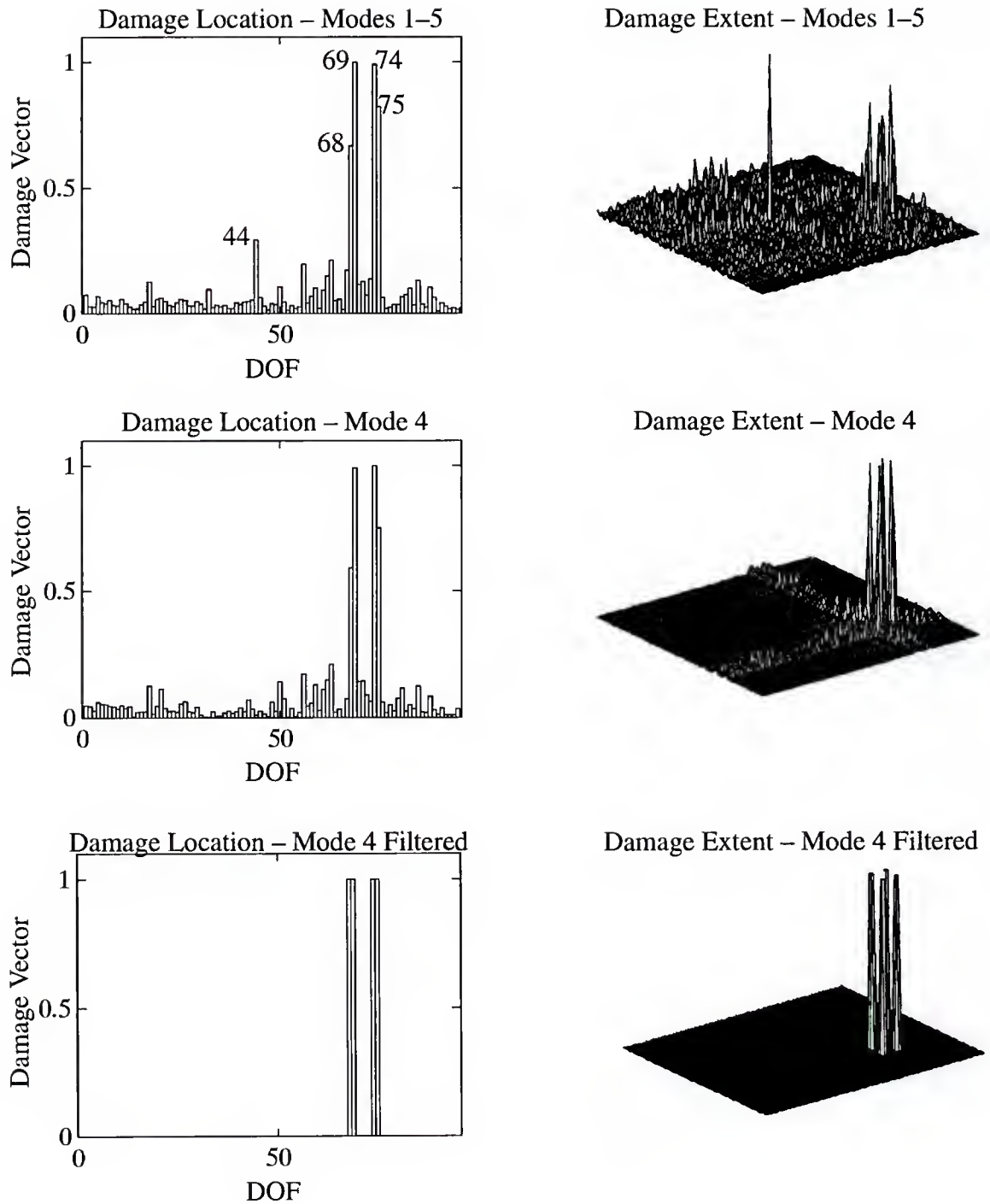


Figure 7.25 NASA 8-bay Truss: Damage Assessment of Case I.

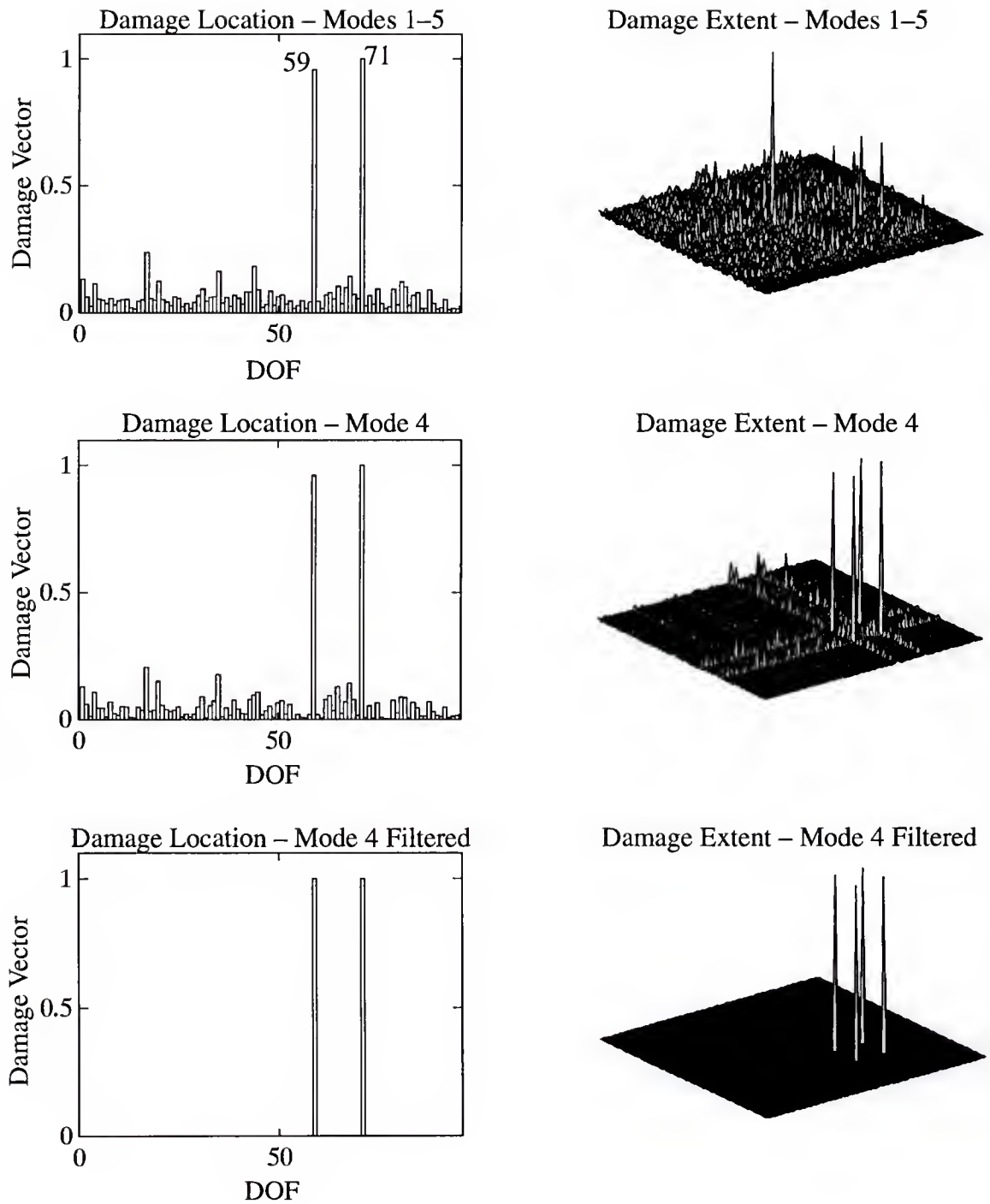


Figure 7.26 NASA 8-bay Truss: Damage Assessment of Case J.



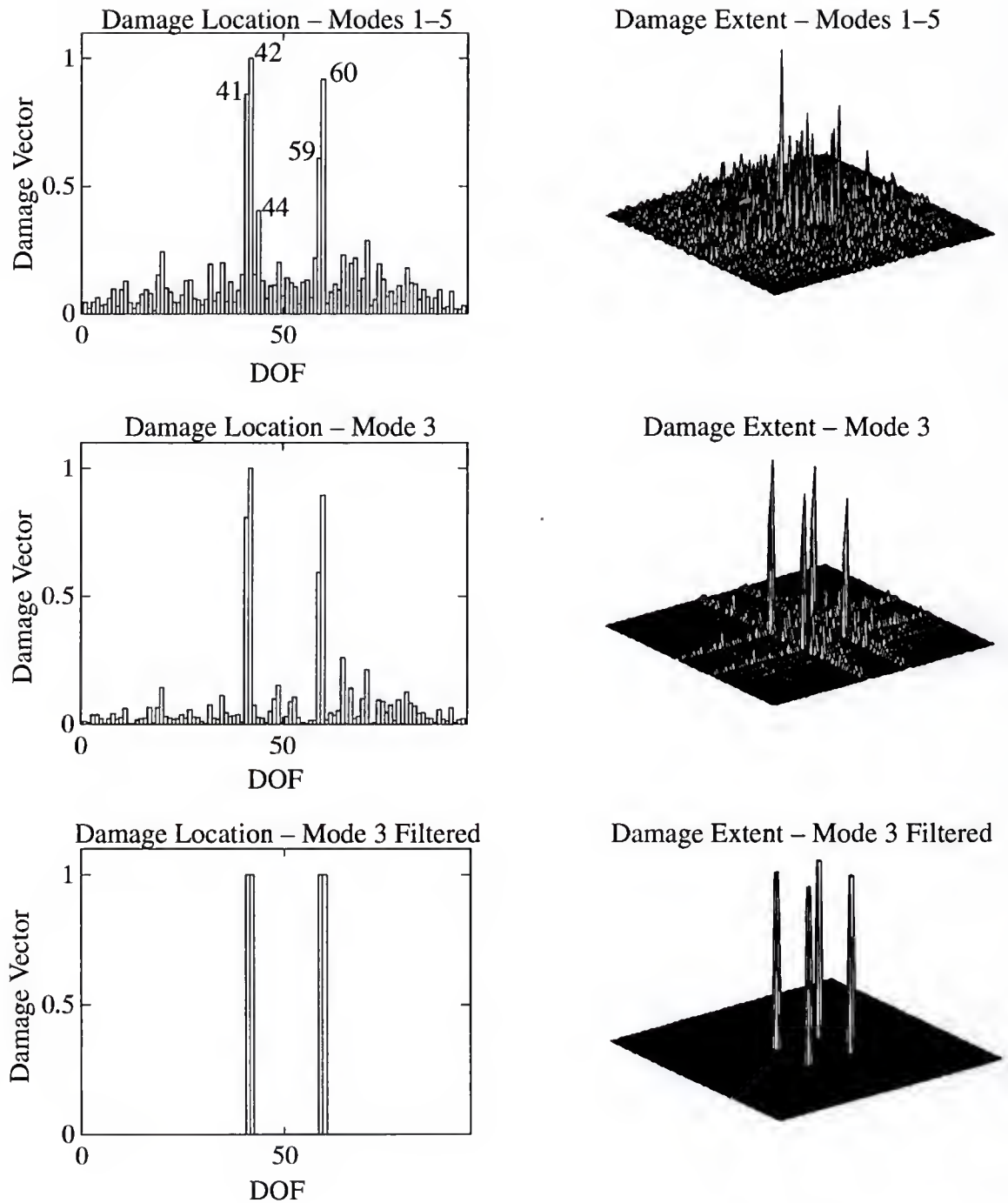


Figure 7.27 NASA 8-bay Truss: Damage Assessment of Case K.

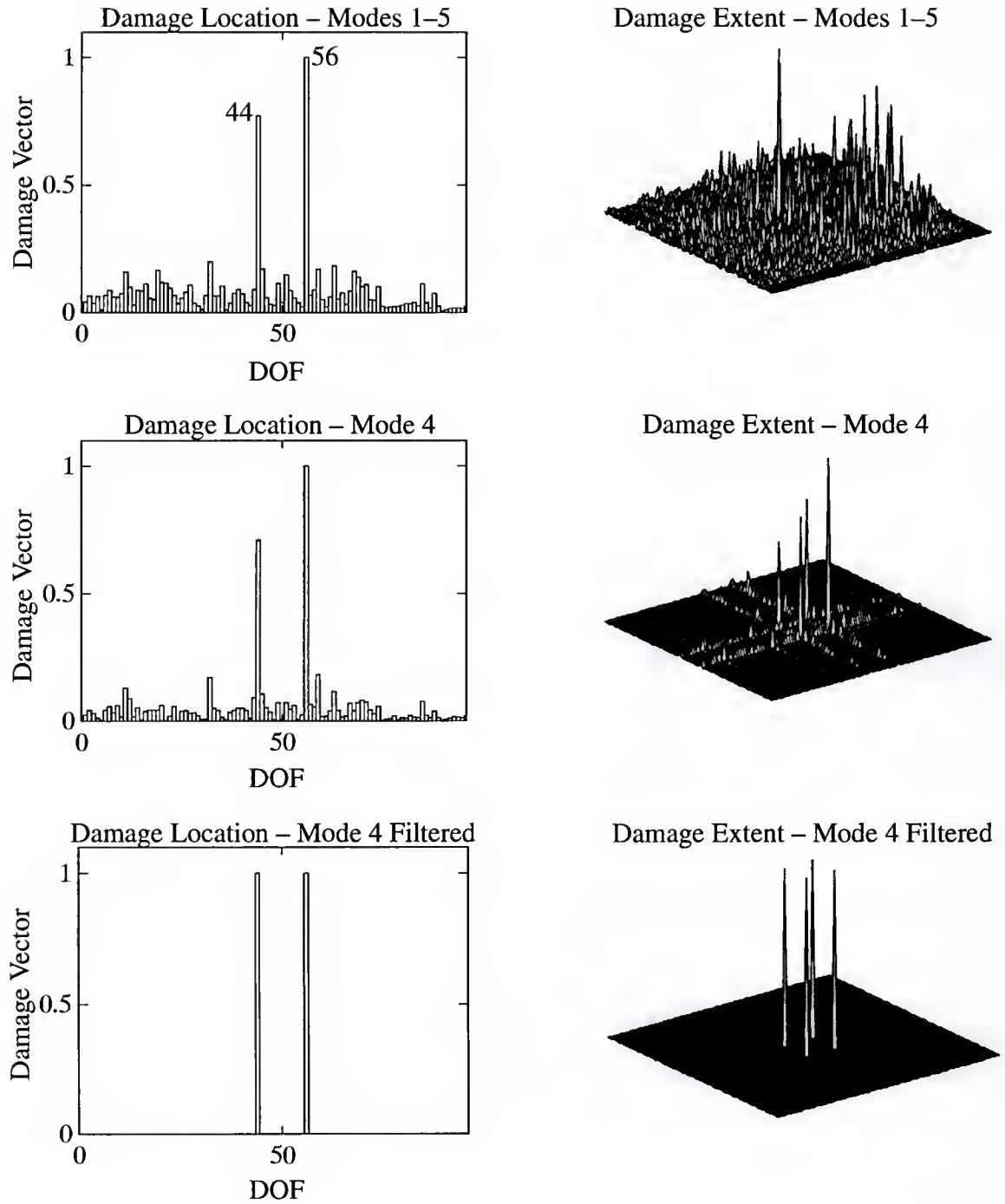
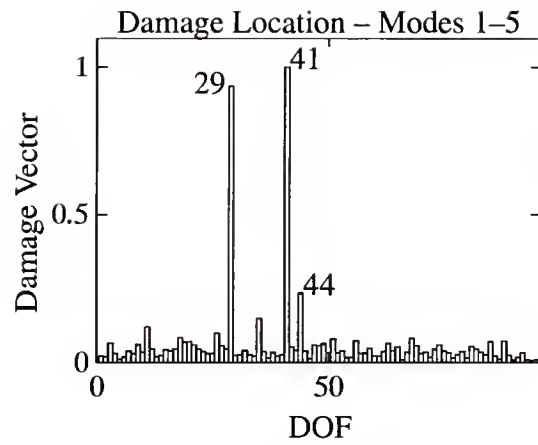
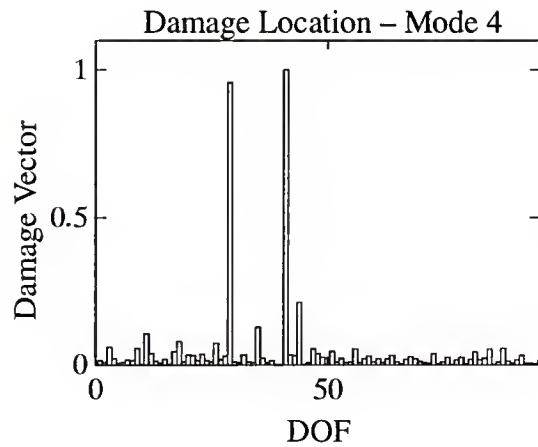
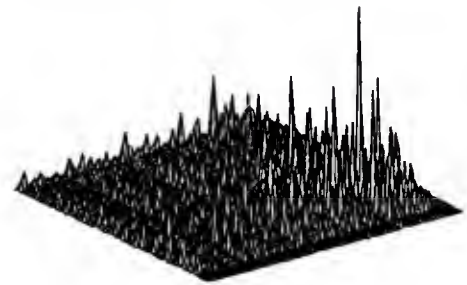


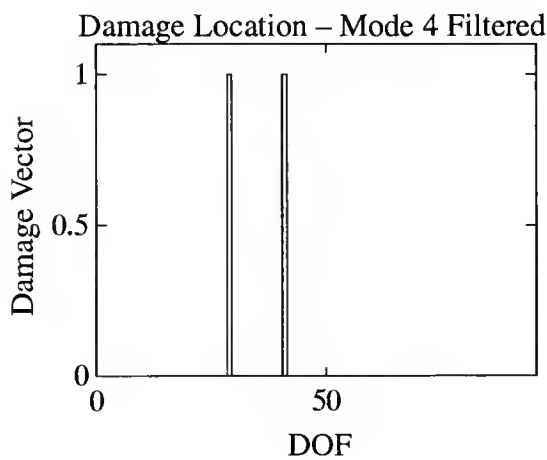
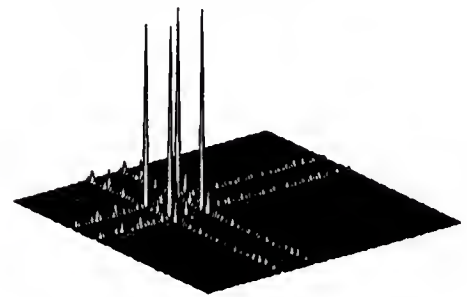
Figure 7.28 NASA 8-bay Truss: Damage Assessment of Case L.



Damage Extent – Modes 1–5



Damage Extent – Mode 4



Damage Extent – Mode 4 Filtered

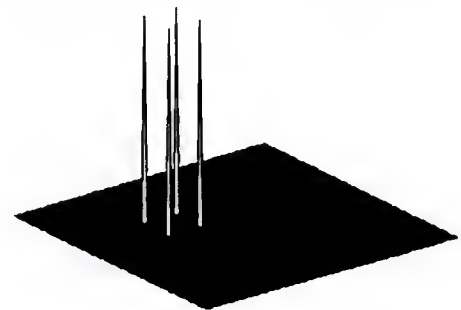


Figure 7.29 NASA 8-bay Truss: Damage Assessment of Case M.

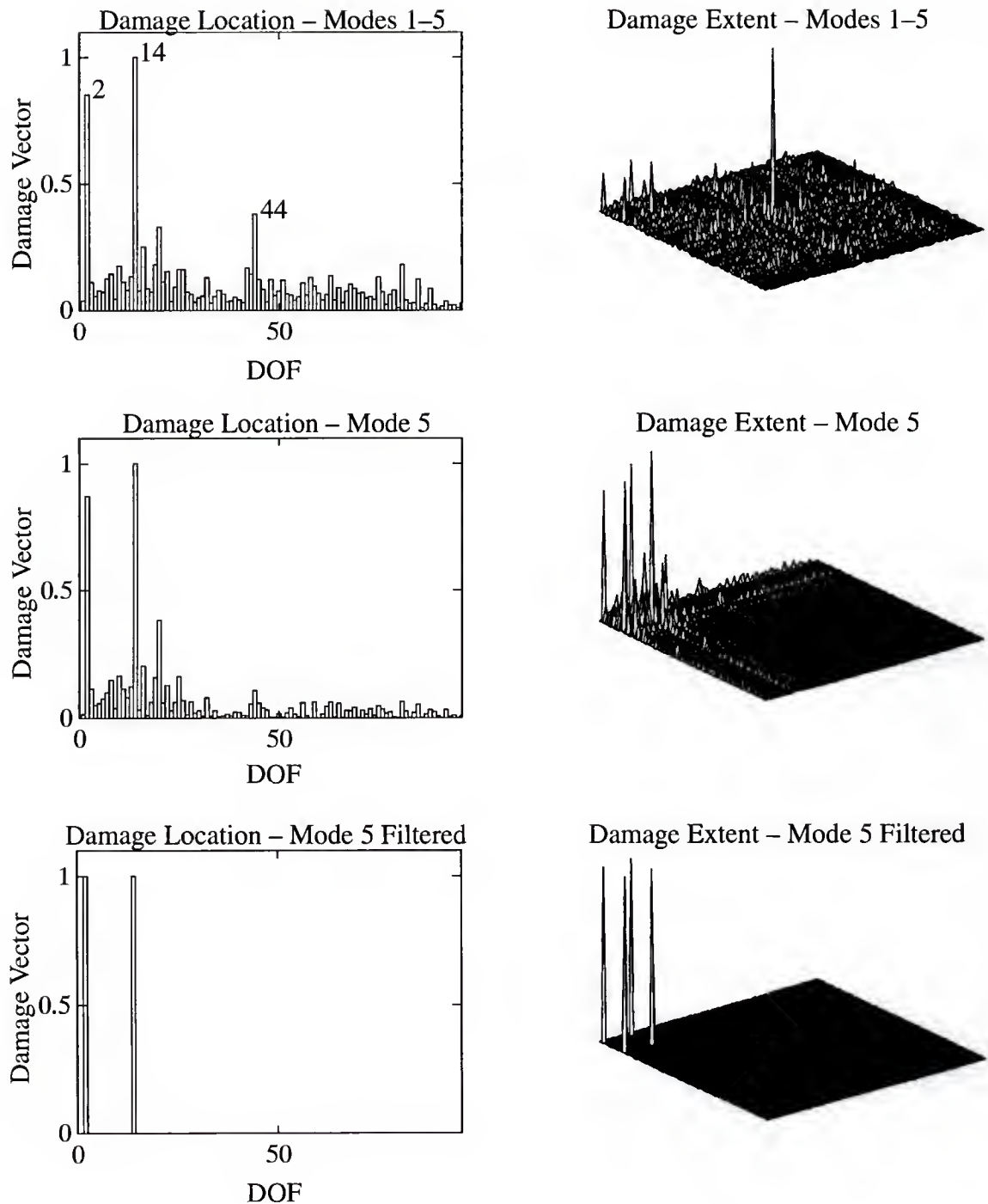


Figure 7.30 NASA 8-bay Truss: Damage Assessment of Case N.

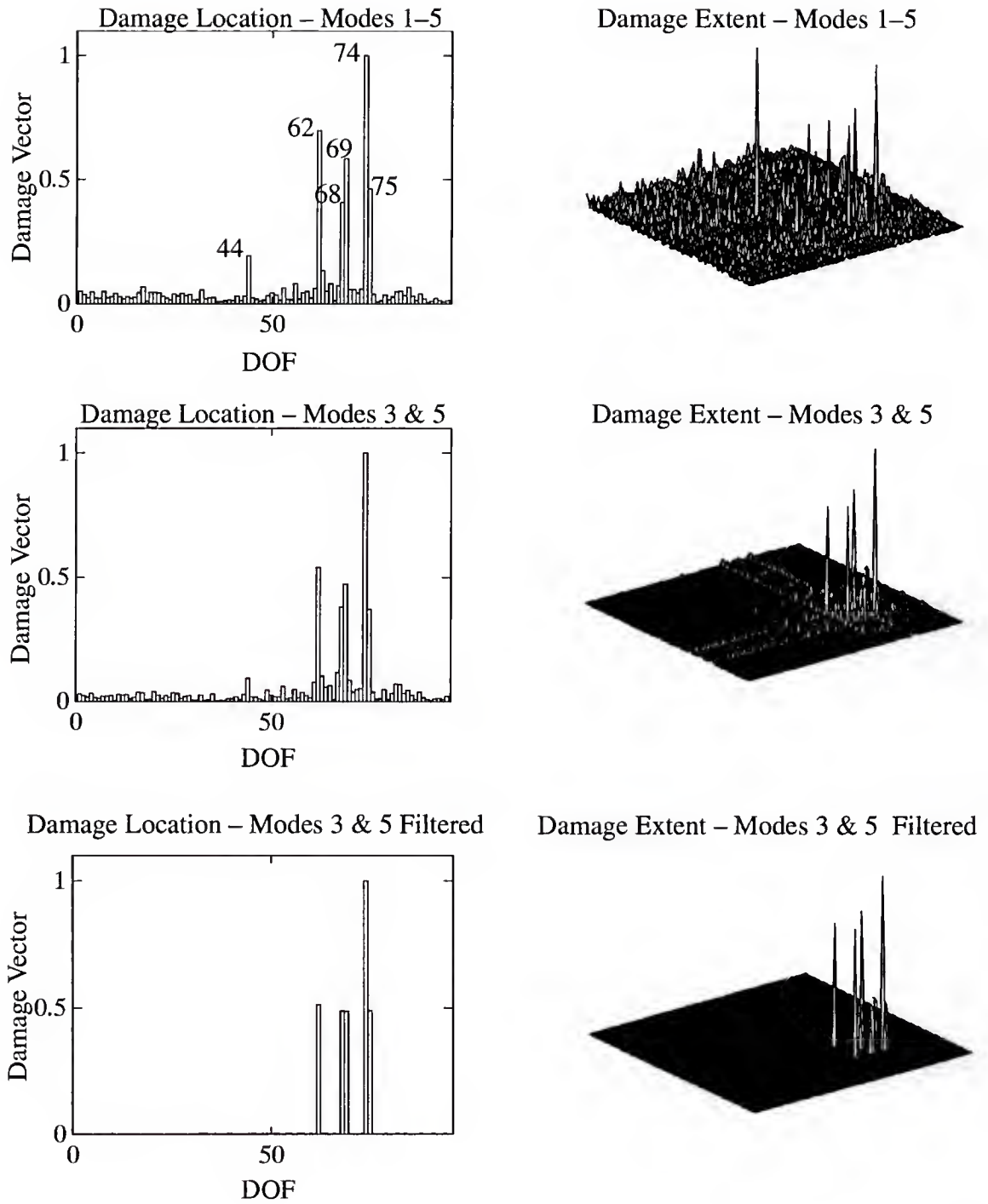


Figure 7.31 NASA 8-bay Truss: Damage Assessment of Case O.



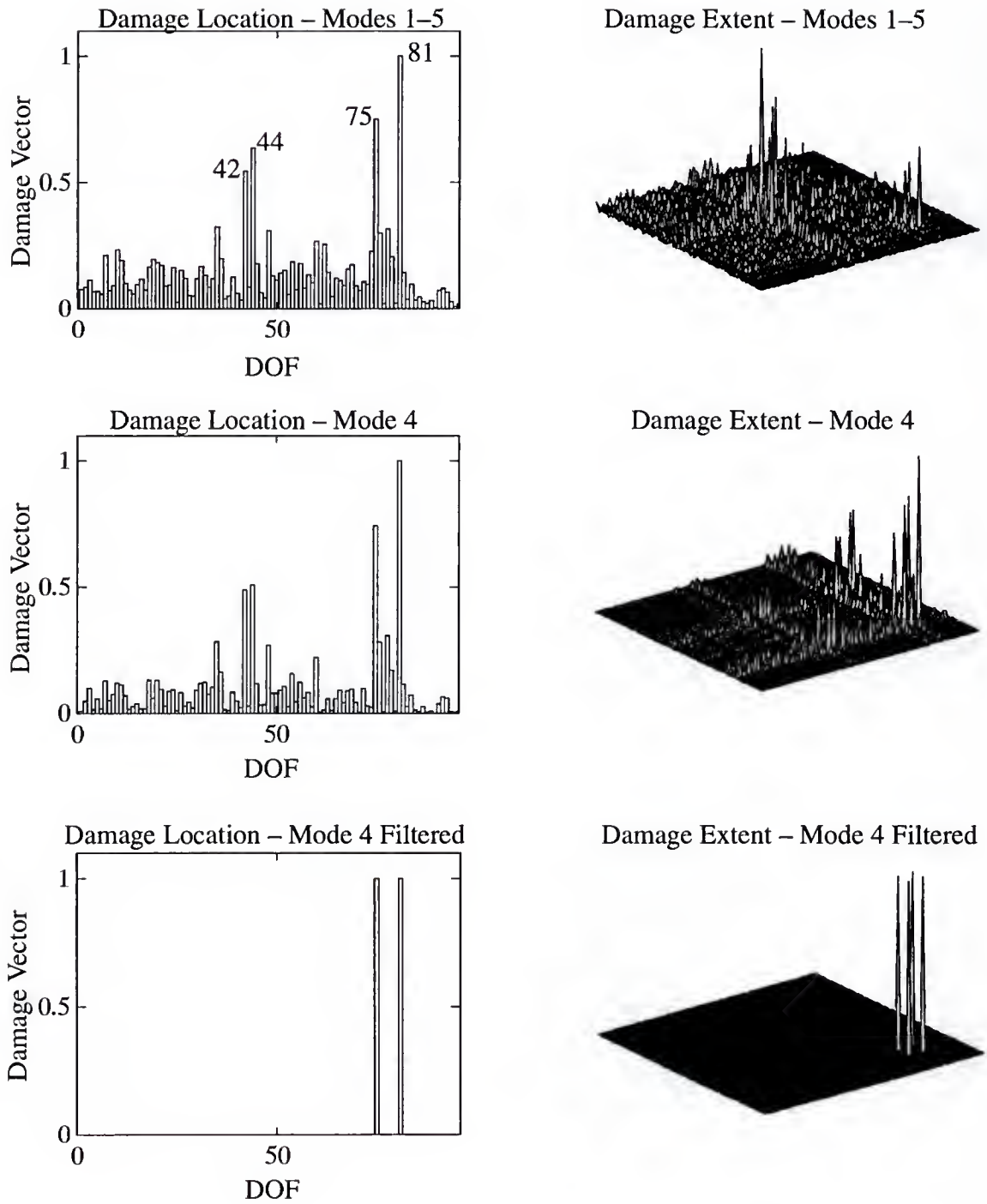


Figure 7.32 NASA 8-bay Truss: Damage Assessment of Case P.

Table 7.7 NASA 8-Bay Truss: Summary of the Damage Assessment Results.

			Without Filtering		With Filtering	
Damage Case	Location Performance	Best mode	Extent (lb/in)	% error	Extent (lb/in)	% error
A	++	1	11,896	8.77	12,865	1.34
C	++	1	11,901	8.73	12,866	1.34
D	++	3	9,789	8.61	8,806	2.30
E	o	4	8,094	37.90	13,454	3.17
F	–	Location not detected				
G	++	1	10,859	16.70	12,971	0.53
H	++	4	12,601	3.37	13,154	0.87
I	++	4	7,568	16.00	10,220	13.39
J	++	4	12,015	7.86	13,176	1.04
K	++	3	6,955	22.80	8,851	1.79
L	+	4	8,421	35.40	12,859	1.39
M	++	4	12,009	7.91	12,882	1.21
N	++	5	10,037	23.00	13,169	0.99
O	++	3, 5	(L) 12,347 (D) 8,451	5.31 6.78	(L) 12,807 (D) 8,878	1.79 1.50
P	+	4	8,815	not def.	13,461	not def.

++ Damage clearly located

+ Damage located with further analysis

– Damage not located

o location narrowed to within two members

(L) Longerons

(D) diagonals

## 7.5 Experimental Study: Mass Loaded Cantilevered Beam

### 7.5.1 Problem Description

This experiment was designed to illustrate the scenario of damage in mass properties. The structure used in this investigation is a cantilevered beam loaded with a non-structural mass. A schematic of this beam is shown in Figure 7.33. The dimensions and properties of the structure are summarized in Table 7.8.

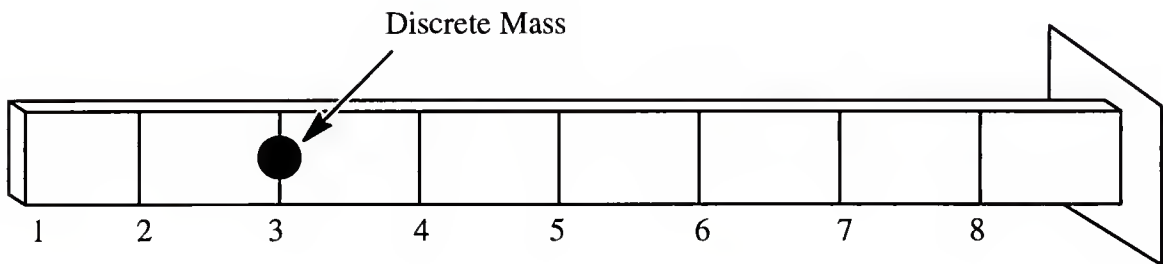


Figure 7.33 The Mass Loaded Cantilevered Beam.

Table 7.8 Mass Loaded Cantilevered Beam Properties.

Beam Length – .86 m
Beam Mass/Length – 1.246 kg/m
Beam Moment of Inertia – $1.458 \times 10^{-9} \text{ m}^4$
Beam Young's Modulus – 69 GPa
Discrete Mass – 0.7938 kg
Discrete Mass Moment of Inertia – $1.1 \times 10^{-3} \text{ kg-m}^2$

An undamped FEM of the mass loaded beam was constructed using beam elements in conjunction with the properties of the non-structural mass. The beam element has two degrees of freedom (DOF) at each node: bending and rotation. A sixteen DOF undamped

FEM was generated using the eight equal length element discretization shown in Figure 7.33. The effect of the non structural mass was considered non-stiffening and concentrated at node 3. This mass was modelled by adding its mass and moment of inertia to node 3 bending and rotation DOFs, respectively. The mass loaded beam, as described above, was considered the “healthy” configuration. Structural damage consisted of the removal of the non-structural mass from the beam.

Experimental modal analysis of the beam was performed on the “healthy and “damaged” beam configurations. Modal parameters were identified using frequency domain techniques and the Rational Fraction Least Square single degree of freedom curve fitting algorithm. The excitation source used was an impact hammer and the driving point measurement was an accelerometer mounted at the free end of the beam. For each configuration (healthy and damaged), four modes of vibration were measured. Each mode consisted of a natural frequency and its corresponding mode shape with measurements at only the eight FEM bending degrees of freedom.

### 7.5.2 Analytical and Experimental Models Dimension Correlation

The number of measured eigenvector components (8) is less than the number of DOFs in the FEM (16). In fact, only the bending DOFs of the beam were measured experimentally. As discussed in Chapter 2, two approaches are available to correlate these dimensions: (i) expansion of the measured eigenvectors or (ii) reduction of the FEM. It was found that a FEM reduction is better suited for this application. Thus, the FEM was reduced using the improved reduction system (IRS) method (O’Callahan, 1989).

### 7.5.3 Refinement of the Original FEM

Table 7.9 shows a comparison between the analytically computed and experimentally measured natural frequencies. From this comparison, it is clear that the original reduced FEM does not accurately predict the dynamic behavior of the “healthy” beam. The first step in this study was to refine the original FEM. For the refinement process, it was assumed that

the original mass matrix is an accurate representation of the structure's mass properties. The inaccuracy of the original FEM was believed to be solely due to modeling errors in the stiffness properties. The algorithm discussed in Section 6.3.2 was used to correct the original reduced stiffness matrix. In order to get a symmetric updated stiffness matrix, the measured mode shapes (eigenvectors) were mass orthogonalized using the Optimum Weighted Orthogonalization technique (Baruch and Bar Itzhack, 1978).

Table 7.9 Analytical and Experimental Frequencies of the “Healthy” Structure.

Mode #	Analytical Frequency (Hz)	Experimental Frequency (Hz)
1	4.5	4.6
2	40.3	41.6
3	96.8	99.8
4	195.9	205.9

#### 7.5.4 Damage Location

The next step of this analysis is to determine the location of the structural damage. Using the refined FEM, and the modal parameters of the four modes of vibration measured from the “damaged” beam, a cumulative damage location vector was calculated (Chapter 5). Since the values of  $\|\underline{z}_{d_i}^j\|$ , as defined in Section 5.3, are of different orders of magnitude the cumulative damage location vector should be computed using Eq. (5.4.2). The upper left corner of Figure 7.34 displays the plot of the unit normalized cumulative damage location vector as calculated by Eq. (5.4.2). From this plot, it is clear that DOF 3 has been affected by damage. This is exactly the bending DOF where the non-structural mass was mounted. The

small numerical elements at all other DOFs can be attributed to experimental measurement noise.

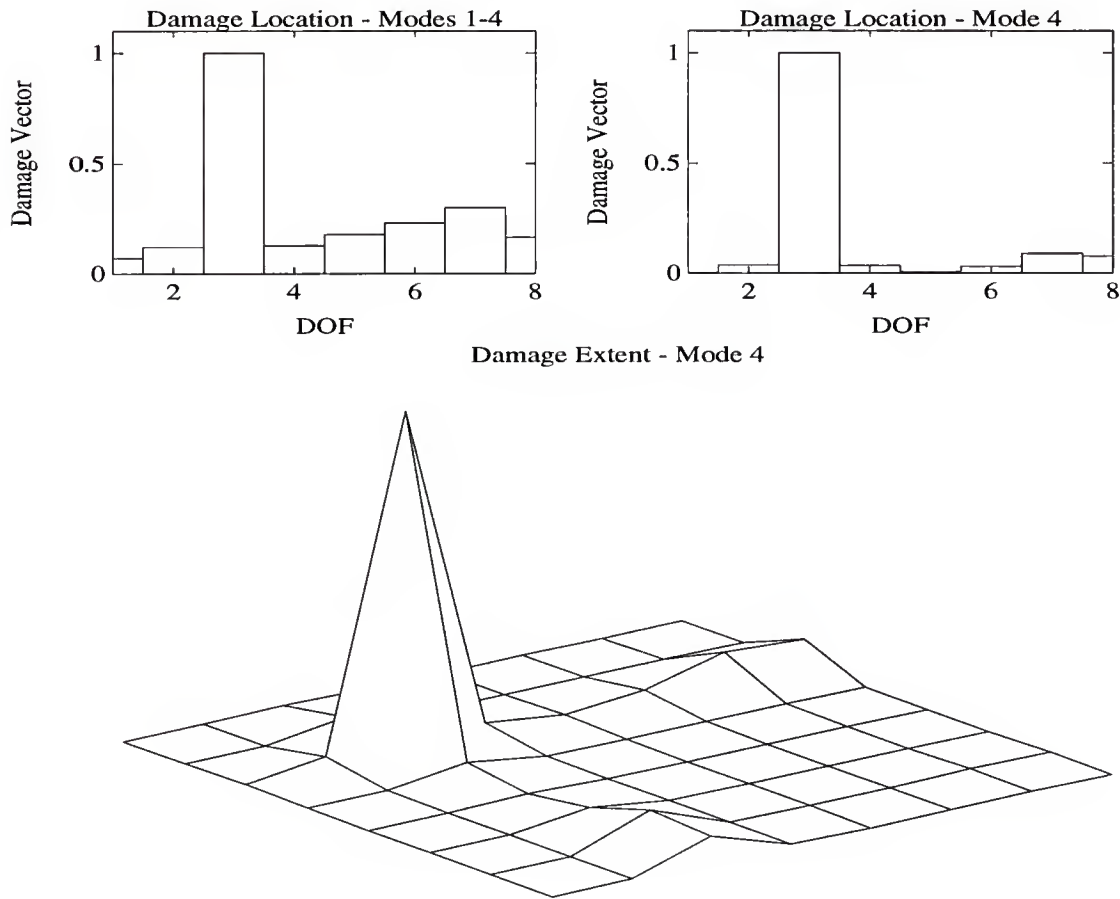


Figure 7.34 Mass Loaded Cantilevered Beam: Damage Assessment

#### 7.5.5 Damage Extent

The final step of this analysis is to determine the extent of structural damage. With knowledge of the damage location, the rank of the “true” mass perturbation matrix,  $\Delta M_d$ , is one since there is only one DOF affected by the damage and that DOF is not connected to the cantilevered end. Hence, in order to compute a rank one  $\Delta M_d$  only one mode of vibration is needed. As discussed earlier, the mode that should be used is the one that most cleanly demonstrates the damage detected by the cumulative damage location vector. The damage



vector  $\underline{d}_4$  was determined to provide the best insight into the state of damage. The damage vector,  $\underline{d}_4$  is shown in the upper right corner of Figure 7.34. The calculated  $\Delta M_d$  using mode 4 data is shown in the lower plot of Figure 7.34. It is clear that the extent calculation has concentrated the major changes at the DOF affected by the damage. From the extent calculation, the mass loss was estimated to be 0.7947 kilograms, which is within 1.1 % of the actual mass loss.

## 7.6 Fifty-Bay Two-Dimensional Truss: Proportionally Damped FEM

### 7.6.1 Problem Description

The structure used in this investigation is the same as the one used in Section 7.3. For convenience, it is shown again in Figure 7.35. This example is used to illustrate the characteristics of the MRPT when dealing with proportionally damped systems in which two of the three property matrices are affected by structural damage. The analytical model of the truss is a 201 DOF FEM which was generated using rod elements. The damping of the “healthy” model is proportional and equal to  $1 \times 10^{-1}$  times the “healthy” mass matrix plus  $5 \times 10^{-7}$  times the “healthy” stiffness matrix. As in the problem of Section 7.3, damage is simulated by reducing the Young’s modulus of two members: the upper longeron of bay three and the lower longeron of bay forty. The modulus of elasticity of the upper longeron of the third bay is reduced from  $E=29 \times 10^6$  psi to  $1 \times 10^3$  psi. The bay forty’s lower longeron is subjected to a complete loss of stiffness (Young’s modulus equal to zero). The damping of the “damaged” model is also proportional and equal to  $1 \times 10^{-1}$  times the “healthy” mass matrix plus  $5 \times 10^{-7}$  times the “damaged” stiffness matrix. Thus, the simulated damage is only affecting the stiffness and damping properties of the structure. Note that the damage in the damping properties is proportional to the damage in the stiffness properties. For our damage assessment analysis, it is assumed that only the first ten “damaged” modes are available. This problem is investigated for three different scenarios. Each scenario corresponds to a different level of random noise added to the “damaged” eigenvectors. In

practice the noise in eigenvector information could be due to both measurement and/or expansion errors.

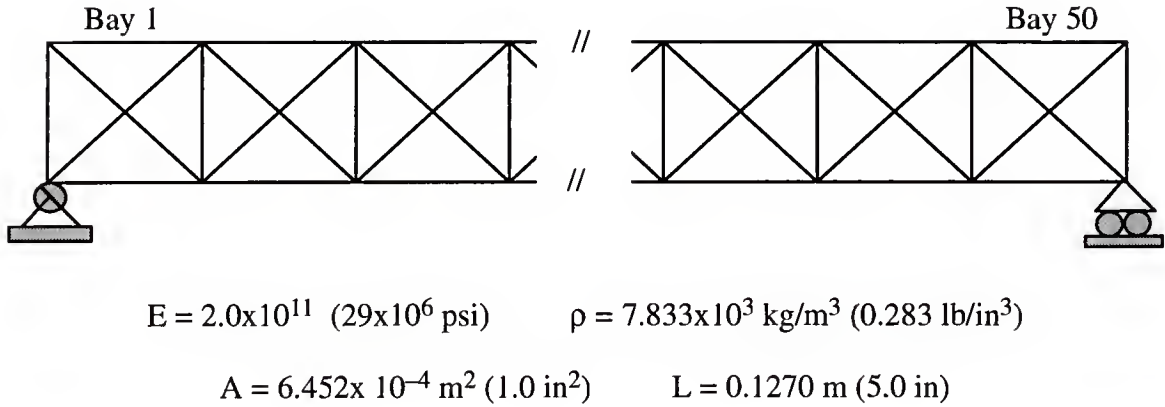


Figure 7.35 50-Bay 2-Dimensional Truss.

### 7.6.2 Damage Location

Cumulative damage location vectors, as defined in Chapter 5, are first computed for all three scenarios using the modal properties of the ten “damaged” modes. In this problem, all rows of matrix  $Z_{d_i}$  (defined in Chapter 5) are of the same order of magnitude; hence either Eq. (5.4.1) or Eq. (5.4.2) can be used to compute the cumulative damage vectors. The upper left plot of Figure 7.36 represents the exact damage computed from the exact damage perturbation matrices ( $\Delta K_d$  and  $\Delta D_d$ ). The upper right plot corresponds to the case where the exact “damaged” eigenvector information is provided to the subspace rotation damage location algorithm. The lower left and right plots correspond to the cases where the exact “damaged” eigenvectors have been corrupted with 2.5% and 5% random noise, respectively. As shown in Figure 7.36, the location algorithm is able to exactly locate the damage when presented with noise free information. Although not as clean, the damage can still be clearly located in the noisy eigenvectors cases.

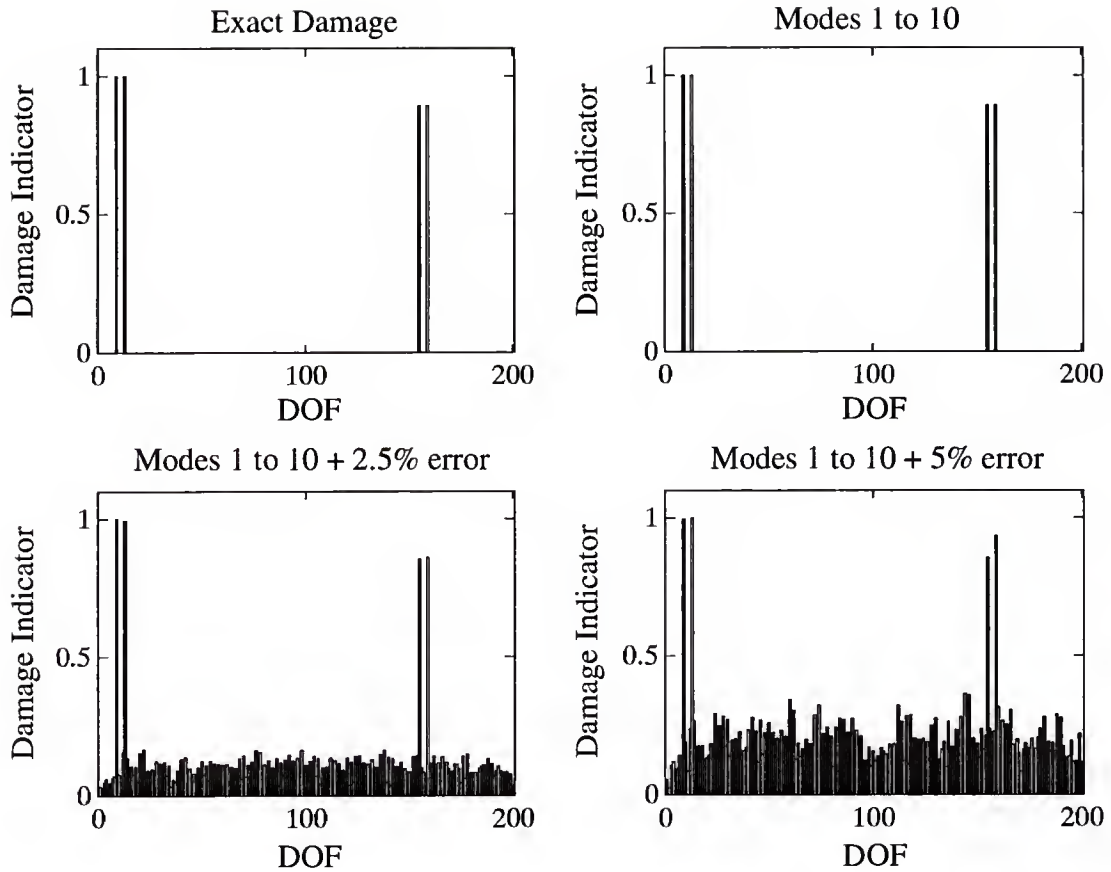


Figure 7.36 50-Bay 2-Dimensional Truss: Damage Location.

### 7.6.3 Damage Extent

The damage location assessed in the previous section can be used in conjunction with the truss finite element connectivity to determine the damaged truss struts. The rank of the “true” perturbation matrix,  $\Delta K_d$  (or  $\Delta D_d$ ), can be found by adding the rank of the element stiffness (or damping) matrix of the damaged struts. Hence, the rank of the perturbation to the stiffness matrix due to damage is two because two struts of rank one element matrices are damaged. Note that the element stiffness matrix of a strut is one since it is modelled as a rod element. Because the damping of the structure is proportional and the mass properties are unaffected by the damage, it is deduced that the rank of the perturbation to the damping matrix is the same as the rank of the perturbation to the stiffness matrix. From propositions

6.1 and 6.2, it is clear that only experimental data from two modes of vibration are needed to compute the extent of the damage. In the noisy situations, the two modes that should be used are the ones that most cleanly demonstrate the damage shown in Figure 7.36. These modes can be determined by inspecting the individual damage vectors. An inspection of the individual damage vectors associated with each “noisy” eigenvector suggests that modes 8 and 9 provide the best insight into the state of the damage. The results of applying the MRPT (Section 6.4.1, Eq. (6.4.6)) to determine the perturbations to the stiffness matrix due to the damage are shown in Figure 7.37. Clearly, from judging the upper right mesh plot of Figure 7.37, the MRPT is able to reproduce the exact damage with only two noise free modes. The algorithm demonstrates good performance when faced with noisy eigendata (lower plots). The percentage errors with respect to the exact stiffness damage for all studied cases are listed in Table 7.10. The perturbations to the damping matrix,  $\Delta D_d$ , due to the damage are estimated by the extent algorithm (Section 6.4.1, Eq. (6.4.4)) with exactly the same accuracy as for  $\Delta K_d$ . In fact, the unscaled mesh plots of the computed  $\Delta D_d$ 's are the same as the ones shown in Figure 7.37. This would be expected since, as reported earlier, the damage in the damping properties is proportional to the damage in the stiffness properties.

Table 7.10 50-Bay 2-Dimensional Truss: Summary of Percentage Error With Respect to the Exact Damage.

Eigenvectors Error	Percentage Error with respect to exact stiffness (or damping)	
	Upper Longeron Of Bay Three	Lower Longeron of Bay Forty
0.0%	0.00	0.00
2.5%	6.60	7.42
5.0%	22.60	15.30

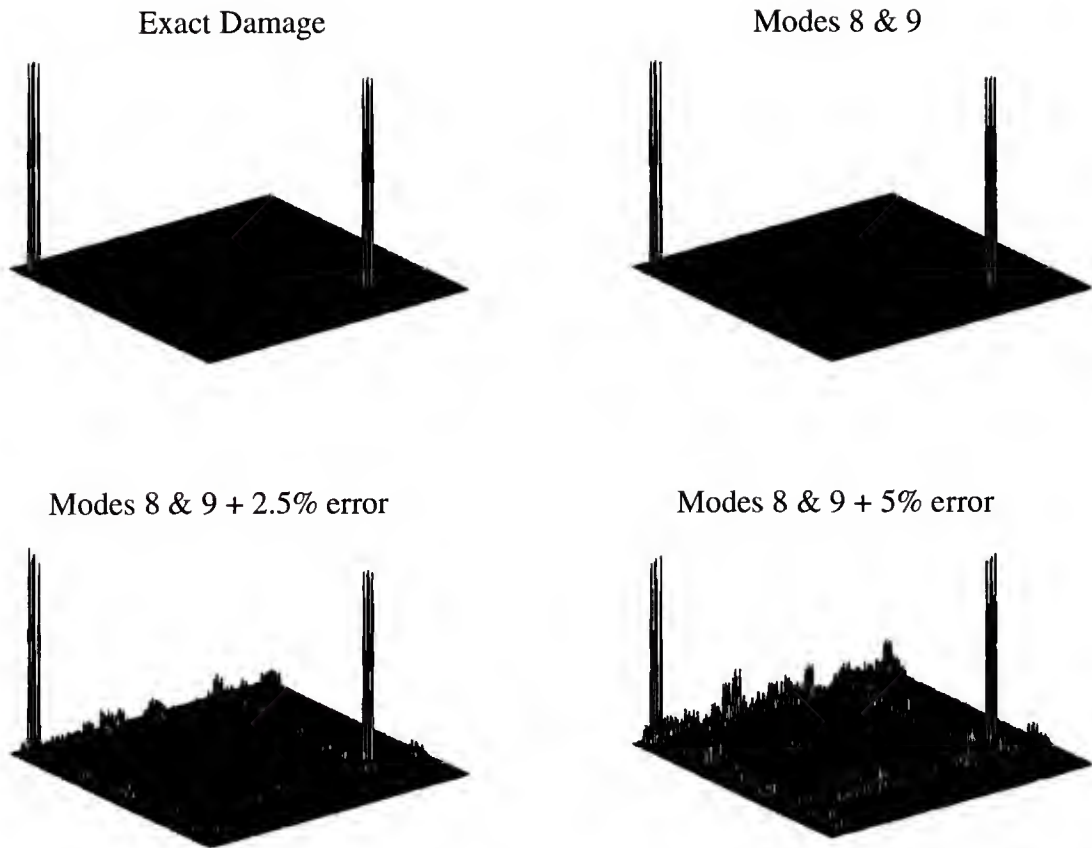


Figure 7.37 50-Bay 2-Dimensional Truss: Damage Extent.

## 7.7 Eight-Bay Two-Dimensional Mass-Loaded Cantilevered Truss

### 7.7.1 Problem Description

The structure under investigation is the eight-bay two-dimensional mass-loaded cantilevered truss shown in Figure 7.38. This structure was designed (Ricles, 1991) to emulate typical properties of space structures: low frequency modes with large non-structural mass. The geometric and material properties of the truss are given in Figure 7.38. The truss consists of 40 struts and 16 nodes. Fourteen of the nodes are loaded with concentrated non-structural mass of magnitude  $2.3 \text{ lbs-sec}^2/\text{in}$  and the remaining two nodes have large lumped masses of magnitude  $47.4 \text{ lbs-sec}^2/\text{in}$ . Each truss strut was modeled as a



rod element with negligible mass. The finite element model has 32 translational DOFs ( 2 DOFs per node). The truss, as described above, is considered the healthy (undamaged) configuration in our study. Two problems based on this structure are presented to illustrate the characteristics of the procedure of applying the MRPT to simultaneously determine the damage extent in all property matrices of undamped ( $M, K$ ) and proportioned damped ( $M, D, K$ ) structures.

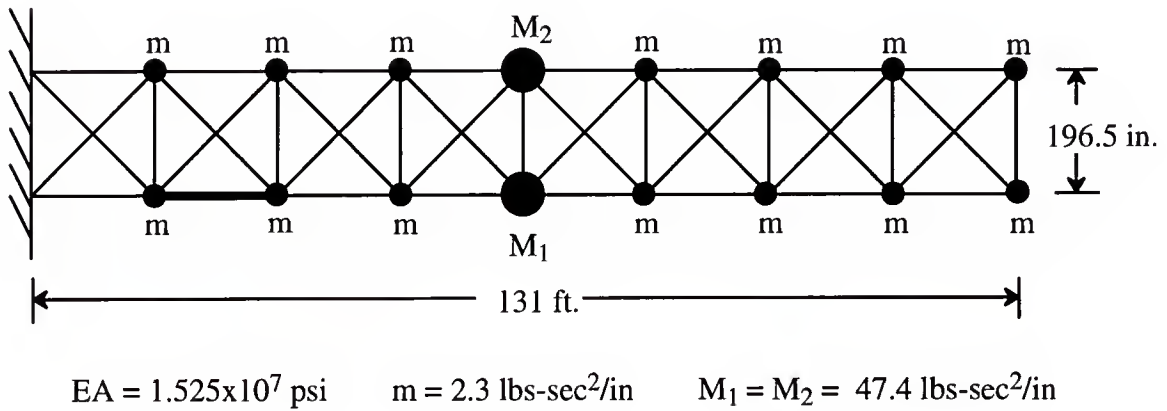


Figure 7.38 The Eight-Bay Two-Dimensional Mass-Loaded Cantilevered Truss.

### 7.7.2 Proportionally Damped Configuration: Damage of Small Order of Magnitude

In this first problem, it is assumed that the damping of the truss is proportional and equal to  $1 \times 10^{-1}$  times the “healthy” mass matrix plus  $1 \times 10^{-6}$  times the “healthy” stiffness matrix. In this example the damage is simulated by a 10% stiffness reduction of the darkened strut and a 5% reduction of mass  $M_1$ . The damping of the “damaged” model is also assumed proportional and equal to  $1 \times 10^{-1}$  times the “damaged” mass matrix plus  $1 \times 10^{-6}$  times the “damaged” stiffness matrix. For the damage analysis, it is assumed that only the first four modes of vibration are available. Each available mode consists of an eigenvalue and an eigenvector with entries at all FEM DOFs. This present problem is similar to a problem



investigated by Ricles (1991) with the exception that in Ricles (1991) the truss was assumed undamped.

### 7.7.2.1 Damage Location

The first step in the analysis is to use the damage location algorithm as discussed in Chapter 5 to determine the location of damage. The left plot of Figure 7.39 represents the unit normalized exact cumulative damage location vector (CDLV) (Eqs. (5.2.4b) and (5.4.2)) computed from the exact perturbation matrices  $\Delta M_d$ ,  $\Delta D_d$  and  $\Delta K_d$ . The unit normalized CDLV computed from the subspace damage location algorithm (Eqs. (5.2.4b) and (5.4.2)) is shown in the right plot of Figure 7.39. As previously proven, the location algorithm is able to exactly locate the damage when presented with noise free data.

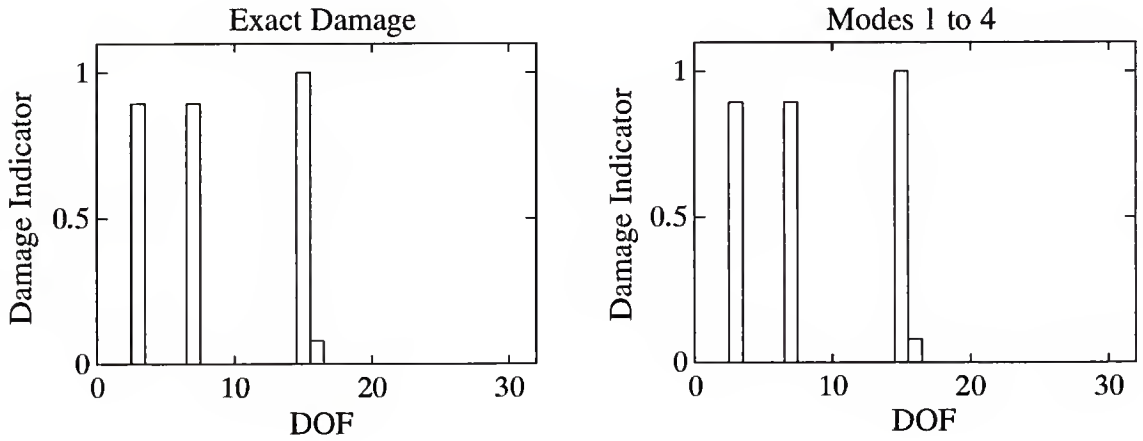


Figure 7.39 Problem 7.7: Cumulative Damage Location Vector: First Four Modes.

### 7.7.2.2 Decomposition of Matrix B

The next step is to decompose matrix B as defined by Eq. (6.4.28) into  $B_m$ ,  $B_d$ , and  $B_k$ . As discussed in Section 6.4.4, the proposed decomposition requires that matrix B be of full rank. A simple singular value decomposition of matrix B computed using all 4 available modes shows that its rank is 3. Therefore, only three of the four available modes should be used. A further investigation reveals that any three of the four modes result in a full rank B.

Hence, any combination of three modes can be used in the decomposition. The three plots in the upper half of Figure 7.40 show the unit normalized exact cumulative vector (Eq. (6.4.35), Section 6.4.4) computed using the exact perturbation matrices,  $\Delta M_d$ ,  $\Delta D_d$  and  $\Delta K_d$ , and the first three modes. The unit normalized cumulative vector associated with the computed  $B_m$ ,  $B_d$ , and  $B_k$  using the proposed decomposition procedure, for the first three modes, are displayed in the lower half of Figure 7.40. A comparison between upper and lower plots shows that the decomposition procedure resulted in the exact  $B_m$ ,  $B_d$ , and  $B_k$  for the associated modes. This is also true if any other combination of three modes was used. Note that the cumulative vectors in Figure 7.40 give information on the effect of the damage on the mass, damping and stiffness properties.

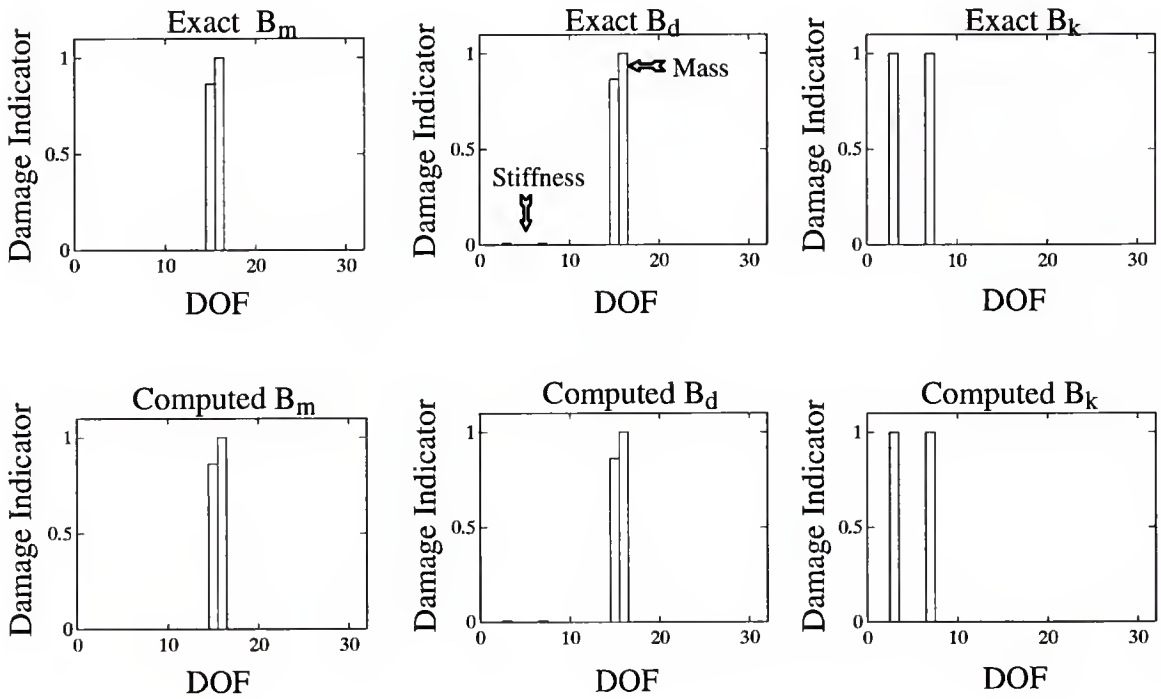


Figure 7.40 Problem 7.7: Cumulative Vectors Associated With the Exact and Computed  $B_m$ ,  $B_d$ ,  $B_k$ : First Three Modes.

### 7.7.2.3 Damage Extent

Now that  $B_m$ ,  $B_d$ , and  $B_k$  have been computed, the final step is to compute the perturbation to the property matrices due to the damage ( $\Delta M_d$ ,  $\Delta D_d$ ,  $\Delta K_d$ ) using the minimum rank perturbation theory (MRPT) as defined in Section 6.4.4. Using the

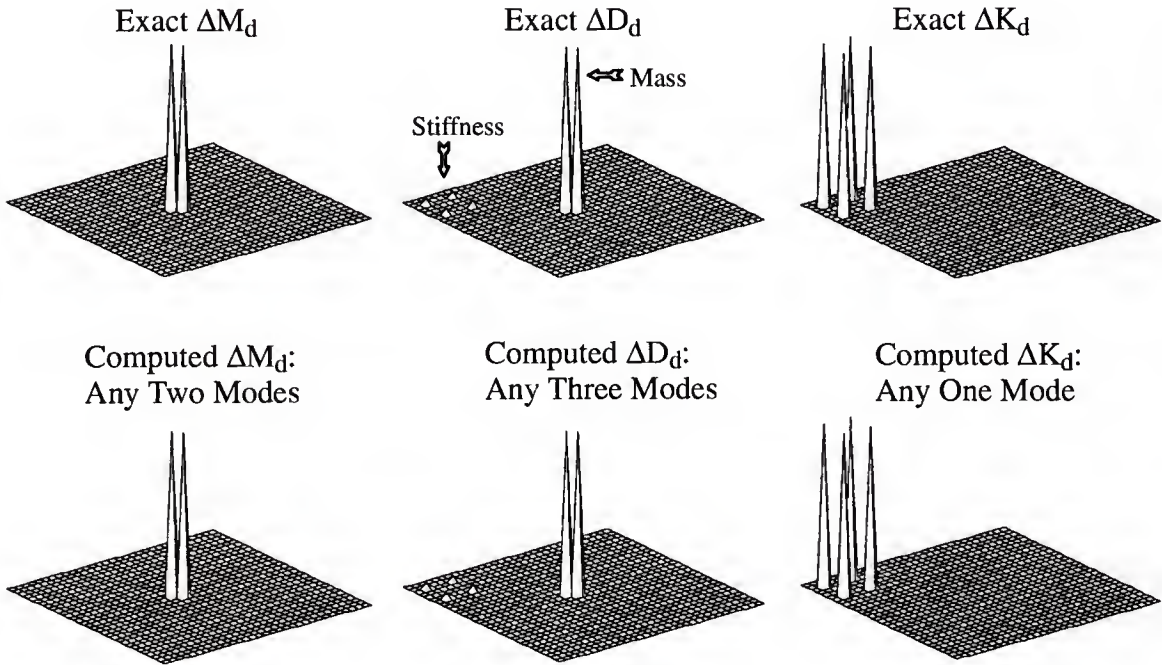


Figure 7.41 Problem 7.7: Exact and Computed  $\Delta M_d$ ,  $\Delta D_d$ ,  $\Delta K_d$

connectivity information of the original FEM along with the information of the damage effect on the three property matrices (shown in Figure (7.39)), it can be deduced that the rank of the “true”  $\Delta M_d$  is two and the rank of the true  $\Delta K_d$  is one. Because of the fact that the damage in the damping is proportional to the damage in the mass and stiffness, it can also be deduced that the rank of the “true”  $\Delta D_d$  is three. The rank information is ascertained by identifying which structural elements connect the damaged DOFs, and then adding up the rank of each damaged structural element. The rank estimation could also be obtained by performing a singular value decomposition on  $B_m$ ,  $B_d$  and  $B_k$ . From the rank information

and propositions 6.1 and 6.2, it is clear that only two modes are needed to compute  $\Delta M_d$  using the MRPT. Likewise, only three modes are needed to compute  $\Delta D_d$  and only one mode is needed to compute  $\Delta K_d$ . Since we are dealing with noise free eigendata, any two, three modes, or any one mode can be used in the computation  $\Delta M_d$ ,  $\Delta D_d$  or  $\Delta K_d$ , respectively. Mesh plots of the exact and computed  $\Delta M_d$ ,  $\Delta D_d$  and  $\Delta K_d$  matrices are shown in Figures 7.41. Again, a comparison between exact and computed  $\Delta M_d$ ,  $\Delta D_d$  and  $\Delta K_d$  shows that the MRPT is able to reproduce the exact damage effect.

In this problem, as shown in this investigation, the proposed damage detection technique is able to assess the damage exactly when three noise free eigenvalues/eigenvectors are used. Unfortunately, in practice, the measured eigendata are always corrupted by noise. To simulate some kind of a practical situation, random noise was added to the eigendata. When using noisy eigendata ( first four modes), the present algorithm was unable to locate the damage. The reason is that the damage as simulated is of small order of magnitude which results in only a small change in the eigendata of the healthy model. In this case, the noise totally masks the damage as reflected in the “measured” noisy eigendata.

### 7.7.3 Undamped Configuration: Damage of Large Order of Magnitude

In this problem, the truss is assumed undamped. The damage is simulated by a 60% stiffness reduction of the darkened strut and a 40% reduction of mass  $M_1$ . For the analysis, it is assumed that only the first five modes of vibration are available. Each available mode consist of an eigenvalue and an eigenvector with entries at all FEM DOFs. This problem is investigated for four different cases. Each case represents a different amount of random noise added to the eigenvectors of the available modes: 0 % , 2.5 % , 5% and 10%.

#### 7.7.3.1 Noise Free Eigendata

The procedures used in the investigation of this case are similar to the one used in the previous problem. The computed/exact cumulative damage location vector and the

cumulative vector associated with  $B_m$  and  $B_k$  are displayed in the first row of plots of Figure 7.42. Likewise, the first row of plots of Figure 7.43 show the computed/exact  $\Delta M_d$  and  $\Delta K_d$  when using noise free data. Again, as previously shown, exact data provides exact results.

### 7.7.3.2 Noisy Eigendata

The effect of introducing noise into the “measured” eigenvectors is shown in the lower three rows of plots in Figures 7.42 and 7.43. In Figure 7.42, it is obvious that as noise is increased, the cumulative damage vector  $B$  (first column) becomes corrupted, to the point that when 10% noise is added it is difficult to ascertain information concerning the state of damage. In performing the decomposition of  $B$  into  $B_m$  and  $B_k$  one should only use those modes of vibrations whose damage vector  $\underline{d}_i$  reflects the same “nature of damage” as the cumulative damage vector  $B$ . For this particular example, only modes 3, 4 and 5 meet this criterion for the cases of 2.5% and 5% random noise. For the 10% noise case, the cumulative damage vector and the individual mode damage vectors did not clearly indicate damage. To maintain a level of consistency, the same mode set (3, 4, 5) was used for the case of 10% noise. The decomposition of  $B$  into  $B_m$  and  $B_k$  for the case of noisy measurements is shown in the remaining rows and columns of Figure 7.42. As shown in Figure 7.42, the added noise has two effects in the decomposition process. The first, which is rather obvious, is that noise causes the appearance of small numerical component at all DOFs, although in the low level noise cases (2.5% and 5%) it is still clear which DOFs have been actually damaged. The second more subtle effect is that the actual decomposition process is no longer exact. This manifests itself in that the computed  $B_m$  has substantial indicators of damage at DOFs in which there is actually only stiffness damage. The same is true for  $B_k$ , in that damage is also indicated at DOFs in which there is only mass damage. These indicators are shown darkened in Figure 7.42.

Figure 7.43 shows the effect of noise on the computed perturbation matrices. Mode selection was based on (i) rank calculation of  $B_m$  and  $B_k$ , and (ii) comparison of individual columns of  $B_m$  and  $B_k$  to their associated cumulative vector. For the cases of 2.5% and 5%



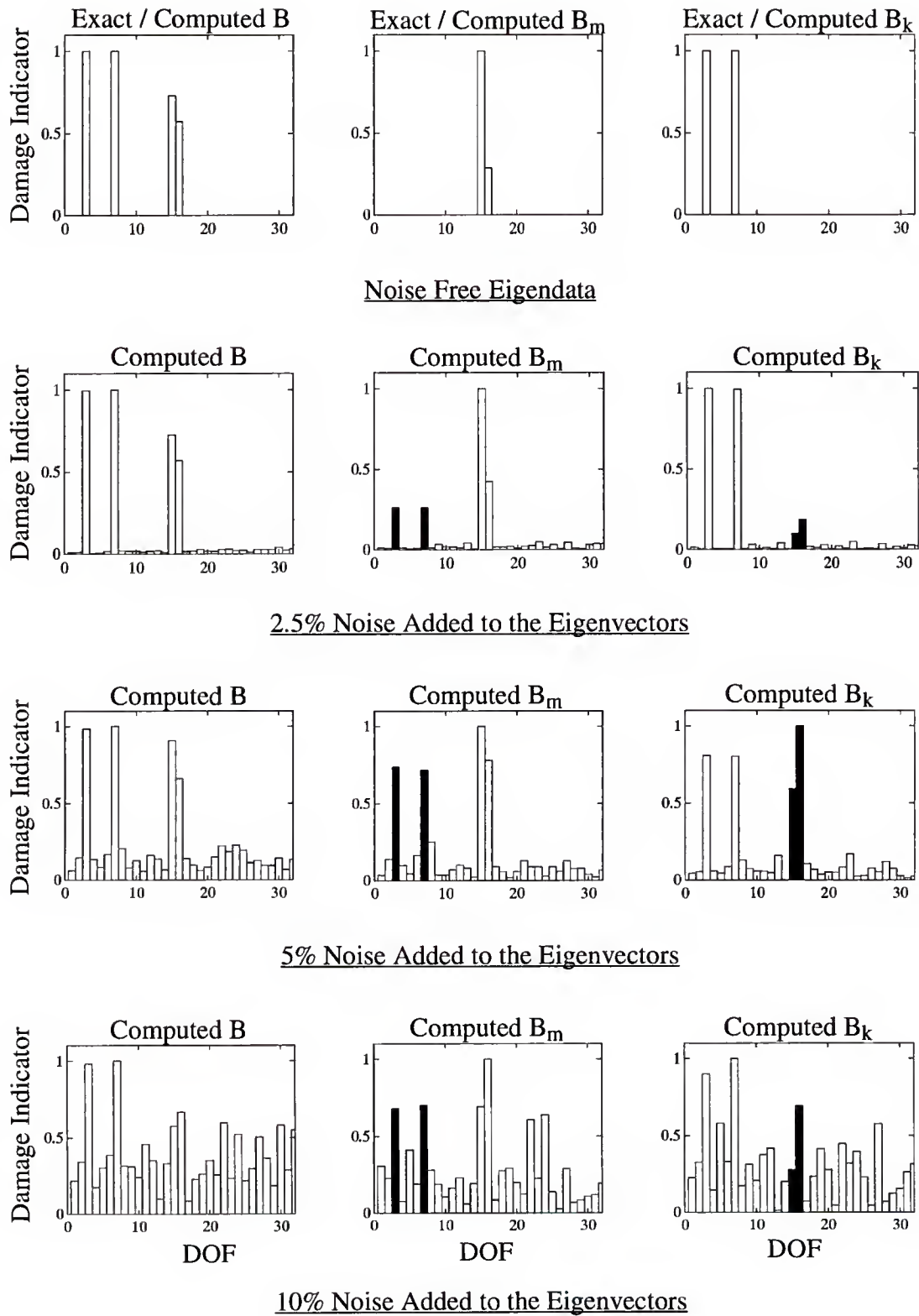


Figure 7.42 Problem7.7: Cumulative Vectors Associated With  $B$ ,  $B_m$ ,  $B_d$ ,  $B_k$   
 $B$  Computed Using Modes 1-4  
 $B_m$ ,  $B_d$ ,  $B_k$  Computed Using modes 3, 4 & 5



noise, the extent calculation stills provides a reasonable indication of damage, although the magnitude of damage is in error. The percentage errors of the estimated mass and stiffness damage with respect to the exact damage are listed in Table 7.11. Figure 7.43 shows the extent calculation with no enhancements.

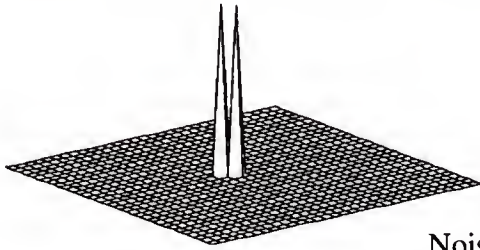
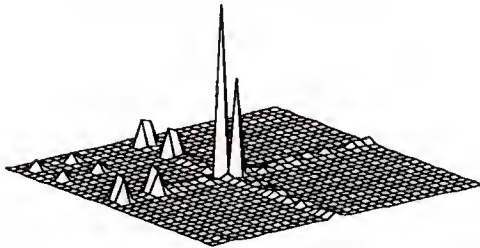
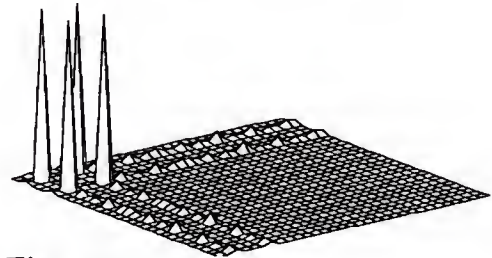
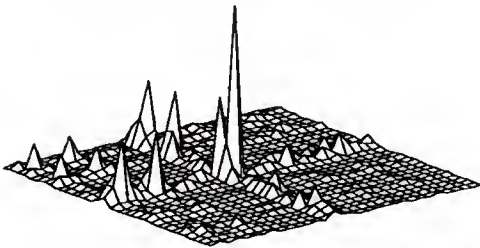
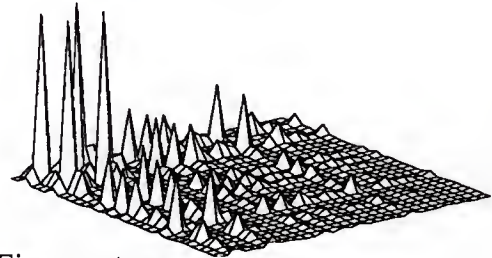
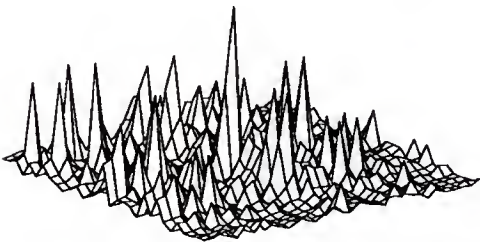
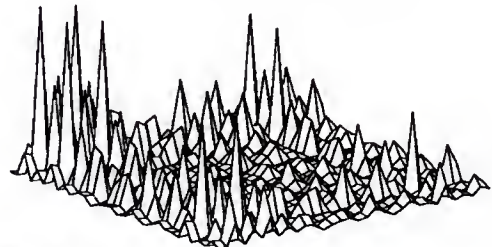
For the case in which 10% noise was added, the damage location and extent algorithm failed. In actual practice, the analysis would have halted after the calculation of the individual and cumulative damage vectors. At that point, inspection of the damage vectors would give no clear indication as to the state of damage. The decomposition of  $B$  into  $B_m$  and  $B_k$  as well as the calculation of the perturbation matrices was just carried out for completeness of the results.

Table 7.11      Problem 7.7: Percentage Error of Damage Estimate with respect to Exact Damage

Noise Added	Percentage Error With Respect to Exact Damage	
	Mass	Stiffness
0.0%	0.00	0.00
2.5%	6.60	9.10
5.0%	99.10	24.60

## 7.8 Summary

A technique that approaches the structural damage assessment problem in a decoupled fashion was demonstrated and evaluated using numerical and actual experimental test data. In all presented examples, the structural damage was first located by using the subspace rotation damage location algorithm formulated in Chapter 5. With location determined, the

Exact / Computed  $\Delta M_d$ : Any two ModesExact / Computed  $\Delta K_d$ : Any One ModeNoise Free EigendataComputed  $\Delta M_d$ : Modes 3 & 5Computed  $\Delta K_d$ : Mode 32.5% Noise Added to the EigenvectorsComputed  $\Delta M_d$ : Modes 3 & 5Computed  $\Delta K_d$ : Mode 35% Noise Added to the EigenvectorsComputed  $\Delta M_d$ : Modes 3 & 5Computed  $\Delta K_d$ : Mode 310% Noise Added to the EigenvectorsFigure 7.43 Problem7.7: Exact and Computed  $\Delta M_d$ ,  $\Delta D_d$ ,  $\Delta K_d$

minimum rank perturbation theory (MRPT) developed in Chapter 6 is then applied to assess the extent of the damage. As illustrated, the decomposition of the damage assessment problem has two distinct advantages. First, each subproblem is shown to be computationally attractive. Second, the decoupling allows engineering judgement to enter into the extent algorithm. By making use of the results of the damage location algorithm, the modes which do not exhibit the damage may be eliminated before the application of the MRPT extent algorithm. In general, the subspace rotation damage location algorithm and the MRPT performed well in assessing damage in all studied examples. The eigenvector filtering algorithm developed in Chapter 5 was shown to be useful in improving the accuracy of the damage extent assessment. The MRPT was also demonstrated to be applicable in model refinement problems.

## CHAPTER 8

### CONCLUSION AND SUGGESTIONS FOR FUTURE WORK

This study investigated the development of four algorithms relevant to the areas of finite element model refinement and structural damage assessment. All four algorithms make use of an original finite element model (FEM) and a subset of experimentally measured eigenvalues and eigenvectors. The first algorithm, termed the inverse/hybrid approach, is a model refinement algorithm with basis in the standard framework of the inverse problem. In the formulation of the inverse/hybrid approach, it is proposed to approximate the unmeasured experimental modes with the corresponding analytical modal information. With a complete hybrid set of experimental and analytical modal parameters, the symmetry of the inaccurate finite element property matrices is enforced by mass orthogonalizing the eigenvectors. An orthogonalization strategy that assigns more credibility to the measured eigenvectors was discussed. Through an example, it was shown that the performance of the inverse/hybrid approach is similar to the algorithm formulated by Baruch and Bar Itzhack (1978).

Next, a subspace rotation technique to improve the performance of an existing model refinement algorithm, termed SEAMRA (Zimmerman and Widengren, 1989), was presented. The mathematical formulation of SEAMRA is based on a control concept known as the eigenstructure assignment. The proposed improvement results in both an enhancement of the eigenvector assignability and a substantial decrease of the computational burden. The enhanced SEAMRA was shown to be suited for both model refinement and structural damage assessment.

An efficient structural damage location algorithm that bypasses the general framework of the model refinement problem was then formulated. The algorithm, also termed the

subspace rotation, is similar to the Modal Force Error Criteria formulated by several researchers. The effects of measurement error on the performance of the subspace rotation were discussed. A new viewpoint that reduces the effects of measurement error for certain classes of structure was developed. Additionally, the use of multi-mode measurements as a technique to overcome the effects of these errors is also discussed. Furthermore, an eigenvector filtering technique was formulated.

A minimum rank perturbation theory (MRPT) was then developed. A number of computationally attractive damage extent algorithms based on the MRPT were formulated. The formulations of the presented MRPT based algorithms are consistent with the effects of most structural damage on FEMs. The formulated algorithms address several damage scenarios for undamped, proportionally damped and nonproportionally damped FEMs. A damage scenario is defined by the effect of the structural damage on the FEM. Two techniques to improve the performances of the MRPT based extent algorithm were discussed. The first technique suggests the exclusion in the damage extent calculations of the measured “damaged” modes that do not reflect the state of the damage as determined by the subspace rotation damage location algorithm. Alternatively, the eigenvector filtering algorithm discussed earlier was shown to be also useful in improving the damage estimate.

Finally, the subspace rotation damage location algorithm and the MRPT based damage extent algorithms were evaluated using both computer simulated and actual experimental data. All issues raised in the formulation of these algorithms were demonstrated. In every problem, the damage assessment process was approached in a decoupled fashion. The location of the damage was first determined. The extent of the damage was then assessed by making use of the results of the damage location. The decoupled approach improves both the accuracy and the efficiency of the extent computations. In general, all evaluated algorithms performed very well in assessing the damage in the examples studied. The algorithms show great promises in handling “real life” structures. This was demonstrate in the investigation of the experimental data and, in particular, the NASA 8-bay truss examples.



To fully demonstrate the practicality of the MRPT based damage extent algorithms and the subspace rotation damage location algorithm in handling “real life” structures, the issue of incomplete eigenvector measurement must be intensively investigated. This problem was pointed out in Chapter 2. Two alternative approaches, model reduction and eigenvector expansion, were discussed as possible solutions to the incomplete measurement problem. These approaches have only been investigated in the context of the model refinement problem. An investigation of their performance vis-a-vis the damage assessment problem is of order. Additionally, formulations of damage assessment algorithms that do not require the use of a finite element model should be considered. This could be useful when dealing with “old” structures that have no analytical model.

## REFERENCES

- Adelman, H. M. and Haftka, R. T. (1986), "Sensitivity Analysis of Discrete Structural Systems," *AIAA Journal*, Vol. 24, No. 5, pp. 823–832.
- Andry, A. N., Shapiro, E. Y., and Chung, J. C. (1983), "Eigenstructure Assignment For Linear Systems," *IEEE Transactions on Aerospace and Electronic Systems*, Vol. AES-19, No. 5, pp. 711–729.
- Baruch, M., (1979), "Optimum Weighted Orthogonalization of Measured Modes," *AIAA Journal*, Vol. 17, No. 1, pp. 120–121.
- Baruch, M., and Bar Itzhack, I. Y. (1978), "Optimum Weighted Orthogonalization of Measured Modes," *AIAA Journal*, Vol. 16, No. 4, pp. 346–351.
- Berman, A., and Nagy, E. J. (1983), "Improvements of a Large Analytical Model Using Test Data," *AIAA Journal*, Vol. 21, No. 8, pp. 1168–1173.
- Brock, J. E. (1968), "Optimal Matrices Describing Linear Systems," *AIAA Journal*, Vol. 6, No. 7, pp. 1292–1296.
- Chen, J. C. and Garba, J. A., (1980), "Analytical Model Improvement Using Modal Test Results," *AIAA Journal*, Vol. 18, No. 6, pp. 684–690.
- Chen, J. C. and Garba, J. A., (1988), "On-Orbit Damage Assessment for Large Space Structures," *AIAA Journal*, Vol. 26, No. 12, pp. 1119–1126.
- Collins, J. D., Hart, G. C., Hasselman, T. K. and Kennedy, B. (1974), "Statistical Identification of Structures," *AIAA Journal*, Vol. 12, No. 2, pp. 185–190.
- Creamer, N. G., and Hendricks, S. L. (1987), "Structural Parameter Identification Using Modal Response Data," Proceedings of the 6th VPI&SU/AIAA Symposium on Dynamics and Controls for Large Structures, Blacksburg, VA, pp. 27–38.
- Ewins, D. J. (1986), *Modal Testing: Theory and Practice*, Bruel & Kjaer, Letchworth, Hertfordshire, England.
- Flanigan, C. C. (1991), "Correction of Finite Element Models Using Mode Shape Design Sensitivity," Proceedings of the 9th International Modal Analysis Conference, Firenze, Italy, pp. 151–159.

- Freed, A. M., and Flanigan, C. C. (1991), "A Comparison of Test-Analysis Model Reduction Methods," *Sound and Vibration*, March, pp. 30–35.
- Fuh, J., Chen S. and Berman A. (1984), "System Identification of Analytical Models of Damped Structures," *Proceedings of the 25th AIAA Structures, Structural Dynamics and Materials Conference*, Palm Springs, CA, pp. 112–122.
- Golub, G. H. and Van Loan, C. F. (1989), *Matrix Computations*, The Johns Hopkins University Press, Baltimore, MD.
- Guyan, R. J. (1965), "Reduction of Stiffness and Mass Matrices," *AIAA Journal*, Vol. 3, No. 2, p. 380.
- Gysin, H. (1990), "Comparison of Expansion Methods for FE Modeling Error Localization," *Proceedings of the 8th International Modal Analysis Conference*, Kissimmee, FL, pp. 195–204.
- Hajela, P. and Soeiro, F. (1990), "Recent Developments in Damage Detection Based on System Identification Methods," *Structural Optimization*, Vol. 2, pp. 1–10.
- Hanagud, S., Meyyappa, M. Cheng, Y. P., and Graig, J. I. (1984), "Identification of Structural Dynamic Systems with Nonproportional Damping," *Proceedings of the 25th AIAA Structures, Structural Dynamics and Materials Conference*, Palm Springs, CA, pp. 283–291.
- Heylen, W., and Saas, P. (1987), "Correlation of Analysis and Test in Modeling of Structures, Assessment and Review," *Proceedings of the 5th IMAC*, London, England, pp. 1177–1182.
- Hughes, T. J. R. (1987), *The Finite Element Method*, Prentice Hall, Englewood Cliffs, NJ.
- Ibrahim, S. R. and Saafan, A. A., (1987), "Correlation of Analysis and Test in Modeling of Structures, Assessment and Review," *Proceedings of the 5th IMAC*, London, England, pp. 1651–1660.
- Inman, D. J., (1989), *Vibration With Control, Measurement, and Stability*, Prentice Hall, Englewood Cliffs, NJ.
- Inman, D. J. and Minas, C. (1990), "Matching Analytical Models with Experimental Modal Data in Mechanical Systems," *Control and Dynamics Systems*, Vol. 37, pp. 327–363.
- Juang, J.-N., and Pappa, R. S. (1985), "An Eigensystem Realization Algorithm for Modal Parameter Identification and Model Reduction," *Journal of Guidance, Control and Dynamics*, Vol. 8, No. 5, pp. 620–627.
- Kabe, A. M. (1985), "Stiffness Matrix Adjustment Using Mode Data," *AIAA Journal*, Vol. 23, No. 9, pp. 1431–1436.

- Kammer, D. C. (1987). "Test-Analysis Model Development Using an Exact Modal Reduction," *International Journal of Analytical and Experimental Modal Analysis*, Vol. 2, No. 4, pp. 175–179.
- Kammer, D. C. (1988), "Optimum Approximation for Residual Stiffness in Linear System Identification," *AIAA Journal*, Vol. 26, No. 1, pp. 104–112.
- Kaouk, M. and Zimmerman D. C. (1993a), "Evaluation of the Minimum Rank Update in Damage Detection: An Experimental Study," Proceedings of the 11th IMAC, Kissimmee, FL, pp. 1061–1068.
- Kaouk, M. and Zimmerman D. C. (1993b), "Structural Damage Assessment Using a Generalized Minimum Rank Perturbation Theory," Proceedings of the 34th AIAA Structures, Structural Dynamics and Materials Conference, La Jolla, CA, pp. 1529–1539.
- Kashangaki, T. A.-L. (1992), "Ground Vibration Tests of a High Fidelity Truss For Verification of on Orbit Damage Location Techniques," NASA Technical Memorandum 107626.
- Kashangaki, T. A.-L., Smith, S. W., and Lim, T. W. (1992), "Underlying Modal Data Issues for Detecting Damage in Truss Structures," Proceedings of the 33rd AIAA Structures, Structural Dynamics and Materials Conference, Dallas, TX, pp. 1437–1446.
- Kidder, R. L. (1973), "Reduction of Structural Frequency Equations," *AIAA Journal*, Vol. 11, No. 6, pp. 119–126.
- Lim, T. W. (1990), "Submatrix Approach to Stiffness Matrix Correction Using Modal Test Data," *AIAA Journal*, Vol. 28, No. 6, pp. 1123–1130.
- Lin C. S. (1990), "Location of Modeling Errors Using Modal Test Data," *AIAA Journal*, Vol. 28, No. 9, pp. 1650–1654.
- Martensson, K. (1971), "On the Matrix Riccati Equation," *Information Sciences*, Vol. 3, pp. 17–49.
- Martinez, D., Red-Horse, J. and Allen, J. (1991), "System Identification Methods for Dynamic Structural Models of Electronic Packages," Proceedings of the 32nd AIAA Structures, Structural Dynamics and Materials Conference, Baltimore, MD, pp. 2336–2346.
- McGowan, P. E. (1991), *Dynamic Test/Analysis Correlation Using Reduced Analytical Models*, M. S. Thesis, Engineering Mechanics, Old Dominion University, Norfolk, VA.
- Meirovitch, L. (1980), *Computational Methods in Structural Dynamics*, Sijhoff & Noordhoff, Alphen aan den Rijn, The Netherlands.



- Meirovitch, L. (1986), *Elements of Vibration Analysis*, McGraw-Hill Book Company, New York.
- Miller, C. A. (1980), "Dynamic Reduction of Structural Model," *Journal of the Structural Division ASCE*, Vol. 106, pp. 2097–2108.
- O'Callahan, J. C. (1989), "A Procedure for an Improved Reduced System (IRS) Model," Proceedings of the Seventh International Modal Analysis Conference, Las Vegas, NV, pp. 17–21.
- O'Callahan, J. C., Avitabile P. A. and Riemer, R. (1989), "System Equivalent Reduction Expansion Process (SEREP)," Proceedings of the Seventh International Modal Analysis Conference, Las Vegas, NV, pp. 29–37.
- Ojalvo, I. U. and Pilon, D. (1988), "Diagnostics for Geometrically Locating Structural Math Model Errors From Modal Test Data,"
- Paz, M. (1984), "Dynamic Condensation," *AIAA Journal*, Vol. 22, No. 5, pp. 724–727.
- Potter, J. E. (1966), "Matrix Quadratic Solutions," *SIAM Journal of Applied Mathematics*, Vol. 14, No. 3, pp. 496–501.
- Ricles, J. M., (1991) "Nondestructive Structural Damage Detection in Flexible Space Structures Using Vibration Characterization," Report NDT-44-001-800 submitted to NASA/JSC.
- Ricles, J. M. and Kosmatka, J. B. (1992), "Damage Detection in Elastic Structures Using Vibratory Residual Forces and Weighted Sensitivity," *AIAA Journal*, Vol. 30, No. 9, pp. 2310–2316.
- Rodden, W. P. (1967), "A Method for Deriving Structural Influence Coefficients from Ground Vibration Tests," *AIAA Journal*, Vol. 5, No. 5, pp. 991–1000.
- Smith, S. W. (1992), "Iterative Use of Direct Matrix Updates: Connectivity and Convergence," Proceedings of the 33rd AIAA Structures, Structural Dynamics and Materials Conference, Dallas TX, pp. 1797–1806.
- Smith, S. W., Baker, J. R., Kaouk, M. and Zimmerman, D. C. (1993), "Mode shape Expansion for Visualization and Model Correction," Proceedings of the 9th VPI&SU Symposium on Dynamics and Control of Large Space Structures, Blacksburg, VA (proceedings to be published).
- Smith, S. W. and Beattie, C. A. (1990), "Simultaneous Expansion and Orthogonalization of Measured Modes for Structure Identification," Proceedings of the AIAA Dynamic Specialist Conference, Long Beach, CA, pp. 261–270.



- Smith, S. W. and Beattie, C. A. (1991), "Secant-Method Adjustment for Structural Models," *AIAA Journal*, Vol. 29, No. 1, pp. 119–126.
- Smith, S. W. and Hendricks, S. L. (1987), "Evaluation of Two Identification Methods for Damage Detection in Large Space Trusses," Proceedings of the 6th VPI&SU/AIAA Symposium on Dynamics, and Controls for Large Space Structures, Virginia Polytechnic Institute and State University, Blacksburg, VA, pp.127–142.
- Soeiro, F. (1990), *Structural Damage Assessment Using Identification Techniques*, Ph.D. Dissertation, Department of Aerospace Engineering, Mechanics, and Engineering Science, University of Florida, Gainesville, FL.
- Srinathkumar, S. (1978), "Eigenvalues/Eigenvectors Assignment Using Output Feedback," *IEEE Transactions on Automatic Control*, Vol. AC-23, 1, pp. 79–81.
- Widengren, M. (1989), *An Analytical Method for the Symmetric Correction of Mathematical Models of Vibrating Systems Using Eigenstructure Assignment*, M.S. Thesis, Department of Mechanics, Royal Institute of Technology, Stockholm, Sweden.
- White, C. W. and Maytum, B. D. (1976), "Eigensolution Sensitivity to Parametric Model Perturbation," *Shock and Vibration Bulletin*, Vol. 46, Part 5, pp. 123–133.
- Zimmerman, D. C., and Kaouk, M. (1992a), "Eigenstructure Assignment Approach for Structural Damage Detection," *AIAA Journal*, Vol. 21, No. 8, pp. 1848–1855.
- Zimmerman, D. C. and Kaouk, M. (1992b), "Structural Damage Detection Using a Subspace Rotation Algorithm," Proceedings of the 33rd AIAA Structures, Structural Dynamics and Materials Conference, Dallas, TX, pp. 2341–2350.
- Zimmerman, D. C. and Smith, S. W., (1992), "Model Refinement and Damage Location for Intelligent Structures," chapter in *Intelligent Structural Systems* (H.S. Tzou, editor), Kluwer Academic Publishers, Amsterdam, The Netherlands.
- Zimmerman, D. C., and Widengren, W. (1989), "Equivalence Relations for Model Correction of Nonproportionally Damped Linear Systems," Proceedings of the Seventh VPI&SU Symposium on the Dynamics and Control of Large Structures, Blacksburg, VA, pp. 523–538.
- Zimmerman, D.C., and Widengren, W. (1990), "Model Correction Using a Symmetric Eigenstructure Assignment Technique," *AIAA Journal*, Vol. 28, No. 9, pp. 1670–1676.

## BIOGRAPHICAL SKETCH

Mohamed Kaouk received a Bachelor of Science in aerospace engineering from the Department of Aerospace Engineering, Mechanics, and Engineering Science at the University of Florida in December of 1988. From the same department, he then received a Master of Science in aerospace engineering in August of 1991.

I certify that I have read this study and that in my opinion it conforms to acceptable standards of scholarly presentation and is fully adequate, in scope and quality, as a dissertation for the degree of Doctor of Philosophy.



---

David C. Zimmerman, Chair  
Associate Professor of Aerospace Engineering,  
Mechanics, and Engineering Science

I certify that I have read this study and that in my opinion it conforms to acceptable standards of scholarly presentation and is fully adequate, in scope and quality, as a dissertation for the degree of Doctor of Philosophy.



---

Lawrence E. Malvern  
Professor Emeritus of Aerospace Engineering,  
Mechanics, and Engineering Science

I certify that I have read this study and that in my opinion it conforms to acceptable standards of scholarly presentation and is fully adequate, in scope and quality, as a dissertation for the degree of Doctor of Philosophy.



---

Bhavani Sankar  
Associate Professor of Aerospace Engineering,  
Mechanics, and Engineering Science

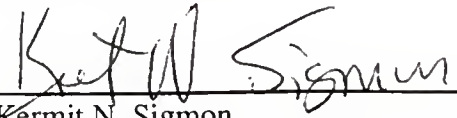
I certify that I have read this study and that in my opinion it conforms to acceptable standards of scholarly presentation and is fully adequate, in scope and quality, as a dissertation for the degree of Doctor of Philosophy.



---

Norman Fitz-Coy  
Assistant Professor of Aerospace Engineering,  
Mechanics, and Engineering Science

I certify that I have read this study and that in my opinion it conforms to acceptable standards of scholarly presentation and is fully adequate, in scope and quality, as a dissertation for the degree of Doctor of Philosophy.



Kermit N. Sigmon  
Associate Professor of Mathematics

This dissertation was submitted to the Graduate Faculty of the College of Engineering and to the Graduate School and was accepted as partial fulfillment of the requirements for the degree of Doctor of Philosophy.

August 1993



Winfred M. Phillips  
Dean, College of Engineering

---

Dean, Graduate School

UNIVERSITY OF FLORIDA



3 1262 08554 0457